



Universiteit
Leiden

The Netherlands

Everyone works better together: rational improvements to radio- and immunotherapy combinations

Frijlink, E.S.

Citation

Frijlink, E. S. (2024, April 4). *Everyone works better together: rational improvements to radio- and immunotherapy combinations*. Retrieved from <https://hdl.handle.net/1887/3731335>

Version: Publisher's Version

License: [Licence agreement concerning inclusion of doctoral thesis in the Institutional Repository of the University of Leiden](#)

Downloaded from: <https://hdl.handle.net/1887/3731335>

Note: To cite this publication please use the final published version (if applicable).

EVERYONE WORKS BETTER TOGETHER:

RATIONAL IMPROVEMENTS TO RADIO- AND
IMMUNOTHERAPY COMBINATIONS



ELSELIEN FRIJLINK

Everyone works better together:

Rational improvements to radio- and immunotherapy combinations.

Eselien Frijlink

Voor mijn ouders

About the cover:

In nature, a continuous synergy exists between plants and pollinators. This synergy is essential for the reproduction of many plant species. Without pollinators like butterflies and bees, the ecosystem would suffer significant disruptions, leading to decreased biodiversity. Butterflies and bees collaborate to enhance different aspects of pollination. Similarly, anti-tumor (immune) therapies, including radiotherapy and immune checkpoint inhibitors, must operate in concert to overcome various bottlenecks in the cancer immunity cycle. This thesis explores how to rationally overcome these bottlenecks to achieve anti-tumor treatment synergy.

Cover design: Irma Frijlink, Parntawan Kidtham | k.parntawan@gmail.com

Printing: Ridderprint | www.ridderprint.nl

ISBN: 978-94-6483-861-9

Copyright © 2024 Elselien S. Frijlink.

All rights reserved. No parts of this book may be reproduced, stored in a retrieval system, or transmitted in any form or by any means, without prior permission of the author.

The research described in this thesis was performed at the Netherlands Cancer Institute – Antoni van Leeuwenhoek hospital (NKI-AVL), Division of Tumor Biology and Immunology and Leiden University Medical Center (LUMC), Department of Immunology. The research was financially supported by the Dutch Cancer Foundation (KWF) (grants 10894 and 11079), a Strategic Fund from the LUMC and the Oncode Institute. The printing of this thesis was financially supported by the NKI-AVL.

Everyone works better together: Rational improvements to radio- and immunotherapy combinations.

Proefschrift

ter verkrijging van
de graad van doctor aan de Universiteit Leiden,
op gezag van rector magnificus prof.dr.ir. H. Bijl,
volgens besluit van het college voor promoties
te verdedigen op donderdag 4 april 2024
klokke 15:00 uur

door

Elselien Stephanie Frijlink
geboren te Naarden
in 1989

Promoter

Prof. Dr. J.G. Borst

Co-Promoter

Dr. I. Verbrugge

The Netherlands Cancer Institute

Promotie Commissie

Prof. Dr. K.E. de Visser

Prof. Dr. F.A. Ossendorp

Prof. Dr. M. Verheij

Radboud University Medical Center

Prof. Dr. S. Janssens

VIB – Ghent University

Dr. Leila Akkari

The Netherlands Cancer Institute

Table of contents

Chapter 1:	General introduction & Scope of the thesis	7
Chapter 2:	PD-1 and CTLA-4 blockade promote CD86-driven Treg responses upon radiotherapy of lymphocyte-depleted cancer <i>Frijlink, E. et al., J. Clin. Invest. - In revision</i>	19
Chapter 3:	Identifying the mechanisms behind tumor-induced Treg priming <i>Frijlink, E. et al.</i>	59
Chapter 4:	Radiotherapy and Cisplatin increase immunotherapy efficacy by enabling local and systemic intratumoral T-cell activity <i>Kroon, P./Frijlink, E. et al., Can. Imm. Res. 2019;7(4): 670-682</i>	77
Chapter 5:	Autotaxin impedes anti-tumor immunity by suppressing chemotaxis and tumor infiltration of CD8 ⁺ T cells <i>Matas-Rico, E./Frijlink, E. et al., Cell Rep. 2021;37(7): 110013</i>	111
Chapter 6:	General discussion	147
Addenda:	English summary	170
	Nederlandse samenvatting	174
	Publications	178
	PhD portfolio	179
	Curriculum Vitae	180
	Acknowledgements	181



1

General Introduction & Scope of thesis

General introduction

The T cell response to cancer

CD8⁺ and CD4⁺ T cells can defend higher organisms against pathogens and cancer through the recognition of foreign (“non-self”) molecules, called antigens. CD8⁺ T cells are particularly effective in targeting tumors, because they can identify intracellular antigens presented by MHC Class I molecules that are expressed on all cell types, including all tumor variants. CD8⁺ T cells differentiate into cytotoxic T lymphocytes (CTL) upon activation that can directly kill infected or cancer cells. In contrast, CD4⁺ T cells recognize antigens presented in the context of MHC Class II, which is predominantly expressed on antigen-presenting immune cells (APCs). They can therefore directly recognize only certain cancers and are primarily involved in immunomodulatory functions. CD8⁺ T cells are activated (primed) in secondary lymphoid organs and after clonal expansion and effector differentiation, go into the blood, from where they can reach and infiltrate infected or cancerous tissues. For successful cancer immunotherapy, a durable and self-sustaining anti-tumor CD8⁺ T cell response is crucial. Efficient priming of effector T cells relies on the activity and migration of dendritic cells (DCs) from the tumor¹. DCs encompass three different lineages, including plasmacytoid (p) DCs and conventional (c)DC type 1 (cDC1) and type 2 (cDC2). cDC1s and cDC2s are discerned in migratory and lymph node-resident subsets². cDCs are specialized in engulfing infected cells and cellular debris, which they process and present as antigens via MHC Class I and II molecules to CD8⁺ and CD4⁺ T cells, respectively. cDCs need to be adequately activated to express specific costimulatory molecules and cytokines to induce (prime) CD8⁺ and CD4⁺ T cell responses. Activation of DCs in cancer depends on the release of danger-associated molecular patterns (DAMPs) from dying cancer cells. Additionally, cDCs require “help” or licensing from CD4⁺ T cells through MHC Class II-mediated interaction to fully mature³⁻⁵. CD4⁺ T cell help equips CD8⁺ T cells with effector and memory functions required to overcome negative regulation^{6,7}. Intravital imaging argues that priming of effective CD8⁺ T cell immunity occurs in two steps: The initial priming step takes place separately for CD8⁺ and CD4⁺ T cells in distinct areas of lymphoid organs, involving cDC1s and cDC2s, respectively. Subsequently, CD8⁺ and CD4⁺ T cells interact with the same lymph node-resident or perhaps migratory cDC1, where CD4⁺ T cells provide their help signals allowing for effector CD8⁺ T cell differentiation to occur^{5,8,9}. cDCs are crucial in determining whether a response by conventional CD8⁺ and CD4⁺ T cells (Tconv) occurs. Insufficient DC activation can lead to tolerogenic mechanisms, including the development of non-responsive (anergic) T cells or the priming of regulatory CD4⁺ T cells (Tregs)¹⁰. Tregs promote immune tolerance by attenuating conventional T cell (Tconv) responses through inhibition of cDC activation and migration^{11,12} or by suppression of effector T cell function¹³.

Thus, a series of intricate and carefully orchestrated steps is required to mount an effective anti-tumor T cell response. Several bottlenecks commonly hinder this response, including the lack of recognizable non-self antigens, insufficient presence of T cells with tumor antigen-specific T

cell receptors (TCRs) in the patient's repertoire, inadequate abundance of cDCs in the tumor, or inadequate activation of cDCs, and effector T cell suppression in the tumor micro-environment (TME). Targeting of these bottlenecks has been the focus of current cancer immunotherapy strategies and has resulted in a surge of clinical trials in the past years^{14,15}. However, only a small fraction of patients with solid tumors benefit from these treatments¹⁶, emphasizing the requirement for a better understanding of the immunogenicity and immune responsiveness of cancers.

Interplay between tumors and the immune system

Recent advances in multi-omic analysis of human cancer have provided valuable insights into the relationship between tumors and the immune system and the impact of the immune response on patient survival^{17,18}. These studies have revealed that tumors of the same type, e.g. non-small cell lung cancer (NSCLC) or colon cancer can present a wide range of immune constellations that can be favorable or unfavorable in terms of overall patient survival and response to immunotherapy. Generally, lymphocyte paucity, in combination with high levels of fibroblasts and/or myeloid cells, is typically associated with a higher mortality rate, whereas a high abundance of lymphocytes, often accompanied by elevated levels of DCs and robust IFN responses, is strongly linked to improved response to antibody-based immunotherapy and overall survival^{17,18}. These "inflamed" tumors usually meet the required conditions for T cell priming in the TdLN, but suboptimal priming, combined with immunosuppression in the TME often impairs their activity, resulting in T cell exhaustion¹⁹. In such cases, antibody-based blockade of the inhibitory pathways imposed by PD-(L)1 or CTLA-4 can restore anti-tumor T cell responses^{20,21}. In contrast, tumors lacking T cells generally experience immunosuppression or immune ignorance at an early stage in development, rendering them unresponsive to the same immunotherapy approaches. For these tumors, strategies should focus on inducing T cell priming rather than overcoming immunosuppression in the TME²².

Tumor progression not only affects the local immune landscape but also triggers systemic immune alterations²³. This leads to a state of general immunosuppression, typically due to the mobilization of immunosuppressive myeloid cells in the host, creating a favorable environment for tumor metastasis to distant organs²⁴. The tumor-draining lymph nodes (TdLNs), acting as downstream lymph draining site for (tumor) tissues, are often the first affected sites. This results in significant immunosuppression that hinders effective tumor-specific T cell responses²⁵, presenting another hurdle for effective cancer immunotherapy.

Cancer immunotherapy

Immunotherapy strategies are designed to overcome barriers that impede effective anti-tumor T cell responses. Among these, therapeutic vaccination aims to expand the pool of tumor-reactive

T cells. This is achieved by incorporating either tumor-associated “self” antigens like cancer-testis antigens, or “non-self” antigens including virus-derived antigens and tumor-specific neoantigens²⁶. However, clinical benefit of vaccination is limited by challenges in antigen identification (for both CD8⁺ and CD4⁺ T cells), inadequate MHC class I expression on tumors, local and systemic immunosuppression and tumor burden²⁶. To overcome these hurdles, adoptive cell therapy (ACT) with autologous or allogeneic tumor-specific T cells was proposed as a promising strategy²⁷. ACT involves infusion of highly active effector T cells, and recent advances in genetic engineering of tumor-specific TCRs and the development of chimeric antigen receptor (CAR)-T cell have further improved its effectiveness, particularly in hematopoietic malignancies. However, outcomes with ACT depend on the presence of defined tumor antigens, the availability of tumor-specific T cells with the appropriate functional capabilities and resistance to exhaustion, and have a risk of life-threatening toxic off-target effects²⁸.

Immunomodulatory antibodies, commonly known as immune checkpoint blockade (ICB), like anti-PD-(L)1 and anti-CTLA-4 alleviate suppression imposed on tumor-specific T cells existing within patients. This approach presents a potential solution to lack of defined tumor-specific antigens. The co-inhibitory receptors PD-1 and CTLA-4 attenuate CD28 costimulation^{29,30}, required to support T cell division, metabolism, and survival³¹ through distinct mechanisms. PD-1 dampens CD28 costimulation by binding to its ligands PD-L1 or PD-L2, which are presented by cDCs. This interaction causes the recruitment of SHP2 tyrosine phosphatase to PD-1, which leads to CD28 dephosphorylation and subsequent signaling inhibition³². CTLA-4, constitutively expressed on Tregs and upregulated by TconvS post activation, downregulates the CD28 ligands CD80 and CD86 from the cell surface of cDCs³⁰. Thereby, it plays a crucial role in peripheral tolerance by establishing Treg-mediated inhibition of the priming of self-reactive T cells³³. Notably, PD-(L)1 blockade can act in the TME, but also promotes T cell priming in the TdLN^{34,35}. Impressive curative responses following CTLA-4 blockade were observed in melanoma³⁶, whereas PD-1 inhibition achieved significant successes in non-small-cell lung cancer³⁷, renal carcinoma³⁸, and head and neck squamous carcinoma³⁹. Additionally, the combination of CTLA-4 and PD-1 blockade can be synergistic, as was first shown in melanoma⁴⁰ and has yielded considerable successes in other difficult-to-treat cancers, including mismatch-repair proficient colorectal cancer⁴¹ and advanced esophageal cancer⁴². However, the mechanism underlying this synergistic response has not yet been fully elucidated^{21,43}. Despite these successes, response rates for most solid tumors are disappointing¹⁶, which can be attributed to the lack of pre-existing T cell responses in these tumors. Thus, especially for cancers displaying robust immunosuppression, immunotherapy approaches should aim to 1) evoke an effective, preferably endogenous, anti-tumor T cell response without the requirement for prior identification of tumor antigens, and 2) overcome prevailing immunosuppression. To achieve this, ICB may be combined with radiotherapy (RT)⁴⁴.

Radiotherapy

RT is a common cancer treatment given to over 50% of patients for curative or palliative purposes⁴⁵. RT inflicts DNA damage and selectively targets tumor cells, owing to their high proliferation rate and frequent loss of DNA repair capabilities. This leads to either a permanent cell cycle arrest or tumor cell death⁴⁶. In contrast to chemotherapy, RT is applied locally to the tumor field and thereby offers the advantage of reduced off-target toxicity to healthy tissues. Moreover, RT not only causes tumor cell death, but also induces local immunomodulatory effects. For example, RT targets endothelial-cellular junctions and enhances the expression of adhesion molecules, potentially resulting in improved permeability and enhanced infiltration of circulating immune cells into the TME⁴⁶. Additionally, RT may expose immunogenic neoantigens by upregulating mutated gene expression^{47,48} and it can potentially increase the expression of MHC Class I on tumor cells⁴⁹. Furthermore, depending on the anatomical location, proliferative state, and level of differentiation, RT may also target other cellular components in the TME, including immunosuppressive cells⁴⁶. Thus, in addition to reducing tumor size, RT can create a more immune-permissive environment, potentially reducing the likelihood of local tumor recurrence.

Radiotherapy and immunogenicity

RT has gained increasing interest for its potential effects on systemic anti-tumor immunity. In 1953, Robin Mole observed that local RT may result in anti-tumor effects outside the field of treatment, described as the abscopal effect⁵⁰. The contribution of the immune system to this effect was not identified until 1979, when it was observed that an intact immune system was crucial for RT-induced tumor control⁵¹. Many years later, the abscopal effect to RT was shown to depend on the recruitment of effector T cells to the tumor⁵². However, the fact that RT could support T cell priming remained unknown for two decades until the groundbreaking study by Lugade, et al.⁵³, who demonstrated that local RT supports the differentiation of tumor-specific effector T cells in the TdLN. These studies not only emphasized the importance of T cells for achieving curative effects with RT, but also highlighted the potential of RT to generate new T cell responses.

Upon causing tumor cell death, RT may release cellular debris, including antigens and DAMPs required to achieve DC maturation and migration to the TdLN⁵⁴. Specifically, RT-induced DNA damage activates the nucleic acid sensor cGAS in tumor cells, leading to the activation of the Stimulator of Interferon Genes (STING) pathway and subsequent production of type I interferons (IFN-I)^{55,56}. Release of IFN-I is crucial to improve the activation and migration of DCs⁵⁷. Thus, RT can essentially kickstart the cancer-immunity cycle to promote endogenous anti-tumor T cell responses⁵⁸. In principle, this may be further supported by concomitant ICB, but the combination of RT and such immunotherapy thus far has not consistently achieved combined curative

responses⁴⁴. This is likely primarily due to our limited understanding of the mechanisms by which RT affects immune responses in tumors with varying immune complexities. Specifically, spontaneously immunogenic tumors containing tumor-specific T cells in the TME prior to treatment may exhibit intratumoral T cell activation upon RT alone⁵⁹ or in combination with ICB⁶⁰. This may lead to regression of the irradiated tumor without the requirement of a systemic T cell response. In contrast, tumors lacking tumor-specific T cells in the TME prior to treatment, require for regression the development of a RT-induced anti-tumor T cell response in the TdLN.

Various factors limit the effectiveness of RT in eliciting systemic anti-tumor T cell responses, including the lack of RT-induced release of antigens and DAMPs^{61,62}, insufficient recruitment of DCs⁶³ and immunosuppression in the TME⁶⁴. Additionally, RT may cause the upregulation of inhibitory molecules, including PD-L1 and CD73^{63,65,66}, further contributing to immunosuppressive effects that could limit curative responses. Importantly, these factors are often overlooked or diluted in pre-clinical mouse studies, as these typically take advantage of tumor models that contain dominant, non-self antigens and therefore poorly reflect human cancers^{53,67-69}. It is currently unclear to what extent RT can induce T cell priming in the human cancer setting, specifically in immunosuppressive tumors lacking a tumor-specific T cell infiltrate prior to treatment. Therefore, we need a comprehensive, mechanistic understanding of how RT affects the T cell response to poorly immunogenic tumors. This is essential to rationally combine RT with specific immunotherapeutic interventions, to achieve a synergistic effect on anti-tumor immunity.

Scope of the thesis

In this thesis, I used mouse tumor models of different immune complexities to define and optimize determinants for RT-induced T cell priming and subsequent anti-tumor immunity. First, I identify, in a tumor model resembling human lymphocyte-depleted cancer, impediments that prevent systemic RT-induced T cell responses and present interventions that overcome these impediments. Next, I describe work investigating the role of RT and other interventions to overcome local T cell suppression in the TME, using different tumor models.

In **chapter 2**, we examined the potential and challenges of using RT to generate novel T cell responses in a tumor model representing human lymphocyte-depleted cancer. We observed that low lymphocyte levels and high myeloid cell content negatively impact overall survival after RT in human tumors. We utilized the transplantable TC-1 tumor model to replicate these immune characteristics in mice. This tumor model is characterized by systemic immunosuppression, indicated by increased monocyte and Treg levels in the TdLN and tumor. In this model, RT promotes CD8⁺ T cell priming in the TdLN, required for RT-induced tumor control. However, concurrent Treg priming, which is spontaneously induced by the tumor and further exacerbated by RT, hindered these responses. We

proved that in this setting, CTLA-4 and PD-1 blockade further enhanced RT-induced Treg responses and resulted in failed tumor control. Mechanistically, we identified CD28 costimulation, engaged upon CTLA-4 and PD-1 blockade, as the main driver of the RT-induced Treg response. We discovered that the CD28-ligand CD86 promoted this Treg response. Inhibition of CD86, but not CD80, prevented RT-induced Treg expansion, enhanced cDC1 activation and CTL priming, and together with anti-PD-1 led to improved RT-induced tumor control and overall survival.

This chapter presents compelling evidence for the potential of RT to induce a potentially tumor eradicating CTL response even in the presence of systemic Treg-based immunosuppression. Furthermore, it emphasizes the significance of considering the patient's tumor immune profile, particularly the Tconv/Treg ratio, when designing combination strategies involving RT. This is crucial, as conventional ICBs may inadvertently promote undesired Treg responses. In addition, we propose CD86 blockade as a promising potential therapeutic target to prevent (RT-induced) Treg responses in the TdLN and tumor.

The influence of Tregs as an impediment to (RT-induced) anti-tumor immunity has received much attention by earlier studies^{64,70,71}. However, clinical targeting of Tregs has been impeded by the limited availability of targetable molecules exclusively expressed by Tregs, and the challenge of identifying targets that can discriminate tumor-specific Tregs from healthy tissue to preserve homeostatic immune tolerance. Thus, a comprehensive characterization of the development and origin of tumor-induced Treg responses is crucial to identify potential targets that can effectively differentiate them from healthy surrounding tissue. In **chapter 3**, we characterize the Treg response triggered by TC-1 tumor development and highlight potential future experiments necessary to better identify the factors to determine potential targets for Tregs.

In **chapter 4**, we study the potential of RT to promote CD8⁺ T cell responses in the TME locally. Here, we investigated the use of RT as a strategy to overcome anti-PD-1 resistance in a transplantable breast carcinoma model. Combined infusion of inhibitory anti-PD-1 and agonistic anti-CD137 facilitated the priming of CTLs, while RT created a T-cell permissive TME. Additionally, the presence of an unirradiated second, contralateral tumor, further emphasized the contribution of RT in supporting local CTL activity, as CTL infiltration in these "metastatic" tumors was not enough to improve tumor control and survival. Rather, low-dose systemic cisplatin infusion created a permissive CTL environment in the non-irradiated lesion, leading to prolonged overall survival. This chapter proposes that even following sufficient CTL priming and infiltration, local immunosuppressive mechanisms within the TME may prevent CTL functionality, alongside PD-1 blockade. In such cases, strategies like RT and cisplatin can be used to overcome these impediments and restore CTL reactivity.

Classically, TMEs have been categorized into "immune desert"; lacking T cell infiltration, "immune excluded"; containing T cell restricted to the tumor border, and "immune infiltrated";

characterized by T cell infiltration⁷². However, the mechanisms that prevent immune infiltration are not completely understood. In **chapter 5**, we uncover a novel role for autotaxin (ATX), a lysophospholipase D secreted by tumor cells and other cells, in preventing CTL infiltration into the TME. Through production of lysophosphatidic acid (LPA), we show that ATX secreted by human melanoma cells prevents T cell migration, predominantly through binding to the G protein-coupled receptor 6 (LPAR6). Upon anti-cancer vaccination of tumor-bearing mice, enforced ATX overexpression in tumor cells did not interfere with the development of systemic T cell responses, but prevented CTL infiltration into the TME, resulting in abrogated tumor control and survival.

This chapter is fundamental in uncovering a potential mechanism employed by tumors to prevent T cell infiltration, even in the presence of optimal CTL responses. In addition, it offers a promising therapeutic opportunity, that may be combined with existing anti-tumor immune interventions for use in the clinic.

Importantly, the findings in **chapter 4** and **chapter 5** illustrate the significance of effectively engaging every step in the cancer-immunity cycle to establish a durable anti-tumor immune response. Specifically, despite the generation of robust tumor-specific CTL responses, either by using immunomodulatory antibodies or by vaccination, tumor control was not achieved unless local immune inhibition was alleviated.

Finally, in **chapter 6**, I discuss the concepts and clinical implications explored throughout this thesis considering the current literature.

References

- 1 Bottcher, J. P. & Reis e Sousa, C. The Role of Type 1 Conventional Dendritic Cells in Cancer Immunity. *Trends Cancer* **4**, 784-792 (2018).
- 2 Murphy, T. L. & Murphy, K. M. Dendritic cells in cancer immunology. *Cell Mol Immunol* **19**, 3-13 (2022).
- 3 Borst, J., Ahrends, T., Babala, N., Melief, C. J. M. & Kastenmuller, W. CD4(+) T cell help in cancer immunology and immunotherapy. *Nat Rev Immunol* **18**, 635-647 (2018).
- 4 Lei, X. *et al.* CD4(+) helper T cells endow cDC1 with cancer-impeding functions in the human tumor micro-environment. *Nat Commun* **14**, 217 (2023).
- 5 Ferris, S. T. *et al.* cDC1 prime and are licensed by CD4(+) T cells to induce anti-tumour immunity. *Nature* **584**, 624-629 (2020).
- 6 Ahrends, T. *et al.* CD4(+) T Cell Help Confers a Cytotoxic T Cell Effector Program Including Coinhibitory Receptor Downregulation and Increased Tissue Invasiveness. *Immunity* **47**, 848-861 e845 (2017).
- 7 Ahrends, T. *et al.* CD4(+) T cell help creates memory CD8(+) T cells with innate and help-independent recall capacities. *Nat Commun* **10**, 5531 (2019).
- 8 Eickhoff, S. *et al.* Robust Anti-viral Immunity Requires Multiple Distinct T Cell-Dendritic Cell Interactions. *Cell* **162**, 1322-1337 (2015).
- 9 Hor, J. L. *et al.* Spatiotemporally Distinct Interactions with Dendritic Cell Subsets Facilitates CD4+ and CD8+ T Cell Activation to Localized Viral Infection. *Immunity* **43**, 554-565 (2015).
- 10 Lutz, M. B. & Schuler, G. Immature, semi-mature and fully mature dendritic cells: which signals induce tolerance or immunity? *Trends Immunol* **23**, 445-449 (2002).
- 11 Binnewies, M. *et al.* Unleashing Type-2 Dendritic Cells to Drive Protective Antitumor CD4(+) T Cell Immunity. *Cell* **177**, 556-571 e516 (2019).
- 12 Bauer, C. A. *et al.* Dynamic Treg interactions with intratumoral APCs promote local CTL dysfunction. *J Clin Invest* **124**, 2425-2440 (2014).
- 13 Vignali, D. A., Collison, L. W. & Workman, C. J. How regulatory T cells work. *Nat Rev Immunol* **8**, 523-532 (2008).
- 14 Kaiser, J. Too much of a good thing? *Science* **359**, 1346-1347 (2018).
- 15 Upadhaya, S. *et al.* Combinations take centre stage in PD1/PDL1 inhibitor clinical trials. *Nat Rev Drug Discov* **20**, 168-169 (2021).
- 16 Haslam, A. & Prasad, V. Estimation of the Percentage of US Patients With Cancer Who Are Eligible for and Respond to Checkpoint Inhibitor Immunotherapy Drugs. *JAMA Netw Open* **2**, e192535 (2019).
- 17 Thorsson, V. *et al.* The Immune Landscape of Cancer. *Immunity* **48**, 812-830 e814 (2018).
- 18 Luca, B. A. *et al.* Atlas of clinically distinct cell states and ecosystems across human solid tumors. *Cell* **184**, 5482-5496 e5428 (2021).
- 19 van der Leun, A. M., Thommen, D. S. & Schumacher, T. N. CD8(+) T cell states in human cancer: insights from single-cell analysis. *Nat Rev Cancer* **20**, 218-232 (2020).
- 20 Huang, A. C. *et al.* T-cell invigoration to tumour burden ratio associated with anti-PD-1 response. *Nature* **545**, 60-65 (2017).
- 21 Wei, S. C. *et al.* Distinct Cellular Mechanisms Underlie Anti-CTLA-4 and Anti-PD-1 Checkpoint Blockade. *Cell* **170**, 1120-1133 e1117 (2017).
- 22 Vonderheide, R. H. The Immune Revolution: A Case for Priming, Not Checkpoint. *Cancer Cell* **33**, 563-569 (2018).
- 23 Hiam-Galvez, K. J., Allen, B. M. & Spitzer, M. H. Systemic immunity in cancer. *Nat Rev Cancer* **21**, 345-359 (2021).
- 24 Peinado, H. *et al.* Pre-metastatic niches: organ-specific homes for metastases. *Nat Rev Cancer* **17**, 302-317 (2017).
- 25 van Pul, K. M. *et al.* Selectively hampered activation of lymph node-resident dendritic cells precedes profound T cell suppression and metastatic spread in the breast cancer sentinel lymph node. *J Immunother Cancer* **7**, 133 (2019).

- 26 Saxena, M., van der Burg, S. H., Melief, C. J. M. & Bhardwaj, N. Therapeutic cancer vaccines. *Nat Rev Cancer* **21**, 360-378 (2021).
- 27 Rosenberg, S. A., Restifo, N. P., Yang, J. C., Morgan, R. A. & Dudley, M. E. Adoptive cell transfer: a clinical path to effective cancer immunotherapy. *Nat Rev Cancer* **8**, 299-308 (2008).
- 28 Sharma, P., Hu-Lieskovan, S., Wargo, J. A. & Ribas, A. Primary, Adaptive, and Acquired Resistance to Cancer Immunotherapy. *Cell* **168**, 707-723 (2017).
- 29 Kamphorst, A. O. *et al.* Rescue of exhausted CD8 T cells by PD-1-targeted therapies is CD28-dependent. *Science* **355**, 1423-1427 (2017).
- 30 Wing, K. *et al.* CTLA-4 control over Foxp3+ regulatory T cell function. *Science* **322**, 271-275 (2008).
- 31 Esensten, J. H., Helou, Y. A., Chopra, G., Weiss, A. & Bluestone, J. A. CD28 Costimulation: From Mechanism to Therapy. *Immunity* **44**, 973-988 (2016).
- 32 Hui, E. *et al.* T cell costimulatory receptor CD28 is a primary target for PD-1-mediated inhibition. *Science* **355**, 1428-1433 (2017).
- 33 Wong, H. S. *et al.* A local regulatory T cell feedback circuit maintains immune homeostasis by pruning self-activated T cells. *Cell* **184**, 3981-3997 e3922 (2021).
- 34 Dammeijer, F. *et al.* The PD-1/PD-L1-Checkpoint Restrains T cell Immunity in Tumor-Draining Lymph Nodes. *Cancer Cell* **38**, 685-700 e688 (2020).
- 35 Fransen, M. F. *et al.* Tumor-draining lymph nodes are pivotal in PD-1/PD-L1 checkpoint therapy. *JCI Insight* **3** (2018).
- 36 Schadendorf, D. *et al.* Pooled Analysis of Long-Term Survival Data From Phase II and Phase III Trials of Ipilimumab in Unresectable or Metastatic Melanoma. *J Clin Oncol* **33**, 1889-1894 (2015).
- 37 Antonia, S. J. *et al.* Four-year survival with nivolumab in patients with previously treated advanced non-small-cell lung cancer: a pooled analysis. *Lancet Oncol* **20**, 1395-1408 (2019).
- 38 Motzer, R. J. *et al.* Nivolumab versus Everolimus in Advanced Renal-Cell Carcinoma. *N Engl J Med* **373**, 1803-1813 (2015).
- 39 Ferris, R. L. *et al.* Nivolumab for Recurrent Squamous-Cell Carcinoma of the Head and Neck. *N Engl J Med* **375**, 1856-1867 (2016).
- 40 Wolchok, J. D. *et al.* Overall Survival with Combined Nivolumab and Ipilimumab in Advanced Melanoma. *N Engl J Med* **377**, 1345-1356 (2017).
- 41 Chalabi, M. *et al.* Neoadjuvant immunotherapy leads to pathological responses in MMR-proficient and MMR-deficient early-stage colon cancers. *Nat Med* **26**, 566-576 (2020).
- 42 Doki, Y. *et al.* Nivolumab Combination Therapy in Advanced Esophageal Squamous-Cell Carcinoma. *N Engl J Med* **386**, 449-462 (2022).
- 43 van der Leun, A. M. *et al.* Dual immune checkpoint blockade induces analogous alterations in the dysfunctional CD8+ T cell and activated Treg compartment. *Cancer Discov* (2023).
- 44 Pointer, K. B., Pitroda, S. P. & Weichselbaum, R. R. Radiotherapy and immunotherapy: open questions and future strategies. *Trends Cancer* **8**, 9-20 (2022).
- 45 Miller, K. D. *et al.* Cancer treatment and survivorship statistics, 2019. *CA Cancer J Clin* **69**, 363-385 (2019).
- 46 Rodriguez-Ruiz, M. E., Vitale, I., Harrington, K. J., Melero, I. & Galluzzi, L. Immunological impact of cell death signaling driven by radiation on the tumor microenvironment. *Nat Immunol* **21**, 120-134 (2020).
- 47 Formenti, S. C. *et al.* Radiotherapy induces responses of lung cancer to CTLA-4 blockade. *Nat Med* **24**, 1845-1851 (2018).
- 48 Lhuillier, C. *et al.* Radiotherapy-exposed CD8+ and CD4+ neoantigens enhance tumor control. *J Clin Invest* **131** (2021).
- 49 Reits, E. A. *et al.* Radiation modulates the peptide repertoire, enhances MHC class I expression, and induces successful antitumor immunotherapy. *J Exp Med* **203**, 1259-1271 (2006).

- 50 Mole, R. H. Whole body irradiation; radiobiology or medicine? *Br J Radiol* **26**, 234-241 (1953).
- 51 Stone, H. B., Peters, L. J. & Milas, L. Effect of host immune capability on radiocurability and subsequent transplantability of a murine fibrosarcoma. *J Natl Cancer Inst* **63**, 1229-1235 (1979).
- 52 North, R. J. Radiation-induced, immunologically mediated regression of an established tumor as an example of successful therapeutic immunomanipulation. Preferential elimination of suppressor T cells allows sustained production of effector T cells. *J Exp Med* **164**, 1652-1666 (1986).
- 53 Lugade, A. A. *et al.* Local radiation therapy of B16 melanoma tumors increases the generation of tumor antigen-specific effector cells that traffic to the tumor. *J Immunol* **174**, 7516-7523 (2005).
- 54 Galluzzi, L., Buque, A., Kepp, O., Zitvogel, L. & Kroemer, G. Immunogenic cell death in cancer and infectious disease. *Nat Rev Immunol* **17**, 97-111 (2017).
- 55 Deng, L. *et al.* STING-Dependent Cytosolic DNA Sensing Promotes Radiation-Induced Type I Interferon-Dependent Antitumor Immunity in Immunogenic Tumors. *Immunity* **41**, 843-852 (2014).
- 56 Vanpouille-Box, C. *et al.* DNA exonuclease Trex1 regulates radiotherapy-induced tumour immunogenicity. *Nat Commun* **8**, 15618 (2017).
- 57 Corrales, L., McWhirter, S. M., Dubensky, T. W., Jr. & Gajewski, T. F. The host STING pathway at the interface of cancer and immunity. *J Clin Invest* **126**, 2404-2411 (2016).
- 58 Chen, D. S. & Mellman, I. Oncology meets immunology: the cancer-immunity cycle. *Immunity* **39**, 1-10 (2013).
- 59 Arina, A. *et al.* Tumor-reprogrammed resident T cells resist radiation to control tumors. *Nat Commun* **10**, 3959 (2019).
- 60 Crittenden, M. R. *et al.* Tumor cure by radiation therapy and checkpoint inhibitors depends on pre-existing immunity. *Sci Rep* **8**, 7012 (2018).
- 61 Blair, T. C. *et al.* Dendritic Cell Maturation Defines Immunological Responsiveness of Tumors to Radiation Therapy. *J Immunol* **204**, 3416-3424 (2020).
- 62 Blair, T. C. *et al.* Fluorescent tracking identifies key migratory dendritic cells in the lymph node after radiotherapy. *Life Sci Alliance* **5** (2022).
- 63 Wennerberg, E. *et al.* CD73 Blockade Promotes Dendritic Cell Infiltration of Irradiated Tumors and Tumor Rejection. *Cancer Immunol Res* **8**, 465-478 (2020).
- 64 Mondini, M. *et al.* CCR2-Dependent Recruitment of Tregs and Monocytes Following Radiotherapy Is Associated with TNF α -Mediated Resistance. *Cancer Immunol Res* **7**, 376-387 (2019).
- 65 Hsieh, R. C. *et al.* ATR-mediated CD47 and PD-L1 up-regulation restricts radiotherapy-induced immune priming and abscopal responses in colorectal cancer. *Sci Immunol* **7**, eabl9330 (2022).
- 66 Deng, L. *et al.* Irradiation and anti-PD-L1 treatment synergistically promote antitumor immunity in mice. *J Clin Invest* **124**, 687-695 (2014).
- 67 Lee, Y. *et al.* Therapeutic effects of ablative radiation on local tumor require CD8⁺ T cells: changing strategies for cancer treatment. *Blood* **114**, 589-595 (2009).
- 68 Takeshima, T. *et al.* Local radiation therapy inhibits tumor growth through the generation of tumor-specific CTL: its potentiation by combination with Th1 cell therapy. *Cancer Res* **70**, 2697-2706 (2010).
- 69 Buchwald, Z. S. *et al.* Tumor-draining lymph node is important for a robust abscopal effect stimulated by radiotherapy. *J Immunother Cancer* **8** (2020).
- 70 Chaudhary, B. & Elkord, E. Regulatory T Cells in the Tumor Microenvironment and Cancer Progression: Role and Therapeutic Targeting. *Vaccines (Basel)* **4** (2016).
- 71 Ji, D. *et al.* Combination of radiotherapy and suppression of Tregs enhances abscopal antitumor effect and inhibits metastasis in rectal cancer. *J Immunother Cancer* **8** (2020).
- 72 Fridman, W. H., Zitvogel, L., Sautes-Fridman, C. & Kroemer, G. The immune contexture in cancer prognosis and treatment. *Nat Rev Clin Oncol* **14**, 717-734 (2017).



2

PD-1 and CTLA-4 blockade promote CD86-driven Treg responses upon radiotherapy of lymphocyte-depleted cancer

Manuscript in revision – J. Clin. Invest.

Elselien Frijlink^{1,2}, Douwe M.T. Bosma², Thomas W. Battaglia³, Julia Busselaar², Mo D. Staal², Inge Verbrugge^{1,4} and Jannie Borst²

¹Division of Tumor Biology and Immunology and Oncode Institute, The Netherlands Cancer Institute, Amsterdam, The Netherlands

²Department of Immunology and Oncode Institute, Leiden University Medical Center, Leiden, The Netherlands

³Division of Molecular Oncology and Immunology and Oncode Institute, The Netherlands Cancer Institute, Amsterdam, The Netherlands

⁴Present address: Genmab, Utrecht, The Netherlands.

Abstract

Radiotherapy (RT) is considered immunogenic, but clinical data demonstrating RT-induced T-cell priming are scarce. Here, we show in a mouse tumor model representative of human lymphocyte-depleted cancer that RT enhances spontaneous priming of regulatory T-cells (Treg) by the tumor. These Tregs impede RT-induced CD8⁺ cytotoxic T-cell (CTL)-mediated tumor control. CTLA-4 or PD-1 blockade, which enables CD28 costimulation, further increased RT-induced Treg responses and failed to improve tumor control. We discovered that upon RT, CD28-ligands CD86 and CD80 differentially affected the Treg response. Only CD86 blockade promoted the PD-L1⁺CD80⁺ costimulatory status of conventional (c)DCs and prevented the Treg response. Blockade of CD86 alone or in combination with PD-1 enhanced intra-tumoral CTL accumulation and significantly increased RT-induced tumor regression and overall survival. We advise that combining RT with PD-1 and/or CTLA-4 blockade may be counterproductive in tumors that are Treg dominant. However, combining RT with CD86 blockade can promote control of such tumors by enabling a CTL response.

Summary

In lymphocyte-depleted cancer, PD-1 and CTLA-4 blockade promote radiotherapy-induced Treg responses in a CD86-dependent manner and prevent CD8⁺ T-cell mediated tumor control.

Introduction

Immunotherapies, particularly antibody-based immune-checkpoint blockade (ICB), are now a mainstay in managing multiple cancer types. However, only a minority of patients shows durable clinical responses¹, which is partially attributed to the immune composition of the tumor². Pan-cancer transcriptome analyses have subdivided human cancer types into different classes, based on the intra-tumoral immune cell composition and cell states^{3,4}. These analyses identified that ICB responsiveness only occurs in tumors that are infiltrated by effector-type CD4⁺ and CD8⁺ T cells⁴. To achieve clinical benefit in poorly immunogenic cancers devoid of effector T-cells, anti-tumor immune interventions therefore should elicit *de novo* T-cell responses⁵. In attempts to accomplish this, ICB is combined with RT in multiple clinical trials⁶. The combination of ICB with RT is attractive for multiple reasons: 1) RT-induced tumor cell death causes tumor debulking, which may alleviate systemic immune suppression, 2) RT can modulate the tumor micro-environment (TME) and render it more permissive for T cell-mediated tumor destruction⁷, and 3) RT can support systemic anti-tumor immunity by generating new tumor-specific T-cell responses in the tumor-draining lymph nodes (TdLNs), in a process called T-cell priming.

The capacity of RT to induce *de novo*, systemic anti-tumor T-cell responses has been much advertised, based on theoretical grounds⁸ and on observations in mouse models⁹⁻¹¹. Upon RT-induced tumor cell destruction, cell debris will be released that contains tumor-derived antigens and danger-associated molecular patterns (DAMPs)^{12,13}. This debris is engulfed locally by migratory, conventional dendritic cells (cDCs) that are activated by DAMPs and subsequently migrate to TdLNs and initiate T-cell responses. To prime CD8⁺ T cells, the cDC1 subset is required that excels in cross-presenting peptides from phagocytosed proteins in MHC class I (MHC-I) molecules. Moreover, activated cDC1s give CD8⁺ T cells the instruction to differentiate into competent CTLs via specific costimulatory and cytokine signals¹⁴. The potential of RT to induce T-cell priming and consequent systemic immunity predicts that it may potentiate abscopal effects, i.e. tumor regression outside the field of radiation. Clinically, such observations are extremely rare¹⁵, indicating that there are impediments in this process⁷. In specific mouse tumor models, RT has repeatedly shown to induce T-cell infiltration not only of the irradiated tumor, but also of a tumor implanted on a non-irradiated site in the same mouse¹⁶⁻¹⁸. However, this observation is primarily restricted to tumors that contain dominant, non-self antigens.

Currently approved ICB immunotherapies, i.e. CTLA-4 and PD-(L)1 blockade, both promote T-cell costimulation by cDCs. PD-1 is a co-inhibitory receptor that attenuates T-cell responses by extinguishing downstream signaling of CD28¹⁹. CD28 costimulatory signals amplify and add to T-cell receptor (TCR)/CD3 signals to support division, metabolism, and survival of newly activated CD4⁺ and CD8⁺ T-cells²⁰. When PD-1 binds either of its ligands PD-L1 or PD-L2, its cytoplasmic tail

recruits the SHP2 tyrosine phosphatase. This enzyme can then dephosphorylate the cytoplasmic tail of activated CD28, thus abrogating its downstream signaling¹⁹. The co-inhibitory receptor CTLA-4 is constitutively expressed on Tregs^{21,22} and downregulates the CD28 ligands CD80 and CD86 on cDCs. Therefore, CTLA-4 attenuates the ability of cDCs to induce CD28 costimulation of conventional, non-regulatory T cells (Tconvs)²³. Thus, CTLA-4 and PD-1 use different mechanisms, but both control T-cell responses by suppressing CD28 costimulation.

Thus far, clinical effects of combining RT with CTLA-4 or PD-1 targeting ICB are disappointing^{6,24-27}. For example, RT as induction treatment did not enhance PD-1 blockade efficacy in metastatic triple negative breast cancer (TNBC) patients, nor did it improve T-cell infiltration in the TME²⁴. Therefore, we must better understand the molecular mechanisms underlying RT-induced T-cell responses. In mouse models, tumors that are spontaneously immunogenic and become infiltrated with tumor-specific effector T cells during their development, have been shown to regress upon RT alone²⁸, or in combination with ICB²⁹, without a requirement for *de novo* T-cell priming. In such T-cell infiltrated tumors, the T cells already present in the TME can apparently exert their effector functions locally upon RT. However, in tumors that lack pre-existing tumor-specific effector T-cells, RT will have to induce new T-cell priming to allow for T-cell mediated tumor control. This may be hampered by lack of antigens and/or DAMPs released by the tumor^{30,31} and/or by tumor-imposed immunosuppression³². We therefore examined in the current study how the T-cell response to RT proceeds in a mouse tumor model representing human lymphocyte-depleted cancer types. We found that Treg priming induced by RT prevented CTL-mediated tumor control. Importantly, CTLA-4 or PD-1 blockade further increased this Treg response. We discovered that selective inhibition of CD86 either alone or in combination with PD-1 blockade prevented the RT-induced Treg response, and enabled CTL priming and tumor control. We advise that combining RT with PD-(L)1 and/or CTLA-4-targeting ICB can be counterproductive in lymphocyte-depleted cancers and identify CD86 as an alternative target for ICB in such cases.

Results

RT response is deficient in T-cell depleted human tumor types

To identify how the tumor immune cell composition influences RT responses in human cancer, we examined the relationship between immune phenotype and RT efficacy in a wide variety of cancers. Using records from The Cancer Genome Atlas (TCGA), we identified five previously characterized pan-cancer immune phenotypes³ in patients for which RT treatment was specified (Figure **S1A,B**). These immune phenotypes are described as “wound healing” (C1), “IFN γ dominant” (C2), “inflammatory” (C3), “lymphocyte depleted” (C4) and “immunologically quiet” (C5). While RT had a positive effect on overall survival (OS) in tumors classified as C1-3 immune subtypes, RT had a negative effect on OS in the C4 and C5 subtypes (Figure **1A**) that are identified by low lymphocyte- and high myeloid cell content³. The remarkably defective response to RT of tumors with a C4 and C5 immune phenotype prompted us to examine the underlying mechanism.

To perform mechanistic studies, we set out to find a mouse tumor model with a C4/C5-like lymphocyte depleted phenotype. We trained a K-nearest neighbor (KNN) classifier to distinguish between the C3 versus C4/C5 immune subtypes (Figure **S1C**) and subsequently applied our model to microarray data of murine (C57BL/6)-derived MC38 and TC-1 tumor models³³. We found similarity between the colon carcinoma cell line MC38 and the C3 subtype and between the lung carcinoma cell line TC-1 and the C4/5 subtype (Figure **1B**). Despite the presence of neo-antigens and virus-related antigens respectively^{34,35}, the MC38 tumor is immunogenic and raises a high T-cell infiltrate¹⁸, whereas the TC-1 tumor does not³⁶. In concert with this, MC38 is responsive to ICB³⁷, whereas TC-1 is not³⁸. Accordingly, flow cytometry analysis revealed a significantly lower proportion of CD8⁺ T cells in TC-1 tumors as compared to MC38 tumors (Figure **1C**).

We assessed how MC38 and TC-1 tumors respond to RT, using three consecutive doses of 8 Gy (3x 8 Gy) or a single dose of 20 Gy, regimens that are described as immune stimulatory in mouse tumor models^{9,39}. Both regimens led to MC38 tumor control, but were much less effective in TC-1 tumor control (Figure **1D**). This agrees with the finding that the pre-existing T-cell infiltrate in the MC38 tumor contributes to the RT response²⁸ and suggests impediments for immune-mediated control of the TC-1 tumor upon RT. We therefore continued our study with the TC-1 tumor to examine the RT-induced T-cell response in this representative of lymphocyte depleted cancer.

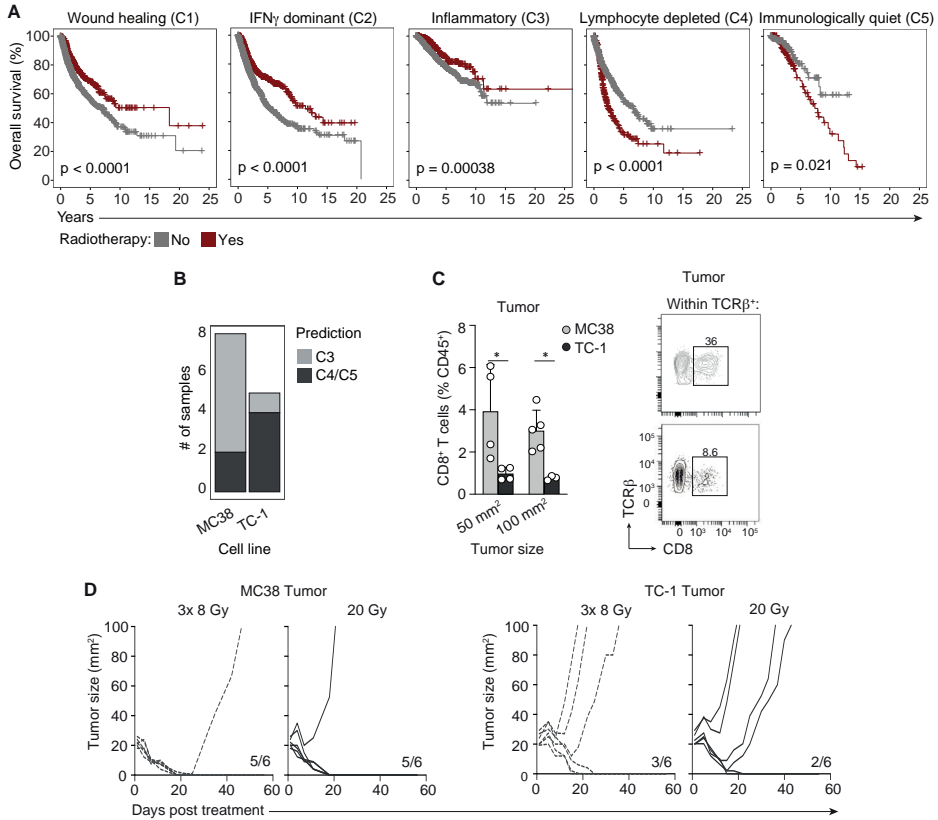


Figure 1. Lymphocyte depleted (C4/5) human cancers have suboptimal response to RT and are modelled by the murine TC-1 tumor.

(A) Kaplan-Meier OS curves obtained from TCGA for patients receiving RT (red) or not (grey) within the C1 “wound healing” (n=2136), C2 “IFN γ dominant” (n=2296), C3 “inflammatory” (n=1903), C4 “lymphocyte depleted” (n=1055) and C5 “Immunologically quiet” (n=354) cancer immune subtypes. Log-rank p-values were generated using a Cox proportional-hazards model. (B) C3 “inflammatory” versus C4/C5 “lymphocyte depleted” model predictions from transcriptome data of C57BL/6- syngeneic MC38 and TC-1 transplantable tumors. (C) Frequency of CD8⁺ T cells among CD45⁺ cells in MC38 (total n=9) and TC-1 (total n=7) tumors measured at the indicated tumor sizes (left), and representative flow cytometry plots (right) depicting the percentage of CD8⁺ T cells within TCR β ⁺ cells in 50 mm² MC38 (grey) and TC-1 (black) tumors. (D) Tumor growth curves of MC38 (n=6/group, left) and TC-1 (n=6/group, right) tumor-bearing mice treated with either 8 Gy over 3 days (3x 8 Gy) or a single dose of 20 Gy RT. Ratios indicate the number of mice out total treated that showed full recovery upon RT. Error bars indicate SD. *P < 0.05, Mann-Whitney test.

Despite high myeloid and Treg content, the RT response of TC-1 is CD8⁺ T-cell dependent

In the TME of the TC-1 tumor, the T-cell compartment, consisting of CD8⁺ and CD4⁺ Tconvs and FOXP3⁺ Tregs, comprised only 11.1% of the CD45⁺ hematopoietic cell infiltrate, as identified by flow cytometry. Conversely, myeloid cells comprised 62.5% of the CD45⁺ cell infiltrate, including macrophages and neutrophils (Figure 2A, Figure S1D). Tumors often raise systemic immune responses that may contribute to immunosuppression⁴⁰. We therefore examined the spontaneous immune response to the TC-1 tumor not only in the tumor, but also in the axillary tumor-draining lymph node (TdLN) and non-TdLN of the mice. Ly6C⁺ monocytes were enriched in the tumor, as well as in the TdLN, but not in the non-TdLN (as compared to the axillary LN in tumor-free mice) (Figure 2B). We analyzed the CD3⁺ lymphocytes in tumor and LNs in detail by spectral flow cytometry. FlowSOM-guided clustering analysis and Uniform Manifold Approximation and Projection (UMAP)-dimension reduction (Figure S1E,F) identified seven main clusters, including CD8⁺ and CD4⁺ (FOXP3⁻) Tconvs, proliferating (Ki67⁺) CD8⁺ and CD4⁺ T cells, central (c)Tregs, effector (e)Tregs and CD4⁺/CD8⁺ T cells. After development in the thymus, Tregs populate secondary lymphoid organs, where they stay as cTregs to prevent responses of autoreactive Tconvs. Alternatively, in response to antigen and inflammatory signals, cTregs can expand and differentiate into eTregs that migrate to peripheral tissues to suppress inflammation²¹. Consistent with these findings, the eTreg population was proliferating and had high expression of the effector marker ICOS, next to steady-state Treg markers FOXP3, CTLA-4 and CD25, whereas cTregs did not proliferate, had no ICOS expression and lower expression of the Treg markers (Figure 2C, Figure S1G). Quantification of the identified populations revealed no increase in proliferating CD8⁺ or CD4⁺ Tconvs in LNs upon TC-1 tumor outgrowth (Figure S1H). However, compared to naïve mice, the frequency of eTregs – but not cTregs – in the TdLN was significantly increased in tumor-bearing mice and eTregs were also present in the tumor (Figure 2D). Thus, during its outgrowth, the TC-1 tumor recruits Ly6C⁺ monocytes to the TdLN and stimulates eTreg formation in the TdLN, and these cells also populate the tumor, highlighting the communication between the tumor and TdLN^{40,41}.

Importantly, RT with either 20 Gy or 3x 8 Gy significantly augmented CD8⁺ T-cell infiltration of the TC-1 tumor, as measured in frequency (Figure 2E, Figure S2A) and absolute cell number (Figure 2F). These tumor-infiltrating CD8⁺ T cells were functional CTLs, as evidenced by the expression of Granzyme B (GZB) and the effector cytokines IFN γ and TNF α (Figure 2G). The intra-tumoral frequency of (FOXP3⁻) CD4⁺ Tconvs was not significantly altered by RT (Figure S2A,B). Systemic depletion of CD8⁺ T cells, but not of CD4⁺ T cells (Figure S2C,D), significantly reduced RT-induced mouse survival (Figure 2H), arguing that the RT-induced CTL response makes a major contribution to control of the TC-1 tumor by RT. This finding suggests that there might be a window of opportunity to improve RT-induced, CTL-mediated control of lymphocyte depleted cancers.

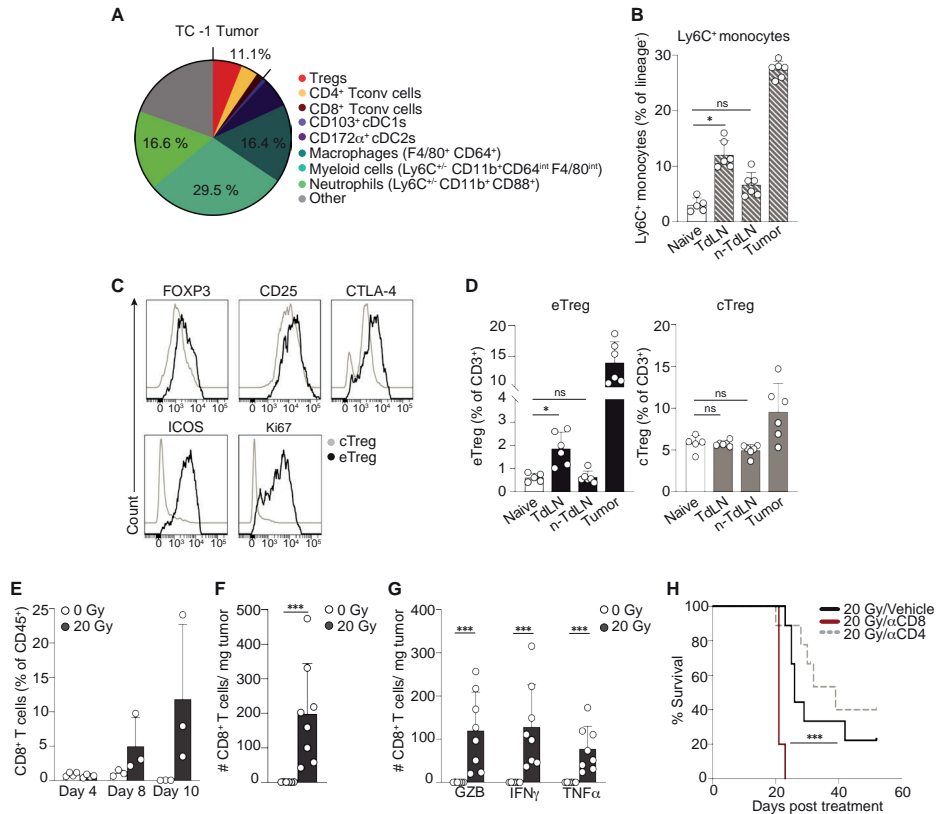


Figure 2. Treg- and myeloid cell-rich TC-1 tumor shows CD8⁺ T-cell dependent RT response.

(A) The frequency of the different indicated immune cell populations among CD45⁺ cells as determined by flow cytometry in 50 mm² TC-1 tumors (n=6). (B-D) Flow cytometric analysis of single cell suspensions from TdLN, non-TdLN and tumors of 100 mm² TC-1 tumor-bearing (n=6) and age-matched naïve mice (n=5). (B) Percentage of Ly6C⁺ monocytes among CD3⁺CD19⁺NK1.1⁻ (lineage⁺) cells found in the axillary LN of naïve mice and in indicated tissues of tumor-bearing mice. (C,D) cTregs and eTregs were defined as indicated in Figure S1E-G. FlowSOM guided clustering was performed on 5000 randomly selected cells per sample within the CD3⁺ lymphocyte population. (C) Representative histograms depicting expression of indicated markers on cTreg and eTreg populations in the right axillary LNs of naïve and TC-1 tumor bearing mice. (D) Percentage of eTregs (left) and cTregs (right) among CD3⁺ cells in the indicated tissues. (E-H) Monitoring by flow cytometry of the CD8⁺ T-cell response to 20 Gy RT (n=3-8) or control (0 Gy, n=3-6) in TC-1 tumors. (E) Frequency of the CD8⁺ T cells among CD45⁺ T cells at the indicated time points post RT. (F) Absolute number (#) of total CD8⁺ T cells or (G) granzyme B (GZB), IFN γ , or TNF α -expressing CD8⁺ T cells per milligram (mg) tumor tissue at day 8 post RT. IFN γ and TNF α were measured after *in vitro* PMA/Ionomycin stimulation. (H) Overall survival of TC-1 tumor-bearing mice treated with 20 Gy RT at day 0 in combination with vehicle (PBS, n=9) or depleting mAbs specific for CD8 (n=5) or CD4 (n=9). ***P < 0.001 (Mantel-Cox analysis). Data are from one experiment representative of at least two experiments. Error bars indicate SD. *P < 0.05, *** P < 0.001, Kruskal-Wallis test with uncorrected Dunn's post hoc analysis in B and D, Mann-Whitney test in F and G. ns; no significance.

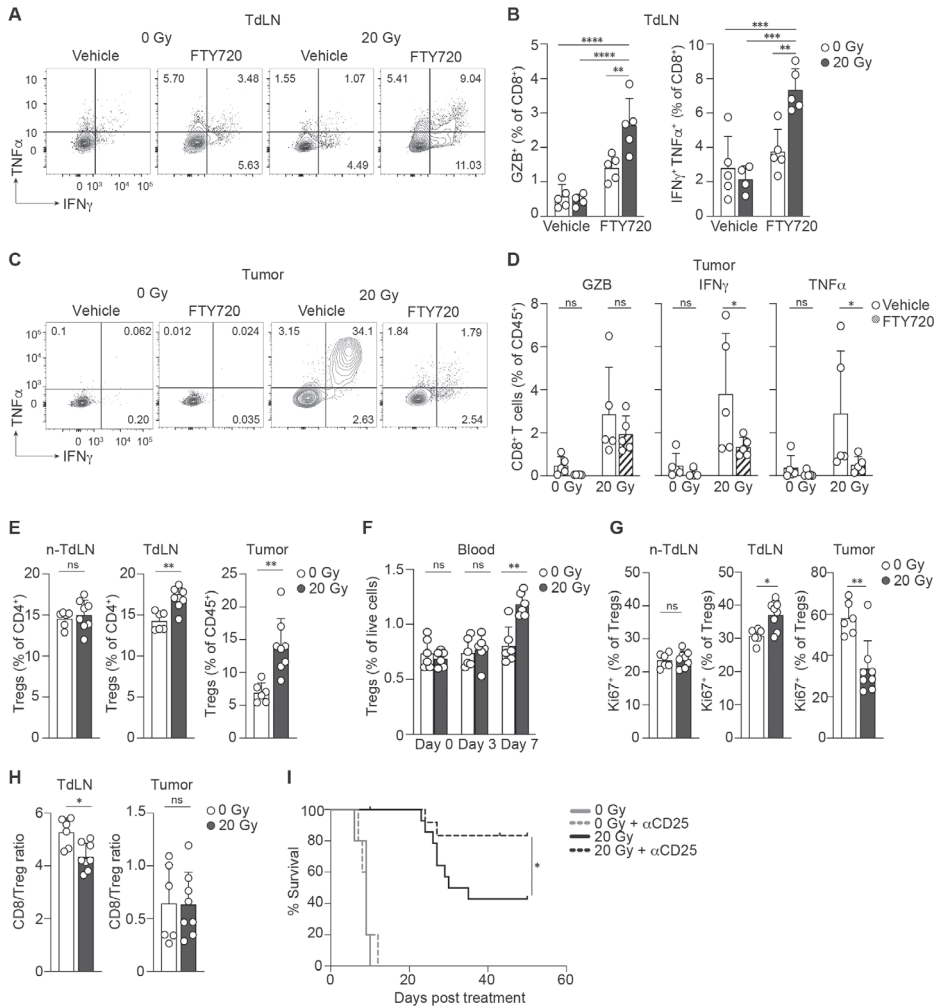
RT of the TC-1 tumor induces CTL priming, next to a Treg response that limits tumor control

The influx of effector CTLs in the irradiated TC-1 tumor likely originated from the induction of a *de novo* CD8⁺ T-cell response in the TdLN, resulting from the release of tumor antigens and DAMPs by RT¹². In highly antigenic mouse models, T-cell priming proved important for durable RT-induced anti-tumor immunity^{9,10}. We wanted to examine whether this is also the case for poorly immunogenic, T-cell depleted tumors such as TC-1. To visualize new T-cell priming after RT, mice were treated with the S1P-receptor agonist FTY720, which traps T cells in LNs⁴². In this way, the window to identify newly primed T cells in the TdLN is enlarged. As done throughout this study, the tumor was selectively irradiated by imaged-guided RT and the mice were treated before and after RT with FTY720 or vehicle. FTY720 efficacy was confirmed by the elimination of circulating CD8⁺ and CD4⁺ T cells in peripheral blood (Figure **S3A**), and treatment with FTY720 did not affect tumor development (Figure **S3B**). At day 8 after RT, T-cell priming and effector differentiation were analyzed in the TdLN. In presence of FTY720, a significant RT-induced increase in GZB⁺- and IFN γ ⁺TNF α ⁺-double expressing CD8⁺ T cells was revealed (Figure **3A,B**), while RT did not alter the frequency of effector phenotype CD4⁺ T cells (Figure **S3C**). Moreover, FTY720 treatment revealed that a large part of the effector CD8⁺ T cells present in the tumor after RT originated from the TdLN, since their frequency in the tumor was significantly reduced upon FTY720 treatment (Figure **3C,D**). The same was observed for effector CD4⁺ T cells (Figure **S3D**). Thus, in the lymphocyte-depleted TC-1 tumor model, RT elicits priming of CD8⁺ T cells that subsequently migrate into the irradiated tumor.

However, despite RT-induced CTL priming, not all TC-1 tumor-bearing mice were cured (Figure **1D**). Since the TC-1 tumor induced Treg priming during its development, and because of the described increase of Tregs in the TME upon RT^{32,43,44}, we considered that RT might enhance the Treg response in the TC-1 tumor setting. Several reports describe that Tregs require antigen-dependent activation and expansion in the TdLN prior to migration to the tumor^{41,45}. We observed that Treg frequencies (Figure **3E**, Figure **S3E**) and absolute numbers (Figure **S3F**), were significantly increased in TdLN and tumor, but not in the non-TdLN, at day 8 after RT. In addition, Treg frequency was increased in blood over time (Figure **3F**) and the percentage of proliferating (Ki67⁺) Tregs was enhanced in the TdLN but not in the non-TdLN following RT (Figure **3G**, Figure **S3G**). This coincided with a significant decrease in the frequency of proliferating Tregs in the TME (Figure **3G**, Figure **S3G**). These data clearly demonstrate RT-induced Treg priming in the TdLN, followed by migration of these cells into the irradiated TME, rather than RT-induced Treg expansion in the TME⁴³. Thus, despite new CD8⁺ T-cell responses, concomitant RT-induced Treg priming significantly lowered the CD8⁺ T cell/Treg ratio in the TdLN, while maintaining the unfavorable CD8⁺ T cell/Treg ratio in the tumor (Figure **3H**). This suggests that Tregs might be an impediment to CTL-mediated tumor control. To test this, we

treated mice with an Fc-modified antibody to CD25⁴⁶ that efficiently depleted peripheral and intra-tumoral Tregs (Figure **S4A,B**), but not CD8⁺ or CD4⁺ Tconvs (Figure **S4C**). This intervention greatly improved TC-1 tumor control and overall survival in mice after 20 Gy RT (Figure **3I**, Figure **S4D,E**). We observed similar effects when mice were treated with 3x 8 Gy (Figure **S4F,G**).

Taken together, these data indicate that in the TC-1 tumor model, Tregs limit RT-mediated tumor eradication, likely by inhibiting the RT-induced CTL response.



← **Figure 3. RT of TC-1 induces concomitant priming of CTL- and Treg responses.**

(A-D) Mice (n=4-5/group) were s.c injected with TC-1 tumor cells and the tumor was treated with 20 Gy RT when it reached ~20 mm² in size (day 0). Mice received FTY720 or vehicle (NaCl) by oral gavage, at days -1, 3 and 5. At day 8, TdLN (A,B) and tumor (C,D) were isolated and the CD8⁺ T-cell response was analyzed by flow cytometry. (A,C) Representative flow cytometry plots depicting the percentage of IFN γ ⁺ and/or TNF α ⁺ cells among CD8⁺ T cells from the TdLN (A) and tumor (C). (B,D) Frequency of GZB⁺, IFN γ ⁺ and/or TNF α ⁺ cells among CD8⁺ T cells from the TdLN (B) and tumor (D). IFN γ and TNF α were measured after in vitro PMA/Ionomycin stimulation for 3 h. (E-H) Monitoring of the (FOXP3⁺ CD25⁺) Treg response to 20 Gy RT (n=6-8) or control (0 Gy, n=6) in TC-1 tumor-bearing mice at day 8 post treatment. (E) Frequency of Tregs among CD4⁺ T cells in the non-TdLN and TdLN, or among CD45⁺ cells within the tumor. (F) In a separate experiment, the percentage of Tregs among live cells measured in blood at the indicated time points (n=6/group). (G) Percentage of Ki67⁺ cells among Tregs in the indicated tissues. (H) The ratio of CD8⁺ T cells to Treg cells in the TdLN and tumor post RT. Data in (G, H) is from the same experiment as in (E). (I) Overall survival of TC-1 tumor-bearing mice treated with 0 Gy (n=5) or 20 Gy RT (n=11-14/group) in combination with a depleting mAb against CD25 or vehicle (PBS) delivered i.p. at day -1 and 5 post RT. *P < 0.05 (Mantel-Cox analysis). Data are from one experiment representative of at least two experiments. Error bars indicate SD. *P < 0.05, **P < 0.01, *** P < 0.001, **** P < 0.0001, two-way Anova with Tukey's post hoc test in A, C and F, Mann-Whitney test in E, G, H. ns; no significance.

CTLA-4 blockade increases the RT-induced Treg response and does not improve tumor control

Blockade of CTLA-4 has been shown to enhance RT-induced tumor regression in mouse models^{47,48} and clinical studies^{25,26,49}. We next explored whether CTLA-4 inhibition could improve CTL-mediated TC-1 tumor control after RT in our lymphocyte-depleted TC-1 tumor setting. To study this, tumors were treated with RT when they reached 20 mm² as before (day 0) and a blocking antibody to CTLA-4, that does not deplete T-cells from tumor tissue^{22,50}, or vehicle was injected on day 0, 3, 6 and 9. Clearly, in the TC-1 tumor setting, anti-CTLA-4 treatment did not improve RT-induced tumor control or overall survival of the mice (Figure 4A,B). Interestingly, CTLA-4 blockade increased the RT-induced Treg response in both TdLN and non-TdLN and the population of Tregs in the tumor remained high (Figure 4C). To more comprehensively characterize how CTLA-4 blockade affected RT-induced T-cell responses, we performed FlowSOM-guided clustering analysis and dimensionality reduction on the CD3⁺ populations in the different tissues (Figure 4D,E). CTLA-4 blockade in context of RT significantly increased the frequencies of both eTregs and cTregs in the non-TdLN and TdLN, while the proportion of eTregs in the tumor did not change compared to RT alone (Figure 4F,G). Importantly, we further observed that RT as a single treatment selectively increased the proportion of eTregs, but not of cTregs, in the TdLN and tumor (Figure 4G), suggesting that RT is required to facilitate cTreg to eTreg conversion. Thus, the TC-1 tumor promotes eTreg priming, RT supports this process in addition to CTLA-4 blockade. Since Tregs are highly dependent on CD28 costimulation for their expansion⁵¹⁻⁵³, we propose that Tregs profit more from CTLA-4 blockade than Tconvs, due to their prevalence in the TdLN of the TC-1 tumor. Tregs may capitalize on the increased availability of CD80 and/or CD86 on cDCs following CTLA-4 blockade, resulting in augmented CD28 costimulation and subsequent Treg priming (Figure 4H).

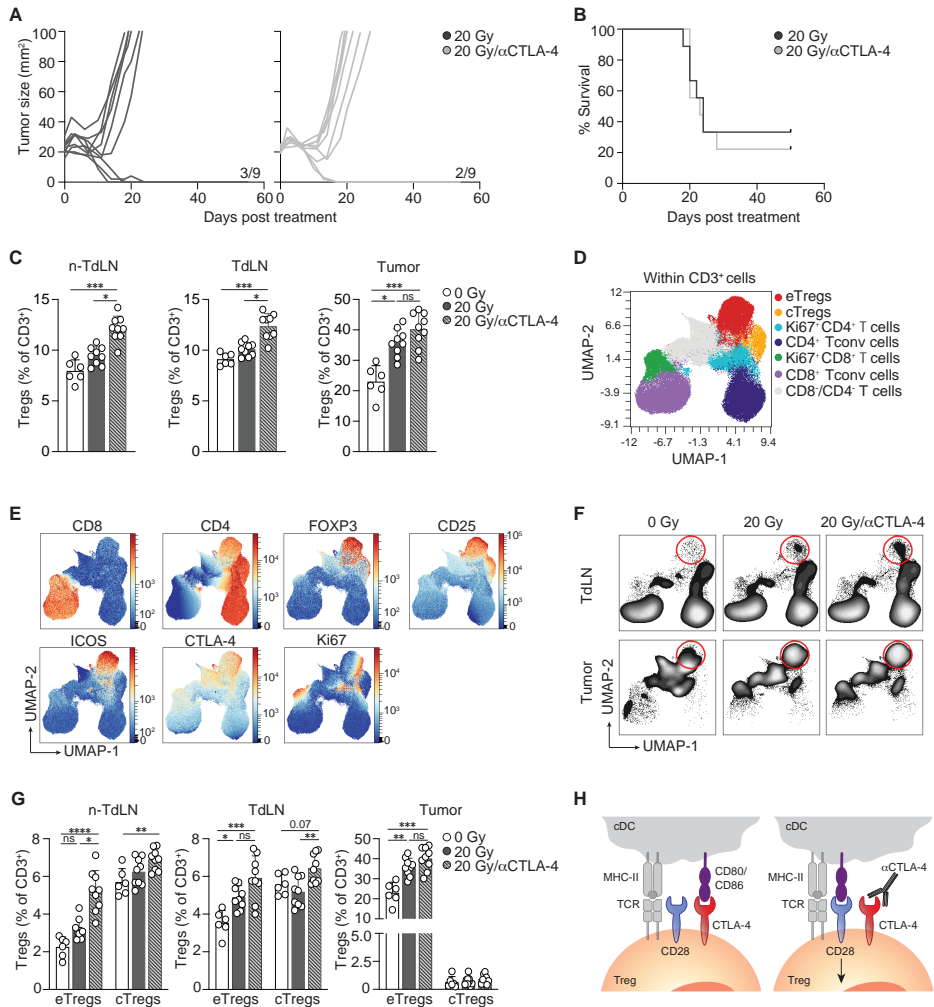


Figure 4. Blockade of CTLA-4 enhances RT-induced eTreg expansion.

Mice bearing TC-1 tumors received RT (20 Gy, n=9) or control treatment (0 Gy, n=6) when tumor size reached 20 mm² (day 0). Treatment with vehicle (PBS) or with a blocking mAb against CTLA-4 was given at day 0, 3, 6 and 9 and responses were monitored longitudinally (A, B) or by performing flow cytometric analysis of the non-TdLN, TdLN and tumor at day 8 post treatment (C-G). (A) Individual tumor growth curves and (B) overall survival of the mice in the indicated treatment groups. (C) Percentage of total Tregs among CD3⁺ lymphocytes in the indicated tissues at day 8. (D-F) UMAP display of 2500 randomly selected CD3⁺ cells per sample found in non-TdLN, TdLN and tumors at day 8 of all mice per treatment group. FlowSOM guided clustering (D) identifying the CD3⁺ cell populations (see also Figure S1E) and (E) representative heat map visualization of the markers that identify the CD3⁺ (T-cell) subpopulations. (F) UMAP visualization of the response of the CD3⁺ subpopulations in TdLN and tumor to the indicated treatments. The circles highlight the eTreg population. (G) Frequencies of eTregs and cTregs identified in (D) among CD3⁺ cells found in the indicated tissues at day 8 post treatment. (H) Graphic visualizing how Tregs could profit from CTLA-4 blockade. Data in this experiment are from one experiment representative of two experiments. Error bars indicate SD. *P < 0.05, **P < 0.01, ***P < 0.001, ****P < 0.0001, Kruskal-Wallis with Dunn's post hoc test. ns; no significance.

CD86 rather than CD80, promotes RT-induced Treg responses

The above findings highlight the importance of the CD28 costimulatory axis in regulating Treg expansion and raise the possibility that the CD28 ligands CD80 and/or CD86 may dictate Treg numbers after RT in the TC-1 tumor model. We therefore selectively blocked CD80 or CD86 in presence of RT and examined the T-cell response in detail by spectral flow cytometry as before, focusing on CD3⁺ T-cell populations (Figure 5A,B). Interestingly, blockade of CD86 significantly reduced the RT-induced eTreg population in non-TdLN, TdLN and tumor (Figure 5C,D). After CD86 blockade, the frequency of eTregs in these tissues were comparable to those in non-irradiated mice (0 Gy). CD86 blockade also diminished the proportion of cTregs in the non-TdLN, suggesting a role for CD86 in the maintenance of steady-state cTregs. In contrast, CD80 blockade in the context of RT only reduced the frequency of eTregs in the TdLN (Figure 5C,D). Thus, in the TC-1 tumor setting, CD86 is the selective CD28-ligand that supports the generation of an eTreg response after RT (Figure 5E).

CD86 blockade in context of RT improves conventional (c)DC costimulatory status and CTL priming

To clarify how CD80/CD86 blockade may impact T-cell priming, we examined the trafficking and phenotype of migratory cDC1 and cDC2 that are responsible for this process⁵⁴⁻⁵⁶. cDC subsets were identified by flow cytometry as indicated in Figure 55A. The absolute number of cDC1s or cDC2 in the TdLN was not altered by RT alone as compared to control. However, cDC1 numbers were significantly increased when RT was combined with CD86 blockade, and there was a similar trend for cDC2s (Figure 6A). CD86 is constitutively expressed on cDCs, while CD80 is upregulated upon activation²⁰. In the context of RT, CD86 blockade significantly increased the expression of CD80, but not CD86 on both cDC1s and cDC2s (Figure 55B,C). CD86 and CD80 blockade did not significantly alter expression of CD40 or PD-L1 on either cDC1s or cDC2s (Figure 55B,C).

On the cDC membrane, CD80 can heterodimerize with PD-L1. This CD80:PD-L1 heterodimer can bind and engage CD28, but cannot bind to PD-1, nor can it be downregulated by CTLA-4^{57,58}. It has been documented that co-expression of CD80 and PD-L1 on cDCs positively correlates with their CTL priming capacity against cancer, in agreement with increased formation of a CD28-costimulatory CD80:PD-L1 heterodimer⁵⁹. We found in the TC-1 tumor model that upon RT, CD86 blockade significantly increased the frequency of cDC1s and cDC2s that co-expressed CD80 and PD-L1 (Figure 6B-D). Furthermore, the frequency of CD80⁺ PD-L1⁺ cells was also increased, whereas the frequency of CD80⁻ PD-L1⁺ cells was decreased. Thus, in the TC-1 model, CD86 blockade in the context of RT likely favors CTL priming by increased presence of migratory cDC1s presenting tumor antigen in the TdLN and their improved costimulatory capacity.

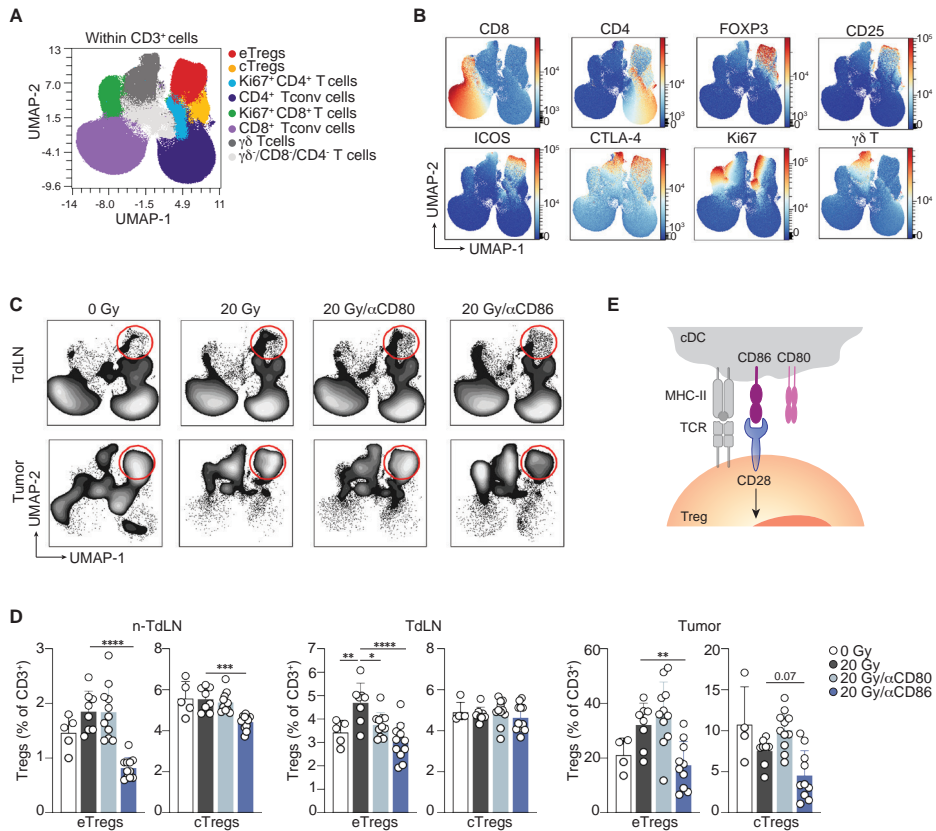


Figure 5. CD86, but not CD80, drives the RT-induced eTreg response.

Mice bearing 20 mm² TC-1 tumors received control treatment (0 Gy, n=5) or 20 Gy RT at day 0 in combination with either vehicle (PBS, n=8) or blocking mAb against CD80 (n=11) or CD86 (n=11) at day 0, 3 and 6. The CD3⁺ lymphocyte response was monitored by flow cytometry in the non-TdLN, TdLN and tumor at day 8 of all treatment groups combined. FlowSOM guided clustering (**A**) identifying the same populations as found in the previous figures and (**B**) representative heat maps of the markers included to determine the CD3⁺ subpopulations. (**C**) Visualization of the response of the CD3⁺ subpopulation in TdLN and tumor to the indicated treatments. The circles highlight the eTreg population. (**D**) Frequencies of eTregs and cTregs identified in (**B**) among CD3⁺ cells found in the indicated tissues at day 8 post treatment. (**E**) Graphic visualization of how CD86, but not CD80, binds CD28 to support Treg expansion. Data are from one experiment representative of two experiments. Error bars indicate SD. *P < 0.05, **P < 0.01, ***P < 0.001, ****P < 0.0001, ordinary one-way Anova with Dunnett's post hoc test in **D**.

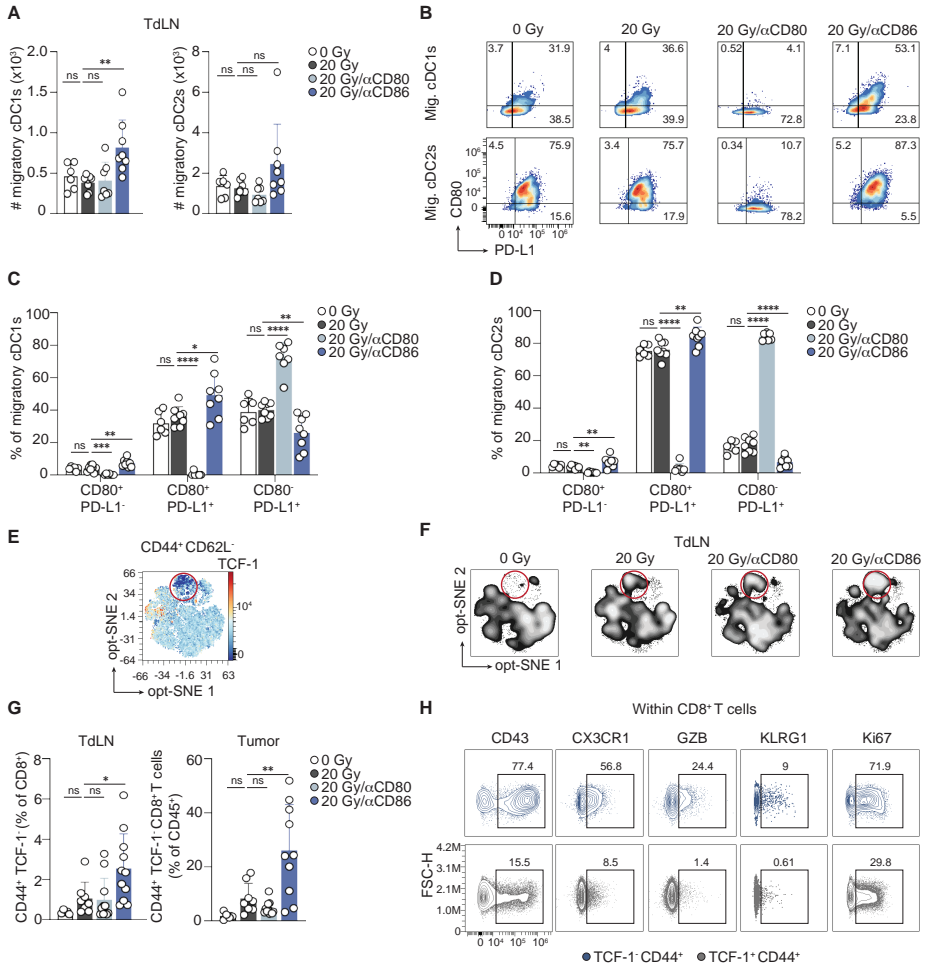


Figure 6. CD86 blockade in context of RT improves the conventional (c)DC costimulatory status and CTL priming.

(A–D) Mice bearing 20 mm² TC-1 tumors received 0 Gy (n=6) or 20 Gy RT at day 0 in combination with either vehicle (PBS, n=8) or blocking mAb against CD80 (n=7) or CD86 (n=8) at day 0, 3 and 6. The cDC response was monitored by flow cytometry in the TdLN at day 8. (A) Absolute counts (#) of migratory cDC1s and cDC2s. (B) Representative concatenated (n=6–8) flow cytometry plots depicting the percentage of CD80⁺ and/or PD-L1⁺ cells among migratory cDC1s and cDC2s in the TdLN per treatment group. Numbers indicate percentages. (C–D) Quantification of the populations represented in (B) among migratory cDC1s (C) and migratory cDC2s (D) from the TdLN. (E–H) The CD8⁺ T cell response was monitored by flow cytometry in the same experiment described in Figure 5. (E,F) Opt-SNE visualization of 1000 randomly selected CD44⁺ CD62L⁻ cells among CD8⁺ T cells per sample found in TdLNs at day 8 concatenated per treatment group. (E) Representative heat map of TCF-1 expression and (F) visualization of the TCF-1⁺ subpopulation in TdLN (encircled) in different treatment groups. (G) Frequency of CD44⁺ TCF-1⁻ cells among CD8⁺ T cells found in the TdLN and among CD45⁺ cells in the tumor at day 8 post treatment. (H) Concatenated (n=11) contour plots depicting expression of the indicated markers on CD44⁺ TCF-1⁻ cells and CD44⁺ TCF-1⁺ cells within CD8⁺ T cells in the TdLN. Numbers indicate percentages. Data are from one experiment representative of two experiments. Error bars indicate SD. *P < 0.05, **P < 0.01, ***P < 0.001, ****P < 0.0001, ordinary one-way Anova with Dunnett’s post hoc test in A, C–E. ns; not significant.

To study CTL priming, we next performed opt-SNE analysis of CD8⁺ T cells with a CD44⁺ CD62L⁻ effector phenotype found in the TdLN. The flow cytometry panel included the marker TCF-1 to monitor CTL effector differentiation, which progresses over a continuum of cellular states depending on the input signals delivered^{60,61}. Loss of TCF-1 expression (a transcription factor encoded by *Tcf7*) is associated with loss of “stemness”⁶² and highlights T cells that are on the path of becoming terminally differentiated short-lived effector T cells⁶³. Contour plot visualization showed significant enlargement of a TCF-1⁻ subpopulation among CD44⁺ CD62L⁻ cells in the TdLN upon RT, which was further increased upon CD86, but not CD80 blockade (Figure 6E,F). Manual gating (Figure 55D) confirmed these findings and showed that CD86 blockade in the context of RT significantly increased the frequency of CD44⁺ TCF-1⁻ cells among CD8⁺ T cells in both TdLN and tumor (Figure 6G). In concordance, phenotypical analysis showed increased expression of the (terminal) effector differentiation markers CD43, CX3CR1, GZB and KLRG1 on the CD44⁺ TCF-1⁻ population as compared to the CD44⁺ TCF-1⁺ population (Figure 6H). Moreover, the CD44⁺ TCF-1⁻ population also showed enhanced Ki67 expression, indicating increased cell cycle activity (Figure 6H). Taken together, these findings indicate that CD86 blockade improves RT-induced CTL priming, expansion and effector differentiation, likely mediated by enhanced cDC1 presence and activity in the TdLN.

RT plus PD-1 blockade increases the Treg response, which is overruled by CD86 blockade resulting in improved tumor control.

PD-1, the key target in current cancer immunotherapy, is considered a hallmark of suboptimally primed CTLs that lack full cytotoxic effector functions^{64,65}. Further analysis of the CD44⁺ TCF-1⁻ population in the tumor after combined RT and CD86 blockade, showed that these cells expressed PD-1, albeit to a lesser extent than the less differentiated CD44⁺ TCF-1⁺ cells (Figure 56A). In fact, we observed that in the tumor, both eTregs and the Ki67⁺ CTLs expressed PD-1 (Figure 7A). PD-1 inhibits CD28 costimulation¹⁹, which is valid for both Tconvs and Tregs. Recent reports describe that in addition to supporting Tconv responses^{64,65}, PD-1 blockade may also promote Treg responses by enabling TCR/CD28 signaling^{66,67}. Therefore, we examined the effect of PD-1 blockade alone, or in combination with CD86 blockade on the RT-induced Treg and CTL response. Strikingly, PD-1 blockade increased RT-induced eTreg priming and tumor infiltration, while these responses were inhibited upon CD86 blockade, as we observed before (Figure 7B,C, Figure 56B,C). Following combined PD-1 and CD86 blockade, the RT-induced eTreg response was abrogated as it was upon CD86 blockade alone, confirming that CD86 is the key driver of the eTreg response. Importantly, following combined PD-1 and CD86 blockade, the RT-induced CTL response was significantly increased in TdLN and tumor (Figure 7B,D, Figure 56B,C). These results agree with the concept that RT-induced Treg priming hampers the induction of a CTL response, as we showed before.

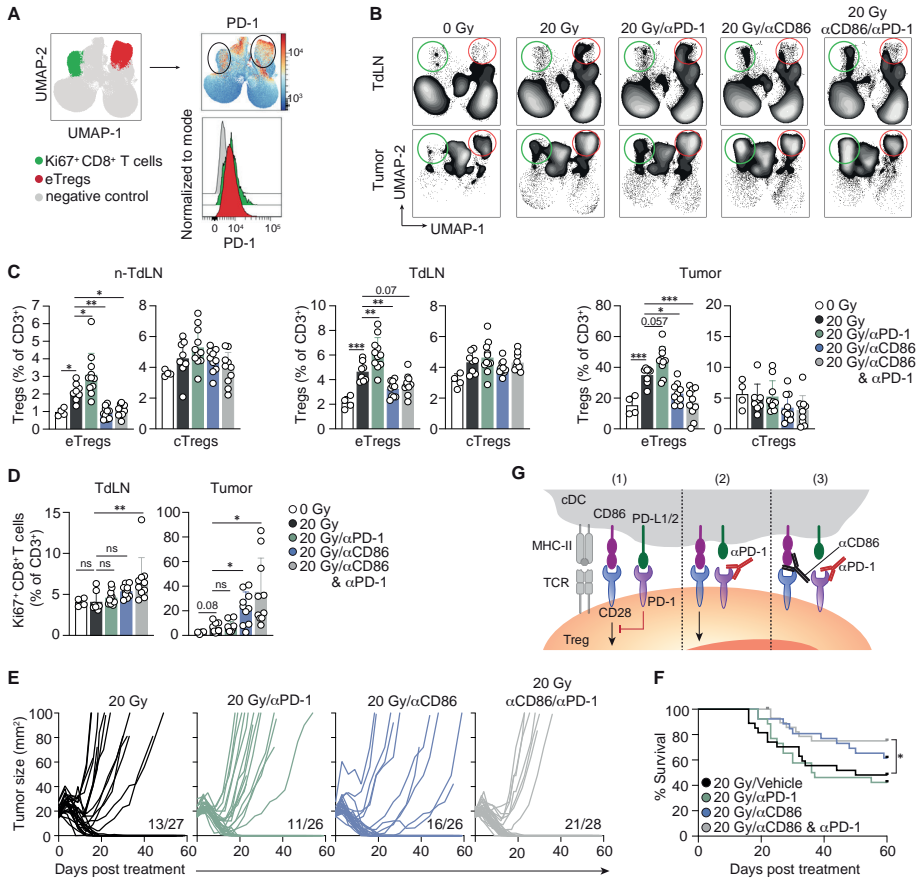


Figure 7. CD86-mediated CD28 costimulation is required for PD-1-dependent eTreg expansion.

(A) PD-1 protein expression of the Ki67⁺ CD8⁺ T cell population (green) and eTreg population (red) in the tumor identified in Figure 5A, depicted as heatmap (upper row) and representative histogram (lower row) of all experimental settings combined. (B,C) Mice bearing TC-1 tumors received control treatment (0 Gy, n=4) or 20 Gy RT at day 0 in combination with either vehicle (PBS, n=8) or blocking mAb against PD-1 (n=11), CD86 (n=10) or a combination of both (n = 10) at day 0, 3 and 6. The CD3⁺ lymphocyte response was monitored by flow cytometry in the non-TdLN, TdLN and tumor at day 8. (B) UMAP visualization of the response of the CD3⁺ subpopulation in TdLN and tumor to the indicated treatments. The red circle highlights the eTreg population, whereas the green circle indicates the Ki67⁺ CD8⁺ T cells (see also Figure S6A,B). (C) Frequencies of eTregs and cTregs identified in Figure S6A among CD3⁺ cells found in the indicated tissues at day 8 post treatment. (D) Quantification of the Ki67⁺ CD8⁺ T cell population among total CD3⁺ cells in the TdLN and tumor at day 8 post treatment. (E) Individual tumor growth curves (F) and overall survival of mice bearing TC-1 tumors receiving RT at day 0 in combination with either vehicle (PBS, n=27) or blocking mAb against PD-1 (n=26), CD86 (n=26) or a combination of both (n=28) at day 0, 3 and 6. Ratios indicate the number of mice that showed full recovery upon treatment compared to total. (G) Illustration depicting the proposed mechanism of action of combined CD86 and PD-1 blockade on Tregs in our setting. (1) PD-L1/L2 offered by dendritic cells (cDCs) ligates PD-1 and prevents downstream signaling of CD28 on Tregs. (2) PD-1 blockade negates this process, resulting in enhanced CD28 costimulation and consequently increased Treg cellular responses. (3) When CD86 blockade is in place, CD28 costimulation is prevented, and additional PD-1 blockade can no longer engage the CD28 costimulatory axis, resulting in an abrogated Treg response. Data are from one experiment representative of two experiments. Error bars indicate SD. *P < 0.05, **P < 0.01, ***P < 0.001, ordinary one-way Anova with Dunnett's post hoc test in C; Brown-Forsythe Anova with Dunnett's T3 post hoc analysis in D; Mantel-Cox analysis in F. ns; no significance.

We next assessed how inhibition of PD-1 and/or CD86 impacted RT-induced tumor control. PD-1 blockade alone failed to enhance RT-induced tumor regression and overall survival, in line with stimulation of the Treg response (Figure 7E,F, Figure S6D). CD86 blockade alone initially improved RT-induced tumor control, but a fraction of these tumors eventually relapsed. Combined PD-1 and CD86 blockade cured 75% of the mice and significantly increased overall survival compared to RT alone. However, combined PD-1 and CD86 blockade did not increase the therapeutic effect as compared to CD86 blockade alone, confirming that CD86 inhibition is the primary factor to alleviate Treg-obstructed RT-induced CTL-mediated tumor control. Taken together, these data indicate that in this lymphocyte-depleted tumor model, RT enhances eTreg priming while restraining tumor-reactive CTL priming and this is further enhanced by PD-1 blockade. This result can be explained by the fact that PD-1 blockade preferentially enables CD28 costimulation on Tregs (Figure 7G). CD86, but not CD80 blockade, counteracts Treg priming through inhibition of CD28 costimulation and thereby facilitates tumor-reactive CTL priming and tumor control by RT.

Discussion

The potential of RT to induce systemic T-cell responses to cancer has recently received much attention, but clinical evidence for abscopal, immune-mediated effects are scarce, even in combination with ICB⁶. We must therefore better understand the ability of RT to induce tumor-controlling T-cell responses, in the context of the divergent impact of different cancer types on the immune response. Comparison of *in vivo* tumor models of varying immunogenicity demonstrated that in immunogenic tumors, CD8⁺ T cells infiltrating the TME contributed to the RT response, while in poorly immunogenic tumors RT failed to elicit a systemic anti-tumor immune response and an abscopal effect¹⁸. We show that the TC-1 tumor model used in our current study recapitulates a “lymphocyte depleted” phenotype represented among human cancer types³ that proves to respond negatively to RT (Figure 1A). Despite expression of HPV-16 derived E6 and E7 antigens, the TC-1 tumor contains a very low amount of Tconvs and primarily contain myeloid populations. We show that the TC-1 tumor invites Tregs and monocytes in the tumor and the TdLN, consistent with systemic immunosuppression, as observed in this type of tumors in the clinic^{68,69}. Nevertheless, the RT response was CD8⁺ T-cell dependent, suggesting that in lymphocyte-depleted tumors, there is an unexploited, favorable T-cell response that should be improved by the correct intervention(s).

To prime CTLs, cDC1s need to be activated and migrate to the TdLN^{54,55}, whereas the cDC2 subset is particularly effective at CD4⁺ T-cell priming, including both Tconvs and Tregs^{56,70}. In the TC-1 tumor setting, RT induced new CTL priming, despite concurrent Treg priming. This suggests that RT produced DAMPs required to activate cDC1s and induced their migration to the TdLN. However, as RT may upregulate signals that prevent cDC1 recruitment to the TME⁷¹, CTL priming in the TC-1 setting may be limited by the number of cDC1s present in the tumor before RT, which was very

low (Figure 2A). As TC-1 has a much higher proportion of cDC2s, cDC2-induced Treg priming may therefore dominate over cDC1-induced CTL priming in the TdLN after RT.

A main role for Tregs lies in prevention or suppression of unwanted Tconv responses against both self- and foreign-antigens⁷². At steady state, “immature” or “tolerogenic” cDCs that express CD86 but no other costimulatory ligands⁷³ migrate from peripheral tissues to dLNs to present self-antigens and prevent responses of sporadic, autoreactive T cells. This role is exerted by cTregs that do not show extensive clonal expansion or relocation to non-lymphoid tissues. A recent study reports that Treg priming may be dictated by the metabolic state of cDC2s, in part through CD86 upregulation, required to promote Treg expansion⁷⁴. Especially in a tumor setting, limited nutrient resources in conjunction with tumor-associated immunosuppressive factors may induce a metabolic state in cDCs that supports Treg priming and/or expansion⁷⁵.

In a tumor setting, Treg accumulation in the TdLN can restrict CTL priming by inhibiting cDC1 activation in the TdLN⁷⁶. CD86 blockade in our model effectively reduced RT-induced eTreg responses, while concurrently increasing the presence of cDC1 cells in the TdLN and enhancing their expression of both CD80 and PD-L1. This enhanced expression is favorable for the formation of a CD28-costimulatory CD80/PD-L1 heterodimer. Accordingly, CD86 blockade selectively improved the CTL response following RT. Based on these data, it is likely that the RT-induced eTreg response in the TdLN in part prevents CTL priming by limiting cDC1 availability and functionality.

Tregs play a role in controlling inflammation resulting from tissue injury, such as inflicted by RT. In this process, cTregs are recruited from dLNs to damaged tissues⁷⁷, where they present an effector (eTreg) phenotype²¹. Murine and human tissue-resident eTregs have a conserved transcriptional signature that is most explicit in tumor-resident eTregs and contains a tissue-repair program⁷⁸. In an irradiated tumor, next to extinguishing inflammatory responses, these eTregs may utilize their repair function to support extracellular matrix remodeling and tumor growth⁷⁹ and therefore may form an impediment to RT efficacy.

In our setting, CD86, but not CD80, drove induction of an eTreg response by RT. In principle, both Tconvs and Tregs can profit from either CD80 or CD86 to receive CD28 costimulation. However, on Tregs, constitutively expressed CTLA-4 imposes an intrinsic constraint for CD28 costimulation. Since CD86 has a lower affinity for CTLA-4 than CD80, it has improved accessibility for CD28 on Tregs and therefore Tregs selectively profit from CD86 costimulation⁸⁰. Upon CTLA-4 blockade, both CD80 and CD86 are available to support the Treg response⁵⁰, especially in our tumor setting where the Treg response is dominant. Interestingly, blockade of CTLA-4 together with RT supported both cTreg and eTreg expansion, whereas RT alone induced an eTreg response. Thus, CTLA-4 inhibition led to CD28 costimulation and consequent expansion of cTregs, while additional signals induced by RT promoted eTreg differentiation.

In certain mouse tumor models (TSA and 4T1 breast cancer and MCA38 colon cancer), CTLA-4 blockade and RT have a combined therapeutic effect^{26,39,47,48}. CTLA-4 likely promoted new T-cell priming in these models, given the increased TCR diversity of tumor-infiltrating T cells observed. Such a combined effect was also found in subsets of patients with metastatic non-small cell lung cancer²⁶ or metastatic melanoma²⁵. In the TC-1 model, however, there was no added therapeutic effect of CTLA-4 blockade to RT, which was explained by increased Treg over CTL priming. It is known that CTLA-4 ICB efficacy largely relies on a high CTL over Treg ratio in the tumor^{81,82}, highlighting that CTLA-4 blockade must favor CTL over Treg priming in this setting⁸². In T-cell depleted tumors, several factors work against a favorable CTL over Treg ratio, e.g. a higher cDC2-over cDC1 ratio in the TME, limited RT-induced adjuvanticity³¹ and/or RT-induced suppressive factors that prevent cDC1 maturation^{71,83}. Reportedly, fractionated low dose RT is superior in eliciting IFN-I dependent optimization of cDC1 for CTL priming. This is because single high dose RT attenuates IFN-I release by promoting DNA degradation via the exonuclease Trex1³⁹. Consequently, 3x8 Gy, but not 20 Gy, cooperated with CTLA-4 blockade to improve systemic anti-tumor immunity in TSA and 4T1 mouse models^{26,39,47,48}. However, in our model, RT induced a strong Treg response to both 3x 8 Gy and 20 Gy and these schedules had no differential therapeutic effect. Thus, in Treg dominant tumors, CTLA-4 blockade may preferentially support Treg expansion⁸⁴ and not improve CTL-based tumor control, regardless of the RT regimen used^{44,85}.

In our tumor setting, PD-1 blockade also exacerbated the RT-induced eTreg response and consequently impeded the therapeutic CTL response. Importantly, it was recently reported that PD-1 blockade can promote Treg responses in cancer patients, which can lead to cancer hyper-progression^{66,86}. These studies showed that both Tregs and Tconvs can profit from CD28 costimulation that is enabled by PD-1 blockade⁴⁹. In tumors that favor Treg- over CTL priming at steady state and that have an exacerbated eTreg response upon RT, the conditions are met for further Treg priming and expansion upon PD-1 blockade. Our discovery that CD86 blockade abrogated the Treg response in this setting is therefore of potential clinical relevance. When CD86 was blocked, PD-1 blockade could not induce Treg expansion upon RT, indicating its dependence on CD86-mediated CD28 costimulation. Importantly, CTL priming depended on CD80-mediated costimulation and was not affected by CD86 blockade, allowing for reversal of the Treg/CTL ratio.

In conclusion, we reveal that in a model of lymphocyte-depleted cancer that favors myeloid and Treg infiltration, CTLA-4 and PD-1 blockade have the opposite effect on RT-induced tumor control than in immunogenic tumors with high Tconv infiltrates. This is due to exacerbation of RT-induced Treg responses that counteract the RT-induced CTL response. We therefore caution that CTLA-4 and/or PD-(L)1 blockade may likewise exacerbate RT-induced Treg responses in human lymphocyte-depleted cancer. Our findings argue that instead, CD86 is a suitable target to inhibit undesired Treg responses and a new candidate to improve Tconv cell responses to poorly immunogenic cancers, particularly in combination with RT.

Methods

TCGA data analysis

Immune subtype classifications among 9126 tumors were collected from Thorsson et al.³. Patient-specific radiotherapy status and survival metrics were gathered from the UCSC Xena Platform using the *UCSCXenaTools* package⁸⁷ of which 7891 tumors had complete information available. Following this, Kaplan-Meier curves were generated for each immune subtype using overall survival (in months) by radiotherapy status (yes vs. no). For the immune subtype prediction, the C4/C5 subtypes were first collapsed into a single immune subtype and tumors derived from the C3 and C4/C5 immune subtypes were selected (n=3939). Following this, features derived from the CIBERSORT deconvolution algorithm and IFN γ signature were subsequently used (n=23). Next, 70% and 30% of the data was split into training and testing datasets, respectively. The training data was first scaled and centered before undergoing a 5-fold repeated cross-validation strategy to predict between C4/C5 vs. C3 using a K-nearest neighbor (KNN) model. The test data was then applied to evaluate model performance.

Murine microarray analysis

Microarray data and metadata was downloaded from *GSE85509* using *GEOquery*. Murine gene symbols were converted to human symbols using the *biomaRt* package. Following this, immune cell types were deconvolved using *CIBERSORT* from the *immunedeconv* package and the IFN γ signature was generated using the Ayers gene signature⁸⁸. Next, the data from the TC-1 and MC38 cell lines were used as input into the trained KNN model for classification.

Tumor cells

The MC38 colon cancer cell line was purchased from Kerfast (Boston, MA) and TC-1 tumor cells (lung epithelial cells engineered to express HPV16 E6 and E7 proteins³⁵) were obtained from Leiden University Medical Center in 2015 and the authors did not perform further authentication. MC38 and TC-1 cells were cultured in DMEM and RPMI 1640 (Gibco, Life Technologies) respectively, supplemented with 10% fetal calf serum (FCS), 0.1 mM non-essential amino acids, 1 mM sodium pyruvate, 2 mM L-glutamine, 10 mM HEPES and penicillin/streptomycin (Roche) at 37°C, 5% CO₂. MC38 and TC-1 cell stocks were tested negative for *Mycoplasma* by PCR, and thawed cells were used within 3 passages for *in vivo* experiments.

Tumor transplantation and RT

Six- to eight-week-old female C57BL/6Rj (B6) mice were purchased from Janvier Laboratories (Le Genest Saint Isle, France). At day -8, mice were anesthetized with isoflurane and injected subcutaneously (s.c.) with either 1x10⁶ MC38 or 1x10⁵ TC-1 tumor cells in 50 μ l HBSS. Tumor size

was measured by calipers in two dimensions and calculated as: area (mm²) = width x length. RT was initiated when the tumors reached 18-25 mm² (indicated as day 0) and mice were randomly assigned to different treatment groups. RT was applied using the SmART⁺ system (Precision X-Ray, North Branford, CT). Mice were anesthetized with isoflurane and a cone-beam CT scan of the mice was performed. The tumor was localized on the CT scan and targeted with RT at 0.1 mm precision using round collimators 1.0 or 1.5 cm in diameter. A single fraction of 8 or 20 Gy (225 peak kilovoltage (kVp), filtered with 0.3 mm of copper (3 Gy/min)) was delivered. For fractionated dosage studies, a single dose of 8 Gy was delivered on days 0, 1 and 2. Control mice (indicated as 0 Gy) were anesthetized and received a cone-beam CT scan but were not exposed to RT. Mice were sacrificed when the tumor diameter reached 15 mm or when the tumor size reached >100 mm². In the survival curves, censored events indicate mice that were sacrificed due to treatment unrelated disease.

Therapeutic antibodies and reagents

Mice received intraperitoneal (i.p.) injections of depleting anti-CD8 α -mAb (2.43, BioXCell) or anti-CD4-mAb (GK1.5, BioXCell) at 200 μ g per mouse in 100 μ l PBS starting at day -1 prior to RT (day 0) followed by days 3, 6 and 9. For Treg depletion experiments, mice were injected i.p. with 250 μ g of depleting mouse IgG2a isotype CD25-mAb⁴⁶ (modified clone of PC61, Evitria) in 100 μ l PBS at day -1 prior to RT and at day 5. Blocking mAbs to CTLA-4 (UC10-4F10-11, BioXCell), PD-1 (RMP1-14, BioXCell), CD80 (1G10, BioXCell) and CD86 (GL-1, BioXCell) were injected i.p. at either 100 μ g (anti-CTLA-4 and anti-PD-1) or 200 μ g (anti-CD80 and anti-CD86) per mouse in 100 μ l PBS at the day of RT (day 0) and days 3, 6, and in case of anti-CTLA-4 also at day 9. Control mice were injected with equal amounts of PBS (vehicle) according to the treatment schedule indicated. The sphingosine-1-phosphate receptor-1 agonist FTY720 (Fingolimod; Cayman Chemical) was dissolved in 0.9% NaCl solution (vehicle) and administered at 2 mg/kg by oral gavage. FTY720 treatment started one day prior to RT and was repeated three times per week throughout the duration of the experiment. All treatments were administered at standardized time points to correct for fluctuations in the adaptive immune response influenced by circadian oscillations⁸⁹.

Tissue preparation and flow cytometry

At the indicated time points, tumor-bearing mice were sacrificed, and the lymphoid tissues and tumors were isolated. We performed intra-tumoral injection of 5% Evans Blue dye (Sigma-Aldrich) in 50 μ l PBS to identify the axillary LN on the tumor bearing side as the TdLN, whereas the contralateral inguinal LN was defined as the non-TdLN. The TdLN was carefully kept out of the field of irradiation to prevent RT-induced attenuation of the adaptive immune responses in the LN⁹⁰. Tumor tissue was mechanically disaggregated using a Mcllwain tissue chopper (Mickle Laboratory Engineering), and a single-cell suspension was prepared by digesting the tissue in collagenase type A (Roche) and 25

µg/ml DNase I (Sigma) in serum-free DMEM for 45 min at 37°C. Enzyme activity was neutralized by addition of medium containing 10% FCS, and the tissue was dispersed by passing through a 70-µm cell strainer. To acquire single cell suspensions of LNs, the tissue was punctured with a 27 G needle followed by incubation in 100 µg/ml Liberase™ TL (Roche) in serum-free DMEM for 30 min at 37°C. Enzyme activity was neutralized as described above and tissue was dispersed by passing through a 70-µm cell strainer. Peripheral blood cells were collected from tail blood of live mice in Microvette CB300 LH tubes (Sarstedt). Red blood cells were lysed in 0.14 M NH₄Cl and 0.017 M Tris-HCl (pH 7.2) for 1 min at room temperature and cell suspensions were washed and stained with relevant mAbs (Table 1). For surface staining, single cells of the isolated tissues were first incubated with anti-CD16/32 (1:50, clone 2.4G2, BD Bioscience) supplemented with 10 µg/ml DNase, to block unspecific Fc receptor binding, for 10 min on ice. Next, surface antibody staining was performed (Table 1) for 30 min in PBS containing 0.5% BSA and 0.01% sodium azide. For intracellular staining of transcription factors and cytokines, cells were fixed and permeabilized with the FOXP3 Transcription Factor Staining Buffer Set according to the manufacturer's protocol (Thermo Fischer Scientific). Dead cells were excluded by using Fixable Viability Near-infra red dye (1:1000, Life Technologies), Zombie Red Fixable Viability Kit (1:5000, BioLegend) or Zombie UV fixable viability Kit (1:500, BioLegend). Cytokine detection in tumor and lymph node single cell preparations was performed following *ex vivo* stimulation in presence of 1 µg/ml GolgiPlug (BD Biosciences) with 50 ng/ml phorbol 12-myristate 13-acetate (PMA, Sigma Aldrich) and 1 µM ionomycin (Sigma Aldrich) dissolved in DMSO and diluted in 100 µl IMDM containing 8% FCS for 3 h at 37°C, 5% CO₂. Control (unstimulated) cells were treated with an equal volume of DMSO in presence of GolgiPlug diluted in IMDM with 8% FCS. Absolute cell numbers were determined by adding AccuCount Blank Particles (7-7.9 µm, Spherotech) to each sample, prior to flow cytometry analysis. Fluorescence minus one (FMO) was used as a negative control for activation markers. Flow cytometry was performed using a BD FACSymphony™ A5 SORP flow cytometer or the 5-laser Cytek Aurora. All generated data was analyzed using FlowJo and OMIQ software (Dotmatics, Boston, MA).

Data analysis

Dimensionality reduction and FlowSOM⁹¹ analysis of flow cytometry data was performed using OMIQ software. Following conventional marker expression analysis, the population of interest was manually gated, and down-sampling was performed to select the maximal number of cells per tissue representative for all tissue types included, as indicated in the figure legends. Tumor samples containing <600 cells of the subsampled population were excluded from further analysis (see Figure 5D). K-means clustering of the indicated populations was performed using FlowSOM, including all markers indicated, except for live/dead and CD45 and in case of the CD8⁺ T cell population (see Figure 6E,F) also without CD3. Dimension reduction and visualization was performed using uniform manifold approximation and projection (UMAP) analysis⁹² and opt-SNE analysis⁹³, including the same markers as described above and by using the default OMIQ settings.

Statistical analysis

All statistical data were analyzed using GraphPad Prism version 9 (GraphPad Software, La Jolla, CA). Statistical analyses were performed as indicated in the figure legends. Ordinary one-way Anova was performed in case sample sizes were $n > 8$, more than three experimental groups were compared and if the assumption for normal distribution was met. In case sample sizes were $n < 8$ and if normal distribution could not be assumed, Kruskal-Wallis analysis was applied. A P value < 0.05 was considered statistically significant; * $p < 0.05$, ** $p < 0.01$, *** $p < 0.001$, **** $p < 0.0001$. Data are presented as mean + S.D.

Study approval

Mice were maintained in individually ventilated cages (Innovive, San Diego, CA) under specific pathogen-free conditions. All mouse experiments were performed in accordance with institutional and national guidelines and were approved by the Animal Welfare Body (IVD) of the Netherlands Cancer Institute.

Author contributions

Conception and design: E.F., J. Bo.

Development of methodology: E.F., T.W.B., I.V.

Experimental advice: D.M.T.B., T.W.B., J. Bu., M.D.S., I.V.

Acquisition of data: E.F., D.M.T.B., T.W.B., J. Bu., M.D.S.

Analysis and interpretation of data: E.F., T.W.B., J. Bo.

Writing of manuscript: E.F., J.Bo.

Critical reading and editing of the paper: D.M.T.B., T.W.B., J. Bu., M.D.S., I.V.

Acknowledgements

We thank dr. Ramon Arens for providing the CD80 and CD86 blocking antibodies, and dr. Sergio Quezada for providing the CD25 IgG2a *in vivo* depletion antibody. We thank all members of the Immunology department at LUMC, and all members of the Tumor Biology & Immunology department at NKI, for their insightful input and helpful discussions. We thank the flow cytometry facility, animal laboratory facility and the intervention unit of the Netherlands Cancer Institute for technical assistance. This work was supported by the Dutch Cancer Society Grant NKI 2017-10894 to I. Verbrugge and J. Borst.

Conflict of Interest:

The authors declare no competing interests.

References

- 1 Haslam, A. & Prasad, V. Estimation of the Percentage of US Patients With Cancer Who Are Eligible for and Respond to Checkpoint Inhibitor Immunotherapy Drugs. *JAMA Netw Open* **2**, e192535 (2019).
- 2 Huang, A. C. *et al.* T-cell invigoration to tumour burden ratio associated with anti-PD-1 response. *Nature* **545**, 60-65 (2017).
- 3 Thorsson, V. *et al.* The Immune Landscape of Cancer. *Immunity* **48**, 812-830 e814 (2018).
- 4 Luca, B. A. *et al.* Atlas of clinically distinct cell states and ecosystems across human solid tumors. *Cell* **184**, 5482-5496 e5428 (2021).
- 5 Chen, D. S. & Mellman, I. Elements of cancer immunity and the cancer-immune set point. *Nature* **541**, 321-330 (2017).
- 6 Pointer, K. B., Pitroda, S. P. & Weichselbaum, R. R. Radiotherapy and immunotherapy: open questions and future strategies. *Trends Cancer* **8**, 9-20 (2022).
- 7 Kroon, P. *et al.* Radiotherapy and Cisplatin Increase Immunotherapy Efficacy by Enabling Local and Systemic Intratumoral T-cell Activity. *Cancer Immunol Res* **7**, 670-682 (2019).
- 8 Formenti, S. C. & Demaria, S. Systemic effects of local radiotherapy. *Lancet Oncol* **10**, 718-726 (2009).
- 9 Lee, Y. *et al.* Therapeutic effects of ablative radiation on local tumor require CD8+ T cells: changing strategies for cancer treatment. *Blood* **114**, 589-595 (2009).
- 10 Takeshima, T. *et al.* Local radiation therapy inhibits tumor growth through the generation of tumor-specific CTL: its potentiation by combination with Th1 cell therapy. *Cancer Res* **70**, 2697-2706 (2010).
- 11 Lugade, A. A. *et al.* Local radiation therapy of B16 melanoma tumors increases the generation of tumor antigen-specific effector cells that traffic to the tumor. *J Immunol* **174**, 7516-7523 (2005).
- 12 Kroemer, G., Galassi, C., Zitvogel, L. & Galluzzi, L. Immunogenic cell stress and death. *Nat Immunol* **23**, 487-500 (2022).
- 13 Golden, E. B. & Apetoh, L. Radiotherapy and immunogenic cell death. *Semin Radiat Oncol* **25**, 11-17 (2015).
- 14 Bottcher, J. P. & Reis e Sousa, C. The Role of Type 1 Conventional Dendritic Cells in Cancer Immunity. *Trends Cancer* **4**, 784-792 (2018).
- 15 Abuodeh, Y., Venkat, P. & Kim, S. Systematic review of case reports on the abscopal effect. *Curr Probl Cancer* **40**, 25-37 (2016).
- 16 Demaria, S. *et al.* Ionizing radiation inhibition of distant untreated tumors (abscopal effect) is immune mediated. *Int J Radiat Oncol Biol Phys* **58**, 862-870 (2004).
- 17 Buchwald, Z. S. *et al.* Tumor-draining lymph node is important for a robust abscopal effect stimulated by radiotherapy. *J Immunother Cancer* **8** (2020).
- 18 Lai, J. Z. *et al.* Abscopal Effects of Local Radiotherapy Are Dependent on Tumor Immunogenicity. *Front Oncol* **11**, 690188 (2021).
- 19 Hui, E. *et al.* T cell costimulatory receptor CD28 is a primary target for PD-1-mediated inhibition. *Science* **355**, 1428-1433 (2017).
- 20 Esensten, J. H., Helou, Y. A., Chopra, G., Weiss, A. & Bluestone, J. A. CD28 Costimulation: From Mechanism to Therapy. *Immunity* **44**, 973-988 (2016).
- 21 Smigielski, K. S. *et al.* CCR7 provides localized access to IL-2 and defines homeostatically distinct regulatory T cell subsets. *J Exp Med* **211**, 121-136 (2014).
- 22 Simpson, T. R. *et al.* Fc-dependent depletion of tumor-infiltrating regulatory T cells co-defines the efficacy of anti-CTLA-4 therapy against melanoma. *J Exp Med* **210**, 1695-1710 (2013).
- 23 Wing, K. *et al.* CTLA-4 control over Foxp3+ regulatory T cell function. *Science* **322**, 271-275 (2008).

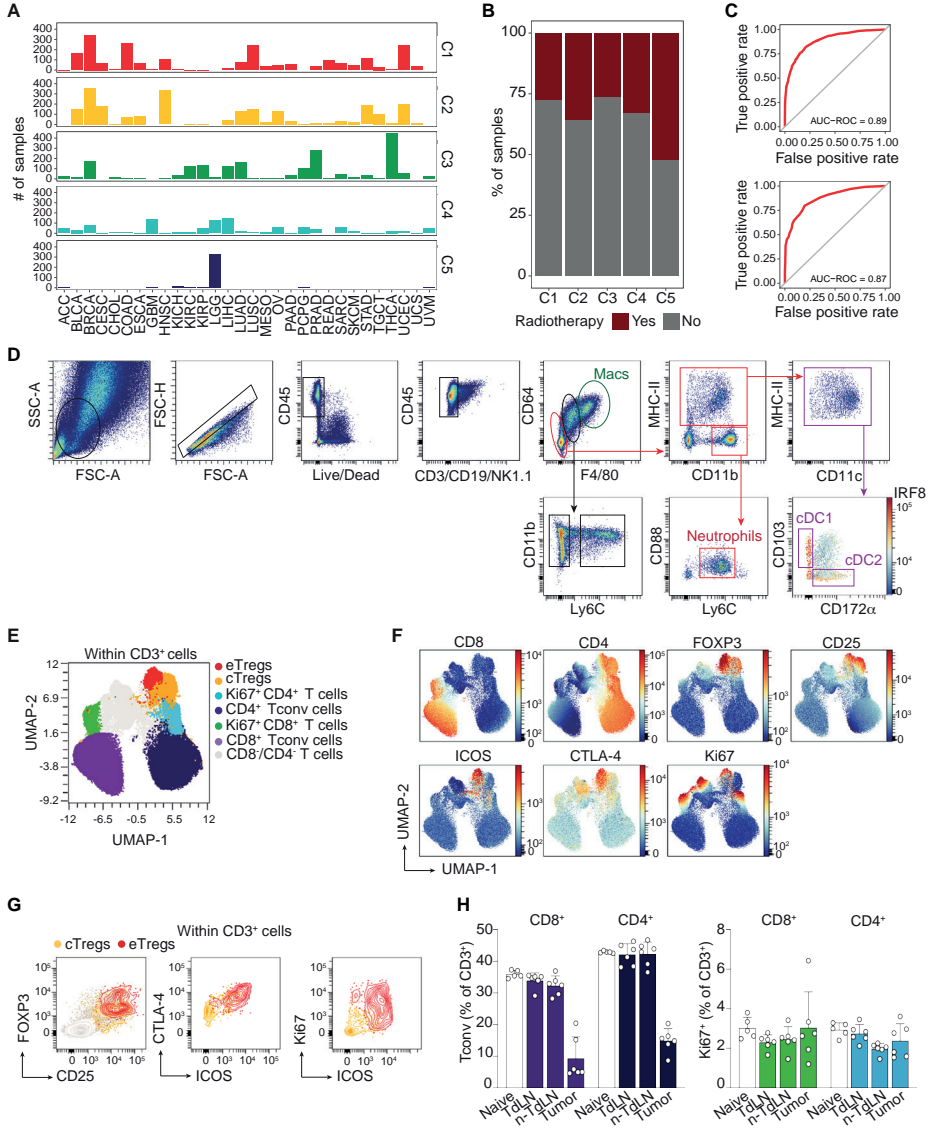
- 24 Voorwerk, L. *et al.* Immune induction strategies in metastatic triple-negative breast cancer to enhance the sensitivity to PD-1 blockade: the TONIC trial. *Nat Med* **25**, 920-928 (2019).
- 25 Twyman-Saint Victor, C. *et al.* Radiation and dual checkpoint blockade activate non-redundant immune mechanisms in cancer. *Nature* **520**, 373-377 (2015).
- 26 Formenti, S. C. *et al.* Radiotherapy induces responses of lung cancer to CTLA-4 blockade. *Nat Med* **24**, 1845-1851 (2018).
- 27 Theelen, W. *et al.* Effect of Pembrolizumab After Stereotactic Body Radiotherapy vs Pembrolizumab Alone on Tumor Response in Patients With Advanced Non-Small Cell Lung Cancer: Results of the PEMBRO-RT Phase 2 Randomized Clinical Trial. *JAMA Oncol* **5**, 1276-1282 (2019).
- 28 Arina, A. *et al.* Tumor-reprogrammed resident T cells resist radiation to control tumors. *Nat Commun* **10**, 3959 (2019).
- 29 Crittenden, M. R. *et al.* Tumor cure by radiation therapy and checkpoint inhibitors depends on pre-existing immunity. *Sci Rep* **8**, 7012 (2018).
- 30 Blair, T. C. *et al.* Dendritic Cell Maturation Defines Immunological Responsiveness of Tumors to Radiation Therapy. *J Immunol* **204**, 3416-3424 (2020).
- 31 Blair, T. C. *et al.* Fluorescent tracking identifies key migratory dendritic cells in the lymph node after radiotherapy. *Life Sci Alliance* **5** (2022).
- 32 Mondini, M. *et al.* CCR2-Dependent Recruitment of Tregs and Monocytes Following Radiotherapy Is Associated with TNF α -Mediated Resistance. *Cancer Immunol Res* **7**, 376-387 (2019).
- 33 Mosely, S. I. *et al.* Rational Selection of Syngeneic Preclinical Tumor Models for Immunotherapeutic Drug Discovery. *Cancer Immunol Res* **5**, 29-41 (2017).
- 34 Hos, B. J. *et al.* Identification of a neo-epitope dominating endogenous CD8 T cell responses to MC-38 colorectal cancer. *Oncoimmunology* **9**, 1673125 (2019).
- 35 Lin, K. Y. *et al.* Treatment of established tumors with a novel vaccine that enhances major histocompatibility class II presentation of tumor antigen. *Cancer Res* **56**, 21-26 (1996).
- 36 Ahrends, T. *et al.* CD4(+) T Cell Help Confers a Cytotoxic T Cell Effector Program Including Coinhibitory Receptor Downregulation and Increased Tissue Invasiveness. *Immunity* **47**, 848-861 e845 (2017).
- 37 Perez-Ruiz, E. *et al.* Prophylactic TNF blockade uncouples efficacy and toxicity in dual CTLA-4 and PD-1 immunotherapy. *Nature* **569**, 428-432 (2019).
- 38 Ahrends, T. *et al.* CD27 Agonism Plus PD-1 Blockade Recapitulates CD4+ T-cell Help in Therapeutic Anticancer Vaccination. *Cancer Res* **76**, 2921-2931 (2016).
- 39 Vanpouille-Box, C. *et al.* DNA exonuclease Trex1 regulates radiotherapy-induced tumour immunogenicity. *Nat Commun* **8**, 15618 (2017).
- 40 Hiam-Galvez, K. J., Allen, B. M. & Spitzer, M. H. Systemic immunity in cancer. *Nat Rev Cancer* **21**, 345-359 (2021).
- 41 Bauer, C. A. *et al.* Dynamic Treg interactions with intratumoral APCs promote local CTL dysfunction. *J Clin Invest* **124**, 2425-2440 (2014).
- 42 Matloubian, M. *et al.* Lymphocyte egress from thymus and peripheral lymphoid organs is dependent on S1P receptor 1. *Nature* **427**, 355-360 (2004).
- 43 Muroyama, Y. *et al.* Stereotactic Radiotherapy Increases Functionally Suppressive Regulatory T Cells in the Tumor Microenvironment. *Cancer Immunol Res* **5**, 992-1004 (2017).
- 44 Ji, D. *et al.* Combination of radiotherapy and suppression of Tregs enhances abscopal antitumor effect and inhibits metastasis in rectal cancer. *J Immunother Cancer* **8** (2020).
- 45 Sainz-Perez, A., Lim, A., Lemerrier, B. & Leclerc, C. The T-cell receptor repertoire of tumor-infiltrating regulatory T lymphocytes is skewed toward public sequences. *Cancer Res* **72**, 3557-3569 (2012).

- 46 Arce Vargas, F. *et al.* Fc-Optimized Anti-CD25 Depletes Tumor-Infiltrating Regulatory T Cells and Synergizes with PD-1 Blockade to Eradicate Established Tumors. *Immunity* **46**, 577-586 (2017).
- 47 Dewan, M. Z. *et al.* Fractionated but not single-dose radiotherapy induces an immune-mediated abscopal effect when combined with anti-CTLA-4 antibody. *Clin Cancer Res* **15**, 5379-5388 (2009).
- 48 Rudqvist, N. P. *et al.* Radiotherapy and CTLA-4 Blockade Shape the TCR Repertoire of Tumor-Infiltrating T Cells. *Cancer Immunol Res* **6**, 139-150 (2018).
- 49 Postow, M. A. *et al.* Immunologic correlates of the abscopal effect in a patient with melanoma. *N Engl J Med* **366**, 925-931 (2012).
- 50 Marangoni, F. *et al.* Expansion of tumor-associated Treg cells upon disruption of a CTLA-4-dependent feedback loop. *Cell* **184**, 3998-4015 e3919 (2021).
- 51 Salomon, B. *et al.* B7/CD28 costimulation is essential for the homeostasis of the CD4+CD25+ immunoregulatory T cells that control autoimmune diabetes. *Immunity* **12**, 431-440 (2000).
- 52 Marangoni, F. *et al.* Tumor Tolerance-Promoting Function of Regulatory T Cells Is Optimized by CD28, but Strictly Dependent on Calcineurin. *J Immunol* **200**, 3647-3661 (2018).
- 53 Tai, X., Cowan, M., Feigenbaum, L. & Singer, A. CD28 costimulation of developing thymocytes induces Foxp3 expression and regulatory T cell differentiation independently of interleukin 2. *Nat Immunol* **6**, 152-162 (2005).
- 54 Broz, M. L. *et al.* Dissecting the tumor myeloid compartment reveals rare activating antigen-presenting cells critical for T cell immunity. *Cancer Cell* **26**, 638-652 (2014).
- 55 Salmon, H. *et al.* Expansion and Activation of CD103(+) Dendritic Cell Progenitors at the Tumor Site Enhances Tumor Responses to Therapeutic PD-L1 and BRAF Inhibition. *Immunity* **44**, 924-938 (2016).
- 56 Binnewies, M. *et al.* Unleashing Type-2 Dendritic Cells to Drive Protective Antitumor CD4(+) T Cell Immunity. *Cell* **177**, 556-571 e516 (2019).
- 57 Sugiura, D. *et al.* Restriction of PD-1 function by cis-PD-L1/CD80 interactions is required for optimal T cell responses. *Science* **364**, 558-566 (2019).
- 58 Zhao, Y. *et al.* PD-L1:CD80 Cis-Heterodimer Triggers the Co-stimulatory Receptor CD28 While Repressing the Inhibitory PD-1 and CTLA-4 Pathways. *Immunity* **51**, 1059-1073 e1059 (2019).
- 59 Oh, S. A. *et al.* PD-L1 expression by dendritic cells is a key regulator of T-cell immunity in cancer. *Nat Cancer* **1**, 681-691 (2020).
- 60 Kaech, S. M. & Cui, W. Transcriptional control of effector and memory CD8+ T cell differentiation. *Nat Rev Immunol* **12**, 749-761 (2012).
- 61 Busselaar, J., Tian, S., van Eenennaam, H. & Borst, J. Helpless Priming Sends CD8(+) T Cells on the Road to Exhaustion. *Front Immunol* **11**, 592569 (2020).
- 62 Zhao, X., Shan, Q. & Xue, H. H. TCF1 in T cell immunity: a broadened frontier. *Nat Rev Immunol* **22**, 147-157 (2022).
- 63 Chen, Z. *et al.* TCF1-Centered Transcriptional Network Drives an Effector versus Exhausted CD8 T Cell-Fate Decision. *Immunity* **51**, 840-855 e845 (2019).
- 64 Philip, M. & Schietinger, A. CD8(+) T cell differentiation and dysfunction in cancer. *Nat Rev Immunol* **22**, 209-223 (2022).
- 65 Dammeyer, F. *et al.* The PD-1/PD-L1-Checkpoint Restrains T cell Immunity in Tumor-Draining Lymph Nodes. *Cancer Cell* **38**, 685-700 e688 (2020).
- 66 Kumagai, S. *et al.* The PD-1 expression balance between effector and regulatory T cells predicts the clinical efficacy of PD-1 blockade therapies. *Nat Immunol* **21**, 1346-1358 (2020).
- 67 Tan, C. L. *et al.* PD-1 restraint of regulatory T cell suppressive activity is critical for immune tolerance. *J Exp Med* **218** (2021).

- 68 Welters, M. J. *et al.* Vaccination during myeloid cell depletion by cancer chemotherapy fosters robust T cell responses. *Sci Transl Med* **8**, 334ra352 (2016).
- 69 Wang, L. *et al.* Connecting blood and intratumoral T(reg) cell activity in predicting future relapse in breast cancer. *Nat Immunol* **20**, 1220-1230 (2019).
- 70 Gerner, M. Y., Casey, K. A., Kastenmuller, W. & Germain, R. N. Dendritic cell and antigen dispersal landscapes regulate T cell immunity. *J Exp Med* **214**, 3105-3122 (2017).
- 71 Wennerberg, E. *et al.* CD73 Blockade Promotes Dendritic Cell Infiltration of Irradiated Tumors and Tumor Rejection. *Cancer Immunol Res* **8**, 465-478 (2020).
- 72 Vignali, D. A., Collison, L. W. & Workman, C. J. How regulatory T cells work. *Nat Rev Immunol* **8**, 523-532 (2008).
- 73 Lutz, M. B. & Schuler, G. Immature, semi-mature and fully mature dendritic cells: which signals induce tolerance or immunity? *Trends Immunol* **23**, 445-449 (2002).
- 74 Pelgrom, L. R. *et al.* LKB1 expressed in dendritic cells governs the development and expansion of thymus-derived regulatory T cells. *Cell Res* **29**, 406-419 (2019).
- 75 Moller, S. H., Wang, L. & Ho, P. C. Metabolic programming in dendritic cells tailors immune responses and homeostasis. *Cell Mol Immunol* **19**, 370-383 (2022).
- 76 Zagorulya, M. *et al.* Tissue-specific abundance of interferon-gamma drives regulatory T cells to restrain DC1-mediated priming of cytotoxic T cells against lung cancer. *Immunity* **56**, 386-405 e310 (2023).
- 77 Li, J., Tan, J., Martino, M. M. & Lui, K. O. Regulatory T-Cells: Potential Regulator of Tissue Repair and Regeneration. *Front Immunol* **9**, 585 (2018).
- 78 Delacher, M. *et al.* Single-cell chromatin accessibility landscape identifies tissue repair program in human regulatory T cells. *Immunity* **54**, 702-720 e717 (2021).
- 79 Wirsdorfer, F. & Jendrossek, V. The Role of Lymphocytes in Radiotherapy-Induced Adverse Late Effects in the Lung. *Front Immunol* **7**, 591 (2016).
- 80 Halliday, N. *et al.* CD86 Is a Selective CD28 Ligand Supporting FoxP3+ Regulatory T Cell Homeostasis in the Presence of High Levels of CTLA-4. *Front Immunol* **11**, 600000 (2020).
- 81 Liakou, C. I. *et al.* CTLA-4 blockade increases IFN-gamma-producing CD4+ICOShi cells to shift the ratio of effector to regulatory T cells in cancer patients. *Proc Natl Acad Sci U S A* **105**, 14987-14992 (2008).
- 82 Quezada, S. A., Peggs, K. S., Curran, M. A. & Allison, J. P. CTLA4 blockade and GM-CSF combination immunotherapy alters the intratumor balance of effector and regulatory T cells. *J Clin Invest* **116**, 1935-1945 (2006).
- 83 Hsieh, R. C. *et al.* ATR-mediated CD47 and PD-L1 up-regulation restricts radiotherapy-induced immune priming and abscopal responses in colorectal cancer. *Sci Immunol* **7**, eabl9330 (2022).
- 84 Kavanagh, B. *et al.* CTLA4 blockade expands FoxP3+ regulatory and activated effector CD4+ T cells in a dose-dependent fashion. *Blood* **112**, 1175-1183 (2008).
- 85 Balazs, K. *et al.* Radiotherapy-Induced Changes in the Systemic Immune and Inflammation Parameters of Head and Neck Cancer Patients. *Cancers (Basel)* **11** (2019).
- 86 Kamada, T. *et al.* PD-1(+) regulatory T cells amplified by PD-1 blockade promote hyperprogression of cancer. *Proc Natl Acad Sci U S A* **116**, 9999-10008 (2019).
- 87 Goldman, M. *et al.* The UCSC Xena platform for public and private cancer genomics data visualization and interpretation. *bioRxiv*, 326470 (2019).
- 88 Ayers, M. *et al.* IFN-gamma-related mRNA profile predicts clinical response to PD-1 blockade. *J Clin Invest* **127**, 2930-2940 (2017).
- 89 Cash, E. *et al.* The role of the circadian clock in cancer hallmark acquisition and immune-based cancer therapeutics. *J Exp Clin Cancer Res* **40**, 119 (2021).

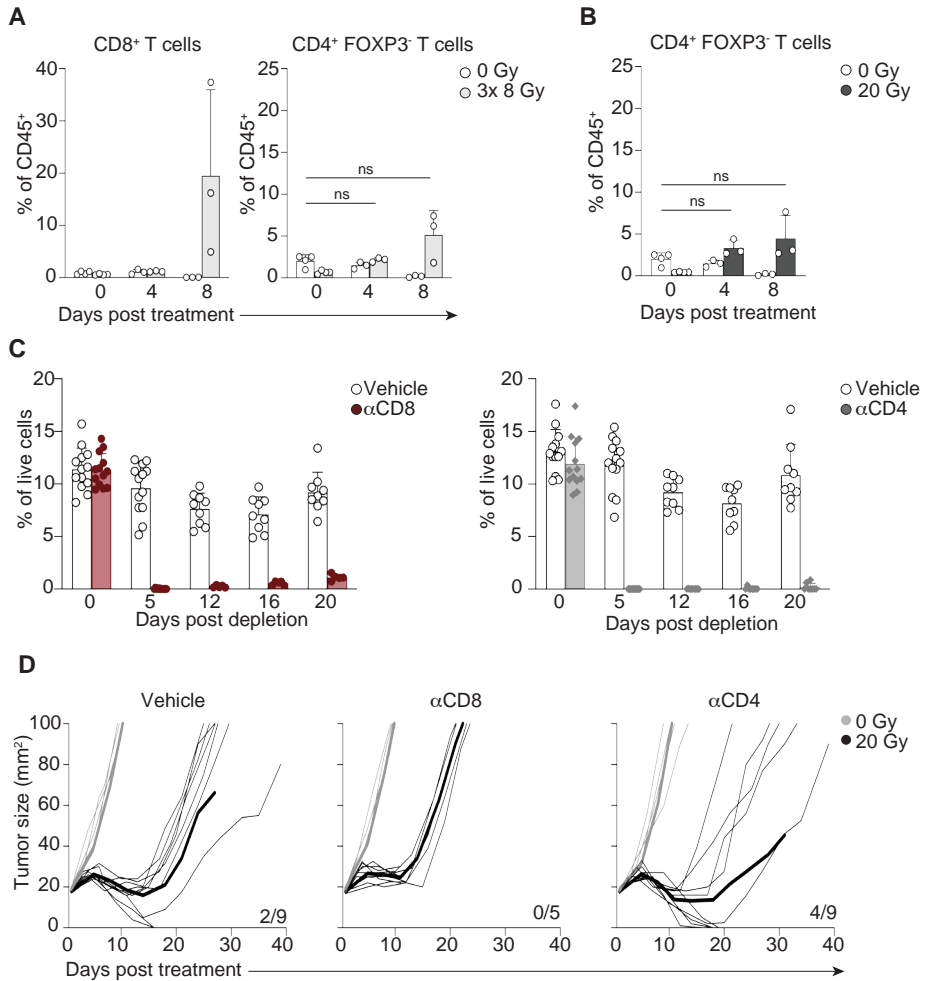
- 90 Marciscano, A. E. *et al.* Elective Nodal Irradiation Attenuates the Combinatorial Efficacy of Stereotactic Radiation Therapy and Immunotherapy. *Clin Cancer Res* **24**, 5058-5071 (2018).
- 91 Van Gassen, S. *et al.* FlowSOM: Using self-organizing maps for visualization and interpretation of cytometry data. *Cytometry A* **87**, 636-645 (2015).
- 92 Becht, E. *et al.* Dimensionality reduction for visualizing single-cell data using UMAP. *Nat Biotechnol* **37**, 38-44 (2018).
- 93 Belkina, A. C. *et al.* Automated optimized parameters for T-distributed stochastic neighbor embedding improve visualization and analysis of large datasets. *Nat Commun* **10**, 5415 (2019).

Supplementary Data



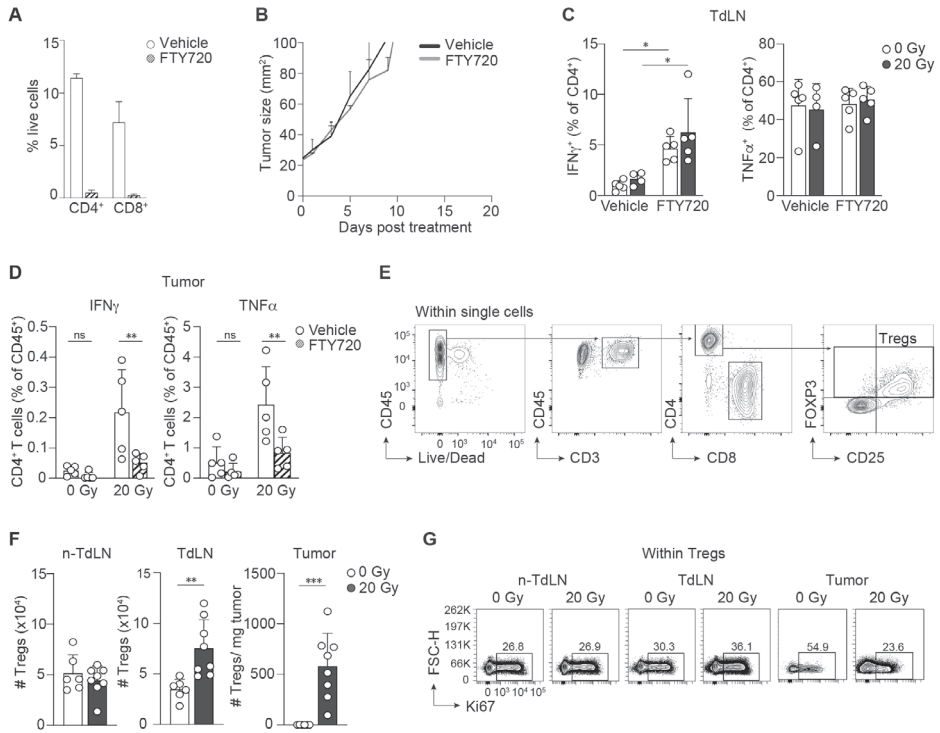
← Supplemental Figure 1- Related to Figure 1 (A – B) and Figure 2 (A – D)

(A) Number of TCGA tumor types (for tumor type abbreviation, see Table 2) classified per immune subtype, among tumors for which RT treatment (yes or no) was known. The total number of samples per tumor immune subtype (C1-C5) is indicated in Figure 1A. (B) Distribution of samples that received RT (red) or not (grey) for each tumor immune subtype. (C) Training (upper panel) and testing (lower panel) receiver operating curves (ROC) and area under the curve (AUC) calculation of a k-nearest neighbor's model training to classify C3 vs. C4/C5 TCGA immune subtypes. Training and testing were split 75% and 25%, respectively. (D) Representative gating strategy of the myeloid populations found in 50 mm² TC-1 tumors. (E-F) UMAP display of 5000 randomly selected CD3⁺ cells per sample found in non-TdLN, TdLN and tumors at day 8 of all treatment groups combined. FlowSOM guided clustering (E) identifying the CD3⁺ cell populations and (F) representative heat map visualization of the markers that identify the CD3⁺ (T-cell) subpopulations. (G) Representative flow cytometry plots overlaying the in (E) identified cTreg and eTreg populations. (H) Percentage of the in (E) identified CD8⁺ and CD4⁺ Tconv populations (left) and Ki67⁺CD8⁺ and Ki67⁺CD4⁺ Tconv populations (right) among the CD3⁺ cells in the indicated tissues. Error bars indicate SD. Data is from one experiment, representative of two experiments.



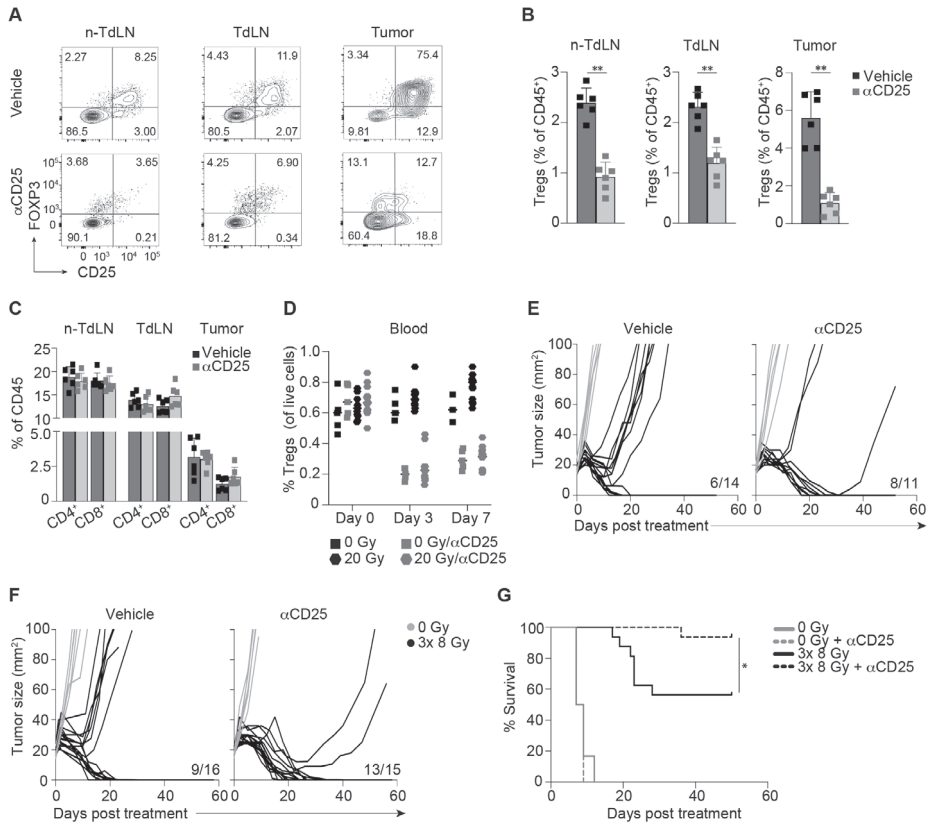
Supplemental Figure 2 – Related to Figure 2 (E - H)

(A,B) Monitoring by flow cytometry of the indicated immune cells over time in TC-1 tumors treated as control (0 Gy, $n = 3-4$ /timepoint) or with either (A) 8 Gy over 3 days (3x 8 Gy, $n=3-4$ /timepoint) or (B) a single dose of 20 Gy RT ($n=3-4$ /timepoint). Error bars indicate SD. Kruskal-Wallis test with Dunn's post hoc analysis. (C,D) TC-1 tumor bearing mice were treated with 20 Gy RT ($n=9$ /group) or control (0 Gy, $n=4$ /group) at day 0 in combination with vehicle (PBS) or depleting mAbs against CD8 or CD4. (C) Frequency of CD8⁺ (left) or CD4⁺ Tconv (right) among live cells in blood over time. The 0 Gy control group and 20 Gy groups are combined (Vehicle (PBS), $n=13$; αCD8, $n=13$; αCD4, $n=13$). (D) Individual tumor outgrowth curves belonging to Figure 2H. Thick lines indicate group averages. Error bars indicate SD. ns; not significant. Data is from one experiment, representative of two experiments.



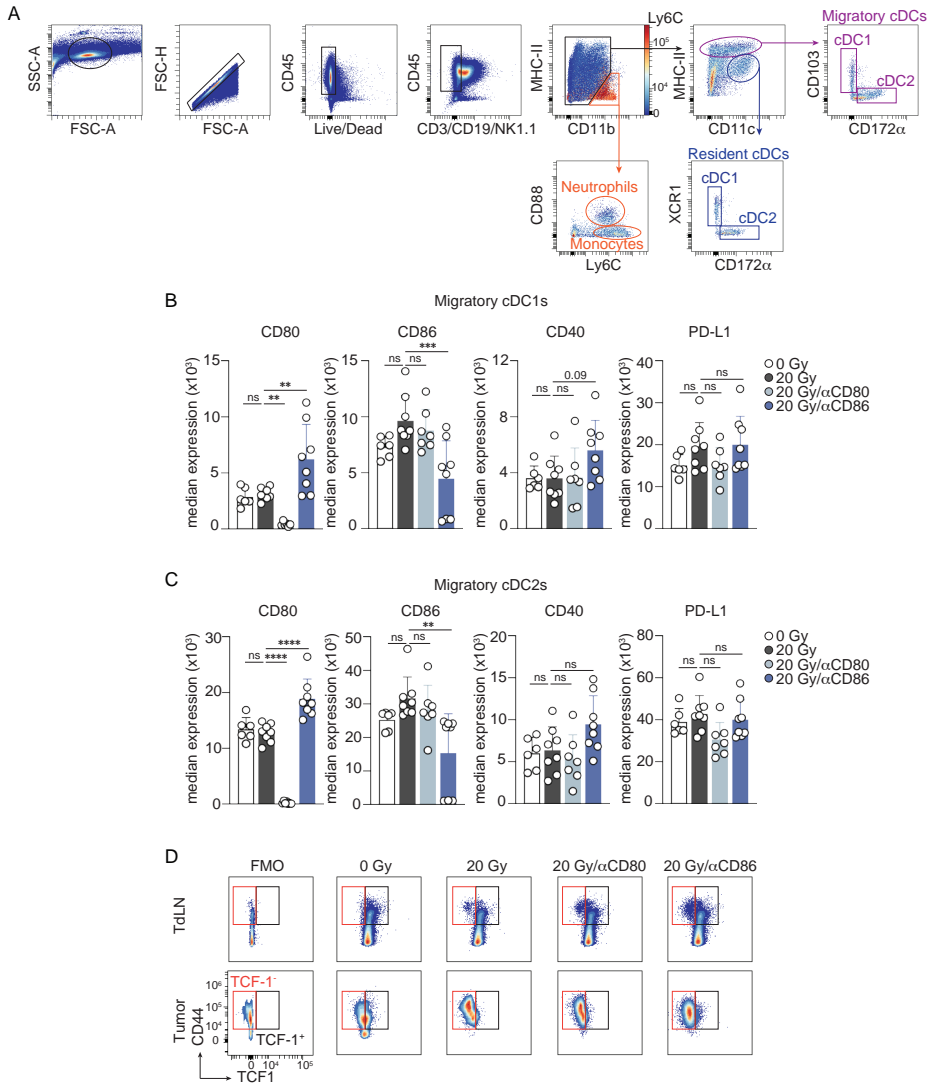
Supplemental Figure 3 – Related to Figure 3 (A – H).

(A-D) Data is from the same experiment described in Figure 3A-D. TC-1 tumor bearing mice received 20 Gy RT (n=4-5/group) or 0 Gy (n=5) when tumor sizes reached ~20 mm² (day 0) in combination with FTY720 or vehicle (NaCl) by oral gavage, starting at day -1 and followed by days 3 and 5. At day 8, the TdLN and tumor were isolated and the CD4⁺ T cell response was analyzed. (A,B) Frequency of CD4⁺ and CD8⁺ Tconv among live cells in blood at day 5 (A) and average tumor outgrowth curves (B) in TC-1 tumor bearing mice treated with 0 Gy and FTY720 or vehicle. (C,D) Frequency of IFN γ ⁺ and TNF α ⁺ cells within CD4⁺ T cells in the TdLN (C) and in the tumor (D) of mice treated with 0 Gy or 20 Gy. (E-G) Monitoring of the (FOXP3⁺ CD25⁺) Treg response to 20 Gy RT (n=8) or 0 Gy (n=6) in TC-1 tumor bearing mice by flow cytometry at day 8 post treatment. (E) Representative gating strategy of Treg cells, based on FOXP3⁺ and CD25⁺ expression. (F) Absolute counts (#) of total Treg cells in the non-TdLN, TdLN and tumor. (G) Representative concatenated (0 Gy, n=6; 20 Gy, n=8) flow cytometry plots depicting Ki67⁺ cells among Treg cells found in the non-TdLN, TdLN and tumor at day 8 post treatment. Numbers indicate the percentage of Ki67⁺ cells. Data is from one experiment, representative of two experiments. Error bars indicate SD. *P < 0.05, **P < 0.01, *** P < 0.001, two-way Anova with Tukey's post hoc test in C and D, Mann-Whitney test in F. ns; not significant.



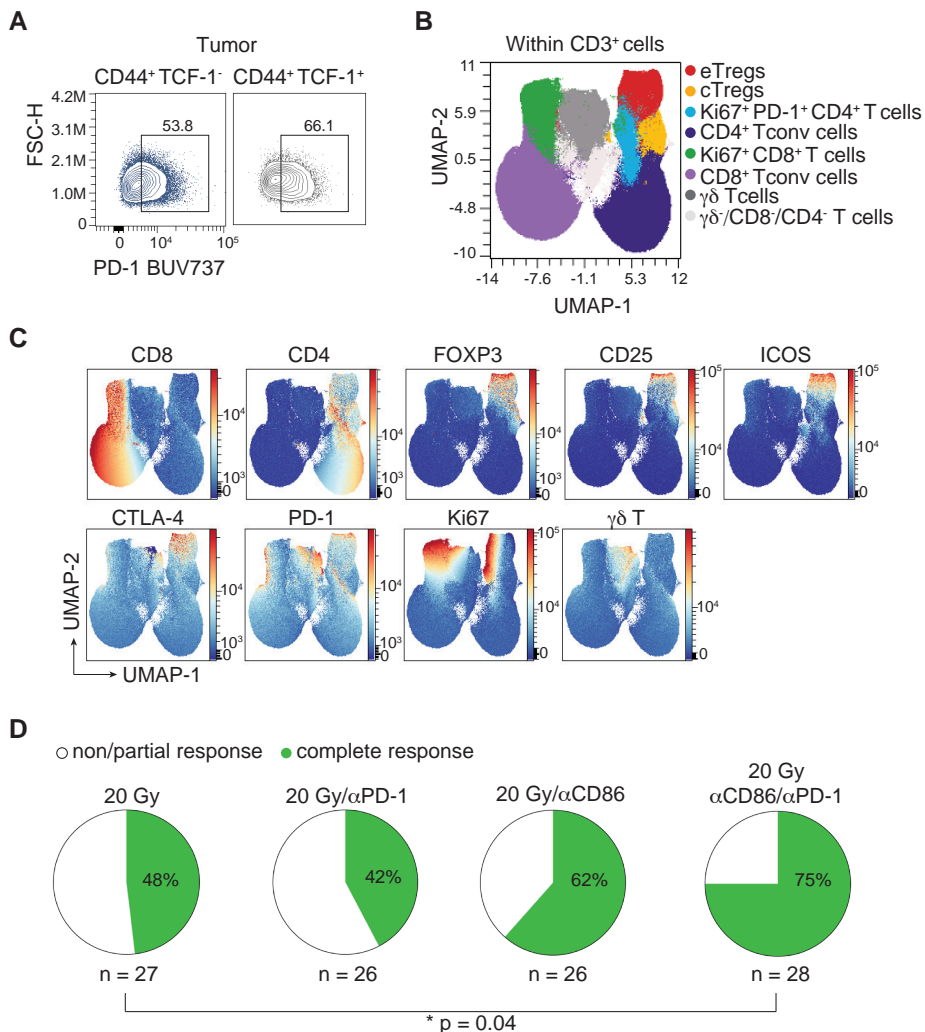
Supplemental Figure 4 - Related to Figure 3(I)

(A-C) TC-1 tumor bearing mice were treated i.p. with a depleting mAb against CD25 (n=6) or vehicle (PBS, n=6) when tumor size reached ~20 mm² (day 0). At day 4, the non-TdLN, TdLN and tumor were harvested and the Treg response was analyzed by flow cytometry. (A) Representative flow cytometry plots and (B) quantification depicting the frequency of total Tregs in the indicated tissues. (C) Proportion of CD4⁺ and CD8⁺ Tcons among CD45⁺ cells found in the indicated tissues following treatment. (D) Frequency of total Tregs among live cells measured in blood over time in the indicated treatment groups and (E) the individual tumor growth curves of the data described in Figure 3I. (F) Individual tumor growth curves and (G) overall survival of TC-1 tumor bearing mice treated with 0 Gy (n=6) or 3x8 Gy (n=15-16) in combination with a depleting mAb against CD25 or vehicle (PBS) at day -1 and 5 post RT. Ratios indicate the number of mice that showed full recovery upon treatment. Data are from one experiment representative of two experiments. Error bars indicate SD. *P < 0.05, **P < 0.01, Mann-Whitney test in B, Mantel-Cox analysis in G and Kruskal-Wallis test with Dunn's post hoc test in H. ns; not significant.



Supplemental Figure 5 – Related to Figure 6

(A) Representative gating strategy of cDC subsets in the TdLN of TC-1 tumor bearing mice. (B,C) Mice bearing 20 mm² TC-1 tumors received control treatment (0 Gy, n=6) or 20 Gy RT at day 0 in combination with either vehicle (PBS, n=8) or blocking mAb against CD80 (n=7) or CD86 (n=8) at day 0, 3 and 6. The cDC response was monitored by flow cytometry in the TdLN at day 8. (B,C) Median expression of the indicated markers found on (B) migratory cDC1s and (C) migratory cDC2s in the TdLN. (D) Representative gating strategy of the CD44⁺ TCF-1⁺ cells (orange) and CD44⁺ TCF-1⁻ cells (black) among CD8⁺ T cells in the TdLN (upper row) and tumor (lower row) for the indicated treatment groups at day 8. FMO; fluorescence minus one. Data are from one experiment representative of two experiments. Error bars indicate SD. **P < 0.01, *** P < 0.001, **** P < 0.0001, ordinary one-way Anova with Dunnett's post hoc test in C, D; ns; not significant.



Supplemental Figure 6 – Related to Figure 7

(A) Mice bearing 20 mm² TC-1 tumors received control treatment (0 Gy, n=5) or 20 Gy RT at day 0 in combination with either vehicle (PBS, n=8) or blocking mAb against CD80 (n=11) or CD86 (n=11) at day 0, 3 and 6. The CD8⁺ T cell response was monitored by flow cytometry in the tumor at day 8. Representative concatenated (n=11) contour plots are depicted for PD-1 expression on the indicated cell populations among CD8⁺ T cells in mice treated with 20 Gy and CD86 blockade. Numbers indicate percentages. (B-C) Mice bearing TC-1 tumors received control treatment (0 Gy, n=4) or 20 Gy RT at day 0 in combination with either vehicle (PBS, n=8) or blocking mAb against PD-1 (n=11), CD86 (n=10) or a combination of both (n=10) at day 0, 3 and 6. The CD3⁺ lymphocyte response was monitored by flow cytometry in the non-TdLN, TdLN and tumor at day 8. UMAP display of 2500 randomly selected CD3⁺ cells per tissue found in non-TdLN, TdLN and tumors at day 8 of all treatment groups combined. FlowSOM guided clustering (B) identifying the CD3⁺ cell populations and (C) representative heat map visualization of the markers that identify the CD3⁺ (T-cell) subpopulations. (D) Pie chart depicting the proportion of TC-1 tumor-bearing mice with complete tumor clearance upon treatment with 20 Gy at day 0, in combination with either vehicle (PBS), or blocking mAb against PD-1, CD86 or both CD86 and PD-1 at day 0, 3 and 6. *P<0.05, Chi-square test.

Table 1: Antibodies & Reagents

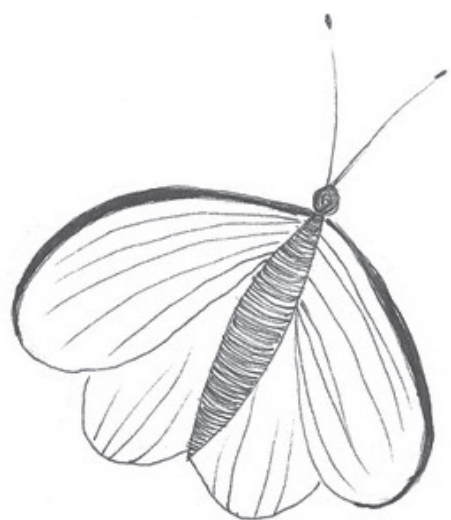
<i>Antigen</i>	<i>Fluorochrome</i>	<i>Flow Cytometry Antibodies</i>			<i>Catalog #</i>
		<i>Clone</i>	<i>Vendor</i>		
CD11c	BUV496	HL3	BD Biosciences	750483	
CD11b	BV510	M1/70	BioLegend	101263	
CD19	PerCP/Cy5.5	6D5	BioLegend	115534	
CD25	BV421	7D4	BD Biosciences	564571	
CD3	PerCP/Cy5.5	17A2	BD Biosciences	560527	
CD3	BV785	17A2	BioLegend	100232	
CD3	PE Cy7	145-2C11	eBiosciences	25-0031-81	
CD4	BV711	GK1.5	BD Biosciences	563050	
CD4	FITC	RM4-4	BioLegend	116003	
CD4	BUV395	GK1.5	BD Biosciences	563790	
CD40	PE Cy5	3/23	BioLegend	124617	
CD43	PE Cy5	1B11	BioLegend	121216	
CD44	BV785	IM7	BioLegend	103059	
CD45	APC/Fire810	30-F11	BioLegend	103173	
CD45	BUV395	30-F11	BD Biosciences	564279	
CD45	BUV563	30-F11	BD Biosciences	612924	
CD62L	APC/Cy7	MEL-14	BD Biosciences	560514	
CD64	AF647	X54-5/7.1	BioLegend	139322	
CD8	PerCP/Cy5.5	53-6.7	eBiosciences	45-0081-82	
CD8	BUV805	53-6.7	BD Biosciences	612898	
CD8	AF700	53-6.7	BioLegend	100730	
CD80	PE/Dazzle 594	16-10A1	BioLegend	B271480	
CD86	BV785	GL-1	BioLegend	B347725	
CD88	BUV805	20/70	BD Biosciences	748611	
CD103	BV711	M290	BD Biosciences	564320	
CD172a	BUV395	P84	BD Biosciences	740282	
CTLA-4	BV605	UC10-4B9	BioLegend	106323	
CX3CR1	PerCP/Cy5.5	SA011F11	BioLegend	B318597	
F4/80	BV421	BM8	BioLegend	123137	
FOXP3	APC	FJK-16S	eBiosciences	25-5773-82	
FOXP3	PE Cy5.5	FJK-16S	eBiosciences	35-5773-80	
Granzyme B	PE	GB11	Sanquin	M2289	
Helios	PE Cy7	22F6	BioLegend	137235	
ICOS	PerCP/Cy5.5	C398.4A	BioLegend	313518	
IFN γ	eFluor450	XMG-1.2	eBiosciences	48-7311-82	
IRF8	APC	V3GYWCH	eBiosciences	17-9852-80	
Ki67	AF700	SolA15	eBiosciences	56-5698-82	
Ki67	eFluor506	SolA15	eBiosciences	69-5698-80	
KLRG1	PE eF610	2F1	Thermo Fisher	4335245	
Ly6C	Pacific Blue	HK1.4	BioLegend	128014	
MHCII	APC-eFluor780	M5/114.15.2	eBiosciences	47-5321-80	
NK1.1	PerCP/Cy5.5	PK136	BioLegend	108727	
PD-1	BUV737	J43	eBiosciences	376-9985-80	
PD-L1 (CD274)	BUV737	MIH5	BD Biosciences	741877	
TCF-1	APC	C63D9	Cell Signaling Technology	376365	
TCR β	PE Cy7	H57-597	BioLegend	109222	
TCR β	BUV563	H57-597	BD Biosciences	748406	
TNF α	PE Cy7	MP6-XT22	BD Biosciences	561041	
yd T cell	BV510	GL3	BioLegend	118131	

Viability dyes		
LIVE/DEAD™ Fixable Near-IR Dead Cell Stain Kit	Thermo Fisher	L10119
Zombie UV™ Fixable Viability Kit	BioLegend	423107
Zombie Red™ Fixable Viability Kit	BioLegend	423109

In vivo antibodies & reagents				
Antigen	Immunogen	Clone	Vendor	Catalog #
CD25	IgG2a	M2A	Evitria	Gift from S. Quezada (under MTA)
CTLA-4	IgG2a fusion protein	UC10-4F10-11	BioXcell	BE0032
PD-1	Rat IgG2a	RMP1-14	BioXcell	BE0146
CD80	Rat IgG2a	1G10	BioXcell	BE0134
CD86	Rat IgG2a	GL-1	BioXcell	BE0025
CD8	Rat IgG2b	2.43	BioXcell	BE0061
CD4	Rat IgG2b	GK1.5	BioXcell	BE0003-1
FTY720			Cayman Chemical Company	10006292

Table 2: TCGA abbreviations

TCGA Abbreviation	Cancer Type
ACC	Adrenocortical carcinoma
BLCA	Bladder urothelial carcinoma
BRCA	Breast invasive carcinoma
CESC	Cervical squamous cell carcinoma and endocervical adenocarcinoma
CHOL	Cholangiocarcinoma
COAD	Colon adenocarcinoma
DLBC	Lymphoid Neoplasm Diffuse Large B-cell Lymphoma
ESCA	Esophageal carcinoma
GBM	Glioblastoma multiforme
HNSC	Head and Neck squamous cell carcinoma
KICH	Kidney Chromophobe
KIRC	Kidney renal clear cell carcinoma
KIRP	Kidney renal papillary cell carcinoma
LGG	Brain Lower Grade Glioma
LIHC	Liver hepatocellular carcinoma
LUAD	Lung adenocarcinoma
LUSC	Lung squamous cell carcinoma
MESO	Mesothelioma
OV	Ovarian serous cystadenocarcinoma
PAAD	Pancreatic adenocarcinoma
PCPG	Pheochromocytoma and Paraganglioma
PRAD	Prostate adenocarcinoma
READ	Rectum adenocarcinoma
SARC	Sarcoma
SKCM	Skin Cutaneous Melanoma
STAD	Stomach adenocarcinoma
TGCT	Testicular Germ Cell Tumors
THCA	Thyroid carcinoma
THYM	Thymoma
UCEC	Uterine Corpus Endometrial Carcinoma
UCS	Uterine Carcinosarcoma
UVM	Uveal Melanoma



3

Identifying the mechanisms behind tumor-induced Treg priming

Elselien Frijlink^{1,2}, Mo D. Staal² and Jannie Borst²

¹Division of Tumor Biology and Immunology and Oncode Institute, The Netherlands Cancer Institute, Amsterdam, The Netherlands

²Department of Immunology and Oncode Institute, Leiden University Medical Center, Leiden, The Netherlands.

Abstract

Tumor emergence is not only associated with local immunosuppression but also induces systemic immune disturbances. Regulatory T cells (Tregs) are among the first immune cells to respond to tumor development and may accumulate in the tumor-draining lymph node (TdLN) before migrating into the tumor. However, the mechanisms underlying tumor-induced Treg priming in the TdLN are poorly characterized. Here, using the mouse TC-1 tumor model, we demonstrate that tumor growth preferentially promotes expansion and initial differentiation in the TdLN of Helios⁺ Tregs, representative for a thymus-derived origin. These Tregs subsequently migrate into the tumor microenvironment (TME), where they adopt a more mature phenotype. We propose future experimental avenues that can reveal mechanisms dictating tumor-induced Treg responses in the TdLN and developmental trajectories of Tregs in healthy tissues and tumors. This information is essential to reveal novel therapeutic targets to inhibit Treg responses without eliciting immune-related adverse effects.

Introduction

Regulatory T cells (Tregs) are critical for maintaining immune homeostasis, but also contribute to an immunosuppressive tumor microenvironment (TME), where they inhibit the function of effector T cells and dendritic cells (DCs)¹. Thus, Tregs may impact the prognosis of various cancer types² and limit the effectiveness of anti-tumor immunotherapy³. Consequently, targeting of Tregs may be attractive to improve therapeutic outcomes, but current approaches are challenged by 1) the shared expression of markers between Tregs and conventional T cells (Tconvs), 2) the difficulty to accurately dissect Treg and Tconv populations in human tumors⁴ and 3) the need to inhibit tumor-associated Tregs, while preserving the ability of Tregs in healthy tissue to maintain tissue homeostasis⁵. Thus, gaining a deeper understanding of these cells in the tumor context may identify better therapeutic targets.

Tregs can be classified into two subsets, based on their tissue of origin: Thymus-derived Tregs (tTregs) develop from immature T cell precursors, recognize self-antigens, and act as guardians against autoimmunity, while peripherally-induced Tregs (pTregs) arise from mature Tconvs and suppress responses against non-self antigens⁴. pTregs are primarily found at mucosal-surfaces, like the colon, and the maternal-fetal interface^{6,7}. tTregs generally circulate between the blood and lymphoid tissue, where they receive signals required to differentiate into effector (e)Tregs. Subsequently, these eTregs migrate into non-lymphoid tissue (NLT) to become tissue-resident Tregs⁸. Within these NLTs, Tregs functionally adapt their differentiation states in response to local CD4⁺ Tconv cells, which produce lineage-specific cytokines associated with T helper (Th)1, Th2, or Th17 cells. In response, Tregs tailor their suppression against the corresponding Tconv population⁹.

In autoimmunity treatment, anti-inflammatory tTregs are preferred due to their stable lineage commitment, while pTregs may revert back into Tconvs that can be pro-inflammatory¹⁰. The precise contributions of these Treg subtypes in cancer remains uncertain, due to the lack of phenotypical and functional markers to distinguish between tTregs and pTregs in human studies, until recently¹¹. Accurate identification of these cells holds promise for developing novel therapeutic approaches. For instance, lineage instability in intra-tumoral Tregs can cause genetic reprogramming¹² and conversion to Tconv cells, evoking anti-tumor immune responses¹³. However, characterization of the T cell receptor (TCR) profiles of human tumor-resident Tregs identified a significant overlap with circulating Tregs isolated from blood, while no parallels were found with Tconvs¹⁴. This finding emphasizes that tumor-resident Tregs likely emerge not from the conversion of Tconvs but rather represent tTregs that are attracted to the TME from the circulation. Insights from single-cell RNA sequencing (scRNAseq) in mice further suggest that tumor-derived Tregs follow adaptation trajectories similar to those observed in NLTs¹⁵, consistent with findings in human breast cancer¹⁶. These Tregs appear to be primed for activation in the (tumor) draining lymph node (TdLN)¹⁵. Thus, tumor-derived Tregs likely are derived from the circulation and show high similarities to tissue-resident Tregs in healthy neighboring tissue. Furthermore, the presence of tumors correlated with elevated levels of Tregs systemically, particularly in the TdLN¹⁷⁻¹⁹. These

Tregs can hinder the initiation of new T cell responses^{20,21}. Although the role of these Tregs in driving metastases is becoming increasingly clear^{18,19}, the exact mechanisms of initial Treg priming in the tumor context remains controversial. Since the TdLNs serve as the site for priming and maintaining tumor-specific Tconv and Treg responses²²⁻²⁴, unraveling the mechanisms that initiate and sustain Treg responses in the tumor setting is of great importance.

We have previously identified that the transplantable C57BL/6-derived lung carcinoma TC-1 tumor model²⁵ resembles human “lymphocyte depleted” cancer^{26,27- under revision}, which is discerned by lymphocyte paucity and high myeloid cell infiltrate. TC-1 tumor growth raised a spontaneous immunosuppressive response in the TdLN, characterized by increased Ly6C⁺ monocytes and effector Tregs^{27- under revision}. Thus, this tumor model allows us to monitor how tumor growth orchestrates immunosuppressive responses beyond the local TME and assess the contribution of TC-1 tumor development to Treg priming in the TdLN, spleen, and tumor. We next integrate our findings and highlight the potential future experiments required to expand upon the current understanding of tumor-induced Treg priming and their differentiation trajectories within healthy and tumor tissue.

Results

Tumor development induces Helios⁺ Treg priming in the tumor draining lymph node

To investigate how TC-1 tumor growth impacts systemic Treg responses, we assessed the abundance of Tregs by flow cytometric analysis in the tumor, TdLN, non-TdLN, and spleen, and compared them to age-matched naïve mice. We observed that Tregs comprise the largest population of CD3⁺ cells in the tumor (Figure 1A). Interestingly, the frequency (Figure 1B) and absolute number (Figure 1C) of Tregs was significantly increased in the axillary TdLN and spleen, but not in the non-TdLN of TC-1 tumor-bearing mice. This data suggests that the TdLN serves as the priming site for tumor-induced Treg expansion, from where Tregs can disseminate systemically. To better visualize this, TC-1 tumor bearing mice received the S1P-receptor agonist FTY720, which restrains T-cell egress from lymphoid organs²⁸. At day 9 post treatment, presence of FTY720 significantly enhanced the proportion of Tregs in the TdLN compared to the control group (Figure 1D). Furthermore, FTY720 treatment significantly reduced the fraction of Tregs present in the tumor, indicating that tumor-infiltrating Tregs originate from the TdLN. These findings were further supported by the increased fraction of proliferating (Ki67⁺) Tregs in the TdLN, while Tregs in the non-TdLN and spleen did not show enhanced proliferation compared to the naïve control group (Figure 1E). Interestingly, analysis of the Treg population across all tissues revealed that regardless of tumor presence, the proliferating Treg subset was primarily characterized by Helios expression (Figure 1F), a marker for tTregs in mice²⁹. Quantitative analysis demonstrated that while both Helios⁺ and Helios⁻ Tregs exhibited increased proliferation in the TdLN of tumor-bearing mice, the majority of the proliferating Tregs expressed Helios (Figure 1G). Furthermore,

upon TC-1 tumor growth, both Helios⁺ and Helios⁻ Tregs showed a significant increase in absolute numbers within the TdLN, but Helios⁺ Tregs constituted the largest Treg population in the TdLN (Figure 1H). Importantly, the majority of tumor-infiltrating Tregs expressed Helios (Figure 1I). Together with the Treg depletion from the tumor upon FTY720 treatment, these data argue that Helios⁺ Tregs expand in the TdLN and subsequently migrate into the tumor.

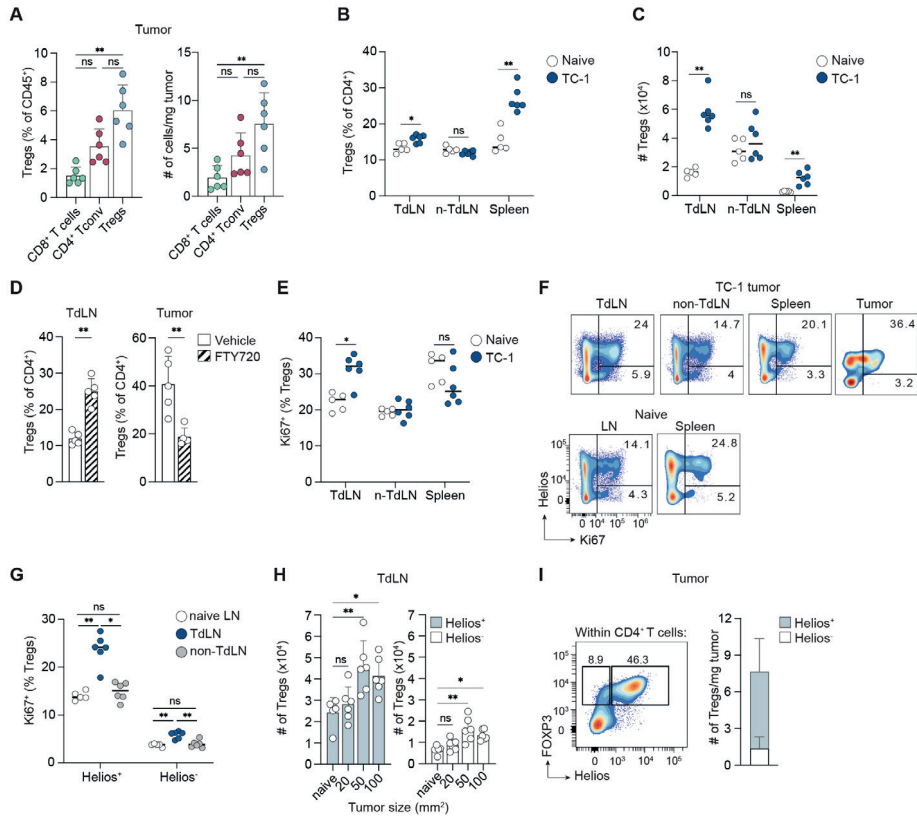


Figure 1. TC-1 tumor development drives priming of Helios⁺ Tregs in the TdLN

Analysis of the CD3⁺ T cell population found in the tumor, TdLN (right axillary LN), non-TdLN (left inguinal LN) and spleen of mice bearing 50 mm² TC-1 tumors (n=6) and age-matched naive mice (n=5) by flow cytometry. (A) Frequency among CD45⁺ cells (left) and absolute number (right) of the indicated populations found in tumor. (B,C) Frequency (B) and absolute number (C) of Tregs in indicated tissues. (D) Mice bearing TC-1 tumors (n=5/group) received FTY720 or vehicle (NaCl) by oral gavage when tumor size reached 20 mm² (day 0), followed by days 3 and 6. Indicated is the percentage of Tregs among CD4⁺ T cells at day 9 post treatment found in the TdLN and tumor. (E) Percentage of Ki67⁺ cells among Tregs in the indicated tissues. (F,G) Representative concatenated (n=5 for naive and n=6 for TC-1 tumor bearing) flow cytometry plots (F) and quantification (G) of the percentage of Ki67⁺ cells positive for Helios⁺ or Helios⁻ Tregs in the indicated tissues. (H) The absolute number of Helios⁺ and Helios⁻ Tregs found in the TdLN of TC-1 tumor bearing mice (n=6/timepoint) at increasing tumor sizes compared to age-matched naive mice (n=5). (I) Representative concatenated (n=6) flow cytometry plot (left) and quantification in absolute numbers (right) of the distribution of Helios⁺ and Helios⁻ Tregs found in the TC-1 tumor at 50 mm².

Data are from one experiment, representative of at least two experiments. Error bars indicate SD. *P < 0.05, **P < 0.01, Mann-Whitney test and Kruskal-Wallis test with Dunn's post hoc analysis. ns; no significance.

Following priming, thymic-derived Tregs acquire an effector phenotype in the tumor

If Tregs were primed in the TdLN and subsequently relocated to the tumor, as suggested by our data, we would expect them to acquire an effector phenotype. We indeed observed a significant increase in the proportion of cells displaying a CD44⁺ CD62L⁻ effector phenotype within the Helios⁺ Treg population, in contrast to Helios⁻ Tregs (Figure 2A,B). Conversely, Helios⁻ Tregs exhibited a higher fraction of cells with a CD44⁻ CD62L⁺ naïve phenotype. Thus, while both Helios⁺ and Helios⁻ Tregs expanded in the TdLN upon TC-1 tumor growth, primarily Helios⁺ Tregs apparently underwent effector differentiation. Reduction analysis of the total Treg population revealed a distinct population in the TdLN that was absent in both naïve and non-TdLNs (Figure 2C). This population encompassed both Helios⁺ and Helios⁻ Tregs, although the majority were Helios⁺ cells (Figure S1A). Clustering analysis confirmed these findings and identified clusters 5, 6 and 7 to be significantly enhanced in the TdLN, but not in the naïve and non-TdLNs (Figure 2D,E). Interestingly, although cluster 4 was not significantly enriched in the TdLN compared to naïve LNs, it is near absent in the non-TdLN. All clusters displayed high expression of ICOS, TNFR2, CTLA-4, GITR. Furthermore, cluster 5 and 7 differentiate from cluster 6 by Helios and enhanced CCR8 expression. In addition, cluster 5 exhibits elevated PD-1, CXCR6, CD39 and OX40 expression, as compared to the other clusters (Figure 2F, S1B), consistent with an NLT-adapted effector phenotype¹⁵. This population is likely primed to migrate and eventually become tissue-resident Tregs. Cluster 7 is highly proliferative, based on the expression of Ki67, which was less pronounced in cluster 6 and not observed in clusters 4 and 5 (Figure 2F, S1B), and probably reflects a precursor population of cluster 5. Thus, TC-1 tumor development drives effector differentiation of both Helios⁻ and Helios⁺ Tregs in the TdLN, yet expansion of Helios⁺ Tregs seems to be preferred.

Following differentiation into effector cells, Tregs move to non-lymphoid tissues, where they undergo further phenotypical adaptations¹⁵. Tumor-derived Tregs apparently undergo similar adaptation trajectories¹⁵, but may exhibit enhanced expression of chemokine receptors, such as CCR8 and CXCR6¹⁶. Similarly, scRNAseq analysis in mice have illustrated a transformation process of Tregs migrating from the TdLN into the TME, where they become tumor-retained Tregs. These Tregs exhibit an upregulated protein expression profile, including enhanced ICOS and CD39 expression³⁰. Correspondingly, tumor-resident Helios⁺ Tregs were enriched for the CD44⁺ CD62L⁻ effector phenotype (Figure S1C) and exhibited increased cell surface expression of ICOS, CTLA-4, GITR and CCR8 as compared to Helios⁺ Tregs found in the TdLN (Figure 2G,H). TNFR2, PD-1 and OX40 expression were not further increased. Additionally, tumor-resident Helios⁺ Tregs uniquely expressed CXCR6 and CD39. Although present in a significantly smaller proportion (Figure 1I), we observed that tumor-resident Helios⁻ Tregs displayed a comparable phenotype to tumor-resident Helios⁺ Tregs (Figure S1C-E). Taken together, these findings suggest that TC-1 tumor growth preferentially drives effector differentiation of Helios⁺ Tregs in the TdLN, which likely enables their subsequent infiltration from the bloodstream into the tumor. In the tumor, the effector Treg phenotype is most explicitly present.

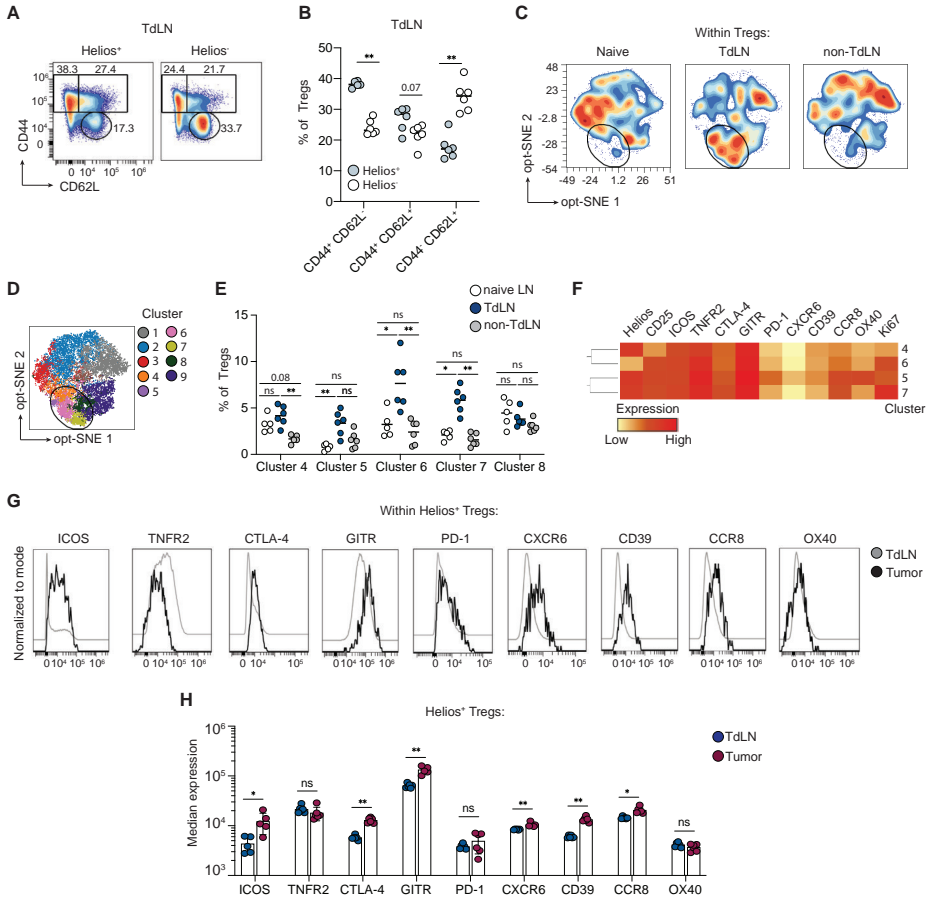


Figure 2. Helios⁺ Tregs acquire a more explicit effector phenotype in the TME.

Phenotypic analysis by flow cytometry of the Treg population found in the TdLN (right axillary LN), non-TdLN (left inguinal LN) and tumor of mice bearing 50 mm² TC-1 tumors (n=6) or age-matched naïve mice (n=5). (A,B) Representative concatenated (n=6) flow cytometry plots (A) and quantification (B) of the percentage of Helios⁺ and Helios⁻ Tregs expressing CD44 and/or CD62L. The numbers in (A) represent percentages. (C) Opt-SNE display of 1000 randomly selected Treg cells per sample found in axillary LNs of naïve mice (n=5), together with TdLN and non-TdLN of TC-1 tumor bearing mice (n=6). Black circle is for visualization purposes only. (D) Opt-SNE visualization of 9 Treg clusters identified by FlowSOM. Black circle visualizes the clusters with upregulated activation markers, as indicated in Figure S1B. (E) Quantification of the indicated clusters identified in (D) in naïve LNs, TdLNs and non-TdLNs. (F) Heatmap overview of the relative expression of the indicated Treg markers among clusters 4, 5, 6 and 7. (G,H) Representative (n = 5-6) concatenated histograms (G) and quantification (H) depicting expression of the indicated markers on Helios⁺ Tregs found in the TdLN and tumor. Results are combined from two separate experiments. Error bars indicate SD. *P < 0.05, **P < 0.01, Mann-Whitney test in (B) and (H). Kruskal-Wallis with Dunn's post hoc test in (E). ns; no significance.

Discussion

Tregs are among the first immune cells to respond to tumor development²⁴, establishing an immunosuppressive environment that could hinder anti-tumor immune responses^{3,31}. These Tregs tend to accumulate in the TdLN before migrating into the tumor²⁴. However, the precise mechanisms governing tumor-induced Treg priming in the TdLN and their subsequent migration into the tumor remain poorly understood. Recent studies found significant overlap in TCR sequences between Tregs isolated from the tumor and blood, but not with Tconv cells^{5,14,32}. This suggests peripheral Treg recruitment and potential activation upon recognition of antigens distinct from those recognized by Tconvs^{33,34}. Additionally, tumor-associated Tregs likely resemble tissue-resident Tregs^{5,15,35}, complicating targeted intervention without affecting healthy tissue Tregs.

To identify potential therapeutic targets, we need to better understand the mechanisms underlying tumor-induced Treg priming and the subsequent migration and adaptation of these Tregs in the TME. Hence, we require effective *in vivo* tumor models that can recapitulate this process. Our study demonstrates that the TC-1 tumor model is suitable for this purpose. Specifically, we identify that tumor development favors expansion of Helios⁺ Tregs, representing tTregs, in the TdLN. These Tregs then migrate into the tumor where they further adopt a matured phenotype. To gain a better understanding of the observed findings, future experiments should focus on the underlying mechanisms governing Treg priming in the tumor setting. For instance, scRNAseq, together with TCR sequencing of Tregs extracted from the TdLN and tumor, compared to healthy LN and lung tissue (considering TC-1 tumors originate from lung epithelial cells²⁵), may identify specific cellular states and pathways distinguishing normal tissue-resident from tumor-specific Tregs. This data may be particularly important to gain insights into the differentiation trajectories of Tregs in the TdLN. Additionally, this data will also provide a better understanding of the overlap between tumor-infiltrating Tregs and those residing in healthy tissue. Particularly, it has been described that Tregs transitioning from the TdLN into the tumor undergo an adaptation process to become tumor-resident Tregs³⁰. However, it remains unclear whether these findings resemble a common tissue-resident adaptation process^{15,36}, or if they are exclusive to the tumor context. This could potentially be addressed by scRNAseq data from our setting. Finally, given the proportion of Helios⁺ Tregs present in the TdLN, CD4⁺ Tconv cells should be analyzed in parallel. By performing TCR sequencing analysis, it could be determined whether these cells are pTregs originating from Tconv conversion within the TdLN³⁷.

An alternative approach worth exploring involves scRNAseq together with multiplex spectral flow cytometry to analyze the immune composition in the TdLN and compare it to healthy LNs. Specifically, it would be interesting to map the myeloid population, including dendritic cells (DCs) and monocytes to identify cellular states that may dictate Treg priming³⁸. By utilizing the fluorescent protein zsGreen, stably transduced in TC-1 tumor cells, sorting strategies could efficiently identify recently migrated DCs and other myeloid populations from the tumor³⁹. This

information may help to identify how tumor development impacts DC and myeloid functional states, potentially favoring Treg differentiation over Tconv priming.

Studies in humans have demonstrated that tumor-resident Tregs acquire an enhanced immunosuppressive phenotype compared to Tregs derived from healthy tissue^{16,40}. This suggests the existence of additional contributing factors that may sustain the intra-tumoral Treg pool and impact their molecular reprogramming, such as local interactions with DCs^{21,41} or macrophages⁴². Considering that TC-1 tumors primarily contain myeloid populations, it would be interesting to better understand the interplay between these cells with tumor-resident Tregs. Immunohistochemistry (IHC) on entire slide images may help to determine the spatial localization of Tregs and DCs or macrophages in the tumor. In addition, intervention studies including CSF1R-targeted depletion^{43,44} or CCR2-inhibitors^{45,46} are required to determine the interaction between macrophages and Tregs. While these interventions may offer clarity regarding the general interplay between these cell types, further exploration into the phenotypic and functional changes occurring in these cells subsequent to these interventions is essential. Particularly, it would be intriguing to dissect the mechanisms employed by myeloid cells that contribute to Treg differentiation within the TME. This can either be through direct interactions with potential co-inhibitory or -stimulatory receptors⁴⁷, or through indirect mechanisms like the release of cytokines^{45,47}. The collective insights from this data could potentially provide a strategy to alleviate immunosuppression within the TME, not by targeting Tregs directly, but by focusing on modulating tumor-resident myeloid cells.

Taken together, we here show that the TC-1 tumor model may be used to delineate the mechanisms guiding tumor-induced Treg differentiation in TdLN and the tumor. Furthermore, we suggest potential avenues for investigating Treg differentiation mechanisms in the tumor context. These efforts are vital for identifying potential therapeutic targets.

Methods

Murine TC-1 tumor cell line

The TC-1 tumor cell line is derived from C57BL/6 lung epithelial cells engineered to express HPV16 E6 and E7 proteins²⁵ and was received from Leiden University Medical Center in 2015. TC-1 cells were cultured in RPMI 1640 (Gibco, Life Technologies), supplemented with 10% fetal calf serum (FCS), 0.1 mM non-essential amino acids, 1 mM sodium pyruvate, 2 mM L-glutamine, 10 mM HEPES and penicillin/streptomycin (Roche) at 37°C, 5% CO₂ and the stock was tested negative for *Mycoplasma* by PCR. Thawed cells were used within 3 passages for *in vivo* experiments.

Mice

Six-to-eight-week old female C57BL/6J mice were obtained from Janvier Laboratories (Le Genest Saint Isle, France) and maintained in individually ventilated cages (Innovive) under specific pathogen-free conditions. All mouse experiments were performed in accordance with institutional and national guidelines and were approved by the Animal Welfare Body (IVD) of the Netherlands Cancer Institute.

Tumor transplantation

Mice were anesthetized with isoflurane and injected subcutaneously (s.c.) with 1×10^5 TC-1 tumor cells in 50 μ l HBSS. Tumor size was measured by calipers in two dimensions and calculated as: area (mm²) = width x length. Mice were sacrificed at the indicated timepoints, when humane endpoint was reached or when the tumor size reached >100 mm².

FTY720 treatment

When tumor size reached 18-20 mm² (day 0), TC-1 tumor bearing mice were treated with the sphingosine-1-phosphate receptor-1 agonist FTY720 (Fingolimod, Cayman Chemical), dissolved in 0.9% NaCl solution (vehicle) and administered at 2 mg/kg by oral gavage. FTY720 treatment was repeated at day 4 and 6 and mice were sacrificed at day 9.

Tissue preparation and flow cytometry

Lymphoid tissues and tumors were harvested from mice at the indicated timepoints. To characterize the TdLN and non-TdLNs, we performed intra-tumoral injection of 5% Evans Blue Dye (Sigma-Aldrich) in 50 μ l PBS under isoflurane, and identified the axillary lymph node as the TdLN, whereas the contralateral inguinal LN was defined as the non-TdLN. Tumor tissue was mechanically disaggregated using a Mcllwain tissue chopper (Mickle Laboratory Engineering), and a single-cell

suspension was prepared by digesting the tissue in collagenase type A (Roche) and 25 µg/ml DNase I (Sigma) in serum-free DMEM for 45 min at 37°C. Enzyme activity was neutralized by addition of medium containing 10% FCS, and the tissue was dispersed by passing through a 70-µm cell strainer. To acquire single cell suspensions of LNs and spleen, the tissue was punctured with a 27 G needle followed by incubation in 100 µg/mL Liberase™ TL (Roche) in serum-free DMEM for 30 min at 37°C. Enzyme activity was neutralized as described above and tissue was dispersed by passing through a 70-µm cell strainer. For surface staining, single cells of the isolated tissues were first incubated with anti-CD16/32 (1:50, clone 2.4G2, BD Bioscience) supplemented with 10 µg/ml DNase, to block unspecific Fc receptor binding, for 10 min on ice. Next, surface antibody staining was performed (Table 1) for 30 min in PBS containing 0.5% BSA and 0.01% sodium azide. For intracellular staining of transcription factors and cytokines, cells were fixed and permeabilized with the FOXP3 Transcription Factor Staining Buffer Set according to the manufacturer's protocol (Thermo Fischer Scientific). Dead cells were excluded by using Fixable Viability Near-infra red dye (1:1000, Life Technologies) or Zombie UV fixable viability Kit (1:500, BioLegend). Absolute cell numbers were determined by adding AccuCount Blank Particles (7-7.9 µm, Spherotech) to each sample, prior to flow cytometry analysis. Fluorescence minus one (FMO) was used as a negative control for activation markers. Flow cytometry was performed using a BD FACSymphony™ A5 SORP flow cytometer or the 5-laser Cytex Aurora. All generated data was analyzed using OMIQ software (Dotmatics, Boston, MA).

Data analysis

Dimensionality reduction and FlowSOM⁴⁸ analysis of flow cytometry data was performed using OMIQ software. Following conventional marker expression analysis, the population of interest was manually gated, and down-sampling was performed to select the maximal number of cells per tissue representative for all tissue types included, as indicated in the figure legends. K-means clustering of the indicated populations was performed using FlowSOM, including all markers indicated, except for live/dead, CD45, CD3 and CD4. Dimension reduction and visualization was performed using uniform manifold approximation and projection (UMAP) analysis⁴⁹, including the same markers as described above and by using the default OMIQ settings.

Statistical analysis

All statistical data were analyzed using GraphPad Prism version 9 (GraphPad Software, La Jolla, CA). Statistical analyses were performed as indicated in the figure legends. A P value < 0.05 was considered statistically significant; *p<0.05, **p<0.01, ***p<0.001, ****p<0.0001. Data are represented as mean + S.D.

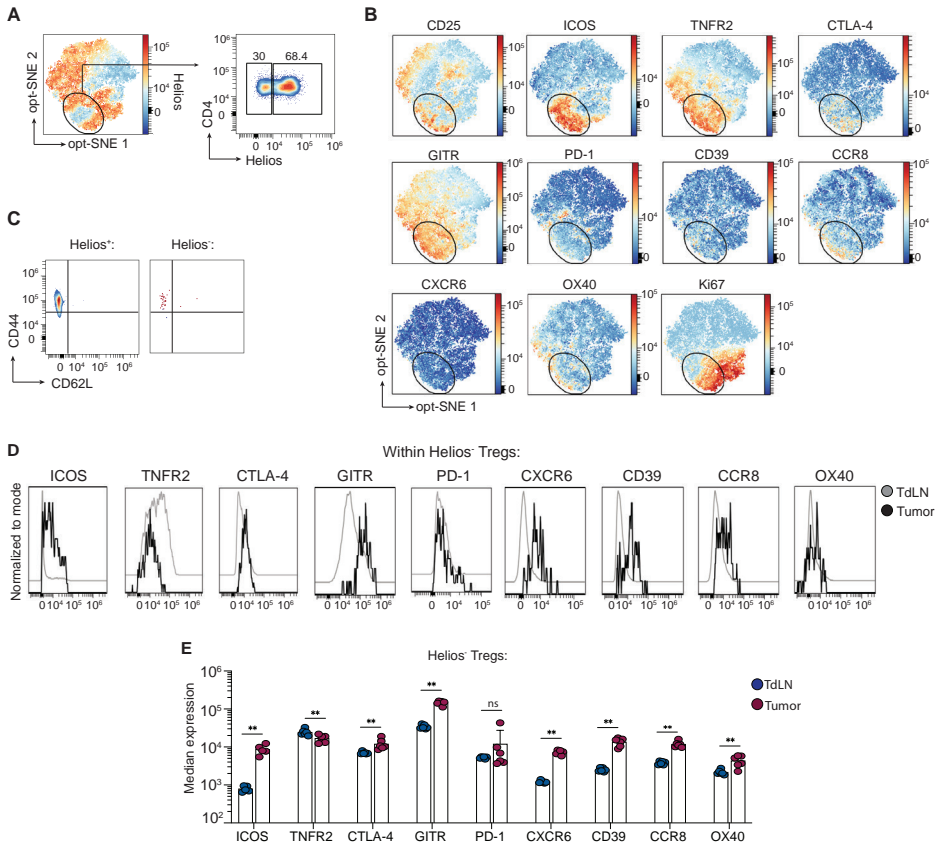
References

- 1 Vignali, D. A., Collison, L. W. & Workman, C. J. How regulatory T cells work. *Nat Rev Immunol* **8**, 523-532 (2008).
- 2 Shang, B., Liu, Y., Jiang, S. J. & Liu, Y. Prognostic value of tumor-infiltrating FoxP3+ regulatory T cells in cancers: a systematic review and meta-analysis. *Sci Rep* **5**, 15179 (2015).
- 3 Kumagai, S. *et al.* The PD-1 expression balance between effector and regulatory T cells predicts the clinical efficacy of PD-1 blockade therapies. *Nat Immunol* **21**, 1346-1358 (2020).
- 4 Wing, J. B., Tanaka, A. & Sakaguchi, S. Human FOXP3(+) Regulatory T Cell Heterogeneity and Function in Autoimmunity and Cancer. *Immunity* **50**, 302-316 (2019).
- 5 Delacher, M. *et al.* Single-cell chromatin accessibility landscape identifies tissue repair program in human regulatory T cells. *Immunity* **54**, 702-720 e717 (2021).
- 6 Josefowicz, S. Z. *et al.* Extrathymically generated regulatory T cells control mucosal TH2 inflammation. *Nature* **482**, 395-399 (2012).
- 7 Samstein, R. M., Josefowicz, S. Z., Arvey, A., Treuting, P. M. & Rudensky, A. Y. Extrathymic generation of regulatory T cells in placental mammals mitigates maternal-fetal conflict. *Cell* **150**, 29-38 (2012).
- 8 Liston, A. & Gray, D. H. Homeostatic control of regulatory T cell diversity. *Nat Rev Immunol* **14**, 154-165 (2014).
- 9 Josefowicz, S. Z., Lu, L. F. & Rudensky, A. Y. Regulatory T cells: mechanisms of differentiation and function. *Annu Rev Immunol* **30**, 531-564 (2012).
- 10 Koenen, H. J. *et al.* Human CD25highFoxp3pos regulatory T cells differentiate into IL-17-producing cells. *Blood* **112**, 2340-2352 (2008).
- 11 Opstelten, R. *et al.* GPA33: A Marker to Identify Stable Human Regulatory T Cells. *J Immunol* **204**, 3139-3148 (2020).
- 12 Yates, K., Bi, K., Haining, W. N., Cantor, H. & Kim, H. J. Comparative transcriptome analysis reveals distinct genetic modules associated with Helios expression in intratumoral regulatory T cells. *Proc Natl Acad Sci U S A* **115**, 2162-2167 (2018).
- 13 Nakagawa, H. *et al.* Instability of Helios-deficient Tregs is associated with conversion to a T-effector phenotype and enhanced antitumor immunity. *Proc Natl Acad Sci U S A* **113**, 6248-6253 (2016).
- 14 Ahmadzadeh, M. *et al.* Tumor-infiltrating human CD4(+) regulatory T cells display a distinct TCR repertoire and exhibit tumor and neoantigen reactivity. *Sci Immunol* **4** (2019).
- 15 Miragaia, R. J. *et al.* Single-Cell Transcriptomics of Regulatory T Cells Reveals Trajectories of Tissue Adaptation. *Immunity* **50**, 493-504 e497 (2019).
- 16 Plitas, G. *et al.* Regulatory T Cells Exhibit Distinct Features in Human Breast Cancer. *Immunity* **45**, 1122-1134 (2016).
- 17 Nunez, N. G. *et al.* Tumor invasion in draining lymph nodes is associated with Treg accumulation in breast cancer patients. *Nat Commun* **11**, 3272 (2020).
- 18 Kos, K. *et al.* Tumor-educated T(regs) drive organ-specific metastasis in breast cancer by impairing NK cells in the lymph node niche. *Cell Rep* **38**, 110447 (2022).
- 19 Reticker-Flynn, N. E. *et al.* Lymph node colonization induces tumor-immune tolerance to promote distant metastasis. *Cell* **185**, 1924-1942 e1923 (2022).
- 20 Zagorulya, M. *et al.* Tissue-specific abundance of interferon-gamma drives regulatory T cells to restrain DC1-mediated priming of cytotoxic T cells against lung cancer. *Immunity* **56**, 386-405 e310 (2023).
- 21 Bauer, C. A. *et al.* Dynamic Treg interactions with intratumoral APCs promote local CTL dysfunction. *J Clin Invest* **124**, 2425-2440 (2014).

- 22 Salmon, H. *et al.* Expansion and Activation of CD103(+) Dendritic Cell Progenitors at the Tumor Site Enhances Tumor Responses to Therapeutic PD-L1 and BRAF Inhibition. *Immunity* **44**, 924-938 (2016).
- 23 Broz, M. L. *et al.* Dissecting the tumor myeloid compartment reveals rare activating antigen-presenting cells critical for T cell immunity. *Cancer Cell* **26**, 638-652 (2014).
- 24 Darrasse-Jeze, G. *et al.* Tumor emergence is sensed by self-specific CD44hi memory Tregs that create a dominant tolerogenic environment for tumors in mice. *J Clin Invest* **119**, 2648-2662 (2009).
- 25 Lin, K. Y. *et al.* Treatment of established tumors with a novel vaccine that enhances major histocompatibility class II presentation of tumor antigen. *Cancer Res* **56**, 21-26 (1996).
- 26 Thorsson, V. *et al.* The Immune Landscape of Cancer. *Immunity* **48**, 812-830 e814 (2018).
- 27 Frijlink, E. *et al.* (2023).
- 28 Matloubian, M. *et al.* Lymphocyte egress from thymus and peripheral lymphoid organs is dependent on S1P receptor 1. *Nature* **427**, 355-360 (2004).
- 29 Thornton, A. M. *et al.* Expression of Helios, an Ikaros transcription factor family member, differentiates thymic-derived from peripherally induced Foxp3+ T regulatory cells. *J Immunol* **184**, 3433-3441 (2010).
- 30 Li, Z. *et al.* In vivo labeling reveals continuous trafficking of TCF-1+ T cells between tumor and lymphoid tissue. *J Exp Med* **219** (2022).
- 31 Deng, L. *et al.* Accumulation of foxp3+ T regulatory cells in draining lymph nodes correlates with disease progression and immune suppression in colorectal cancer patients. *Clin Cancer Res* **16**, 4105-4112 (2010).
- 32 Wang, L. *et al.* Connecting blood and intratumoral T(reg) cell activity in predicting future relapse in breast cancer. *Nat Immunol* **20**, 1220-1230 (2019).
- 33 Hindley, J. P. *et al.* Analysis of the T-cell receptor repertoires of tumor-infiltrating conventional and regulatory T cells reveals no evidence for conversion in carcinogen-induced tumors. *Cancer Res* **71**, 736-746 (2011).
- 34 Sainz-Perez, A., Lim, A., Lemercier, B. & Leclerc, C. The T-cell receptor repertoire of tumor-infiltrating regulatory T lymphocytes is skewed toward public sequences. *Cancer Res* **72**, 3557-3569 (2012).
- 35 Malchow, S. *et al.* Aire-dependent thymic development of tumor-associated regulatory T cells. *Science* **339**, 1219-1224 (2013).
- 36 Li, C. *et al.* TCR Transgenic Mice Reveal Stepwise, Multi-site Acquisition of the Distinctive Fat-Treg Phenotype. *Cell* **174**, 285-299 e212 (2018).
- 37 Alonso, R. *et al.* Induction of anergic or regulatory tumor-specific CD4(+) T cells in the tumor-draining lymph node. *Nat Commun* **9**, 2113 (2018).
- 38 Maldonado, R. A. & von Andrian, U. H. How tolerogenic dendritic cells induce regulatory T cells. *Adv Immunol* **108**, 111-165 (2010).
- 39 Binnewies, M. *et al.* Unleashing Type-2 Dendritic Cells to Drive Protective Antitumor CD4(+) T Cell Immunity. *Cell* **177**, 556-571 e516 (2019).
- 40 De Simone, M. *et al.* Transcriptional Landscape of Human Tissue Lymphocytes Unveils Uniqueness of Tumor-Infiltrating T Regulatory Cells. *Immunity* **45**, 1135-1147 (2016).
- 41 Marangoni, F. *et al.* Expansion of tumor-associated Treg cells upon disruption of a CTLA-4-dependent feedback loop. *Cell* **184**, 3998-4015 e3919 (2021).
- 42 Casanova-Acebes, M. *et al.* Tissue-resident macrophages provide a pro-tumorigenic niche to early NSCLC cells. *Nature* **595**, 578-584 (2021).
- 43 Kos, K. *et al.* Tumor-associated macrophages promote intratumoral conversion of conventional CD4(+) T cells into regulatory T cells via PD-1 signalling. *Oncoimmunology* **11**, 2063225 (2022).

- 44 Gyori, D. *et al.* Compensation between CSF1R+ macrophages and Foxp3+ Treg cells drives resistance to tumor immunotherapy. *JCI Insight* **3** (2018).
- 45 Mondini, M. *et al.* CCR2-Dependent Recruitment of Tregs and Monocytes Following Radiotherapy Is Associated with TNFalpha-Mediated Resistance. *Cancer Immunol Res* **7**, 376-387 (2019).
- 46 Liang, H. *et al.* Host STING-dependent MDSC mobilization drives extrinsic radiation resistance. *Nat Commun* **8**, 1736 (2017).
- 47 Lindau, D., Gielen, P., Kroesen, M., Wesseling, P. & Adema, G. J. The immunosuppressive tumour network: myeloid-derived suppressor cells, regulatory T cells and natural killer T cells. *Immunology* **138**, 105-115 (2013).
- 48 Van Gassen, S. *et al.* FlowSOM: Using self-organizing maps for visualization and interpretation of cytometry data. *Cytometry A* **87**, 636-645 (2015).
- 49 Becht, E. *et al.* Dimensionality reduction for visualizing single-cell data using UMAP. *Nat Biotechnol* **37**, 38-44 (2018).

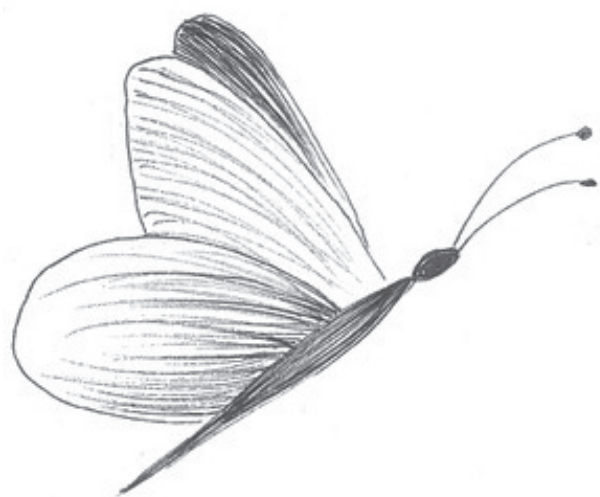
Supplementary Data

**Supplemental Figure 1 – Related to Figure 2.**

Phenotypic analysis by flow cytometry of the Treg population found in the TdLN, non-TdLN and tumor of mice bearing 50 mm² TC-1 tumors (n=6) or age-matched naïve mice (n=5). **(A,B)** Opt-SNE visualization of 1000 randomly selected Tregs per sample found in axillary LNs of naïve mice (n = 5), together with TdLN and non-TdLN of TC-1 tumor bearing mice (n=6). **(A)** Heatmap display (left) and representative flow plots (right) showing Helios expression. The figure on the right shows Helios expression as found among clusters 4-8 (see Figure 2D). The numbers indicate percentages. **(B)** Representative heatmap visualization of the markers used to identify different activation states among Tregs. **(C)** Representative concatenated (n=6) flow cytometry plots of the proportion of tumor-derived Helios⁺ and Helios⁻ Tregs expressing CD44 and/or CD62L. **(D,E)** Representative concatenated (n=6) histograms **(D)** and quantification **(E)** depicting expression of the indicated markers on Helios⁺ Tregs found in the TdLN and tumor. Error bars indicate SD. **P < 0.01, Mann-Whitney test in **(E)**. ns; no significance.

Table 1: Antibodies & Reagents

Flow Cytometry Antibodies				
→ Antigen	Fluorochrome	Clone	Vendor	Catalog #
CD25	BV421	7D4	BD Biosciences	564571
CD3	PerCP eF710	500A2	eBiosciences	46-0033-82
CD3	BV785	17A2	BioLegend	100232
CD4	BUV395	GK1.5	BD Biosciences	563790
CD45	APC/Fire810	30-F11	BioLegend	103173
CD45	BUV563	30-F11	BD Biosciences	612924
CD8	BB515	53-6.7	BD Biosciences	564422
CD8	BUV805	53-6.7	BD Biosciences	612898
CTLA-4	BV605	UC10-4B9	BioLegend	106323
FOXP3	APC	FJK-16S	eBiosciences	25-5773-82
FOXP3	PE Cy5.5	FJK-16S	eBiosciences	35-5773-80
Helios	PE Cy7	22F6	BioLegend	137235
ICOS	PerCP Cy5.5	C398.4A	BioLegend	313518
CD39	BUV805	24DMS1	eBiosciences	368-0391-82
TNFR2	PE	TR75-89	BioLegend	113405
Ki67	AF700	SoIA15	eBiosciences	56-5698-82
Ki67	eFluor506	SoIA15	eBiosciences	69-5698-80
CXCR6	APC/Cy7	SA051D1	BioLegend	151124
GITR	R718	DTA-1	BD Optibuild	2285946
OX40	SB780	OX-86	eBiosciences	78-1341-82
CCR8	BV711	SA214G2	BioLegend	150320
PD-1	BUV737	J43	eBiosciences	376-9985-80
CD44	BV785	IM7	BioLegend	103059
CD62L	APC/Cy7	MEL-14	BD Biosciences	560514
Viability dyes				
LIVE/DEAD™ Fixable Near-IR Dead Cell Stain Kit			Thermo Fisher	L10119
Zombie UV™ Fixable Viability Kit			Biolegend	423107
In vivo antibodies & reagents				
Antigen	Immunogen	Clone	Vendor	Catalog #
FTY720			Cayman Chemical Company	10006292



4

Radiotherapy and Cisplatin increase immunotherapy efficacy by enabling local and systemic intratumoral T-cell activity

Cancer Immunology Research. 2019;7(4): 670-682

Paula Kroon^{1*}, **Elselien Frijlink^{1*}**, Victoria Iglesias-Guimaraes¹, Andriy Volkov¹, Marit M. van Buuren¹, Ton N. Schumacher^{1,2}, Marcel Verheij³, Jannie Borst^{1#}, and Inge Verbrugge^{1#}

** Shared first authors*

Shared senior authors

¹Division of Tumor Biology and Immunology, The Netherlands Cancer Institute-Antoni van Leeuwenhoek, 1066 CX Amsterdam, The Netherlands.

²Division of Molecular Oncology and Immunology, OncoCode Institute, The Netherlands Cancer Institute-Antoni van Leeuwenhoek, 1066 CX Amsterdam, The Netherlands. ³Department of Radiation Oncology, The Netherlands Cancer Institute-Antoni van Leeuwenhoek, 1066 CX Amsterdam, The Netherlands.

Abstract

To increase cancer immunotherapy (IT) success, PD-1 blockade must be combined with rationally selected treatments. Here, we examined, in a poorly immunogenic mouse breast cancer model, the potential of antibody-based immunomodulation and conventional anticancer treatments to collaborate with anti-PD-1 treatment. One requirement to improve anti-PD-1-mediated tumor control was to promote tumor-specific cytotoxic T-cell (CTL) priming, which was achieved by stimulating the CD137 costimulatory receptor. A second requirement was to overrule PD-1-unrelated mechanisms of CTL suppression in the tumor microenvironment (TME). This was achieved by radiotherapy (RT) and cisplatin treatment. In the context of CD137/PD-1-targeting IT, RT allowed for tumor elimination by altering the TME, rather than intrinsic CTL functionality. Combining this radioimmunotherapy regimen with low-dose cisplatin improved CTL-dependent regression of a contralateral tumor outside the radiation field. Thus, systemic tumor control may be achieved by combining IT protocols that promote T-cell priming with (chemo)radiation protocols that permit CTL activity in both the irradiated tumor and (occult) metastases.

Running title

Chemo-radio-immunotherapy in PD-1 resistant breast cancer.

Introduction

Cancer immunotherapies include adoptive T-cell therapy, therapeutic vaccination, and/or antibody-based immunomodulation. From a technical perspective, antibody-based immunomodulation is relatively straightforward, because immunomodulatory antibodies can essentially be delivered in the same way as conventional anticancer drugs. Immunomodulatory antibodies approved for cancer immunotherapy (IT) are designed to target the T-cell coinhibitory receptors PD-1 or CTLA-4, and single or combined treatment induces durable responses in about one third of patients with solid tumors¹. Still, the majority of patients do not benefit from this treatment approach². Compared with targeting CTLA-4, targeting PD-1 is generally more successful and associated with fewer autoimmune symptoms³. Therefore, targeting PD-1 currently serves as the backbone for developing new combination therapies. To choose combinations rationally, insight into their combined mechanism of action is required.

CD8⁺ cytotoxic T lymphocytes (CTL) can recognize (tumor-derived) intracellular peptides presented on the cell surface by MHC class I molecules. As MHC class I molecules are expressed on virtually all body cells, CTLs can in principle target any cancer type. CD4⁺ T cells also promote antitumor immunity, either by direct cytotoxic activity or by promoting the activity of CTLs and other immune cells⁴. Several groups postulated that successful IT relies on a tumor-specific T-cell response that is self-sustained by continuous generation of new effector T cells (T cell priming) and support of their activity^{5,6}. To enable this cycle, the tumor must essentially act as its own 'vaccine' by releasing both recognizable antigens and 'danger' signals. Dendritic cells (DCs) can then present these antigens to naïve T cells and provide appropriate costimulatory and cytokine signals needed to induce T cell clonal expansion and effector differentiation. However, in immunogenic tumors that have given rise to a T-cell response throughout their development, negative feedback mechanisms reduce effector T-cell functions. These mechanisms include the activity of regulatory T cells (Tregs) and suppressive activity of myeloid cells, stromal cells, and even the tumor cells themselves⁷. For example, PD-L1 can be expressed on tumor cells and/or other (immune) cell types present in the tumor, and can inhibit T-cell function via PD-1⁸. Successful IT requires the elimination of such suppressive mechanisms.

Blocking CTLA-4 enables CD28 costimulation⁹, which may promote new T-cell priming and effector T-cell activity. Blocking CTLA-4 and PD-1 promotes T-cell activity inside tumors in a complementary fashion¹⁰ and blocking CTLA-4 promotes T-cell priming in patients with cancer¹¹. Concomitant targeting of CTLA-4 and PD-1 is associated with increased autoimmunity¹² and this combination should likely be avoided when developing new IT strategies. A potential alternative, targeting CD137 (also known as 4-1BB or TNFRSF9) using agonistic antibodies is currently in phase III clinical trials¹³ and is being tested in combination with PD-1 blockade in phase 1b clinical trials¹⁴. CD137 is

a costimulatory receptor that belongs to the Tumor Necrosis Factor (TNF) receptor family, and its signaling promotes the priming and maintenance of CTL responses by delivering pro-survival and other signals to CD8⁺ T cells and DCs¹⁵.

Both radiotherapy (RT) and chemotherapy induce tumor cell destruction, which leads to release of antigens and 'danger' signals¹⁶. In principle, these events may lead to new T-cell priming. However, the likelihood that priming will occur without IT-based assistance is low, because RT almost never gives rise to an 'abscopal' effect, i.e. regression of a tumor mass outside the radiation field¹⁷. Extrapolating from mouse models¹⁸, conventional chemotherapeutic drugs may have immunomodulatory actions in human, but thus far, this question has not been a systemically address in the clinic.

Here, we examined the potential of using RT and a routinely co-applied conventional chemotherapy (cisplatin) to assist IT in evoking a systemic, tumor-eradicating T-cell response. We provide evidence that RT and chemotherapy make tumors permissive to CTL activity. These data argue that conventional anticancer regimens can be combined rationally with IT to improve systemic tumor control and increase tumor clearance rates and patient outcome.

Results

Immunotherapy (IT) with CD137 agonism and PD-1 blockade promotes T-cell priming

As a model system, we used mice with syngeneic AT-3 breast cancer cells implanted orthotopically into the fat pad and treated with IT and/or RT after the tumor reached >20mm². Standard IT consisted of a blocking antibody to PD-1 and an agonistic antibody to CD137 (Figure 1A), targets which are expressed on DCs and on T cells in lymphoid organs and tumor tissue (Figure S1). In this setting, IT and RT as individual treatments merely delayed tumor outgrowth, whereas combined treatment (i.e. RIT) resulted in tumor clearance in the majority of the mice (Figure 1B). We have previously shown that combined PD-1 blockade and CD137 agonism is more effective at enhancing RT-induced tumor control than single PD-1 blockade or CD137 agonism and that tumor control in this setting relies on CD8⁺ T cells^{19,20}.

Among single modality treatments, CD137 agonism, but not RT or PD-1 blockade induced a T-cell response (Figure 1C), as determined by the appearance of CD4⁺ and CD8⁺ T cells with a CD43⁺ effector phenotype in blood posttreatment²¹. PD-1 blockade further increased CD4⁺ and CD8⁺ T-cell responses when combined with CD137 agonism (Figure 1C,D). Finally, when IT with both antibodies was combined with RT, CD4⁺ and CD8⁺ T-cell responses were also induced, as measured by a significant increase in effector phenotype T cells in the blood and a similar increase in the

(inguinal) tumor-draining lymph node (dLN) (Figure 1D,E). These data suggest that IT with CD137 agonist antibody promotes T-cell priming, which is increased by PD-1 blockade and not impeded by concurrent RT.

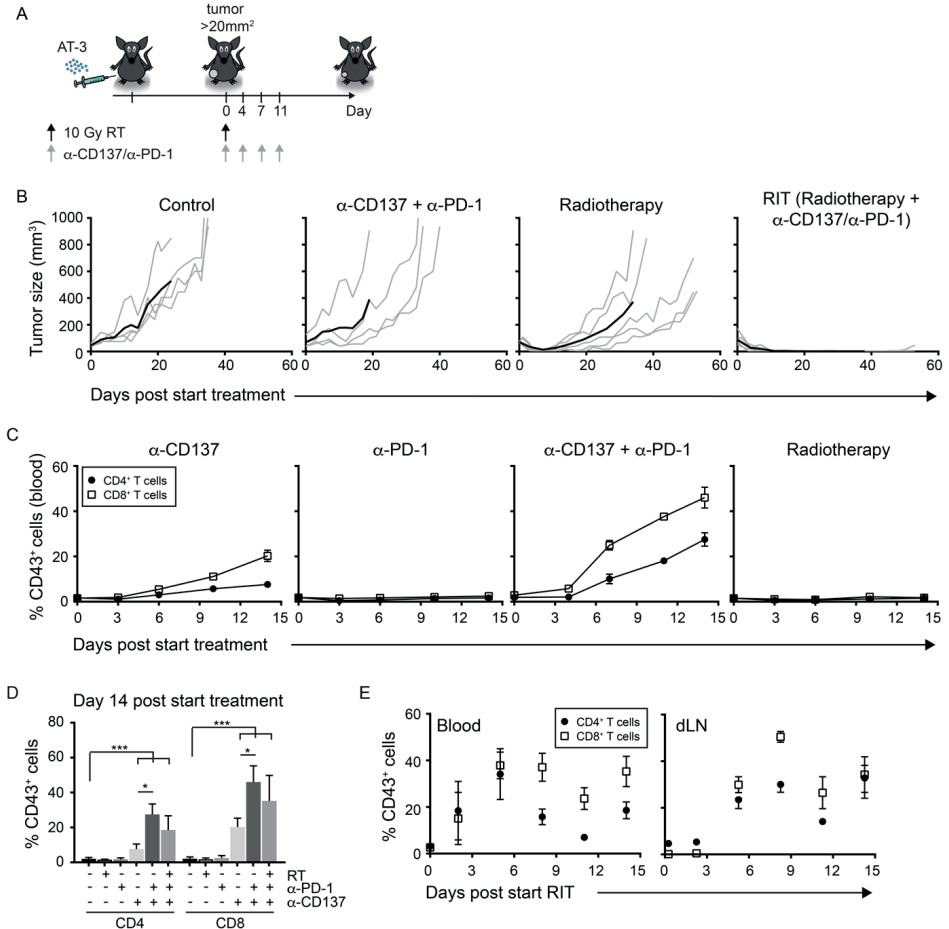


Figure 1. Immunotherapy with CD137 agonism and PD-1 blockade promotes T-cell priming.

(A) Experimental set-up. (B) Tumor growth curves measured in mice receiving the indicated therapies (n=4–5/group). Gray lines, individual mice; black line, group average. (C) CD43 expression on CD4⁺ and CD8⁺ T cells in blood, in tumor-bearing mice (n=5/group) at indicated time points posttherapy. (D) Pooled data (mean +SD) from C and E, showing the frequency of effector phenotype T cells in blood on day 14 side-by-side. (E) CD43 expression on CD4⁺ and CD8⁺ T cells, in the blood (left) and draining lymph node (dLN) of tumor-bearing mice (n=4–5/group), at different time points after RIT (*, P < 0.01; ***, P < 0.001).

Control of the irradiated tumor by radio-immunotherapy (RIT) requires T-cell priming

To examine whether newly primed T cells contributed to tumor control after RIT, we treated mice with the drug FTY720 that induces the internalization of the sphingosine 1 phosphate receptor 1 (S1PR1). T cells use the S1PR1 to egress from secondary lymphoid organs and the drug prevents them from doing so²². RIT was applied while the mice were treated with FTY720 or vehicle (Figure 2A, Figure S2A). To assess T-cell priming and resulting effector T-cell generation, we measured the percentage of CD4⁺ and CD8⁺ T cells in the dLN that could produce the effector cytokines TNF α and/or IFN γ . RIT increased the percentage of CD8⁺ effector T cells, and these cells significantly accumulated in the dLN upon FTY720 treatment (Figure 2B, left). In contrast, TNF α -producing CD4⁺ effector T cells were not increased by RIT, nor did these cells accumulate in the dLN upon FTY720 treatment (Figure 2B, right). These data indicate that RIT induced new priming of CD8⁺ T cells and that FTY720 treatment effectively ‘trapped’ these newly primed T cells in the dLN.

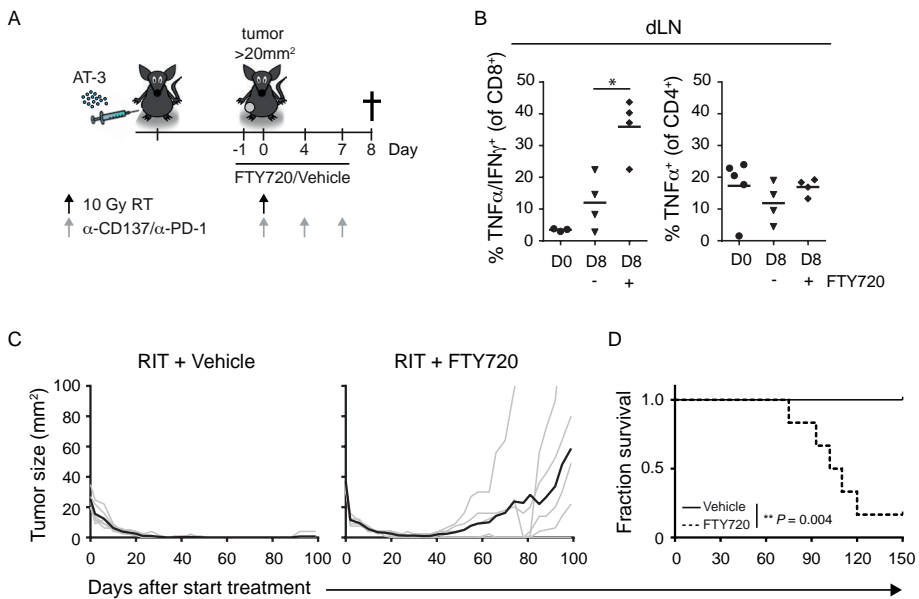


Figure 2. Control of the irradiated tumor by RIT requires T-cell priming.

(A) Experimental set-up for B. (B) Percentage of CD4⁺ (right) and CD8⁺ T cells (left) in the dLN that produce TNF α /IFN γ or TNF α in response to *in vitro* restimulation, before (D0, closed circles) or 8 days (D8) after starting RIT, in presence (closed diamonds) or absence (closed triangles) of FTY720 (*, $P < 0.05$). Tumor growth (C) and survival curves (D) of AT-3 tumor-bearing mice ($n=6$ /group) receiving RIT with FTY720 or vehicle.

Whereas 100% of the mice cleared their tumor and survived long term upon RIT, concurrent FTY720 treatment significantly increased tumor outgrowth (Figure 2C) and reduced overall survival (Figure 2D). FTY720 treatment did not reduce the therapeutic effect of RT or IT alone (Figure S2B). Thus, RIT leads to T-cell priming and these newly primed T cells make a critical contribution to regression of the irradiated tumor.

RIT does not induce regression of an abscopal tumor, despite infiltration with newly primed CTLs

Given that RIT induces T-cell priming, we hypothesized that the resulting systemic T-cell response could also act against a nonirradiated tumor in the same host. We tested this by implanting two tumors into the same mouse; one in the left fat pad and the other in the contralateral flank. Only the latter tumor was irradiated (Figure 3A). The T-cell response and tumor regression were examined for both tumors.

We found that after RIT the percentage of CD8⁺ T cells among total CD45⁺ (hematopoietic) cells increased significantly in both irradiated and nonirradiated tumors (Figure 3B, right). The RIT-induced increase of CD8⁺ T cells in the nonirradiated tumor was largely prevented by FTY720 treatment (Figure 3B, right), indicating that this increase was largely due to new T-cell priming. The CD4⁺ T-cell response following RIT was much less pronounced (Figure 3B). Histologic analysis confirmed that CD8⁺

T cells accumulated to a similar extent following RIT in both irradiated and nonirradiated tumors (Figure 3C). Infiltration by CTLs, capable of producing IFN γ and TNF α and the cytotoxic effector molecule Granzyme B, was of similar magnitude in irradiated and nonirradiated tumors (Figure 3D). In contrast, accumulation of CD4⁺ T cells that could produce TNF α or Granzyme B was not evident (Figure 3E). As compared with IT alone, RIT delayed outgrowth of the irradiated tumor, but not of the nonirradiated tumor (Figure 3F, Figure S3A). As overall survival was defined by the time for any the two tumors to reach 100 mm², RIT did not improve overall survival of mice as compared with IT alone (Figure 3G). (Hypo)fractionated RT is more effective than single-dose RT in enhancing abscopal tumor control by IT in certain mouse models^{23,24}. However, 3 x 8 Gy (hypo)fractionation also did not enhance IT-induced control of nonirradiated AT-3 tumors (Figure S3B, C). Thus, CTLs that are raised by RIT are present in equal measure in the irradiated and nonirradiated tumor, yet these CTLs can only eliminate the irradiated tumor.

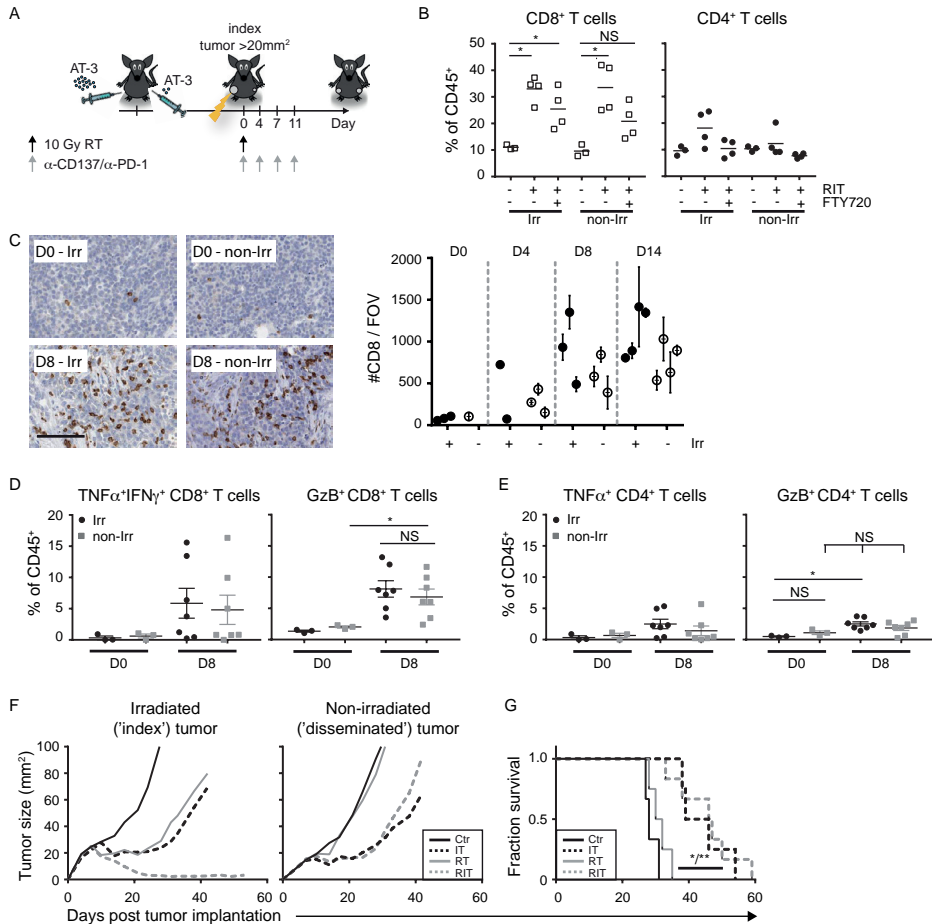


Figure 3. RIT leads to comparable infiltration of irradiated and nonirradiated tumors with T cells, but the nonirradiated tumor does not regress.

(A) Experimental set-up. (B) Percentage of CD4⁺ and CD8⁺ T cells within the CD45⁺ cell population in the irradiated (Irr) and nonirradiated (non-Irr) tumors before (-) or 8 days after the start of RIT, in the presence or absence of FTY720. * P < 0.05. C, AT-3 tumor sections (n=3 mice/group) were stained for CD8 before treatment (D0) or 4, 8, or 14 days after the start of RIT. Left, representative images; right, summary data. Quantification in the right represents the average (SD) of 5 fields of view (FOVs) for 3 irradiated (filled circles) and 3 nonirradiated tumors (open circles). Images represent 1/6th of a FOV; scale bar, 100 μm. (D, E) Percentage of TNFα⁺IFNγ⁺ or Granzyme B (GzB)⁺ CD8⁺ T cells (D) and CD4⁺ T cells (E) within the CD45⁺ cell population isolated from irradiated and nonirradiated tumors before (D0) and 8 days after starting RIT. Each symbol represents a single tumor, and the mean is indicated. *, P < 0.05. (F) Mean tumor growth in mice (n=5–6/group) that received no therapy (Ctr), RT (10 Gy, R), alone or in combination with IT. (G) Survival curve for mice treated as indicated. *, P < 0.05, between the Ctr and IT groups; **, P < 0.01 between the Ctr and RIT groups and between the RT and RIT groups.

The abscopal effect of RIT is not limited by T cell priming, intratumoral neutrophils/macrophages

We next addressed a number of potential factors that might prevent RIT-induced CTLs from eliminating the nonirradiated tumor. We first assessed whether the size of the tumor-specific effector CTL pool was a limiting factor. For this purpose, we identified the peptide SNPTY SVM from MMTV-Polyoma virus middle-T (PyMT) as an MHC class I-restricted antigen that could raise T-cell immunity to AT-3 tumor cells (Figure **S4A-F**). This enabled us to purposely generate tumor-specific CTL memory *in vivo* by vaccinating mice with plasmid (p)DNA encoding this epitope (Figure **4A**), designed according to ref²⁵. Vaccinated mice were challenged with two AT-3 tumors and treated with RIT (Figure **4B**). Also, in this setting, RIT did not enhance control of the nonirradiated tumor (Figure **4C**) or improve survival of mice (Figure **4D**), as compared with IT alone. These data suggest that the magnitude of the tumor-specific CTL response was not the limiting factor for systemic tumor control following RIT.

We next examined which mechanisms of T-cell suppression other than PD-1/PD-L1 interaction may operate in the nonirradiated AT-3 tumors. Treg frequency was low in the irradiated and nonirradiated tumors and did not change significantly following RIT (Figure **4E**), suggesting that it did not correlate with CTL-mediated tumor control.

Tumor-resident neutrophils and macrophages can also locally impair CTL function²⁶. Following RIT, a decrease in the frequency of F4/80⁺MHCII⁺ TAMs was observed in irradiated, but not in nonirradiated tumors (Figure **4F**, left). The frequency of Ly6G⁺Ly6C^{low} neutrophils did not change after RIT (Figure **4F**, right). In addition, antibody-mediated depletion of neutrophils or TAMs (Figure **S4G**) did not improve control of nonirradiated tumors (Figure **S4H**), nor did it increase overall survival following RIT (Figure **4G**).

Following RIT, the frequency of NK cells and NK-T cells was decreased in irradiated and nonirradiated tumors to a similar extent. There was also no difference in the frequency of Ly6C^{hi}Ly6G⁻ inflammatory monocytes, CD103⁺ DCs, and CD11b⁺ DCs in irradiated as compared to nonirradiated tumors (Figure **4H**). Thus, the presence of these cell types did not correlate with CTL-mediated tumor control.

Although RT can upregulate cell surface expression of MHC class I²⁷, it did not increase MHC class I expression on nonhematopoietic cells in the AT-3 tumor *in vivo*, as determined on day 3 and 8 post RT (Figure **S4I**). Taken together, these data suggest that the magnitude of the tumor-specific CTL response, PD-1 signaling, Tregs, neutrophils, TAMs, NK(T) cells, inflammatory monocytes, DCs, or MHC class I expression were not key factors that limited CTL activity in the nonirradiated tumor after RIT.

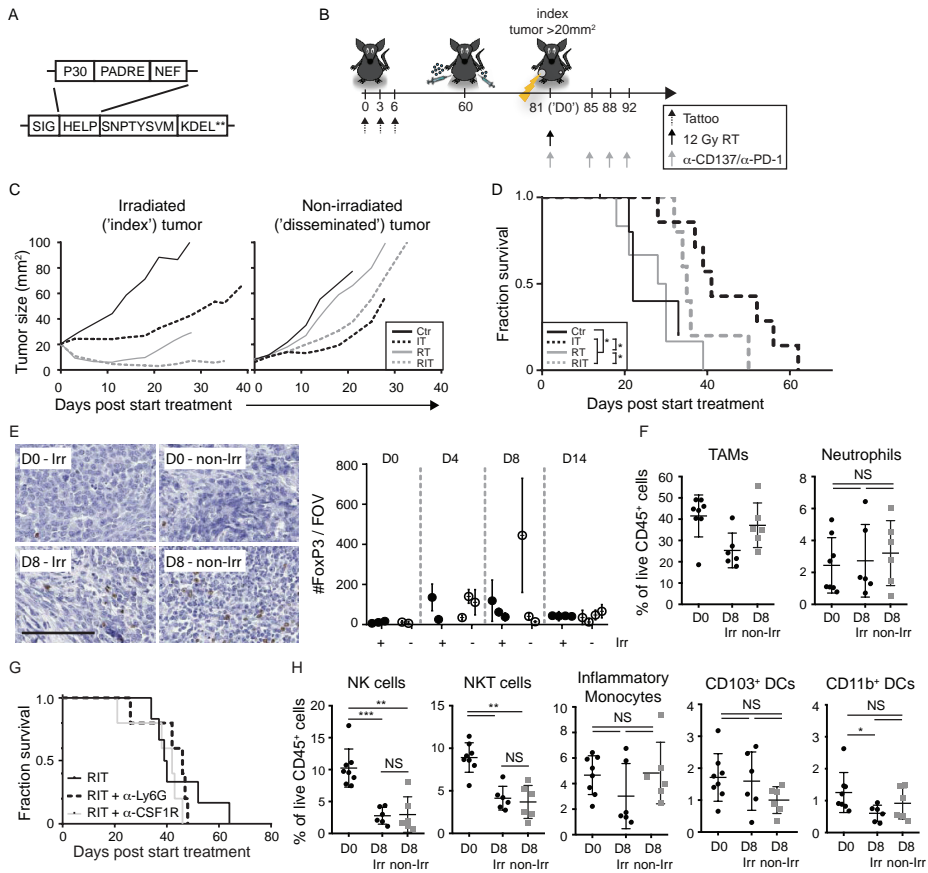


Figure 4. Optimizing tumor-specific T-cell priming, depletion of neutrophils or TAMs is insufficient to control nonirradiated AT-3 tumors following RIT.

(A) The vaccine encodes the H-2K^b-binding PyMT epitope SNPTY SVM and MHC II "helper" epitopes. **, Double stop codon. (B) Experimental set-up. Mean tumor size (C) and survival curves (D) of 5–7 mice/group that received the indicated treatments. *, $P < 0.05$. (E) FoxP3⁺ regulatory T cells in irradiated (Irr) and nonirradiated (non-Irr) tumors before treatment (D0) and on the indicated days after the start of RIT ($n=3$ /group). Images, representative FoxP3 staining of 10% of a FOV; scale bar, 100 μ m. Quantification (right): mean (SD) of 5 FOVs for 3 irradiated (filled circles) and 3 nonirradiated tumors (open circles). (F,H) TAMs, neutrophils (F), NK cells, NKT cells, inflammatory monocytes, CD103⁺ DCs, CD11b⁺ DCs (H) in untreated (D0), irradiated (Irr), and nonirradiated (non-Irr) tumors on day 8 (D8) after RIT. Each symbol represents an individual tumor, and the mean (SD) is shown (*, $P < 0.05$; **, $P < 0.01$; ***, $P < 0.001$). (G) Survival curve of tumor-bearing mice that receive RIT in the presence or absence of antibodies targeting Ly6G or CSF1R ($n=5$ /group).

RIT induces a TME characterized by reduced cell proliferation and increased tissue repair

RIT led to the same degree of CTL infiltration in the irradiated and nonirradiated tumors, whereas only the irradiated tumor regressed, suggesting that CTLs can exert their activity on tumor cells only after the tumor has been altered by irradiation. To understand the immunomodulatory effect of irradiation in the context of IT, we performed mRNA sequencing (RNA-seq). Eight days after RIT (allowing sufficient time for T cells to infiltrate both tumors: see Figure 3), we sorted the effector (CD43⁺ CD8⁺ T cells (i.e. 'CTLs'), CD45⁺ hematopoietic cells (excluding CD43⁺CD8⁺ T cells) and CD45⁻ tumor/stromal cells (Figure 5A). Statistical analysis of normalized read counts revealed the differential expression of 805 genes in CTLs (Figure 5B), 1107 genes in the hematopoietic cells (Figure 5C), and 3045 genes in the tumor/stromal cells (Figure 5D). These genes encode a wide diversity of proteins (Table S1) that perform a multitude of cellular functions.

We identified groups of biological processes that were differentially modulated between the cell populations at the irradiated and nonirradiated tumor sites. In all three cell populations, gene sets associated with cell division, DNA replication and repair, and chromatin remodeling were significantly downregulated in the irradiated tumor (Figure 5E-G), congruent with the cells receiving a DNA-damaging input in the form of irradiation.

In the CTLs, we additionally identified a small group of gene sets associated with negative regulation of cytokine expression (Figure 5E), that included both *Foxp3* and *Il10* (Table S1), which may report effects of irradiation. We did not identify gene sets associated with increased CTL-intrinsic effector function that could explain the increased CTL efficacy in the irradiated tumor. This finding is consistent with our functional data regarding CD8⁺ T cells, showing that both irradiated and non-irradiated tumors are infiltrated with effector-phenotype CTLs after RIT (see Figure 3D).

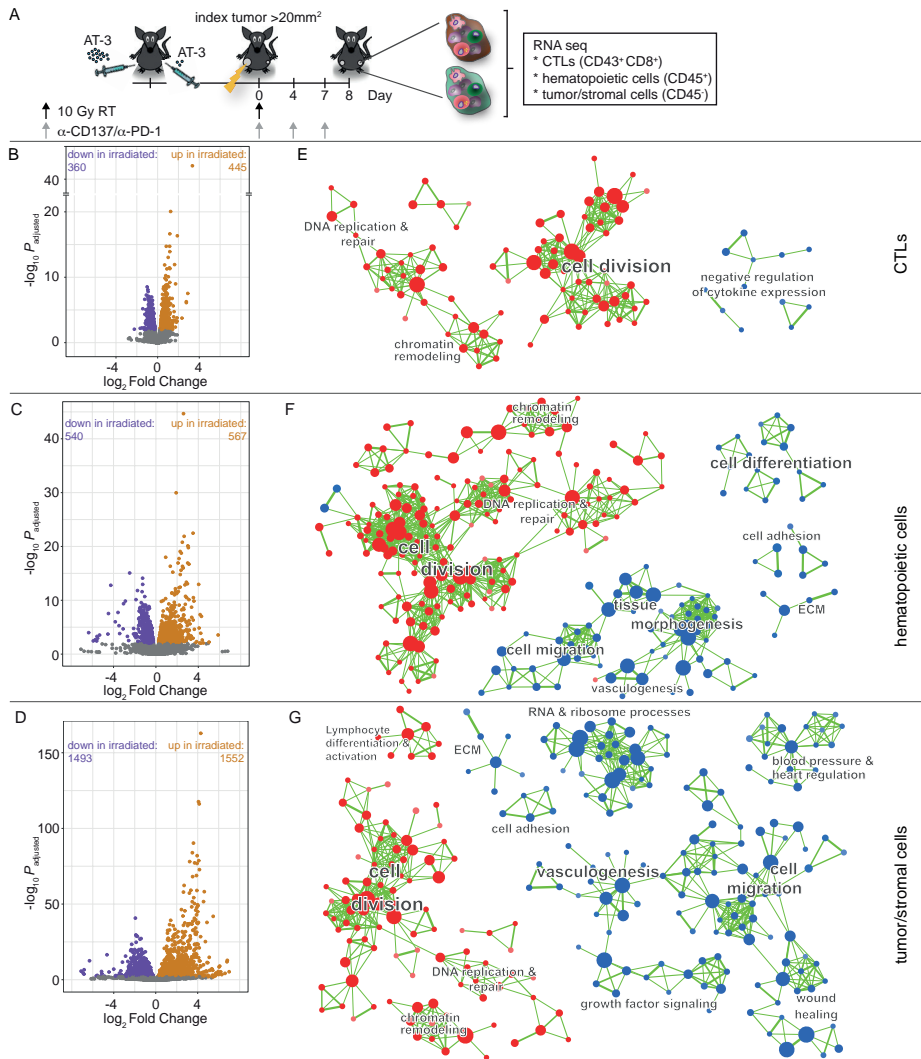


Figure 5. RIT induces a CTL-permissive TME that is characterized by gene signatures associated with reduced cell proliferation and increased response to tissue injury.

(A) Experimental set-up. (B–D) Volcano plots of the indicated cell populations showing significant (adjusted $P < 0.01$) transcriptomic changes in the irradiated compared with the nonirradiated tumor. Purple, orange, and gray dots represent downregulated, upregulated, or unchanged genes, respectively. (E–G) Enrichment Maps showing significantly enriched gene sets (biological processes) in blue (enriched in the irradiated tumor) and red (enriched in the nonirradiated tumor). Gene sets that share a high number of genes are clustered together, and the thickness of the green lines represents the number of shared genes. Clusters of similar biological processes are labeled.

In the hematopoietic and tumor/stromal cells, we identified several biological processes that were significantly different between the irradiated and nonirradiated tumor sites (Figure 5F and G). These included overlapping processes and genes in the hematopoietic and tumor/stromal cells, such as increased cell migration e.g. *Cxcl17*, *Cxcl14*), vasculogenesis (e.g. *Vegfc*, *Egfl7l*), and cell adhesion/extracellular matrix (ECM; e.g. *Selp*, *Mmp3*, see also Table S1). In addition, and unique to the tumor/stromal cell population, we identified increased expression of gene sets associated with RNA/ribosome processes (e.g. *Rps19*, *Rps12*) and wound healing (e.g. *Pdgfb*, *Cxcl12*) in the irradiated tumor as compared to the nonirradiated tumor (Figure 5F, G). Increased expression of proapoptotic *Bax* was observed specifically in the tumor/stromal cells of the irradiated tumor (Table S1).

Taken together, these RNA-seq data revealed that the TME of the irradiated tumor was different from that of the nonirradiated tumor. RT inflicted a DNA damage response in all cell populations in the tumor and led to tissue repair, as suggested by increased protein translation, angiogenesis and cell migration. This gene expression profile was associated with increased CTL activity against the tumor cells, most likely through CTL-extrinsic effects.

Cisplatin functionally mimics the RT-induced, T cell permissive TME and increases RIT efficacy

Next, we aimed to create a 'CTL-permissive' TME in the nonirradiated tumor to allow for systemic CTL-based tumor eradication following RIT. We tested low-dose cisplatin chemotherapy to achieve this effect (Figure 6A) for the following reasons: *i*) Cisplatin has partially the same mode of action as RT by inducing DNA damage, *ii*) cisplatin combined with RT is standard-of-care in the treatment of different types of cancer and *iii*) (low-dose) cisplatin has been shown to support T-cell function in (pre-)clinical vaccination studies¹⁸.

We found that low-dose cisplatin delayed tumor outgrowth, and that adding cisplatin treatment to RIT further improved control of nonirradiated tumors (Figure 6B and C) and increased overall survival (Figure 6D). This enhanced therapeutic effect was CD8⁺ T-cell-dependent (Figure 6D), even though cisplatin modestly reduced the magnitude of the T-cell response following RIT (Figure 5SA and 5SB). In the absence of RT, cisplatin treatment also enhanced the antitumor effect of this IT approach (Figure 5SC and 5SD). Thus, systemic cisplatin treatment functionally mimicked the localized effects of RT, allowing CTL-mediated growth delay of the non-irradiated tumor and prolonging overall survival following RIT.

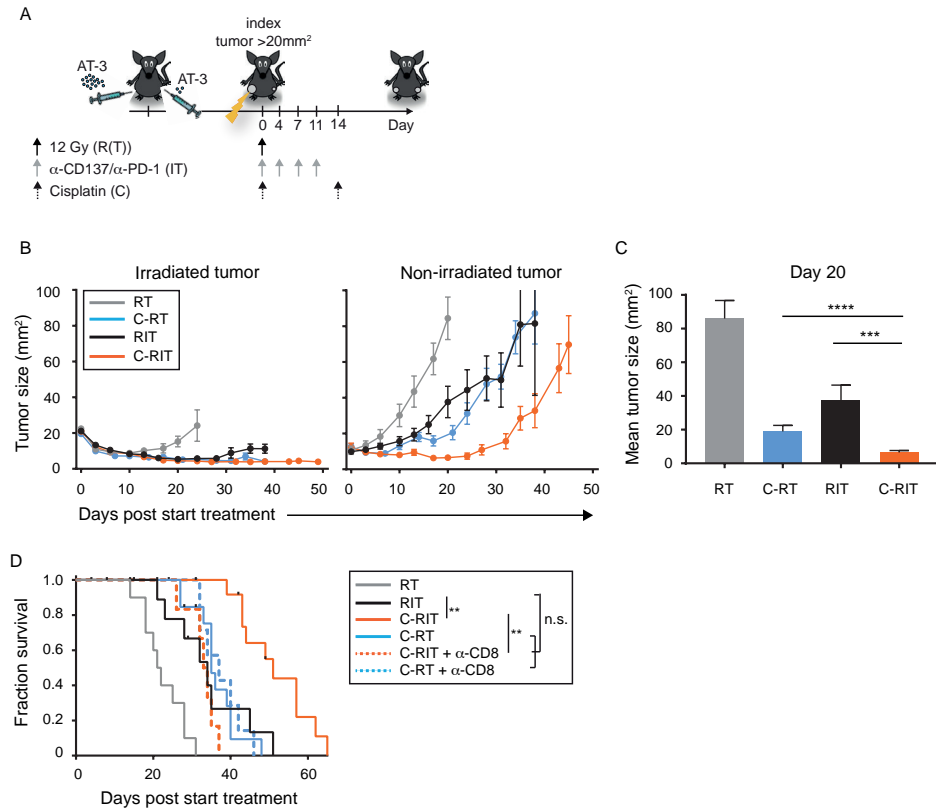


Figure 6. Cisplatin increases the therapeutic efficacy of RIT.

(A) Experimental set-up. (B) Mean tumor growth (SEM) of irradiated and nonirradiated tumors. Mean tumor size (\pm SEM) of nonirradiated tumors on day 20 (C) and survival curves of the indicated groups of mice; where indicated a CD8-depleting antibody (α -CD8) was administered one day before the start of treatment (D). Data shown are pooled data from 3 independent experiments of 4–7 mice/group in each experiment. ** $P < 0.01$; ***, $P < 0.001$; ****, $P < 0.0001$; n.s., not significant.

Discussion

There is an unmet clinical need to improve responses to PD-1 blockade, which currently forms the backbone for IT combinations². The PD-1 coinhibitory receptor is associated with tyrosine phosphatase activity that inhibits CD3/CD28 signalling⁸. In this way, the PD-1 ‘checkpoint’ can impede both T-cell priming and effector function. In patients with cancer, PD-1 blockade thus far seems to primarily relieve effector T cells from PD-L1/2-based suppression in the TME²⁸. Therefore, this approach is likely to be most effective as standalone treatment for immunogenic cancers in which T cells have already infiltrated the tumor²⁹. IT of poorly immunogenic cancers that have not raised a T-cell response will by definition require interventions that induce tumor-specific T-cell priming. Even in immunogenic cancers that respond to PD-1 blockade alone, new T-cell priming

is expected to strengthen and broaden the anti-tumor immune response, thereby increasing efficacy and combatting resistance⁶. In addition, immune suppression within the TME will preexist in immunogenic tumors and may develop in poorly immunogenic tumors once a T-cell response is raised, resulting from negative feedback control. PD-1/PD-L1 interactions are only a small part of this feedback control, which is exerted by diverse immune- and nonimmune cells in the TME. Effective antitumor immunity requires both priming of tumor-specific T-cells and a CTL-permissive TME. Here, we show that RT and conventional chemotherapy can promote intratumoral CTL activity by modulating the TME and by synergizing with an IT that enables T-cell priming.

We here identified that the murine AT-3 breast cancer cell line carries a foreign antigen MHC class I-restricted antigen 'SNPTY SVM'. Few T cells were present within AT-3 tumors at steady-state. PD-1 blockade alone had no therapeutic effect, but CD137 agonism induced CTL priming and anti-tumor immunity. CD137 triggering on activated CD8⁺ T cells stimulates proliferation, survival and possibly effector differentiation¹⁵, supporting CTL priming. Furthermore, CD137 triggering on DCs and other myeloid cell types can lead to the upregulation of costimulatory ligands CD80/CD86 (e.g.³⁰), which may help to overcome peripheral tolerance and induce T-cell responses to tumor antigens. In the TME, CD137 agonism may support CTL function by similar mechanisms. CD137 mAb can also stimulate hypoxic, CD137-expressing endothelial cells to recruit T cells into the tumor³¹. We found that PD-1 blockade aided CD137-stimulated CTL priming, supporting evidence that the PD-1 checkpoint can also limit T-cell priming, as observed previously (e.g.³²).

We predict that combining PD-1 blockade with any form of immunomodulation that induces CTL priming will be generally useful clinically. CTLA-4 blockade (e.g.²⁴) and CD27 agonism³³ can exert similar effects in distinct tumor models. In our current study and previous ones^{19,20,34}, agonistic antibody to CD137 administered either intratumorally or intraperitoneally, did not lead to weight loss or other overt pathology of the mice in the context of RIT. In humans, in which CD137 agonist antibody is applied systemically, combination with PD-1 blockade has comparable side-effects as PD-1 blockade alone, suggesting the approach is feasible¹⁴.

In the IT setting with combined PD-1 blockade and CD137 agonism, AT-3 tumors were not eliminated, despite a robust CTL response. In adoptive tumor-specific T-cell therapy, a robust CTL response is often also not sufficient for tumor control³⁵, highlighting that CTL suppression in the TME can pose an additional bottleneck for systemic antitumor immunity. Our study demonstrates that RT can alter the state of the TME to permit effective CTL activity, under conditions where PD-1 blockade cannot. Newly primed CTLs raised by our RIT protocol contributed to control of the irradiated tumor. Having a second, nonirradiated tumor in the same mouse allowed us to pinpoint the immune modulating effects of RT. The nonirradiated tumor was similarly infiltrated by newly primed CTLs as the irradiated tumor, but did not regress, indicating that impediments beyond

PD-1 signaling hampered abscopal tumor control. In a CT26 transplantable tumor model, control of the irradiated tumor by combined RT and PD-1 blockade was also found to be partly dependent on newly primed T cells. In that model, control of a simultaneously implanted nonirradiated tumor was also improved by PD-1 blockade³⁶. In that case, PD-1 signaling was the key impediment for CTL activity in the TME, whereas in our AT-3 model, additional impediments were in place. In PyMT-induced tumors, stimulation of TAMs with TLR7/9 agonists (imiquimod, CpG) allowed them to reactivate tumor-resident T cells³⁷. However, in the AT-3 model, the CTL-enabling effect of RT could not be reproduced by depletion of neutrophils or TAMs. TAMs can also phagocytose dead tumor cells and enable antigen cross-presentation by DCs. Altering the functional state of TAMs may be preferred over their depletion to enhance intratumoral CTL activity.

Comparative transcriptome analysis of cell populations from the irradiated and the nonirradiated tumors in the same mice revealed that a 'CTL-permissive' TME was associated mostly with changes in CTL-extrinsic, rather than CTL-intrinsic gene signatures. We did not identify gene sets within the CTLs that could explain enhanced efficacy in the irradiated tumor. This indicates that the intrinsic quality of the CTLs that infiltrated the irradiated and nonirradiated tumor after RIT is similar and of good quality, which we also validated by *ex vivo* flow cytometry. Differentially expressed genes identified in the CTLs were associated with negative regulation of cytokine production and included *Foxp3* and *Il10*. We speculate that this is an immune regulatory signature that arose in CTLs that experienced and survived RT. It is unlikely that this population contributed to enhanced tumor control. Instead, our data suggest that CTL-extrinsic parameters (an altered TME) were decisive for CTL efficacy in the irradiated tumor after RIT. The differentially expressed genes only allow speculation regarding the mechanisms involved. Increased vasculogenesis identified in the irradiated tumor did not alter CTL infiltration into the irradiated tumor as compared with the nonirradiated tumor, as measured 8 days after RIT. Reduced proliferation of the tumor cells might have improved CTL-mediated tumor cell death by allowing T cells more time to complete killing. Potential sensitization of tumor cells to apoptosis by upregulation of *Bax* may have contributed to increased CTL-mediated tumor control in the irradiated tumor. RNA- and ribosome-associated processes were upregulated in irradiated tumor/stromal cells, suggestive of increased protein synthesis. RT enhances protein synthesis in an mTOR-dependent manner and increases peptide presentation by MHC and tumor cell immunogenicity²⁷. We accordingly found that mTOR inhibition reduced the therapeutic efficacy of our RIT regimen²⁰. Finally, processes that were altered nontranscriptionally may have allowed increased CTL efficacy in the irradiated tumor in our experimental setting.

In the rapidly developing RIT field, tumor cell destruction by RT is seen as a mode of vaccination, due to the release of antigens and 'danger' signals. Thus, the field emphasizes the potential of RT to contribute to CTL priming, which may result in systemic antitumor immunity and 'abscopal effects'

on nonirradiated tumor masses, when adequately supported by additional interventions^{23,24,38}. RT may help to release danger-associated molecular patterns such as calreticulin or HMGB1 and/or cytosolic double-stranded DNA that can activate type I IFN signalling²⁴. Such signals activate DCs from a 'tolerogenic' into an 'immunogenic' state³⁹. In tumors that fail to deliver sufficient tumor antigens to DCs *de novo*, RT-induced debulking of the tumor could help to reach the 'antigen threshold' required for inducing a CTL response. Our study emphasizes that RT also modulates the TME to overcome T cell suppression. Combination of IT and RT may lead to regression of tumor masses outside of the field of radiation (e.g.^{40,41}). However, to qualify systemic tumor regression as 'abscopal' effect of RT, it is required that RT also contributes to the systemic treatment effect, that is, synergistic with IT. Most likely, this can only be achieved when T cells are newly primed as a result of the combined treatment and exert their cytotoxic activity within the nonirradiated tumor.

We show that low-dose cisplatin can facilitate CTL activity in nonirradiated AT-3 tumors in mice treated with PD-1/CD137 targeting therapy, thereby functionally mimicking the immunomodulatory effects of RT. On the basis of our findings, 're-purposing' cisplatin at low-dose as an immunomodulatory drug may help to convert a CTL-suppressive TME into a CTL-permissive one. It will be of interest to test whether the immunomodulating effects of RT and cisplatin that are revealed here and their effective combination with CD137/PD-1 targeting therapy can also lead to increased and systemic antitumor effects in other mouse tumor models, such as the poorly immunogenic *MMTV-PyMT* breast cancer⁴². In general, our findings indicate that systemic tumor control may be achieved by combining IT protocols that promote T cell-priming with chemoradiation protocols that permit CTL activity in both the irradiated tumor and (occult) metastases.

Materials and Methods

Cells

AT-3 cells are derived from the MMTV-Polyoma virus middle-T (PyMT) transgenic mouse, backcrossed to C57BL/6⁴² and were received from the Peter MacCallum Cancer Centre (Melbourne, Australia) in 2012. AT-3 cells were cultured in DMEM, supplemented with 10% fetal calf serum (FCS), 0.1 mmol/L nonessential amino acids, 1 mmol/L sodium pyruvate, 2 mmol/L L-glutamine, 10 mmol/L HEPES, and 30 μ mol/L β -mercaptoethanol at 37°C, 10% CO₂. AT-3 cells were tested negative for *Mycoplasma* by PCR, and cells thawed from this 'master stock' were routinely used within 6 passages (approximately 3 weeks) for *in vitro* and *in vivo* experiments. PyMT protein expression in AT-3 cells was validated by Western blot analysis, but the cells were not further authenticated in the past year.

Mice

Six-eight-week-old female C57BL/6JRj (B6) mice were obtained from Janvier Laboratories (Le Genest Saint Isle, France) or from in-house breeding within the Netherlands Cancer Institute (NKI, Amsterdam, the Netherlands) and maintained in individually ventilated cages (Innovive) under specific pathogen-free conditions. All mouse experiments were performed in accordance with institutional and national guidelines and were approved by the Committee for Animal Experimentation at the NKI.

Therapeutic antibodies and reagents

Agonistic rat anti-mouse CD137 (clone 3H3, IgG2a)⁴³ was purified from hybridoma supernatant by affinity chromatography on protein-G. Rat anti-mouse PD-1 mAb (clone RMP1-14, IgG2a) and isotype control (2A3) were purchased from BioXCell. FTY720 was purchased from Cayman Chemical and cisplatin Pharmachemie BV (RVG 101430).

Tumor transplantation and therapy

AT-3 cell transplantation and therapy were performed essentially as described previously^{19,20}, with minor modifications. Briefly, mice were anesthetized with isoflurane, and injected with 1×10^6 AT-3 cells into the fourth mammary fat pad. In some experiments, mice were injected with 0.5×10^6 AT-3 cells into this fat pad on one side and with 2.5×10^6 AT-3 cells on the contralateral flank. The latter tumor was irradiated, and the other tumor served as the non-irradiated 'abscopal' tumor. Tumor size was measured using a caliper, and treatment was initiated when the tumors reached 20-25mm². Therapy was done with n=5-10 mice per group. RT was applied using an XRAD225-Cx system (Precision X-Ray), as described previously^{20,34}. In brief, the mice were anesthetized with

isoflurane and a cone-beam CT scan of the mice was performed. The tumor(s) were localized on the CT scan and targeted with RT at 0.1-mm precision using round collimators 1.0 or 1.5 cm in diameter. A single fraction of 10-12 Gy (225 peak kilovoltage (kVp), filtered with 0.3 mm of copper (3 Gy/minute) was delivered. Control mice were anesthetized and underwent a cone-beam CT scan, but were not exposed to RT. Immunomodulatory mAbs toPD-1 and CD137 or an isotype control mAb were diluted in PBS. The antibodies were administered twice weekly for 2 weeks either intraperitoneally (PD-1 mAb, 100 µg per injection), or intratumorally (CD137 mAb, 25 µg in 10 µl per injection), with the first dose delivered immediately after RT treatment. For some experiments, cisplatin was administered intravenously at 4 mg/kg on day 0 (i.e., immediately after RT) and on day 14. Tumor transplantation and therapy for RNAseq experiments was performed identically, with the exception that CD137 mAb was delivered i.p. (100 µg). The sphingosine-1-phosphate receptor-1 agonist FTY720 was diluted in saline (vehicle) and administered at 2 mg/kg by oral gavage. FTY720 treatment started one day prior to RT and was repeated three times per week throughout the duration of the experiment. All mice were sacrificed when the tumor(s) reached 100-200 mm². A tumor size of 100 mm² was set at a designated end point.

DNA vaccination

The DNA vaccination vector 'SIG-HELP-SNPTY SVM.KDEL' was generated by ligating annealed codon-optimized oligos (FW: 5'TCGAGAGCAACCCACCTACAGCGTGATGAAGGACGAGCTGTAATAAT3' and RV: 5'CTAGATTATTACAGCTCGTCCTTCATCACGCTGTAGGTGGGGTTGCTC3') encoding SNPTY SVM.KDEL and *XhoI* and *XbaI* restriction sites in the *XhoI/XbaI* linearized pVax-HELP vector designed by Oosterhuis and colleagues²⁵, and described in detail by Ahrends and colleagues³³. For DNA vaccination, the hair on a hind leg was removed using depilating cream (Veet; Reckitt Benckiser) on day -1. On days 0, 3 and 6, the mice were anesthetized with isoflurane, and 15 µl of a solution containing 2 mg/ml plasmid DNA in 10 mmol/L Tris and 1 mmol/L EDTA, pH 8.0, was applied to the hairless skin with a Permanent Make-up Up Tattoo machine (MT Derm GmbH), using a sterile disposable 9-needle bar with a needle depth of 1 mm and an oscillating frequency of 100 Hz for 45 seconds.

Flow cytometry

At the indicated time points, tumor-bearing mice were sacrificed, and tumor and lymphoid tissue were harvested. The tumors were mechanically chopped using a McIlwain tissue chopper (Mickle Laboratory Engineering) and a single-cell suspension was prepared by digesting the tissue in collagenase type A (Roche) and 25 µg/ml DNase (Sigma) in serum-free DMEM medium for 45 min at 37°C. Enzyme activity was neutralized by addition of DMEM containing 8% FCS, and the tissue was dispersed by passing through a 70-µm cell strainer. Single cells were first stained with PE- or APC-conjugated H-2K^b PyMT₂₄₆₋₂₅₃ (SNPTY SVM) tetramers for 15 min at 20°C in the dark. For

surface staining, cells were incubated with Fc receptor antibody (1:50, clone 2.4G2), followed by fluorochrome-conjugated antibodies (see below) for 30 min on ice in the dark in PBS containing 0.5% BSA and 0.01% sodium azide. Intracellular staining following restimulation with PMA and ionomycin was performed as described previously²⁰. 7AAD (1:20; eBioscience) or Fixable Viability Dye eFluor 780 (1:1000; eBioscience), Zombie Red Fixable Viability Kit (1:5000, Biolegend) or DAPI (Invitrogen) was added to exclude dead cells. All experiments were analyzed using a BD LSRII, BD Fortessa or BD Symphony A5 flow cytometer with Diva software and the generated data were analyzed using FlowJo software.

Fluorochrome-conjugated mAbs with the following specificities were used for flow cytometry and obtained from BD Pharmingen unless otherwise specified: CD8-FITC (1:100, clone 56-6.7), CD4-eFluor450 (1:200, clone GK1.5), TCR β -PECy5 (1:200; clone H57-597), CD43-PerCPCy5.5 (1:200, clone 1B11 (BioLegend, San Diego, CA)), CD45.2-eFluor605 (1:50; clone 30-F11), CD4-FITC (1:100, clone GK1.5), CD8-V450 (1:300, clone 56-6.7), CD11b-AF700 (1:200, clone M1/70), CD8-AF700 (1:200, clone 56-6.7), IFN γ -APC (1:100, clone XMG1.2), TNF α -PECy7 (1:200, clone MP6-XT22), CD4-BV711 (1:200, clone GK1.5), CD8 α -PerCPCy5.5 (1:200, clone 56-6.7), CD3 ϵ -PECy7 (1:50, clone 145-2C11), NK1.1-APC-eFluor780 (1:200, clone PK136), CD11b-BV786 (1:400, clone M1/70), FOXP3-APC (1:50, clone FJK-165), Ly6C-eFluor450 (1:400, clone HK1.4), Ly-6G-AF700 (1:200, clone 1A8), CD45-BUV395 (1:200, clone 3-F11), PE (1 μ l/sample, clone PE001), I-A/I-E-AF700 (1:400, Clone M5/114.15.2, BioLegend), CD11c-PECy7 (1:200, clone HL3), XCR1-PerCPCy5.5 (1:200, Clone ZET, BioLegend), CD11b-BUV395 (1:50, Clone M1/70), CD45-BUV563 (1:200, clone 3-F11), CD45R/B220-eFluor450 (1:200, clone RA3-6B2), CD103-BV711 (1:50, clone M290), and F4/80-BV510 (1:50, clone BM8, BioLegend).

Within the live, single, CD45⁺ cells, we gated and defined the cell populations as follows: CD8⁺ T cells (TCR β ⁺CD8⁺), CD4⁺ T cells (TCR β ⁺CD4⁺), Tumor-associated macrophages (TAMs, F4/80⁺MHCII⁺), Neutrophils (Ly6G⁺Ly6C^{int}), inflammatory monocytes (Ly6G⁺Ly6C^{hi}, as described in e.g.⁴⁴, NK cells (NK1.1⁺CD3⁻), NKT cells (NK1.1⁺CD3⁺), CD103⁺ DCs (F4/80⁻CD11c⁺MHCII⁺CD103⁺), CD11b⁺ DCs (F4/80⁻CD11c⁺MHCII⁺CD11b⁺).

Prediction of PyMT peptides and generation of PyMT-H-2K^b/D^b multimers

To identify AT-3 tumor antigens, we first used epitope prediction tools to define PyMT-derived peptides that could potentially bind to H-2K^b and/or H-2D^b MHC class I molecules. These peptides were then synthesized by the peptide facility at the NKI (Amsterdam, the Netherlands), and MHC tetramers were produced by UV-induced peptide exchange as described previously⁴⁵. In brief, 28 peptides of PyMT (protein ID: NP_041265.1) predicted to bind either H-2K^b or H-2D^b (NetPan MHC 3.0 and NetPan MHC 4.0) were synthesized by the peptide facility at the NKI. These peptides were

individually exchanged into H-2K^b or H-2D^b molecules that had been refolded with a UV-sensitive peptide, allowing the generation of monomers with multiple specificities via a single reaction⁴⁵. The resulting monomers were subsequently multimerized and conjugated to phycoerythrin (PE) or allophycocyanin (APC) and then used to screen for T-cell reactivity to MHC I-restricted PyMT epitopes using flow cytometry.

RNA preparation and sequencing

Using flow cytometry, CD43⁺ CD8⁺ T cells ('CTLs'), CD45⁺ hematopoietic cells, and CD45⁻ (tumor/stromal) cells were isolated from both the irradiated and non-irradiated tumors of 9 mice per experimental group, and material from 3 mice was pooled per sample to retrieve sufficient RNA. Cells were collected in RLT lysis buffer (QIAGEN) and total RNA was extracted using the RNeasy mini kit (QIAGEN) in accordance with the manufacturer's instructions. The integrity of the total RNA was assessed using a 2100 Bioanalyzer System (Agilent). Only RNA samples with an RNA Integrity Number (RIN) > 8 were used to create the library. Poly-A-selected RNA libraries were prepared using the TruSeq RNA library protocol (Illumina) and the resulting libraries were sequenced using an Illumina HiSeq2500 with V4 chemistry, with 50-bp single-end reads per lane.

Transcriptomics analysis of illumina sequencing data

Sequencing reads in FASTQ files were mapped to the mouse genome (build GRCm38.77) using Tophat v2.1⁴⁶, and the read summarization program HTseq-count⁴⁷ was used to count uniquely mapped reads against annotated genes. Differential expression analysis was performed using the DESeq2 package in R⁴⁸. *P*-values were corrected for multiple comparisons, based on the False Discovery Rate (FDR), with significance considered at a *q*-value <0.01. Volcano plots were generated using ggplot2 (<https://www.springer.com/gp/book/9780387981413>).

Normalized read counts were used as input for Gene Ontology (GO) Gene Set Enrichment Analysis (GSEA) version 3.0^{49,50} to identify groups of biological processes that were differentially expressed between cell populations obtained from the irradiated site and cell populations obtained from the nonirradiated site. We used the MSigDB C5 collection to identify enriched GO biological processes (BP). GSEA was performed with default parameters and gene set permutations were used. To gain a better overview of the linked biological processes, we generated enrichment maps using the Enrichment Map app v3.1.0, using cut-off values set at Q = 0.1 and Jaccard Overlap Combined = 0.375. We illustrated the largest gene set clusters and manually assigned the more general processes that these clusters represent.

The RNA-seq data reported in this paper have been deposited in the ArrayExpress database at EMBL-EBI (www.ebi.ac.uk/arrayexpress) under accession number E-MTAB-6914.

Immunohistochemical analysis

Harvested tumors were fixed for 24 h in ethanol (50%), acetic acid (5%), and formalin (3.7%), embedded in paraffin, and then sectioned randomly at 5 μm . The sections were then stained as described previously³⁴. In brief, fixed sections were rehydrated and then incubated with primary antibodies to CD8 (eBioscience; clone 4SM15) and Foxp3 (eBioscience; clone FJK-16s). Endogenous peroxidases were blocked with 3% H_2O_2 and the sections were then incubated with biotin-conjugated secondary antibodies, followed by incubation with HRP-conjugated streptavidin-biotin (DAKO). The substrate was developed using diaminobenzidine (DAB; DAKO). We included negative controls to determine background staining, which was negligible. The stained sections were digitally processed using an Aperio ScanScope (Aperio) equipped with a 20x objective. ImageJ software was used to quantify the number of positive cells in 3-5 random fields of view (FOV) per slide.

Statistical Analysis

All summary data were analyzed using GraphPad Prism version 6 (GraphPad Software). Differences between various treatment groups were analyzed using the Mann-Whitney *U* Test. Differences in survival curves were analyzed using the Log Rank (Mantel-Cox) test. Differences with *P*-value <0.05 were considered statistically significant.

Disclosure of Potential Conflicts of Interest

No potential conflicts of interest were disclosed.

Authors' Contributions

Conception and design: P. Kroon, M. Verheij, J. Borst, I. Verbrugge
Development of methodology: P. Kroon, T.N. Schumacher

Acquisition of data (provided animals, acquired and managed patients, provided facilities, etc.): P. Kroon, E. Frijlink, V. Iglesias-Guimaraes, I. Verbrugge

Analysis and interpretation of data (e.g., statistical analysis, biostatistics, computational analysis): P. Kroon, E. Frijlink, V. Iglesias-Guimaraes, A. Volkov, M.M. Van Buuren, J. Borst, I. Verbrugge

Writing, review, and/or revision of the manuscript: P. Kroon, E. Frijlink, A. Volkov, M.M. Van Buuren, M. Verheij, J. Borst, I. Verbrugge
Administrative, technical, or material support (i.e., reporting or organizing data, constructing databases): P. Kroon, E. Frijlink

Study supervision: J. Borst, I. Verbrugge

Acknowledgments

We thank animal facility personnel for mouse husbandry, J.-J. Sonke and A. Khmelinskii for help in the small-animal radiotherapy facility, the Intervention Unit for help with the mouse experiments, R. Kerkhoven, A. Velds, M. Nieuwland, and I. de Rink of the genomics core facility for assistance and bioinformatics support with RNA sequencing, H. Yagita (Juntendo School of Medicine, Tokyo, Japan) for anti-CD137 (3H3), M. Toebe for assistance in generating tetramers, H. Hilkmann and D. El Atmioui at the Peptide Production Facility for generating the peptides, J. Walker and N. Goense for technical assistance, K. de Visser and the Borst laboratory for helpful discussions, M. van den Broek for critical reading of the manuscript. Supported by the Dutch Cancer Society (grants NKI 2013-5951, 10764, to I. Verbrugge; 10894, to I. Verbrugge and J. Borst) and a Health Holland public-private partnership grant in collaboration with Elekta (grant LSHM15036; to J.-J. Sonke).

References

- 1 Iwai, Y., Hamanishi, J., Chamoto, K. & Honjo, T. Cancer immunotherapies targeting the PD-1 signaling pathway. *Journal of biomedical science* **24**, 26 (2017).
- 2 Sharma, P., Hu-Lieskovan, S., Wargo, J. A. & Ribas, A. Primary, Adaptive, and Acquired Resistance to Cancer Immunotherapy. *Cell* **168**, 707-723 (2017).
- 3 Buchbinder, E. I. & Desai, A. CTLA-4 and PD-1 Pathways: Similarities, Differences, and Implications of Their Inhibition. *American journal of clinical oncology* **39**, 98-106 (2016).
- 4 Melssen, M. & Slingluff, C. L., Jr. Vaccines targeting helper T cells for cancer immunotherapy. *Current opinion in immunology* **47**, 85-92 (2017).
- 5 Chen, D. S. & Mellman, I. Oncology meets immunology: the cancer-immunity cycle. *Immunity* **39**, 1-10 (2013).
- 6 Spitzer, M. H. *et al.* Systemic Immunity Is Required for Effective Cancer Immunotherapy. *Cell* **168**, 487-502 e415 (2017).
- 7 Munn, D. H. & Bronte, V. Immune suppressive mechanisms in the tumor microenvironment. *Current opinion in immunology* **39**, 1-6 (2016).
- 8 Hui, E. *et al.* T cell costimulatory receptor CD28 is a primary target for PD-1-mediated inhibition. *Science* **355**, 1428-1433 (2017).
- 9 Krummel, M. F. & Allison, J. P. CD28 and CTLA-4 have opposing effects on the response of T cells to stimulation. *The Journal of experimental medicine* **182**, 459-465 (1995).
- 10 Wei, S. C. *et al.* Distinct Cellular Mechanisms Underlie Anti-CTLA-4 and Anti-PD-1 Checkpoint Blockade. *Cell* **170**, 1120-1133 e1117 (2017).
- 11 Kvistborg, P. *et al.* Anti-CTLA-4 therapy broadens the melanoma-reactive CD8+ T cell response. *Science translational medicine* **6**, 254ra128 (2014).
- 12 Sznol, M. *et al.* Pooled Analysis Safety Profile of Nivolumab and Ipilimumab Combination Therapy in Patients With Advanced Melanoma. *Journal of clinical oncology : official journal of the American Society of Clinical Oncology* **35**, 3815-3822 (2017).
- 13 Makkouk, A., Chester, C. & Kohrt, H. E. Rationale for anti-CD137 cancer immunotherapy. *European journal of cancer* **54**, 112-119 (2016).
- 14 Tolcher, A. W. *et al.* Phase Ib Study of Utomilumab (PF-05082566), a 4-1BB/CD137 Agonist, in Combination with Pembrolizumab (MK-3475) in Patients with Advanced Solid Tumors. *Clinical cancer research : an official journal of the American Association for Cancer Research* **23**, 5349-5357 (2017).
- 15 Bartkowiak, T. & Curran, M. A. 4-1BB Agonists: Multi-Potent Potentiators of Tumor Immunity. *Frontiers in oncology* **5**, 117 (2015).
- 16 Galluzzi, L., Buque, A., Kepp, O., Zitvogel, L. & Kroemer, G. Immunogenic cell death in cancer and infectious disease. *Nat Rev Immunol* **17**, 97-111 (2017).
- 17 Abuodeh, Y., Venkat, P. & Kim, S. Systematic review of case reports on the abscopal effect. *Curr Probl Cancer* **40**, 25-37 (2016).
- 18 van der Sluis, T. C. *et al.* Vaccine-induced tumor necrosis factor-producing T cells synergize with cisplatin to promote tumor cell death. *Clinical cancer research : an official journal of the American Association for Cancer Research* **21**, 781-794 (2015).
- 19 Verbrugge, I. *et al.* Radiotherapy increases the permissiveness of established mammary tumors to rejection by immunomodulatory antibodies. *Cancer Res* **72**, 3163-3174 (2012).
- 20 Verbrugge, I. *et al.* The curative outcome of radioimmunotherapy in a mouse breast cancer model relies on mTOR signaling. *Radiation research* **182**, 219-229 (2014).

- 21 Jones, A. T. *et al.* Characterization of the activation-associated isoform of CD43 on murine T lymphocytes. *Journal of immunology* **153**, 3426-3439 (1994).
- 22 Matloubian, M. *et al.* Lymphocyte egress from thymus and peripheral lymphoid organs is dependent on S1P receptor 1. *Nature* **427**, 355-360 (2004).
- 23 Dewan, M. Z. *et al.* Fractionated but not single-dose radiotherapy induces an immune-mediated abscopal effect when combined with anti-CTLA-4 antibody. *Clin Cancer Res* **15**, 5379-5388 (2009).
- 24 Vanpouille-Box, C. *et al.* DNA exonuclease Trex1 regulates radiotherapy-induced tumour immunogenicity. *Nat Commun* **8**, 15618 (2017).
- 25 Oosterhuis, K., Aleyd, E., Vrijland, K., Schumacher, T. N. & Haanen, J. B. Rational design of DNA vaccines for the induction of human papillomavirus type 16 E6- and E7-specific cytotoxic T-cell responses. *Human gene therapy* **23**, 1301-1312 (2012).
- 26 Coffelt, S. B., Wellenstein, M. D. & de Visser, K. E. Neutrophils in cancer: neutral no more. *Nature reviews. Cancer* **16**, 431-446 (2016).
- 27 Reits, E. A. *et al.* Radiation modulates the peptide repertoire, enhances MHC class I expression, and induces successful antitumor immunotherapy. *J Exp Med* **203**, 1259-1271 (2006).
- 28 Herbst, R. S. *et al.* Predictive correlates of response to the anti-PD-L1 antibody MPDL3280A in cancer patients. *Nature* **515**, 563-567 (2014).
- 29 Ayers, M. *et al.* IFN-gamma-related mRNA profile predicts clinical response to PD-1 blockade. *J Clin Invest* **127**, 2930-2940 (2017).
- 30 Futagawa, T. *et al.* Expression and function of 4-1BB and 4-1BB ligand on murine dendritic cells. *International immunology* **14**, 275-286 (2002).
- 31 Palazon, A. *et al.* The HIF-1alpha hypoxia response in tumor-infiltrating T lymphocytes induces functional CD137 (4-1BB) for immunotherapy. *Cancer discovery* **2**, 608-623 (2012).
- 32 Probst, H. C., McCoy, K., Okazaki, T., Honjo, T. & van den Broek, M. Resting dendritic cells induce peripheral CD8+ T cell tolerance through PD-1 and CTLA-4. *Nat Immunol* **6**, 280-286 (2005).
- 33 Ahrends, T. *et al.* CD27 Agonism Plus PD-1 Blockade Recapitulates CD4+ T-cell Help in Therapeutic Anticancer Vaccination. *Cancer Res* **76**, 2921-2931 (2016).
- 34 Kroon, P. *et al.* Concomitant targeting of programmed death-1 (PD-1) and CD137 improves the efficacy of radiotherapy in a mouse model of human BRAFV600-mutant melanoma. *Cancer immunology, immunotherapy : CII* **65**, 753-763 (2016).
- 35 Baruch, E. N., Berg, A. L., Besser, M. J., Schachter, J. & Markel, G. Adoptive T cell therapy: An overview of obstacles and opportunities. *Cancer* **123**, 2154-2162 (2017).
- 36 Dovedi, S. J. *et al.* Fractionated radiation therapy stimulates anti-tumor immunity mediated by both resident and infiltrating polyclonal T-cell populations when combined with PD1 blockade. *Clinical cancer research : an official journal of the American Association for Cancer Research* (2017).
- 37 Engelhardt, J. J. *et al.* Marginating dendritic cells of the tumor microenvironment cross-present tumor antigens and stably engage tumor-specific T cells. *Cancer cell* **21**, 402-417 (2012).
- 38 Rodriguez-Ruiz, M. E. *et al.* Abscopal Effects of Radiotherapy Are Enhanced by Combined Immunostimulatory mAbs and Are Dependent on CD8 T Cells and Crosspriming. *Cancer research* **76**, 5994-6005 (2016).
- 39 Gupta, A. *et al.* Radiotherapy promotes tumor-specific effector CD8+ T cells via dendritic cell activation. *J Immunol* **189**, 558-566 (2012).
- 40 Twyman-Saint Victor, C. *et al.* Radiation and dual checkpoint blockade activate non-redundant immune mechanisms in cancer. *Nature* **520**, 373-377 (2015).

- 41 Kwon, E. D. *et al.* Ipilimumab versus placebo after radiotherapy in patients with metastatic castration-resistant prostate cancer that had progressed after docetaxel chemotherapy (CA184-043): a multicentre, randomised, double-blind, phase 3 trial. *Lancet Oncol* **15**, 700-712 (2014).
- 42 Stewart, T. J. & Abrams, S. I. Altered immune function during long-term host-tumor interactions can be modulated to retard autochthonous neoplastic growth. *Journal of immunology* **179**, 2851-2859 (2007).
- 43 Shuford, W. W. *et al.* 4-1BB costimulatory signals preferentially induce CD8+ T cell proliferation and lead to the amplification in vivo of cytotoxic T cell responses. *The Journal of experimental medicine* **186**, 47-55 (1997).
- 44 Franklin, R. A. *et al.* The cellular and molecular origin of tumor-associated macrophages. *Science* **344**, 921-925 (2014).
- 45 Toebe, M. *et al.* Design and use of conditional MHC class I ligands. *Nature medicine* **12**, 246-251 (2006).
- 46 Trapnell, C., Pachter, L. & Salzberg, S. L. TopHat: discovering splice junctions with RNA-Seq. *Bioinformatics* **25**, 1105-1111 (2009).
- 47 Anders, S., Pyl, P. T. & Huber, W. HTSeq--a Python framework to work with high-throughput sequencing data. *Bioinformatics* **31**, 166-169 (2015).
- 48 Love, M. I., Huber, W. & Anders, S. Moderated estimation of fold change and dispersion for RNA-seq data with DESeq2. *Genome Biol* **15**, 550 (2014).
- 49 Subramanian, A. *et al.* Gene set enrichment analysis: a knowledge-based approach for interpreting genome-wide expression profiles. *Proceedings of the National Academy of Sciences of the United States of America* **102**, 15545-15550 (2005).
- 50 Mootha, V. K. *et al.* PGC-1alpha-responsive genes involved in oxidative phosphorylation are coordinately downregulated in human diabetes. *Nat Genet* **34**, 267-273 (2003).

Supplementary Data

Table S1 can be accessed under the following link:

<https://aacrjournals.org/cancerimmunolres/article/7/4/670/469504/Radiotherapy-and-Cisplatin-Increase-Immunotherapy>

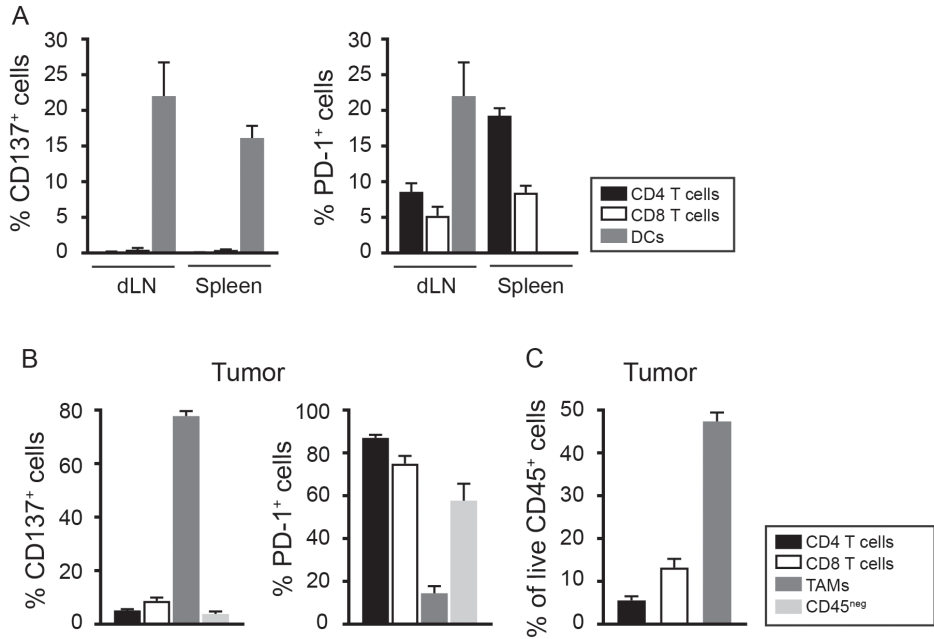


Figure S1. Related to Figure 1. Expression of the immunotherapy targets CD137 and PD-1 in AT-3 tumor-bearing mice. AT-3 tumor-bearing mice (n=3) were sacrificed, and the indicated tissues were harvested. **(A)** Percentage CD137⁺ and PD-1⁺ cells in the CD4⁺T (TCRβ⁺CD4⁺), CD8⁺T (TCRβ⁺CD8⁺), and dendritic cell (DC; CD11c⁺MHCII⁺) populations measured in the tumor draining lymph node (dLN) and spleen. **(B)** Percentage of CD137⁺ and PD-1⁺ cells in the indicated cell populations isolated from the tumor tissue. TAMs; tumor-associated macrophages. **(C)** Percentage of CD4⁺, CD8⁺T cells and TAMs within the CD45⁺ population isolated from the tumor tissue.

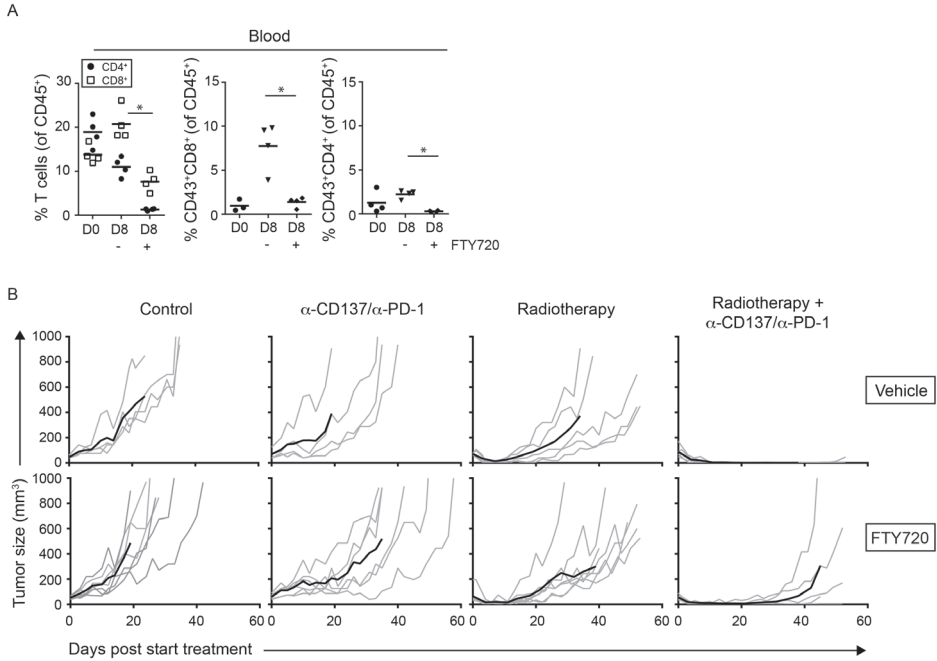


Figure S2. Related to Figure 2. Depletion of effector phenotype T cells from the circulation following RIT combined with FTY720 treatment.

(A) Mice (3-4 per group) bearing an established AT-3 tumor (>20mm²) received either saline or FTY720 3x weekly in combination with RIT (see Figure 2A for the experimental set-up). The percentage of the (CD43⁺) CD4⁺ and CD8⁺ T cells within the CD45⁺ population was measured in the blood before (D0) or 8 days after (D8) the start of RIT. (B) Tumor growth curves of the AT-3 tumor-bearing mice (4-5 per group) receiving radiotherapy (10 Gy), immunotherapy (α -CD137/ α -PD-1 mAbs) alone or in combination or mock-treatment, in presence or absence of FTY720; grey lines: individual tumor growth curves, black lines: average of the group.

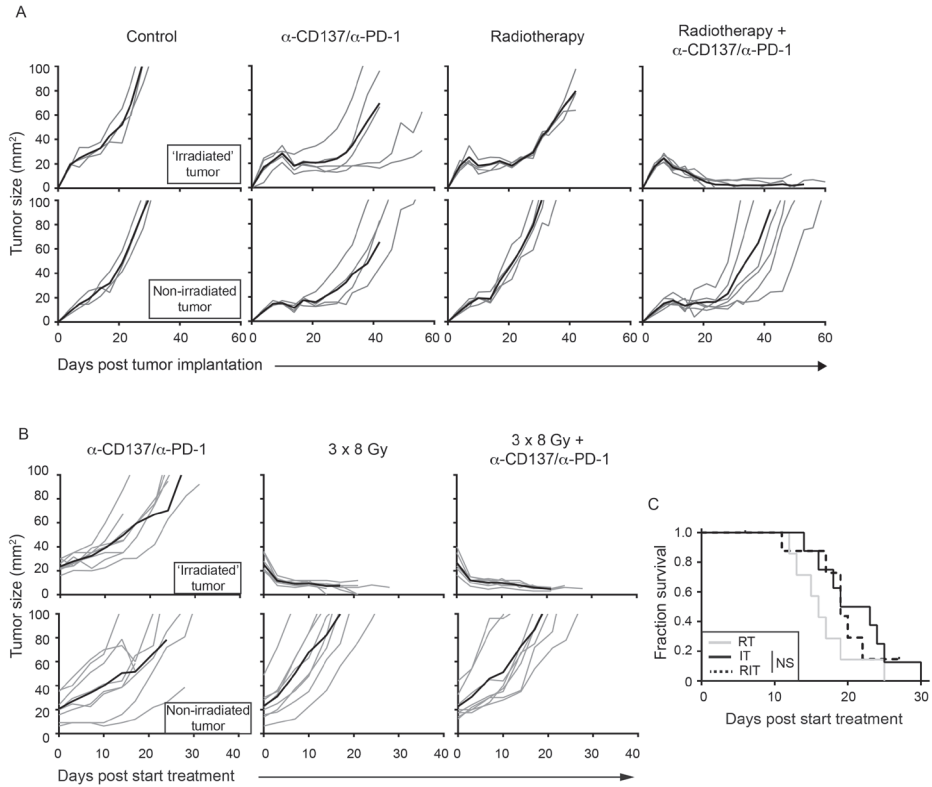


Figure S3. Related to Figure 3. Time course of tumor size following radio-immunotherapy delivered as one dose or in 3x 8 Gy fractions.

(A and B) Time course of tumor size in mice treated as indicated. In each plot, the gray and black lines represent individual tumors and the mean of the group, respectively. (C) Survival curve of mice bearing bilateral AT-3 tumors, treated radiotherapy (RT: 3x 8 Gy) alone, immunotherapy alone (IT), or both RT and IT (RIT).

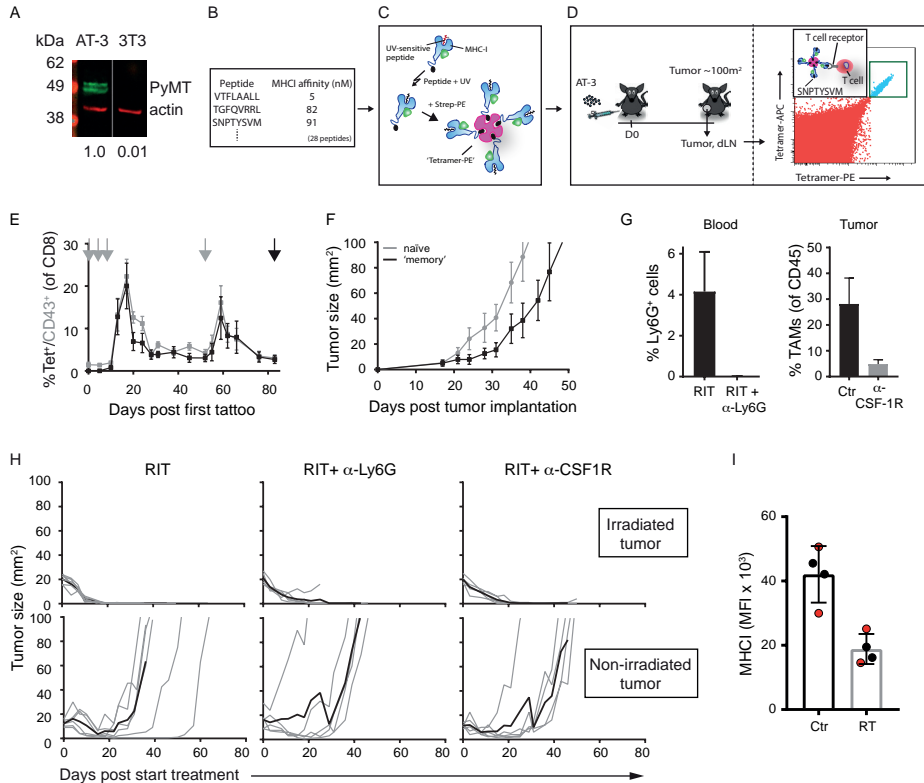


Figure S4. Related to Figure 4. Identification of an AT-3 tumor specific (CD8) T cell epitope, and targeting either Ly6G or CSF1R does not improve RIT-mediated control of non-irradiated tumor.

(A) PyMT and actin immunoblot AT-3 or 3T3 cell lysates. Note that the left and right lanes are from the same blot and the relative PyMT expression levels are shown below the image. (B) A total of 28 PyMT peptides that are predicted to bind to MHC-I with the indicated affinity were synthesized; note that only the three peptides with the highest affinity are shown. (C) Peptide-MHC multimers (“tetramers”) were generated for the 28 peptides as shown. (D) CD8⁺ T cells from the AT-3 tumor and dLN were analyzed for tetramer-binding, identifying SNPTYSVVM as a tumor antigen. (E-F; related to Figure 4A-D) Mice (6 per group) received SNPTYSVVM vaccination (for details see Figure 4A) on days 0,3, 6 and 52 (gray symbols). On day 83 (the black arrow), the mice were implanted with AT-3 tumor cells. (F) Time course of the tumor size of “memory” mice (i.e. the mice shown in Figure S4E that received DNA vaccination at the times indicated by the black arrow), and age-matched naïve mice (shown in gray lines) after implantation with 2×10^5 AT-3 tumor cells in the fourth mammary fat pad. (G; related to Figure 4G) Percentage of Ly6G⁺ (left) and TAMs (right) measured in the blood and tumor tissue of mice treated with RIT in the absence or presence of anti-Ly6G or anti-CSF-1R mAbs. (H) Time course of the size of the irradiated and non-irradiated tumors in the mice treated as indicated. The gray and black lines represent individual and average data, respectively, for the mice shown in Figure 4G. (I) MHC I expression on tumor/stromal cells (CD45⁺) from mice bearing irradiated (10:37 PM) and non-irradiated (Ctr) AT-3 tumors. Data shown is from Day 3 (red circles) and Day 8 (black circles) after treatment (2 mice per timepoint).

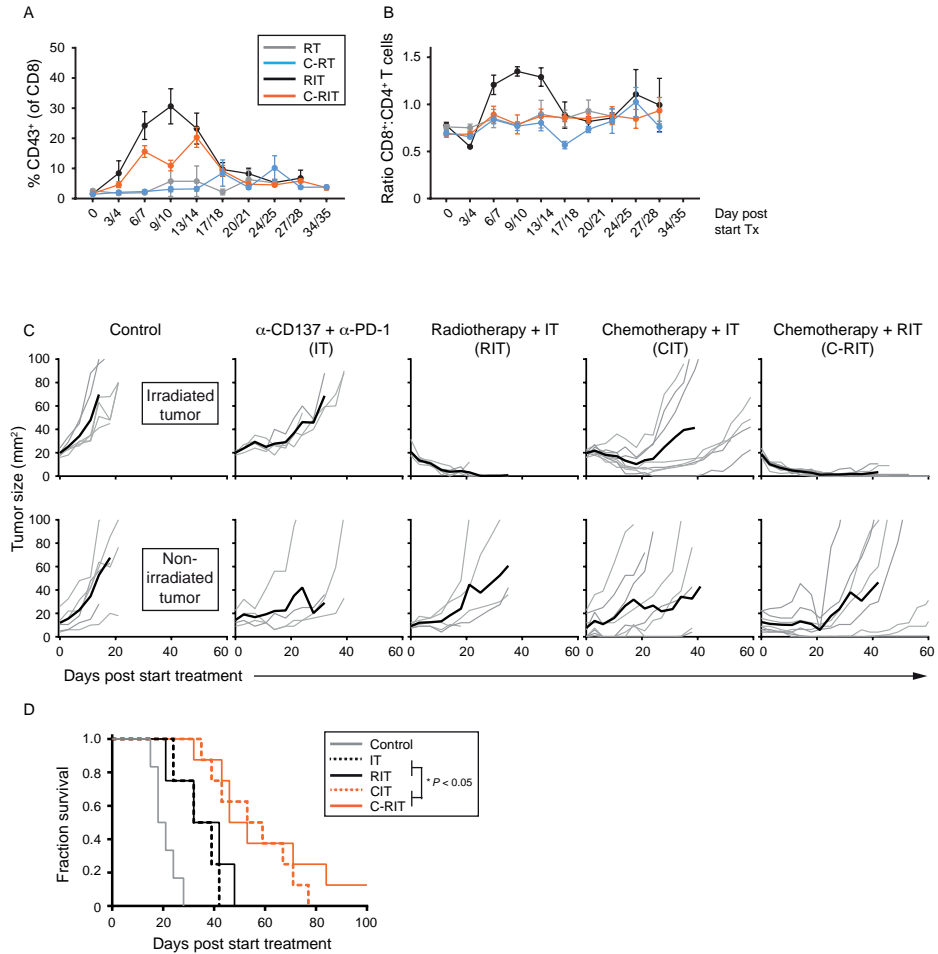
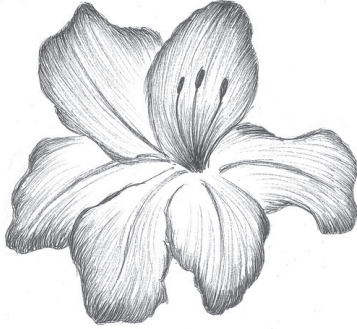
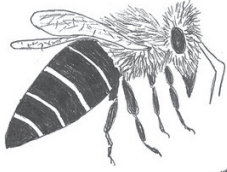


Figure S5. Related to Figure 6. Cisplatin modestly reduces the RIT-induced increase in CD8:CD4 T cell ratio and enhances (R)IT-mediated control of non-irradiated tumors.

Peripheral blood collected from the same mice shown in Figure 6B,C were analyzed for the percentage of CD43⁺ cells within the CD8⁺ T cell population (A) and the CD8⁺:CD4⁺ T cell ratio (B) on the indicated days. (C) Individual (grey lines) and average (black line) tumor growth curves and (D) survival curves of mice treated with the indicated therapies.



Autotaxin impedes anti-tumor immunity by suppressing chemotaxis and tumor infiltration of CD8⁺ T cells

Cell Reports. 2021;37(7): 110013

Elisa Matas-Rico,^{1,10,11,16,*} **Elselien Frijlink**,^{2,3,16} Irene van der Haar Àvila,^{2,3,12} Apostolos Menegakis,^{3,4} Maaïke van Zon,⁵ Andrew J. Morris,⁶ Jan Koster,⁷ Fernando Salgado-Polo,^{1,3} Sander de Kivit,^{2,3,13} Telma Lança,^{3,5} Antonio Mazzocca,⁸ Zoë Johnson,⁹ John Haanen,⁵ Ton N. Schumacher,^{3,5} Anastassis Perrakis,^{1,3} Inge Verbrugge,^{2,3,14} Joost H. van den Berg,^{5,15} Jannie Borst,^{2,3,13,17,*} and Wouter H. Moolenaar^{1,17,18,*}

¹Division of Biochemistry, Netherlands Cancer Institute, Amsterdam, the Netherlands

²Division of Tumor Biology and Immunology, Netherlands Cancer Institute, Amsterdam, the Netherlands

³Oncode Institute, Utrecht, the Netherlands

⁴Division of Cell Biology, Netherlands Cancer Institute, Amsterdam, the Netherlands

⁵Division of Molecular Oncology and Immunology, Netherlands Cancer Institute, Amsterdam, the Netherlands

⁶Division of Cardiovascular Medicine, Gill Heart Institute and Lexington Veterans Affairs Medical Center, University of Kentucky, Lexington, KY, USA

⁷Laboratory for Experimental Oncology and Radiobiology, Amsterdam UMC, Amsterdam, the Netherlands

⁸Interdisciplinary Department of Medicine, University of Bari School of Medicine, Bari, Italy

⁹Onctura SA, Campus Biotech Innovation Park, Geneva, Switzerland

¹⁰Present address: Department of Cell Biology, Genetics and Physiology, Málaga University, Málaga, Spain ¹¹Present address: Genitourinary Cancer Translational Research Group,

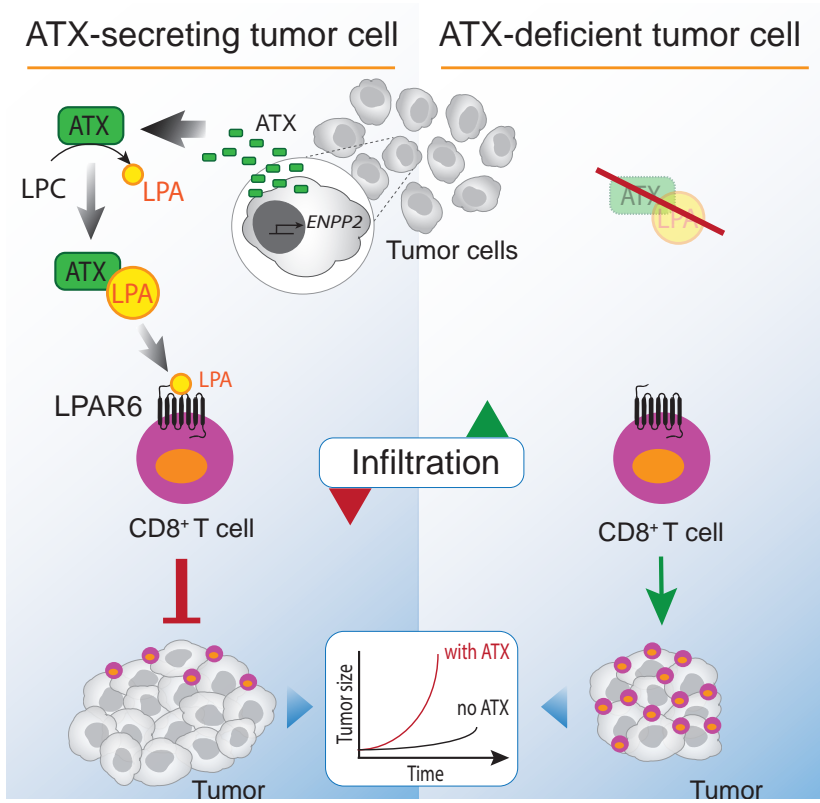
The Institute of Biomedical Research in Málaga (IBIMA), Málaga, Spain, ¹²Present address: Amsterdam UMC, Department of Molecular Cell Biology and Immunology, Amsterdam UMC,

Amsterdam, the Netherlands, ¹³Present address: Department of Immunology, Leiden University Medical Center, Leiden, the Netherlands, ¹⁴Present address: Janssen Pharmaceutica NV, Beerse,

Belgium, ¹⁵Present address: CellPoint BV, Oegstgeest, the Netherlands

¹⁶**These authors contributed equally**, ¹⁷Senior author, ¹⁸Lead contact.

Graphical Abstract



Abstract

Autotaxin (ATX; *ENPP2*) produces lysophosphatidic acid (LPA) that regulates multiple biological functions via cognate G protein-coupled receptors LPAR1-6. ATX/LPA promotes tumor cell migration and metastasis via LPAR1 and T cell motility via LPAR2, yet its actions in the tumor immune microenvironment remain unclear. Here, we show that ATX secreted by melanoma cells is chemorepulsive for tumor-infiltrating lymphocytes (TILs) and circulating CD8⁺ T cells *ex vivo*, with ATX functioning as an LPA-producing chaperone. Mechanistically, T cell repulsion predominantly involves G $\alpha_{12/13}$ -coupled LPAR6. Upon anti-cancer vaccination of tumor-bearing mice, ATX does not affect the induction of systemic T cell responses but, importantly, suppresses tumor infiltration of cytotoxic CD8⁺ T cells and thereby impairs tumor regression. Moreover, single-cell data from melanoma tumors are consistent with intratumoral ATX acting as a T cell repellent. These findings highlight an unexpected role for the pro-metastatic ATX-LPAR axis in suppressing CD8⁺ T cell infiltration to impede anti-tumor immunity, suggesting new therapeutic opportunities.

Introduction

Efficient infiltration of T cells into tumors is associated with positive outcome in several cancer types and determines the response to immunotherapies^{1,2}. Chemokines through their G protein-coupled receptors (GPCRs) are major drivers of T cell migration into tumors, thereby playing a crucial role in the immune response to cancer and influencing tumor fate³⁻⁵. However, tumors develop various strategies to exclude T cells and suppress T cell-mediated immunogenicity, for example via tumor-intrinsic chemokine silencing and production of immunosuppressive cytokines⁶⁻¹⁰. Yet, our understanding of factors that regulate the trafficking of tumor-infiltrating lymphocytes (TILs), either positively or negatively, is incomplete and requires identification of new tractable targets^{11,12}. Here, we explore a role for autotaxin (ATX) in this process.

ATX (encoded by *ENPP2*) is a unique lysophospholipase D (lysoPLD) that is secreted by diverse cell types to produce the lipid mediator and GPCR agonist lysophosphatidic acid (LPA) from abundantly available extracellular lysophosphatidylcholine (LPC)¹³⁻¹⁵. ATX was originally defined as an “autocrine motility factor” secreted by melanoma cells and characterized as a metastasis-enhancing ecto-phosphodiesterase^{16,17}. The ATX-LPA signaling axis plays a key role in a wide variety of biological and pathophysiological processes, ranging from vascular and neural development¹⁸ to lymphocyte homing¹⁹, inflammation, fibrosis, and tumor progression^{20,21}. Unfortunately, however, detailed assessment of ATX function *in vivo* is hampered by the embryonic lethality of ATX-deficient mice¹⁸.

LPA (mono-acyl-*sn*-glycero-3-phosphate) acts on six specific GPCRs, termed LPAR1–LPAR6 or LPA₁₋₆, showing both unique and shared signaling activities and tissue distributions^{22,23}. LPAR1–LPAR3 belong to the so-called EDG subfamily of GPCRs alongside the sphingosine 1-phosphate (S1P) receptors, whereas the disparate LPAR4-6 members are related to the P2Y purinergic receptor family^{22,24}. It is further of note that ATX interacts with cell-surface integrins and/or heparan sulfate proteoglycans thereby facilitating delivery of LPA to its cognate receptors in a highly localized manner^{19,25-27}.

Numerous studies have documented a critical role for ATX and/or LPA in stimulating cell migration, tumor cell dispersal, invasion, and metastasis, mediated primarily by LPAR1²⁸⁻³². LPAR1 also mediates the recruitment and activation of fibroblasts, a prototypic ATX-secreting cell type, and thereby can promote tissue fibrosis³³⁻³⁵. Activated fibroblasts constitute a large part of solid tumors, producing cytokines and extracellular matrix to enhance metastasis^{36,37}. Interestingly, LPAR1–LPAR3 commonly mediate enhanced cellular responses, whereas non-EDG receptors LPAR4–LPAR6 can exert counter-regulatory actions in that they suppress the migration and invasion of diverse cell types, depending on their dominant G protein-effector pathways³⁸⁻⁴⁰.

In the immune system, ATX is abundantly expressed in high-endothelial venules (HEVs) that control lymphocyte entry from blood into lymphoid tissue^{19,41}. Acting predominantly through LPAR2, HEV-secreted ATX promotes the random motility of naive T cells to enhance their transmigration into secondary lymphoid organs and thereby contributes to the control of systemic T cell responses^{19,41-43}. Thus, the ATX-LPA signaling axis regulates the migratory activities of both tumor cells and T cells mainly via LPAR1 and LPAR2, respectively. However, its actions in the tumor immune microenvironment remain unclear, particularly the dominant LPAR signaling pathways and how ATX/LPA may affect antigen-specific T cell responses and effector T cell activity in a tumor context.

Here, we show that ATX/LPA antagonizes the migration of patient-derived TILs and healthy blood-derived CD8⁺ T cells *ex vivo*, and define G $\alpha_{12/13}$ -coupled LPAR6 as a T cell migration inhibitory receptor. By eliciting a robust immune response upon anti-cancer vaccination of tumor-bearing mice, we demonstrate that secreted ATX antagonizes tumor infiltration of cytotoxic CD8⁺ T cells and thereby impedes tumor control in a therapeutic setting. Concordantly, single-cell analysis of melanoma tumors shows a negative correlation between intratumoral *ENPP2* expression and CD8⁺ T cell infiltration. By revealing ATX as a suppressor of anti-tumor immunity, our findings shed light on its multifaceted actions in the tumor microenvironment.

Results

Through LPA production, ATX secreted by melanoma cells is chemorepulsive for TILs and peripheral CD8⁺ T cells

Melanoma cells are known for their high ATX expression levels among many human cancer cell lines⁴⁴ and solid tumors (Figures **S1A** and **S1B**). This feature is unrelated to genetic changes (<https://www.cbioportal.org>), but rather reflects high ATX expression in skin melanocytes, a highly motile cell type. We set out to examine how melanoma cell-secreted ATX affects the migration of *ex vivo* expanded melanoma TILs and peripheral blood CD8⁺ T cells. Patient-derived TILs constitute a heterogeneous population of T cells in distinct functional states and other immune cells⁴⁵. During their *ex vivo* expansion driven by anti-CD3 antibody and IL-2 (see methods), TILs become enriched in CD8⁺ and CD4⁺ T cells and are then used for adoptive TIL therapy in patients⁴⁶.

We first analyzed the effects of LPA and ATX/LPC on the transwell migration of TILs (isolated from two patients). As a positive control, we used chemokine CXCL10 that signals via CXCR3 to promote effector T cell migration and is implicated in enhancing cancer immunity^{4,47}. Strikingly, LPA strongly suppressed the basal migration rate of TILs (up to 5-fold in patient 1) when assayed over a period of 2 h, in a concentration-dependent manner (Figures **1A** and **1B**). LPA was capable of antagonizing TIL migration toward CXCL10 (Figure **1C**). LPA was also chemo-repulsive for

peripheral blood CD8⁺ T cells isolated from healthy donors (Figure 1D). When TILs or CD8⁺ T cells were exposed to recombinant ATX (20 nM) together with its substrate LPC (1–5 mM), their transwell migration was similarly suppressed (Figure 1E).

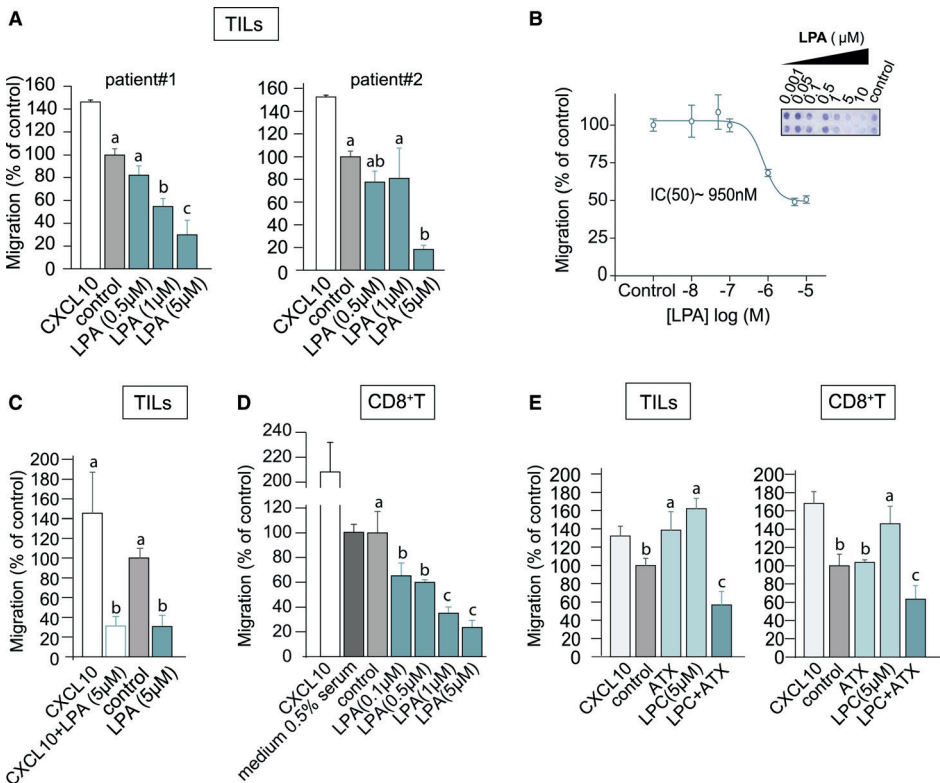


Figure 1. LPA and ATX/LPC are chemorepulsive for TILs and peripheral CD8⁺ T cells

(A) Transwell migration of *ex vivo* expanded TILs from two melanoma patients stimulated with LPA(18:1) at the indicated concentrations. Chemokine CXCL10 (1 mM) was used as positive control; “control” refers to serum-free medium. Agonists were added to the bottom wells and incubation was carried out for 2 h at 37°C. (B) LPA dose-dependency of migration. The inset shows a representative transwell filter after staining. Migration was quantified by color intensity using ImageJ. (C) LPA overrules CXCL10-induced TIL chemotaxis. LPA(18:1) was added together with CXCL10 at the indicated concentrations. (D) Migration of CD8⁺ T cells isolated from peripheral blood, measured in the absence (control) and presence of the indicated concentrations of LPA(18:1). Note that the presence of 0.5% serum has no effect. (E) Recombinant ATX (20 nM) added together with the indicated concentrations of LPC(18:1) recapitulates the inhibitory effects of LPA(18:1) on TILs and CD8⁺ T cells. (A and C–E) Results are representative of three independent experiments each performed in technical triplicates and expressed as means ± SEM; bars annotated with different letters were significantly different according to Fisher’s least significant difference (LSD) test ($p \leq 0.05$) after ANOVA.

We next analyzed melanoma cell supernatants for their modulatory activity on T cell migration. In addition, we measured concurrently secreted ATX protein and lysoPLD activity. Culture media (containing 0.5% serum) conditioned by melanoma cells (MDA-MB-435 and A375) for 24 h

markedly suppressed the basal migration and CXCL10-induced chemotaxis of TILs and peripheral CD8⁺ T cells (Figure 2A). Secreted ATX protein was readily detected by immunoblotting (Figure 2B), whereas lysoPLD activity was detected simultaneously (Figure 2C). By contrast, conditioned media from either ATX knockdown melanoma cells (Figure 2D) or ATX-deficient MDA-MB-231 breast carcinoma cells (Figure 2F) lacked chemorepulsive activity (Figures 2E and 2F). TIL migration could be rescued by incubating melanoma media with established ATX inhibitors, notably PF-8380 and IOA-289 (formerly CRT750)⁴⁸ (Figure 2G). Together, these results show that LPA-producing ATX released from melanoma cells is a major T cell repellent.

ATX as an LPA-producing chaperone

We investigated the relationship between ATX-mediated T cell repulsion and extracellular LPA levels. It is well established that LPA in freshly isolated plasma increases to high levels due to constitutive ATX-catalyzed LPC hydrolysis⁴⁹. Extracellular LPA comprises distinct molecular species that differ in their acyl chain composition and binding affinity for individual LPA receptors²³. We measured LPA species in media from melanoma cells conditioned at 0, 24, and 48 h using liquid chromatography-tandem mass spectrometry (LC-MS/MS)⁵⁰ (Figure 3A). LPA(12:0), LPA(16:0), LPA(18:0), LPA(18:1), and LPA(20:4) were the predominant species in media containing 0.5% serum (Figure 3B). Remarkably, total LPA in TIL-repulsive media declined to very low levels within 24h, despite the fact that ATX activity increased concurrently (Figures 2B, 2C, 3C, and 3E); by contrast, the corresponding LPC species in these media remained constant or increased over time (Figure 3D). Hence, the loss of LPA in the face of ATX activity is not due to substrate depletion. Depletion of extracellular LPA by melanoma cells has been reported previously⁵¹ and is due to its degradation by cell-associated lipid phosphate phosphatases⁵².

That ATX is fully bioactive at near-zero steady-state LPA levels can be explained by the fact that ATX binds LPA in its “exit tunnel” where it is protected from degradation⁵³⁻⁵⁶. These results thus support the notion that ATX both produces and “chaperones” LPA for local delivery to its receptors at the cell surface.

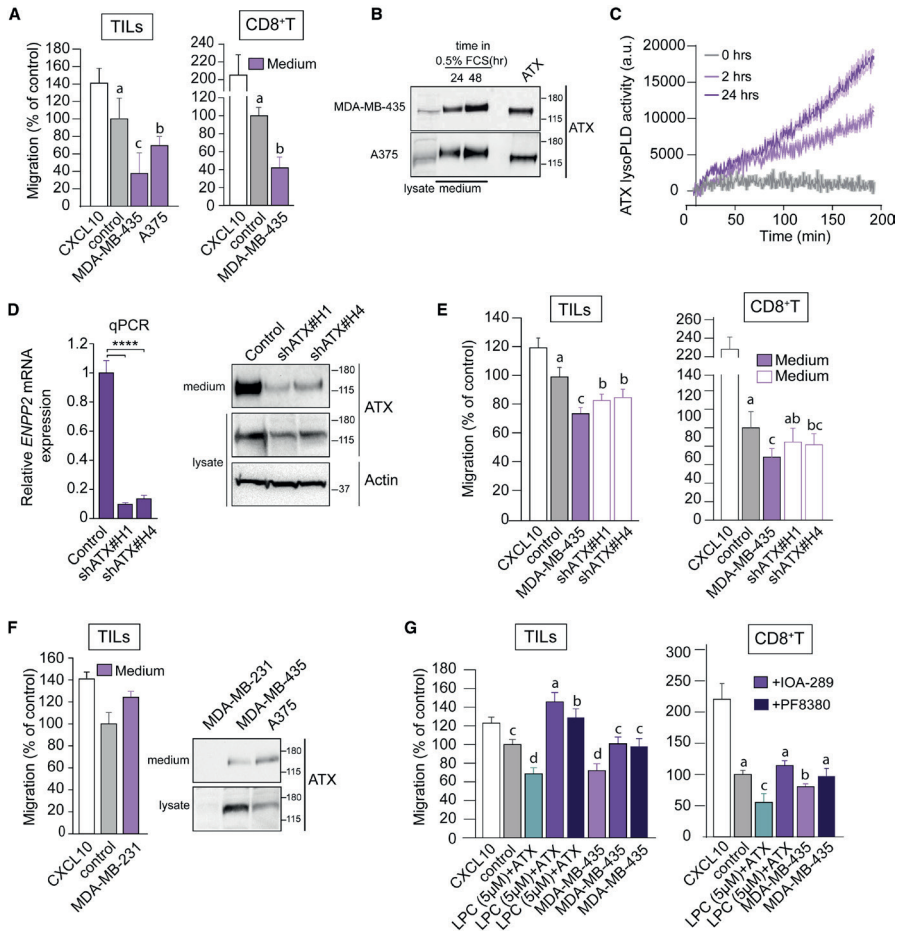


Figure 2. ATX secreted by melanoma cells repels TILs and peripheral CD8⁺ T cells

(A) Melanoma-conditioned medium from MDA-MB-435 and A375 cells (collected after 24 h) is chemorepulsive for TILs and blood-derived CD8⁺ T cells. Experimental conditions as in Figure 1. (B) Immunoblot showing ATX expression in medium and cell lysates of MDA-MB-435 and A375 melanoma cells. Cells were incubated in DMEM with 0.5% FCS for 24 or 48 h. Recombinant ATX (20 nM) was used as positive control (right lane). (C) LysoPLD activity accumulating in melanoma-conditioned media over time. Medium from MDA-MB-435 cells was collected after 2 and 24 h, and lysoPLD activity was measured as choline release from added LPC(18:1). (D) ATX (*ENPP2*) mRNA expression (relative to cyclophilin) in control and *ENPP2*-depleted MDA-MB-435 cells stably expressing short hairpin RNAs (shRNAs) against ATX. Maximal *ENPP2* knockdown was obtained with shRNA 1 and 4 (of 5 different hairpins). Data represent the mean \pm SEM of three independent experiments using triplicate samples; **** $p < 0.0001$ (unpaired Student's t test). Right: immunoblot analysis of ATX expression using shRNA 1 and 4. Actin was used as loading control. (E) Melanoma-conditioned medium from ATX knockdown MDA-MB-435 cells (collected after 24 h) lacks chemorepulsive activity for CD8⁺ T cells and TILs. (F) Conditioned media from ATX-deficient MDA-MB-231 breast carcinoma cells lack chemo-repulsive activity for TILs compared to media from ATX-expressing melanoma cells (MDA-MB-435 and A375; cf. A). Right panel: ATX immunoblots from the indicated media and cell lysates. (G) ATX inhibition restores the migration TILs and CD8⁺ T cells exposed to melanoma cell-conditioned media. Cells were plated at day 0 in medium containing 10% FCS. After 16 h, cells were exposed to medium containing 0.5% FCS and ATX inhibitors (PF-8380 or IOA-289). Conditioned media were collected after 24 h. (A and D–G) Representative data of three independent experiments each performed in triplicate. Values are expressed as mean \pm SEM; bars annotated with different letters were significantly different according to Fisher's least significant difference (LSD) test ($p \leq 0.05$) after ANOVA.

TIL repulsion involves LPAR6

The T cell repelling activity of ATX/LPA markedly contrasts to its chemotactic activity for tumor cells, strongly suggesting involvement of different LPA receptors. We examined the LPAR expression repertoire in TILs and blood-derived CD8⁺ T cells using qPCR. *Ex vivo* expanded melanoma TILs (isolated from eight patients) consistently express high levels of *LPAR6* in addition to considerably lower levels of *LPAR2*; an identical pattern was detected in ovarian carcinoma-derived TILs (Figure 4A, and data not shown). LPAR6 was also the predominant non-EDG LPA receptor in peripheral blood CD8⁺ T cells alongside LPAR4 and LPAR5 (Figure 4B), in agreement with publicly available data (<https://www.immgen.org>; <http://biogps.org>). LPAR4 and LPAR5 may have been lost from TILs during tumorigenesis or their *ex vivo* expansion, scenarios that warrant further investigation. Incubating TILs with a novel xanthylene-based LPAR6 antagonist, named XAA⁵⁷, partially overcame T cell repulsion by LPA (Figure 4C). We therefore conclude that repulsion of TILs and peripheral blood CD8⁺ T cells is primarily mediated by LPAR6, without excluding possible additional anti-migratory roles for LPAR4 and LPAR5.

LPAR6 (P2RY5) preferentially couples to the $G\alpha_{12/13}$ -RhoA pathway that drives cytoskeletal contraction, suppression of cell motility, and other cellular responses^{23,58-60}. The function of LPAR6 in T cells has remained largely unexplored despite its high expression in immune cells (<http://biogps.org>). In contrast to LPAR6, LPAR2 couples to G_i -mediated Rac GTPase activation and other G protein-effector routes and thereby promotes the random motility of T cells^{19,41}, as schematically illustrated in Figure 4D.

Impact of ATX on the induction of systemic T cell responses and tumor infiltration of cytotoxic CD8⁺ T cells

Having shown that ATX through generation and protection of LPA repels TILs and blood-derived CD8⁺ T cells *ex vivo*, we next investigated how ATX affects the anti-tumor T cell response *in vivo*. We took advantage of an anti-cancer vaccination model using subcutaneously (s.c.) implanted TC-1 epithelial tumor cells that express the HPV16 E7 oncogene⁶¹. TC-1 tumors lack spontaneous T cell infiltration; however, tumor-specific CD8⁺ T cell infiltration can be induced by vaccination, as we and others previously described^{62,63}. The DNA vaccine we employed encodes HPV E7 in a gene shuffled configuration to provide a strong MHC class I-restricted CD8⁺ T cell epitope and HPV-unrelated MHC class II-restricted epitopes that elicit CD4⁺ T cell “help.” These “helped” CD8⁺ T cells have optimal cytotoxic and migratory abilities that allow for effective tumor rejection. Specifically, they readily extravasate and infiltrate into the tumor due to upregulation of chemokine receptors and matrix metalloproteases⁶³. This therapeutic setting provides a window to examine the impact of ATX on anti-tumor T cell responses and tumor rejection.

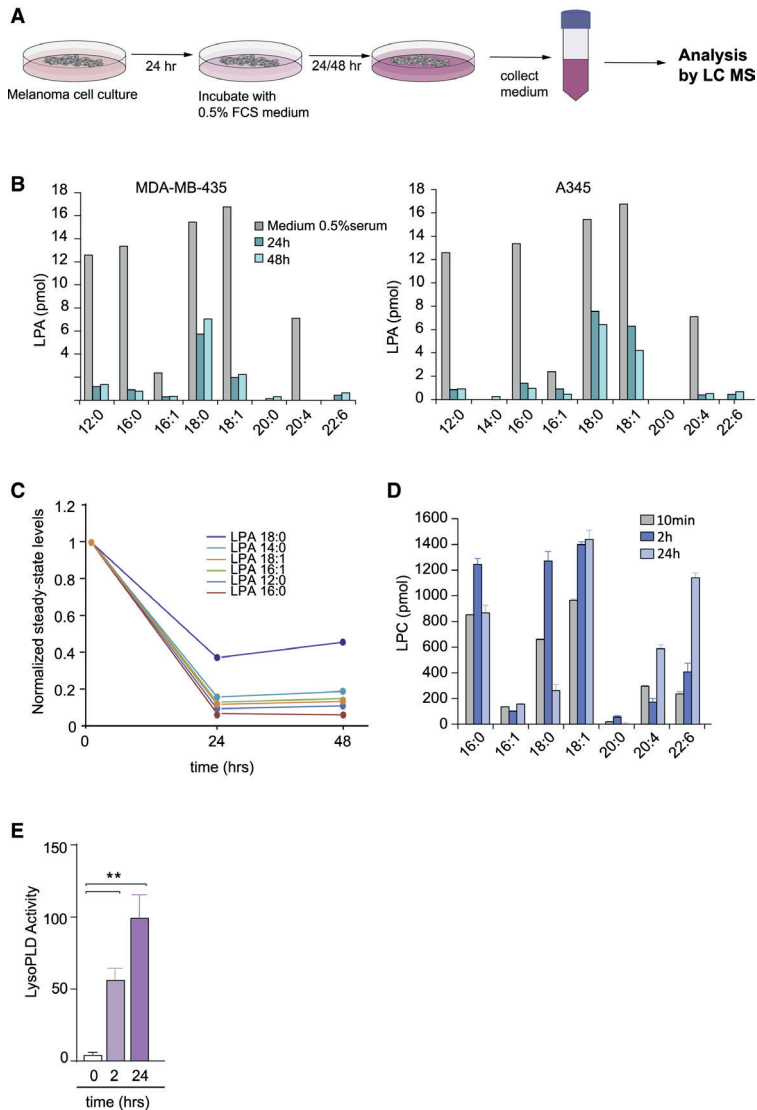


Figure 3. Lysolipid species and secreted lysoPLD activity in conditioned media from melanoma cells

(A) Preparation of cell-conditioned media. Melanoma cells in 10-cm dishes were cultured for 24 h, washed, and then incubated in DMEM containing 0.5% FCS. Media were harvested after 24 and 48 h, and centrifuged to remove cell debris. LPA species were measured using LC/MS/MS. (B) Determination of LPA species in conditioned medium from MDA-MB-435 and A375 melanoma cells, measured at $t = 0$, 24, and 48 h, using LC/MS/MS. Predominant serum-borne LPA species are (12:0), (16:0), (18:0), (18:1) and (20:4). Note LPA depletion from the medium (within 24 h) upon incubation with ATX-secreting melanoma cells. (C) Time-dependent decline of the indicated serum-borne LPA species by melanoma cells. Graph shows normalized steady-state LPA levels in conditioned media from MDA-MB-435 cells. (D) LPC species in conditioned medium from MDA-MB-435 cells, measured at $t = 10$ min, 2 h and 24 h, using LC/MS/MS. Note that LPC levels tend to increase over time. Values from one experiment performed in triplicate and expressed as mean \pm SEM. (E) Secreted lysoPLD activity increases over time. Medium from MDA-MB-435 cells was collected after 2 and 24 h, and lysoPLD activity was measured as choline release from added LPC(18:1). Values from three independent experiments each performed in triplicate and expressed as mean \pm SEM; ** $p < 0.01$ (unpaired Student's t test).

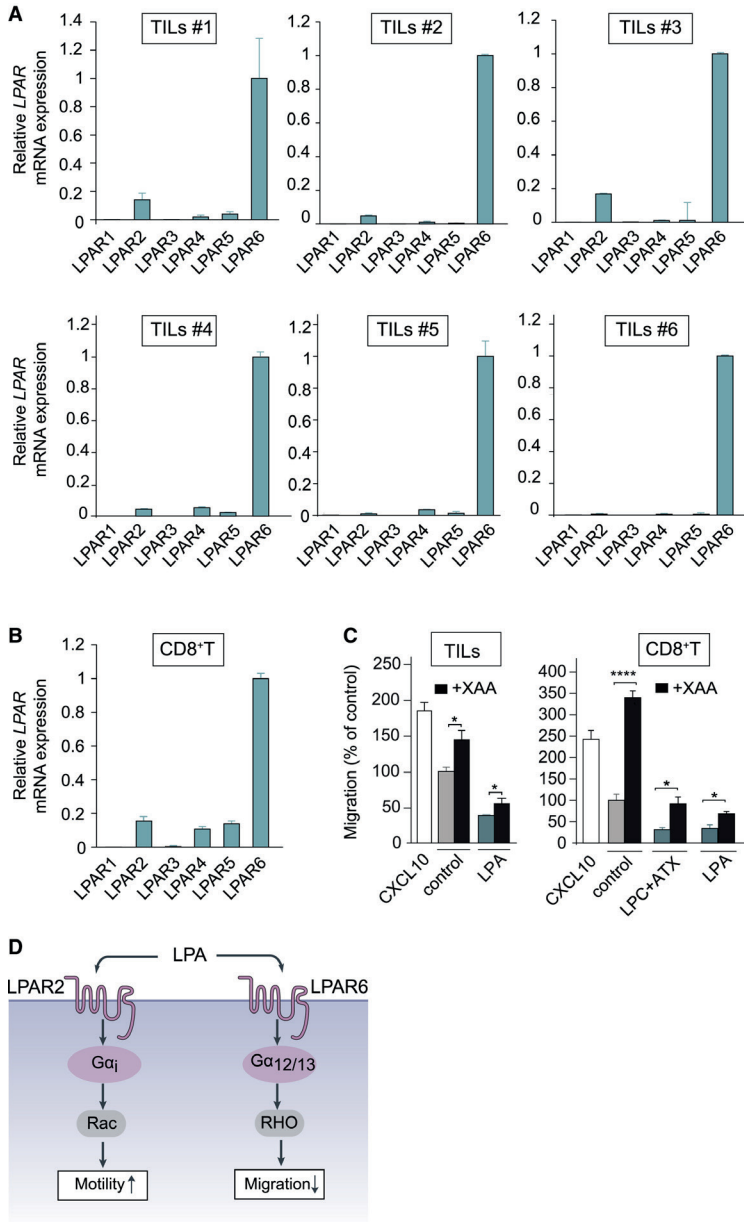


Figure 4. LPAR expression in TILs and peripheral CD8⁺ T cells

(A) LPAR expression repertoire in *ex vivo* expanded TILs from six patients (qPCR analysis relative to cyclophilin). TIL values are expressed as mean \pm SD. (B) LPAR expression in peripheral CD8⁺ T cells from two healthy donors. Values are expressed as mean \pm SD. (C) LPAR6 antagonist XAA restores transwell migration of TILs (left panel) and CD8⁺ T cells (right panel) in response to LPA or ATX plus LPC. Conditions as in Figure 1. Cells were treated with XAA (10 mM) or vehicle control (0.5% DMSO) for 24 h. Data represent the mean \pm SEM of three independent experiments using triplicate samples. * $p < 0.05$, **** $p < 0.0001$ (unpaired Student's t test). (D) Schematic illustration of dominant G-protein coupling and signaling outcomes of LPAR2 versus LPAR6.

Because TC-1 cells were found to lack ATX expression, we generated ATX-expressing TC-1 (TC-1^{ATX}) cells and confirmed that they secrete active ATX (Figures **S2A** and **S2B**). Enforced ATX expression did not significantly alter the growth rate of s.c. injected TC-1 tumor cells (Figures **S2C** and **S2D**). This agrees with previous tumor implantation studies showing that ATX-LPAR signaling has little effect on primary tumor growth, but does promote metastasis to distant organs mainly through LPAR1^{29,32,64}.

ATX does not affect induction of systemic T cell responses

We examined how tumor cell-derived ATX may affect the induction of CD8⁺ and CD4⁺ T cell responses after vaccination. For this purpose, mice were vaccinated on days 8, 11, and 14 after implantation of wild-type (WT) or ATX-expressing TC-1 tumor cells (Figure **5A**). After vaccination, T cells are primed in the vaccine-draining lymph node from where they egress as differentiated effector T cells into the blood and then infiltrate the tumor via chemotaxis⁶³. Primed HPV E7-specific CD8⁺ T cells were detected by flow cytometry using H-2D^b/ E7₄₉₋₅₇ MHC tetramers (Tet) (Figure **5B**). We monitored vaccine-induced T cell responses in blood over time (Figures **5C–5E**). The HPV E7-specific systemic CD8⁺ T cell response measured in blood was similar in TC-1^{WT} and TC-1^{ATX} tumor-bearing mice (Figures **5C** and **S3A**), as was the frequency of CD8⁺ T cells with a CD44⁺

CD62L⁻ effector phenotype (Figures **5D** and **S3B**). Likewise, the frequency of vaccine-induced CD4⁺ T cells showing a CD44⁺ CD62L⁻ effector phenotype increased to a similar extent in both groups of tumor-bearing mice (Figures **5E** and **S3C**). Analysis of the spleens (at day 10 after vaccination) showed no differences in the systemic distribution of HPV E7-specific CD8⁺ T cells (Figure **5F**), nor in their differentiation into granzyme B (GZB)- and interferon gamma (IFN γ)-expressing cytotoxic T lymphocytes (CTLs) (Figure **5G**). CD4⁺ T cell responses in the spleen were also similar between both groups of tumor-bearing mice, as measured by the frequency of IFN γ -expressing cells among conventional (FOXP3⁻) CD4⁺ T cells (Figures **S3D** and **S3E**). Finally, ATX expression did not influence the frequency of FOXP3⁺ CD4⁺-regulatory T cells (Tregs) (Figure **S3F**). Thus, secreted ATX does not affect the induction of systemic CD8⁺ and CD4⁺ T cell responses upon vaccination, either in magnitude or quality.

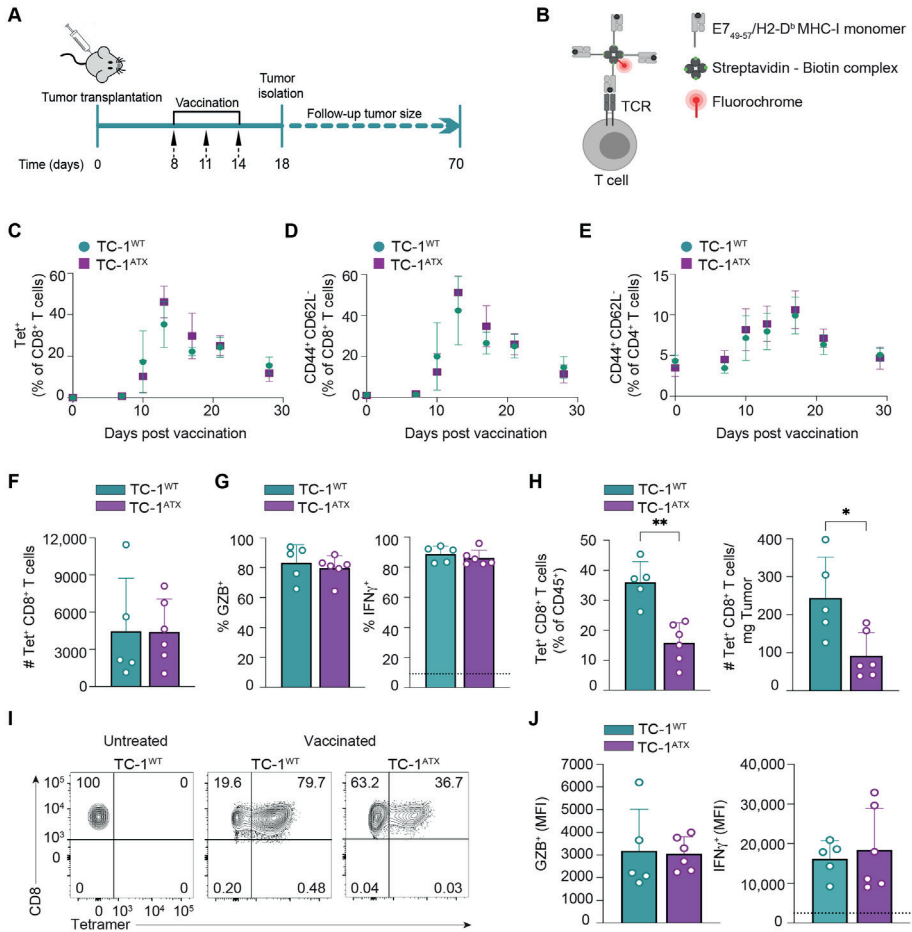


Figure 5. Enforced ATX expression in tumor cells does not affect induction of T cell responses by vaccination (A) Experimental set-up in the anti-cancer vaccination model. Mice were injected s.c. with wild-type (TC-1^{WT}) or ATX-expressing (TC-1^{ATX}) tumor cells on day 0, vaccinated on days 8, 11, and 14 and were either sacrificed on day 18, or monitored until day 70. Tumor cells were injected into one flank and the vaccine DNA was “tattooed” into the depilated skin of the opposing flank. Data are from one experiment representative of two experiments. (B) The DNA vaccine encodes HPV-E7 protein together with tumor-unrelated helper epitopes. The CD8⁺ T cells that have a TCR specific for the immunodominant E7₄₉₋₅₇ peptide presented in H-2D^b can be detected with MHC class I (MHC-I) tetramers. A tetramer is made by folding E7₄₉₋₅₇ peptide with MHC-I monomer, conjugating this to biotin and multimerizing it with fluorochrome-conjugated streptavidin. (C–E) Monitoring of the T cell response to vaccination in peripheral blood by flow cytometry in TC-1^{WT} (n=6) and TC-1^{ATX} (n=5) tumor-bearing mice. (C) Frequency of H-2D^b/E7₄₉₋₅₇ tetramer positive (Tet⁺) cells among total CD8⁺ T cells. (D and E) Frequency of cells with a CD44⁺CD62L⁻ effector phenotype among total CD8⁺ T cells (D) or total CD4⁺ T cells (E). (F–J) Analysis of the CD8⁺ T cell response in spleen (F–J) and tumor (H and J) on day 18 in TC-1^{WT} (n = 5) and TC-1^{ATX} (n = 6) tumor-bearing mice. (F) Absolute number of tetramer positive (Tet⁺) CD8⁺ T cells in spleen. (G) Frequency of granzyme B (GZB)⁺ and IFN γ ⁺ cells among Tet⁺ CD8⁺ T cells in spleen. IFN γ was measured after *ex vivo* PMA/ionomycin stimulation. The dotted line indicates IFN γ signal in unstimulated cells. (H) Frequency among CD45⁺ hematopoietic cells (left) and absolute number (#, right) of Tet⁺ CD8⁺ T cells in TC-1^{WT} and TC-1^{ATX} tumors. (I) Representative flow cytometry plots indicating the percentage of Tet⁺ cells among total CD8⁺ T cells in TC-1^{WT} and TC-1^{ATX} tumors after vaccination and in TC-1^{WT} tumors of non-vaccinated (untreated) mice. (J) Mean fluorescence intensity (MFI) of GZB⁺ and IFN γ ⁺ cells within Tet⁺ CD8⁺ T cells in TC-1^{WT} and TC-1^{ATX} tumors. IFN γ was measured as in (G). (C–H and J) Data are expressed as mean \pm SD; *p < 0.05, **p < 0.01 (Mann-Whitney U test).

ATX repels cytotoxic CD8⁺ T cells from the tumor and impairs tumor control

We then investigated how ATX affects anti-tumor immunity and tumor fate after vaccination. Tumor infiltration of vaccine-induced effector CD8⁺ T cells was analyzed by flow cytometry and immunohistochemistry. Enforced ATX expression significantly reduced the infiltration of HPV E7-specific CD8⁺ T cells into the tumor, in both absolute numbers and frequency among total hematopoietic (CD45⁺) cells (Figures 5H and 5I). ATX did not alter the intrinsic cytotoxicity of the infiltrating CD8⁺ T cells, based on the similar expression levels of GZB and IFN γ in Tet⁺ CD8⁺ T cells retrieved from TC-1^{WT} and TC-1^{ATX} tumors (Figure 5J). Tumor-derived ATX did not oppose tumor infiltration by conventional (FOXP3⁻) CD4⁺ T cells (Figure 53G), nor did it affect their effector quality as inferred from IFN γ expression levels (Figure 53H). Numbers of infiltrating CD4⁺ Treg cells were also similar between TC-1^{WT} and TC-1^{ATX} tumors (Figure 53I). In conclusion, ATX expression by TC-1 tumors impaired infiltration of vaccine antigen-specific CD8⁺ T cells from the blood into the tumor, without affecting CTL quality or infiltration of conventional CD4⁺ T cells and Treg cells into the tumor.

We verified the flow cytometric data by examining T cell infiltration through quantitative CD8 staining in whole tumor sections by immunohistochemistry. As illustrated in Figure 6A, vaccine-induced CD8⁺ T cells were less capable of penetrating ATX-expressing tumors compared to parental tumors.

In the parental TC-1^{WT} tumors, CD8⁺ T cells were evenly dispersed throughout the tumor, according to analysis of multiple whole tumor sections. In TC-1^{ATX} tumors, however, CD8⁺ T cells were detected in separate fields, leaving large parts of the tumor non-infiltrated. Quantitative analysis confirmed reduced CD8⁺ T cell infiltration in ATX-expressing tumors (Figure 6B). Tumor infiltration of CD4⁺ T cells and Tregs was not affected by ATX expression (Figures 6C and 6D), in agreement with the flow cytometric data.

We determined the impact of ATX expression on vaccine-induced TC-1 tumor control, following the experimental protocol of Figure 5A. Vaccination of mice bearing either TC-1^{WT} or TC-1^{ATX} tumors initially resulted in tumor regression (Figure 6E). Importantly, however, vaccine-induced growth delay of ATX-expressing tumors was significantly reduced in comparison to TC-1^{WT} tumors, as was the overall survival rate of mice bearing TC-1^{ATX} tumors (Figures 6F and 6G). Collectively, these findings demonstrate that ATX released by tumor cells impairs cytotoxic CD8⁺ T cell infiltration and dispersion throughout the tumor and thereby impairs tumor control in a therapeutic setting.

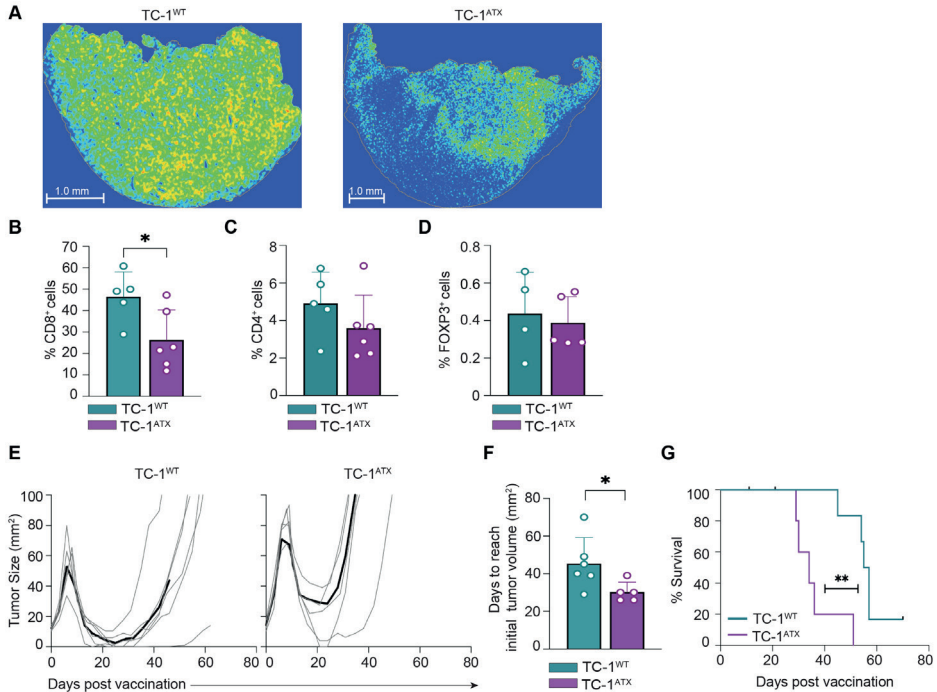


Figure 6. Enforced ATX expression in tumor cells inhibits infiltration of effector CD8⁺ T cells and impedes vaccine-induced tumor control

(A–F) Tumor analysis by immunohistochemistry on day 18 in the same mice as analyzed in Figure 5. (A) Representative heatmaps of CD8⁺ immunostainings of tumor sections from vaccinated mice bearing TC-1^{WT} or TC-1^{ATX} tumors. (B–D) Quantification in percentages of CD8⁺ (B, representative for the data shown in A), CD4⁺ (C), and FOXP3⁺ (D) cells out of all nucleated cells as assessed by immunostaining of tumor sections from vaccinated mice bearing TC-1^{WT} or TC-1^{ATX} tumors. Data are depicted as mean + SD, **p* < 0.05 (Mann-Whitney U test).

(E–G) TC-1^{WT} (*n* = 6) and TC-1^{ATX} (*n* = 5) tumor-bearing mice received vaccination as outlined in Figure 5 and tumor growth was monitored over time up to day 70. (E) Individual growth curves of TC-1^{WT} and TC-1^{ATX} tumors in vaccinated mice. Black lines represent group average. (F) Tumor growth delay following vaccination, expressed as number of days required to reach a tumor size corresponding to that at day 7 (see E). Data are depicted as mean + SD, **p* < 0.05 (Mann-Whitney U test). (G) Overall survival curves of tumor-bearing mice. ***p* < 0.01 (Mantel-Cox analysis). Data in this figure are from one experiment representative of two independent experiments.

Intratumoral *ENPP2* expression in melanoma negatively correlates with CD8⁺ T cell infiltration

Finally, we sought clinical evidence for intratumoral ATX functioning as a CD8⁺ T cell repellent in melanoma. Of note, abundant *ENPP2* expression is detected not only in melanoma but in virtually all solid tumors (<https://www.cbioportal.org>), showing remarkably little correlation with *ENPP2* expression in the corresponding cancer cell lines (Figures S1A and S1B). This supports the view that a substantial part of the tumor *ENPP2* transcripts is derived from non-malignant stromal cells, notably cancer-associated fibroblasts (CAFs) and adipocytes known for their high ATX expression levels, depending on the cancer type^{28,65}.

We analyzed *ENPP2* expression patterns and CD8⁺ T cell infiltration using single-cell RNA-sequencing (scRNA-seq) results from 32 melanoma tumors (prior to immunotherapy) in which diverse cell subsets can be distinguished⁶⁶. *ENPP2* expression in individual cells (n = 7,186) and its association with CD8⁺ T cell infiltration was examined in all subsets, namely malignant cells, CD8⁺ and CD4⁺ T cells, B cells, natural killer (NK) cells, CAFs, tumor-associated macrophages, and endothelial cells. Figure **7A** shows the melanoma samples grouped by individual cell types. Whereas lymphocytes do not express ATX, significant *ENPP2* expression was detected not only in malignant cells and CAFs but also in macrophages and endothelial cells (Figure **7B**). Tumors with the highest intratumoral *ENPP2* expression—in both cancer and stromal cells— contained significantly fewer CD8⁺ T cells, whereas low *ENPP2* expression correlated with enhanced CD8⁺ T cell infiltration, as quantified by Pearson's correlation analysis ($r = 0.4$; $p = 0.01$) (Figure **7C**).

Elevated *ENPP2* expression in melanoma samples was also associated with reduced CD4⁺ T cell infiltration, but not with macrophage accumulation (Figures **S4A** and **S4B**). Although ATX-mediated repulsion of CD4⁺ T cells was not observed in the above vaccination model, differences in the functional state of the respective CD4⁺ T cell populations or species-specific receptor expressions might account for this discrepancy. Despite some caveats concerning the interpretation of scRNA-seq results, as will be discussed below, the single-cell transcriptomics analysis is consistent with our *in vivo* findings, namely that intratumoral ATX repels CD8⁺ T cells from the tumor. Collectively, our findings support a model of intratumoral ATX/LPAR signaling (Figure **7D**) to be discussed below.

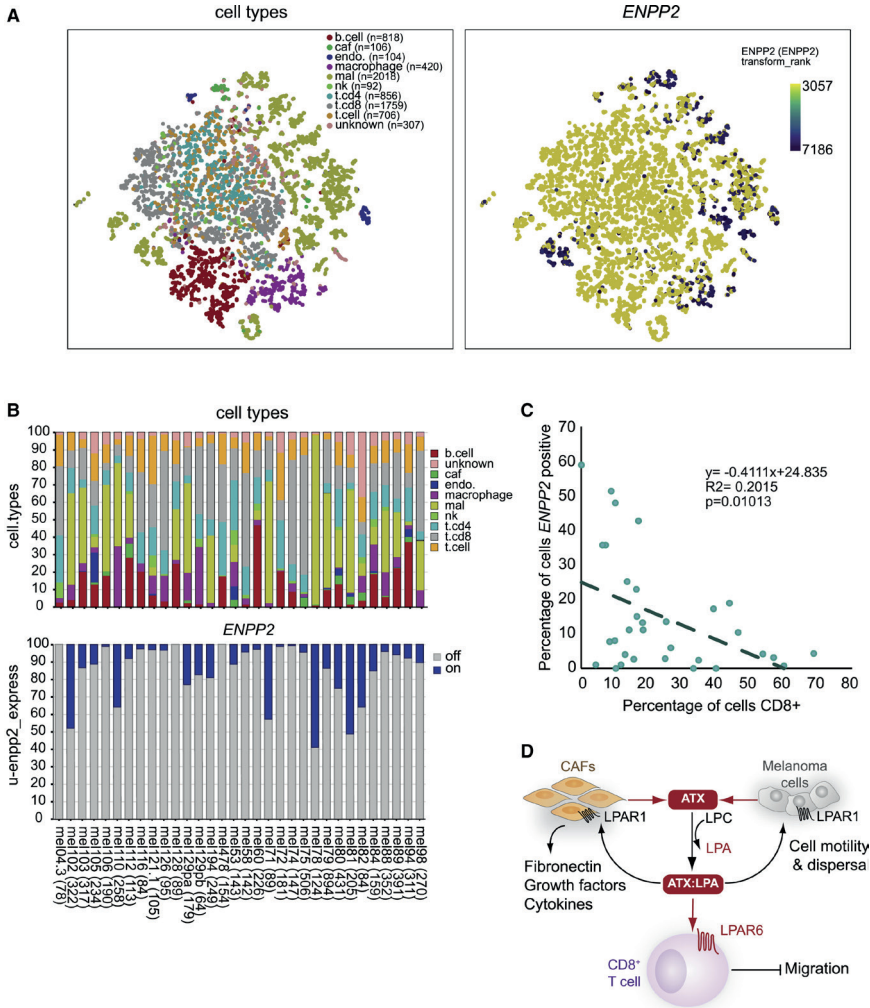


Figure 7. Single-cell analysis of *ENPP2* expression in melanoma tumors and its inverse correlation with CD8⁺ T cell accumulation

(A) t-distributed stochastic neighbor embedding (tSNE) embedding of 7,186 single cells (complexity = 5) from 32 melanoma patients as described⁶⁶. Data were used to project patients, inferred cell types, and log₂ *ENPP2* expression values, respectively, as described in methods. Right panel shows *ENPP2* expression (blue/purple dots high expression) as overlay on single cells presented in the left panel. Intratumoral *ENPP2* expression is detected in malignant cells (mal), cancer-associated fibroblasts (caf), macrophages, and endothelial cells (endo), but not in lymphocytes (T, B, and NK cells). (B) Stacked bar graph showing the percentages of inferred cell type per individual patient sample (top), and the percentage of *ENPP2*-expressing cell types (bottom). (C) Inverse correlation between intratumoral *ENPP2* expression and CD8⁺ T cell accumulation. Pearson correlation between the percentage of inferred *ENPP2*-expressing cells and CD8⁺-positive cells ($R = 0.4$; $p = 0.01$). (D) Model of the melanoma immune microenvironment. In this model, ATX is secreted by melanoma cells and diverse stromal cells, particularly fibroblasts (CAFs), to convert extracellular LPC into LPA. ATX functions as an LPA-producing chaperone (ATX:LPA) that carries LPA to its GPCRs and exerts dual actions: it suppresses T cell infiltration through G_{12/13}-coupled LPAR6, while it promotes melanoma cell dispersal and activates CAFs via LPAR1 (mainly via G_i). Activated CAFs release growth factors and produce extracellular matrix. Random T cell motility mediated by LPAR2 is not illustrated (see Figure 4D). See text for further details.

Discussion

The signaling mechanisms that contribute to the exclusion of CD8⁺ T cells from tumors remain poorly understood, which hampers progress in improving immunotherapy efficacy^{7,11,12}. Tumor-intrinsic mechanisms underlying T cell exclusion involve, for example, transcriptional chemokine silencing^{9,10} and production of immunosuppressive cytokines such as transforming growth factor β (TGF- β)^{6,67}. However, secreted factors and T cell GPCRs that counteract T cell infiltration remain to be identified.

Here, we demonstrate that LPA-producing ATX secreted by tumor cells is a major repellent for human TILs and healthy CD8⁺ T cells under *ex vivo* conditions, with a dominant anti-migratory role for $G\alpha_{12/13}$ -coupled LPAR6. Moreover, we show that secreted ATX repels cytotoxic CD8⁺ T cells from s.c. engrafted tumors to impede anti-tumor immunity and tumor regression in a therapeutic setting.

ATX/LPA is widely known for its chemotactic activities toward both normal and tumor cells, acting mainly via LPAR1, and to enhance the random motility of T cells via LPAR2^{19,43}. Unexpectedly, we initially observed T cell chemo-repulsive effects of exogenous ATX/LPA and melanoma cell-secreted ATX of TILs and peripheral blood CD8⁺ T cells *ex vivo*, with ATX/LPA antagonizing the migration toward chemokine CXCL10 (Figures 1 and 2). Whereas CD8⁺ T cells express multiple LPA receptors, the unique LPAR expression pattern in TILs and the use of a novel LPAR6 antagonist allowed us to define LPAR6 as the predominant T cell anti-migratory receptor (Figure 4). In this respect, it should be emphasized that biological outcome is determined by the balance in expression of GPCRs that signal mainly via G_i (i.e., chemokine and chemotactic EDG receptors LPAR1–LPAR3) versus those that couple predominantly to the $G\alpha_{12/13}$ -RhoA pathway, notably anti-chemotactic non-EDG receptors LPAR4–LPAR6, as exemplified by the present findings.

Contrary to prevailing notions, secreted ATX failed to raise extracellular LPA levels as its lysoPLD activity was outperformed by cell-associated LPA-degrading activity (Figure 3). By binding LPA in its “exit tunnel,” presumably at a 1:1 ratio, ATX protects bioactive LPA from degradation⁵³⁻⁵⁶ and, as such, functions as an LPA-producing “chaperone.” Based on its calculated lifetime⁶⁸, the ATX:LPA complex can diffuse over a relatively long distance in the extracellular milieu⁵³ and hence may shape an ATX/LPA gradient and its paracrine signaling range. Precisely how ATX releases LPA to its cognate receptors upon interaction with the cell surface awaits further functional and structural studies.

LPAR6 (P2RY5) now joins the few select GPCRs that counteract T cell chemotaxis through the $G\alpha_{12/13}$ -RhoA pathway. Among them, EDG-family sphingosine-1-phosphate receptor S1PR2 is arguably the best characterized member^{69,70}, but a role for S1PR2 in immuno-oncology has not been documented to date. LPAR6 (P2RY5) is of special interest as it displays its highest expression

in immune cells and is strongly induced upon activation of chicken T cells through as-yet-unknown mechanisms^{71,72}. Furthermore, LPAR6 prefers 2 acyl- rather than 1-acyl-LPA species as ligand²³, which may explain the relatively high IC₅₀ value for 1-oleyl-LPA observed in T cell migration assays (Figure 1B). Although its non-EDG relatives LPAR4 and LPAR5 were not detected in *ex vivo* expanded TILs (Figure 4A), the latter receptor is nonetheless of immuno-oncological importance since its genetic deletion in mice enhances T cell receptor activity and anti-tumor responses⁷³. To what extent LPAR6 and LPAR5 may act redundantly or synergistically in T cell signal transmission remains to be investigated.

Building on our *in vitro* findings, we pursued the impact of tumor-intrinsic ATX on T cell responses in the mouse TC-1 tumor model that is often used in anti-cancer vaccination studies^{63,74}. For this purpose, we stably expressed ATX in TC-1 cells that lack endogenous *Enpp2* expression and confirmed their LPA-producing activity. Vaccination induces the simultaneous activation of CD4⁺ and CD8⁺ T cells to optimize the cytotoxic T cell response in magnitude and quality⁶³. “Helped” CD8⁺ T cells acquire chemokine receptors to increase their migration capacity and enhanced metalloprotease activity that enables them to invade tumor tissue to promote tumor regression^{63,74}. We established that tumor-intrinsic ATX has no effect on vaccine-induced CD4⁺ and CD8⁺ T cell responses (Figure 5). The cytotoxic CD8⁺ T cells thus displayed optimal effector capacity independent of ATX activity. Importantly, despite the robust anti-tumor immune response, tumor-intrinsic ATX was capable of significantly impeding tumor infiltration of cytotoxic CD8⁺ T cells and suppressing tumor rejection (Figure 6). These findings highlight a key role for LPA-producing ATX in suppressing anti-tumor immunity in a therapeutic setting. By inference, LPAR6 most likely plays a dominant role in mediating ATX-induced T cell repulsion *in vivo*, possibly in concert with LPAR5, but this needs further investigation. Further development of specific LPAR6 antagonists would enable a robust pharmacological characterization and help dissect the ATX-LPAR immune signaling network in further detail.

In a clinical setting, single-cell analysis of melanoma tumors⁶⁶ showed significant *ENPP2* expression in malignant cells, CAFs, tumor-associated macrophages, and endothelial cells, which further accentuates the complexity of ATX/LPA signaling in the tumor microenvironment (Figures 7A–7C). Consistent with our *in vivo* findings, intratumoral *ENPP2* expression positively correlated with CD8⁺ T cell exclusion. *ENPP2* expression was also associated reduced CD4⁺ T cell infiltration in these tumors (Figure S4). These findings should be validated in future immuno-histochemical analyses of select patient samples.

Taken together with previous evidence, our findings support a simplified model of the tumor (melanoma) microenvironment illustrated in Figure 7D. In this model, LPA-producing ATX is secreted by both tumor and stromal cells and—complexed with LPA—counteracts tumor

infiltration of CD8⁺ T cells mainly via G_{12/13}-coupled LPAR6, while it activates tumor cells and pro-tumorigenic fibroblasts (CAFs) in autocrine/paracrine loops via LPAR1, which signals predominantly via G_i. ATX/LPA-stimulated tumor cells acquire a pro-metastatic phenotype, whereas activated fibroblasts drive immune escape by generating a physical barrier to TILs and by secreting immunosuppressive molecules⁷⁵. Because ATX is abundantly expressed in most solid tumors (Figure **S1B**), this model obviously extends beyond melanoma to many cancer types. Because the tumor microenvironment is heterogeneous and cancer type-specific, ATX/LPA signaling outcome will critically depend on the composition and LPAR expression repertoire of the immune cell infiltrate, and likely also on the spatial arrangement of ATX-secreting stromal cells within the tumor.

In conclusion, by suppressing anti-tumor immunity while promoting metastasis via different LPA receptors, the ATX-LPAR signaling axis creates a T cell-excluding, pro-tumorigenic microenvironment that is amenable to therapeutic intervention. Our findings pave the way for addressing outstanding questions on the ATX-LPAR axis in other immunotherapeutic settings, such as genetically engineered melanoma models and/or patient-derived xenografts (PDX) engrafted in humanized mouse models^{76,77}. Such clinically relevant models should provide further insight into the dual pro-tumor actions of ATX; furthermore, they will offer an opportunity to evaluate the anti-tumor benefits of pharmacological ATX inhibition, for example in combination with immune checkpoint inhibitors.

Limitations of the study

Our study has several limitations. Although LPAR6 acts as a migration-inhibitory receptor for peripheral blood CD8⁺ T cells, and ex vivo expanded TILs, its role in ATX-mediated T cell repulsion in tumor-bearing mice, as reported here, remains to be established by using *Lpar6*^(-/-) mice. Furthermore, our correlative single-cell analysis of ATX expression in melanoma tumors (Figure **7**) should be viewed with caution because scRNA-seq studies do not detect all transcripts in every single cell, and intratumoral *ENPP2* expression is not necessarily predictive of secreted ATX activity in the tumor microenvironment.

Methods

Cell culture and materials

MDA-MB-435 and A375M melanoma cells were grown in Dulbecco's modified Eagle's medium (DMEM) supplemented with 10% fetal bovine serum (FBS) at 37°C under 5% CO₂. Patient-derived TILs cells were grown in Roswell Park Memorial Institute (RPMI) 1640 medium supplemented with 10% human serum at 37°C under 5% CO₂. Human CD8⁺ T cells were isolated from buffy coats, activated with anti-CD3 and CD28 mAbs that were plate-bound and expanded in RPMI 1640 medium supplemented with 10% human serum and 100 IU/mL IL-2 and 5 ng/ml IL-15 at 37°C under 5% CO₂. Interleukins and CXCL10 were from PeproTech. LPA(1-oleoyl) was obtained from Avanti Polar Lipids. Human ATX was produced in HEK293 Flip-in cells and purified as previously described⁵⁴. Fibronectin and PF-8380 were purchased from Sigma- Aldrich. IOA-289 (formerly CRT750) was synthesized as previously described⁴⁸.

Isolation and expansion of melanoma-derived TILs

TIL isolation and expansion was started by generation of a single cell suspension by enzymatic digestion of the resected metastatic tumor material obtained by surgery. Resulting cell suspensions were cultured in the presence of 6000 IU/ml IL-2 (Proleukin, Novartis) for two to four weeks. During the subsequent Rapid Expansion Protocol of two weeks, T cells were cultured in 50% RPMI/50% AIM-V medium in the presence of 3,000 IU/ml IL-2, 30 ng/ml anti-CD3 antibody (OKT-3, Miltenyi) and irradiated autologous PBMCs (feeder cells in 200-fold excess over TIL).

Isolation of peripheral CD8⁺ T cells

Human peripheral blood mononuclear cells (PBMCs) were isolated from fresh buffy coats using Ficoll-Paque Plus (GE Healthcare) gradient centrifugation. Total CD8⁺ T cells were isolated using magnetic sorting with CD8 microbeads (Miltenyi Biotec). Blood samples were obtained from anonymized healthy male donors with written informed consent in accordance to guidelines established by the Sanquin Medical Ethical Committee.

Conditioned media

Conditioned media were collected from MDA-MB435 and A375M cells. Sub-confluent 10-cm dishes of melanoma cells were washed with PBS and incubated in DMEM containing 0.5% FCS. Conditioned medium was harvested after 24 and 48 hrs, and centrifuged for 30 min at 4000 rpm in a tabletop centrifuge to remove cell debris.

Transwell migration assays

T cell migration was measured using 48-well chemotaxis chambers (Neuro Probe, Inc.) equipped with 5 μm -pore polycarbonate membranes (8 μm -pore for melanoma cells), which were coated with fibronectin (1 $\mu\text{g}/\text{ml}$). Cells ($1 \times 10^6/\text{ml}$) were added to the upper chamber. Migration was assessed after 2 hrs for TILs and CD8⁺ T cells at 37°C in humidified air containing 5% CO₂. Migrated cells were fixed in Diff-Quik Fix and stained using Diff-Quik II. Migration was quantified by color intensity measurements using Image J software.

ATX lysoPLD activity

ATX enzymatic activity in conditioned media was measured by steady-state choline release from exogenously added LPC using a coupled reaction, as detailed elsewhere⁵⁴. Briefly, media were centrifuged for 45 min at 4,500 rpm, upon which 75 μl of the supernatants were plated on 96-well plates together with 600 μM LPC(18:1), 1 U ml⁻¹ choline oxidase, 2 U ml⁻¹ horseradish peroxidase (HRP) and 2 mM homovanillic acid (HVA), reaching a final volume of 100 μl . ATX activity was measured by HVA fluorescence at $\lambda_{\text{ex}}/\lambda_{\text{em}} = 320/460$ nm every 30 s for at least 160 min at 37°C with a Pherastar plate reader (BMG Labtech). Since ATX activity in vitro presents a ~15-min lag phase, the subsequent linear slope (60-160 min) was used to perform all analyses. Triplicate measures were statistically analyzed by an unpaired t test.

Western blotting

Cells were washed in ice-cold PBS (phosphate-buffered saline containing 2 mM Ca²⁺ and Mg²⁺), lysed in RIPA buffer with protease inhibitors and spun down. Equal amounts of proteins were determined by BCA protein assay kit (Pierce), separated by SDS-PAGE using pre-cast gradient gels (4-12% Nu-Page Bis-Tris, Invitrogen) and transferred to nitrocellulose membranes. The membrane was blocked for 1 hr at room-temperature in 5% skimmed milk in TBST. Incubation with antibodies was done overnight at 4°C, followed by 1 hr incubation with horseradish peroxidase- conjugated secondary antibodies (DAKO, Glostrup, Denmark). Proteins were visualized using ECL Western blot reagent (GE Healthcare, Chalfont St. Giles, UK).

qPCR analysis

Expression levels of LPA receptors and ATX/ENPP2 were quantified by RT-qPCR. Total RNA was isolated using GeneJET purification kit (Fermentas). cDNA was synthesized by reverse transcription from 2 mg RNA with oligodT 15 primers and SSII RT enzyme (Invitrogen). qPCR was performed on a 7500 Fast System (Applied Biosystems) as follows: 95°C for 2 min followed by 40 cycles at 95°C for 15 s followed by 60°C for 1 min. 200 nM forward and reverse primers, 16 ml SYBR Green Supermix (Applied Biosystems) and diluted

cdNA were used in the final reaction mixture. Cyclophilin was used as reference gene and milliQ was used as negative control. Normalized expression was calculated following the equation $NE = 2^{-(Ct\ target - Ct\ reference)}$. Primers used: LPA1 forward AATCGGGATACCATGATGAGT, CCAGGAGTCCAGCAGATGATAAA; LPA2 forward CGCTCAGCCTGGTCAAAGACT, TTGCAGGACTCACAGCCTAAAC; LPA3 forward AGGACACCCATGAAGCTAATGAA, GCCGTCGAGGAGCAGAAC; LPA4 forward CCTAGTCCTCAGTGGCGGTATT, CCTTCAAAGCAGGTGGTGGTT; LPA5 forward CCAGCGACCTGCTCTTCAC, CCAGTGGTGCAGTGCCTAGT; LPA6 forward AAAGTGGTCTGTCAGGAGAAGT, CAGGCAGCAGATTCATTGTCA; ENPP2 forward ATTACAGCCACCAAGCAAGG, TCCCTCAGAGGATTTGTCAT; Cyclophilin forward CATCTGCACTGCCAAGACTGA and reverse TTGCCAAACACCACATGCTT.

ATX knockdown melanoma cells

To generate ATX knockdown melanoma cells, we used five human *ENPP2* shRNAs in the lentiviral vector pLKO1: (TRC human shRNA library; TRCN0000048993, TRCN0000048995-TRCN0000048997 and TRCN0000174091). To generate particles for stable infections, HEK293T cells were transfected with single shRNA hairpins using the calcium phosphate protocol; the virus particles were collected at 48 hrs after transfection. *ENPP2* stable knockdown cells were selected and maintained in medium containing 2 µg/ml puromycin.

Lipid extraction and LC-MS/MS measurements of LPA

Extraction of lipids from cell-free conditioned media was done using acidified organic solvents and measurement of seventeen LPA species was accomplished using LC-MS/MS. Quantitation of LPA species was achieved using LPA(17:0) as an internal standard. Experimental details can be found elsewhere⁵⁰.

Studies in mice

Six to eight-week old female C57BL/6Jrj (B6) mice were obtained from Janvier Laboratories (Le Genest Saint Isle, France) and maintained in individually ventilated cages (Innovive, San Diego, CA) under specific pathogen-free conditions. All mouse experiments were performed in accordance with institutional and national guidelines and were approved by the Committee for Animal Experimentation at the NKI.

Tumor cells and subcutaneous transplantation

TC-1 tumor cells are lung epithelial cells engineered to express HPV16 E6 and E7 proteins⁶¹. Cells were obtained from the Leiden University Medical Center in 2015, and the authors did not perform further authentication. TC-1 cells stably overexpressing ATX were generated by retroviral

transduction and ATX overexpression was validated by Western blotting (Supplementary Figure 3A). TC-1 cells were cultured in medium, supplemented with 10% fetal calf serum (FCS), 0.1 mM non-essential amino acids, 1 mM sodium pyruvate, 2 mM L-glutamine, 10 mM HEPES and antibiotics at 37°C, 5% CO₂. TC-1 cell stock was tested negative for Mycoplasma by PCR, and cells thawed from this stock were used within 3 passages for in vitro and in vivo experiments. On day 0, mice were anesthetized with isoflurane and injected s.c. with 1×10^5 TC-1 tumor cells. Tumor size was measured by calipers in two dimensions and calculated as: area (mm²) = width x length. Mice were monitored twice per week. Mice were sacrificed when the tumor diameter reached 15 mm or when the tumor size reached 100 mm². In the survival curves, censored events indicate mice were sacrificed before treated tumors reached 100 mm².

Anti-cancer vaccination

The HELP-E7SH plasmid DNA vaccine was described previously and validated in detail. Intra-epidermal DNA “tattoo” vaccination was performed as described in the same papers. Briefly, the hair on a hind leg was removed using depilating cream (Veet, Reckitt Benckiser) prior to vaccination, mice were anesthetized and 15 µl of 2 mg/ml plasmid DNA solution in 10 mM Tris, 1 mM EDTA, pH 8.0 was applied to the hairless skin with a Permanent Make Up tattoo device (MT Derm GmbH, Berlin, Germany), using a sterile disposable 9-needle bar with a needle depth of 1 mm and oscillating at a frequency of 100 Hz for 45 sec.

Tissue preparation and flow cytometry

At the indicated days, blood was sampled from live mice or mice were sacrificed and lymphoid tissues and tumors were harvested. Peripheral blood cells were collected by tail bleeding in Microvette CB300 LH tubes (Sarstedt). Red blood cells were lysed in 0.14 M NH₄Cl and 0.017 M Tris-HCl (pH 7.2) for 1 min at room temperature and cell suspensions were washed and stained with relevant mAbs, as indicated below. Tumor tissue was mechanically disaggregated using a Mcllwain tissue chopper (Mickle Laboratory Engineering), and a single-cell suspension was prepared by digesting the tissue in collagenase type A (Roche) and 25 µg/ml DNase (Sigma) in serum-free DMEM medium for 45 min at 37°C. Enzyme activity was neutralized by addition of DMEM containing 8% FCS, and the tissue was dispersed by passing through a 70-µm cell strainer. Lymphoid tissue was dispersed into single cells passing it through a 70-µm cell strainer. Single cells were first stained with APC-conjugated E759-57/H-2D^b tetramers (Peptide and tetramer facility, Immunology department, Leiden University Medical Center) for 15 min at 4°C in the dark. After tetramer staining, tumor cells were incubated with 2% normal mouse serum with 10 µg/ml DNase for 15 min on ice. For surface staining, cells were incubated for 30 min on ice in the dark with fluorochrome-conjugated antibodies and 0.5 µl anti-APC mAb (clone APC003, BioLegend)

per sample in PBS, 0.5% BSA, 0.01% sodium azide to increase intensity of tetramer staining. LIVE/DEAD™ Fixable Near-IR Dead Cell Stain Kit (1:1000, Invitrogen) was added to exclude dead cells. Intracellular staining of cytokines and transcription factors was performed after cell fixation and permeabilization using the FOXP3 Transcription Factor Staining Buffer Set according to the manufacturer's protocol (Thermo Fischer Scientific). The following fluorochrome-conjugated mAbs were used for flow cytometry and obtained from BD Pharmingen (Breda, the Netherlands) unless otherwise specified: CD45.2-BUV395 (1:200; clone 30-F11), TCRβ-PECy7 (1:100; clone H57-597), CD3-PECy7 (1:100, clone 145-2C11, eBiosciences), CD8-BUV805 (1:300, clone 53-6.7), CD4- BV711 (1:200, clone GK1.5), FOXP3-PECy5.5 (1:100, clone FJK-16s, eBiosciences), CD44- BV785 (1:200, clone IM7, BioLegend), CD62L-FITC (1:100, clone MEL-14, eBioscience), IFNγ- eF450 (1:200, clone XMG-1.2, eBioscience), Granzyme B-PE (1:200, clone GB11, Sanquin Amsterdam). To detect cytokine production, whole cell preparations from tumor and lymphoid tissue were plated in 100 μl IMDM/8% FCS in a 96-well U-bottom plate. Cells were treated with 50 ng/ml phorbol 12-myristate 13-acetate (PMA, Sigma Aldrich, Zwijndrecht, The Netherlands) and 1 μM ionomycin (Sigma Aldrich) dissolved in DMSO and diluted in culture medium. Control (unstimulated) cells were treated with an equal volume of DMSO diluted in culture medium. GolgiPlug (1 μg/ml; BD Biosciences) was added to all wells before incubating the cells for 3 hr at 37 °C, 5% CO₂. To determine absolute cell numbers AccuCount Blank Particles (Spherotech) were added to the samples, prior to analysis. For all experiments, cells were analyzed using a BD Symphony A5 flow cytometer with Diva software, and the generated data were analyzed using FlowJo software.

Immuno-histochemical analysis

Harvested tumors were fixed for 24 hrs in aqueous solution with 50% ethanol, 5% acetic acid and 3.7% formalin, embedded in paraffin, and then sectioned randomly at 5 mm. For immunostaining, sections were rehydrated and incubated with primary antibodies to CD8 (eBioscience; clone 4SM15), CD4 (eBioscience; clone 4SM95) and FOXP3 (eBioscience; clone FJK-16s). Endogenous peroxidases were blocked with 3% H₂O₂, and the sections were then incubated with biotin-conjugated secondary antibodies, followed by incubation with HRP-conjugated streptavidin-biotin (DAKO). The substrate was developed using diaminobenzidine (DAB) (DAKO). We included negative controls to determine background staining, which was negligible. For the assessment of immune-cell infiltration in the tumor cross-sections, the immuno-stained slides were scanned and digitally processed using the Panoramic 1000 scanner (3DHISTECH, Hungary) equipped with a 20x objective. Digital whole slide images of CD8-, CD4- and FOXP3-stained serial tissue sections were registered with the HE sections in HALOTM image analysis software version (3.2.1851.229) (Indica Labs, Corrales, NM). The tumor area within the stained sections were

manually annotated and all nuclei within the tumor area (hematoxylin and/or DAB staining) were automatically segmented with the use of the commercially available Indica Labs – Multiplex IHC v2.3.4 algorithm module. Optimized parameters for the detection of nuclei signal included nuclear weight (1 for hematoxylin and 0.066 for DAB staining), nuclear contrast threshold (0.44), minimum nuclear optical density (0.095), nuclear size (11.3 – 220.7), minimal nuclear roundness (0.033) and nuclear segmentation aggressiveness (0.536). The optimized module parameters for the cytoplasmic and membrane detection included DAB-markup color (198, 163, 122) with the DAB-nucleus positive threshold (0.1105, 2.5, 2.5). The algorithm module parameters were kept constant for the analysis of all the sections across the different lymphocyte stainings. Next, with the utilization of the algorithm the total cell number within the tumor area (per section per staining) was automatically determined along with the equivalent number of each lymphocyte classification as DAB-positive cells. For the quantification analysis, the fraction (percentage) of DAB-positive cells (determined either via nucleus or cytoplasmic/membrane staining) over the total number of cells within the tumor area was used.

Single-cell RNA-seq analysis of human melanoma tumors

Single-cell data from 32 melanoma tumors (Jerby-Arnon et al., 2018) was downloaded from NCBI GEO (gse115978) and exported to the R2 platform (<http://r2.amc.nl>, Mixed Melanoma SC - Regev - 7186 - tpm - gse115978). tSNE clustering was applied to 7186 cells. A complexity of 5 was chosen to represent the cohort. Inferred cell type information was extracted from the GEO dataset. Expression of *ENPP2* and other annotations were projected onto the tSNE embedding. In every patient sample, the percentage of *ENPP2*-expressing cells was correlated to the percentage of cells inferred to be CD8⁺-positive. All analyses of the single-cell data were performed in the R2 genomics analysis and visualization platform.

Statistical analyses

For in vitro migration assays, a two-tailed unpaired Student's t-test was applied. A P value < 0.05 was considered statistically significant; *, p<0.05; **, p<0.005; ***, p<0.001; and ****, p<0.0001. Data from mouse studies were analyzed using GraphPad Prism version 9 (GraphPad Software, La Jolla, CA). Differences between various treatment groups were analyzed using the Mann-Whitney U Test. Differences in survival curves were analyzed using the Log Rank (Mantel-Cox) test. Differences with P values <0.05 were considered statistically significant.

Acknowledgements

We thank Paula Voabil, Jos Urbanus, Yanling Xiao, Marjolein Mertz, and Juan Manuel Alba for their help with experiments and data analysis, Kees Franken for making MHC tetramers, Junken Aoki for providing anti-ATX antibodies, and Tomasz Ahrends and Anne van der Leun for helpful discussions and sharing unpublished data. This work was supported by private funding to W.H.M. and grants from the Dutch Cancer Society (NKI 2013-5951 and 10764 to I.V. and NKI 2017-10894 to J.B. and I.V.), the German Research Foundation (DFG) (ME 4924/1-1 to A. Mazzocca), and the NIH (P30 GM127211 to A.J.M.). E.M.-R. is supported by a “Ramón y Cajal” Award (RYC2019-027950-I) from Ministerio de Ciencia e Innovación (MICINN), Spain.

Author contributions

Conceptualization, J.H., Z.J., T.N.S., I.V., J.v.d.B., J.B., and W.H.M.; investigation, E.M.-R., E.F., I.v.d.H.A., A. Menegakis, A. Mazzocca, M.v.Z., A.J.M., J.K., F.S.-P., I.V., and J.v.d.B.; methodology, E.M.-R., E.F., I.v.d.H.A., M.v.Z., A.J.M., J.K., F.S.-P., S.K., T.L., J.H., Z.J., T.N.S., A.P., I.V., J.v.d.B., J.B., and W.H.M.; data analysis, E.M.-R., E.F., I.v.d.H.A., A. Menegakis, M.v.Z., A.J.M., J.K., F.S.-P., S.K., T.L., Z.J., A.P., I.V., J.v.d.B., J.B., and W.H.M.; validation, E.M.-R., E.F., I.v.d.H.A., M.v.Z., A.P., I.V., J.v.d.B., and W.H.M.; visualization, E.M.-R., E.F., I.v.d.H.A., A. Menegakis, M.v.Z., J.K., F.S.-P., I.V., and J.B.; writing, E.M.-R., E.F., J.B., and W.H.M.; supervision, J.B. and W.H.M.

Declaration of interests

Z.J. is an employee and shareholder of iOnctura SA, a company developing an ATX inhibitor for use in cancer.

References

- 1 Fridman, W. H., Zitvogel, L., Sautes-Fridman, C. & Kroemer, G. The immune contexture in cancer prognosis and treatment. *Nat Rev Clin Oncol* **14**, 717-734 (2017).
- 2 Ribas, A. & Wolchok, J. D. Cancer immunotherapy using checkpoint blockade. *Science* **359**, 1350-1355 (2018).
- 3 Jacquelot, N., Duong, C. P. M., Belz, G. T. & Zitvogel, L. Targeting Chemokines and Chemokine Receptors in Melanoma and Other Cancers. *Front Immunol* **9**, 2480 (2018).
- 4 Nagarsheth, N., Wicha, M. S. & Zou, W. Chemokines in the cancer microenvironment and their relevance in cancer immunotherapy. *Nat Rev Immunol* **17**, 559-572 (2017).
- 5 Ozga, A. J., Chow, M. T. & Luster, A. D. Chemokines and the immune response to cancer. *Immunity* **54**, 859-874 (2021).
- 6 Battle, E. & Massague, J. Transforming Growth Factor-beta Signaling in Immunity and Cancer. *Immunity* **50**, 924-940 (2019).
- 7 Joyce, J. A. & Fearon, D. T. T cell exclusion, immune privilege, and the tumor microenvironment. *Science* **348**, 74-80 (2015).
- 8 Kerdidani, D. *et al.* Wnt1 silences chemokine genes in dendritic cells and induces adaptive immune resistance in lung adenocarcinoma. *Nat Commun* **10**, 1405 (2019).
- 9 Spranger, S., Bao, R. & Gajewski, T. F. Melanoma-intrinsic beta-catenin signalling prevents anti-tumour immunity. *Nature* **523**, 231-235 (2015).
- 10 Spranger, S. & Gajewski, T. F. Impact of oncogenic pathways on evasion of antitumour immune responses. *Nat Rev Cancer* **18**, 139-147 (2018).
- 11 Anandappa, A. J., Wu, C. J. & Ott, P. A. Directing Traffic: How to Effectively Drive T Cells into Tumors. *Cancer Discov* **10**, 185-197 (2020).
- 12 van der Woude, L. L., Gorris, M. A. J., Halilovic, A., Figdor, C. G. & de Vries, I. J. M. Migrating into the Tumor: a Roadmap for T Cells. *Trends Cancer* **3**, 797-808 (2017).
- 13 Umezu-Goto, M. *et al.* Autotaxin has lysophospholipase D activity leading to tumor cell growth and motility by lysophosphatidic acid production. *J Cell Biol* **158**, 227-233 (2002).
- 14 Tokumura, A. *et al.* Identification of human plasma lysophospholipase D, a lysophosphatidic acid-producing enzyme, as autotaxin, a multifunctional phosphodiesterase. *J Biol Chem* **277**, 39436-39442 (2002).
- 15 Perrakis, A. & Moolenaar, W. H. Autotaxin: structure-function and signaling. *J Lipid Res* **55**, 1010-1018 (2014).
- 16 Nam, S. W. *et al.* Autotaxin (NPP-2), a metastasis-enhancing motogen, is an angiogenic factor. *Cancer Res* **61**, 6938-6944 (2001).
- 17 Stracke, M. L. *et al.* Identification, purification, and partial sequence analysis of autotaxin, a novel motility-stimulating protein. *J Biol Chem* **267**, 2524-2529 (1992).
- 18 van Meeteren, L. A. *et al.* Autotaxin, a secreted lysophospholipase D, is essential for blood vessel formation during development. *Mol Cell Biol* **26**, 5015-5022 (2006).
- 19 Kanda, H. *et al.* Autotaxin, an ectoenzyme that produces lysophosphatidic acid, promotes the entry of lymphocytes into secondary lymphoid organs. *Nat Immunol* **9**, 415-423 (2008).
- 20 Mills, G. B. & Moolenaar, W. H. The emerging role of lysophosphatidic acid in cancer. *Nat Rev Cancer* **3**, 582-591 (2003).
- 21 Benesch, M. G. K., MacIntyre, I. T. K., McMullen, T. P. W. & Brindley, D. N. Coming of Age for Autotaxin and Lysophosphatidate Signaling: Clinical Applications for Preventing, Detecting and Targeting Tumor-Promoting Inflammation. *Cancers (Basel)* **10** (2018).

- 22 Yanagida, K., Kurikawa, Y., Shimizu, T. & Ishii, S. Current progress in non-Edg family LPA receptor research. *Biochim Biophys Acta* **1831**, 33-41 (2013).
- 23 Yung, Y. C., Stoddard, N. C. & Chun, J. LPA receptor signaling: pharmacology, physiology, and pathophysiology. *J Lipid Res* **55**, 1192-1214 (2014).
- 24 Hisano, Y. & Hla, T. Bioactive lysolipids in cancer and angiogenesis. *Pharmacol Ther* **193**, 91-98 (2019).
- 25 Hausmann, J. *et al.* Structural basis of substrate discrimination and integrin binding by autotaxin. *Nat Struct Mol Biol* **18**, 198-204 (2011).
- 26 Houben, A. J. *et al.* The polybasic insertion in autotaxin alpha confers specific binding to heparin and cell surface heparan sulfate proteoglycans. *J Biol Chem* **288**, 510-519 (2013).
- 27 Fulkerson, Z. *et al.* Binding of autotaxin to integrins localizes lysophosphatidic acid production to platelets and mammalian cells. *J Biol Chem* **286**, 34654-34663 (2011).
- 28 Auciello, F. R. *et al.* A Stromal Lysolipid-Autotaxin Signaling Axis Promotes Pancreatic Tumor Progression. *Cancer Discov* **9**, 617-627 (2019).
- 29 David, M. *et al.* Cancer cell expression of autotaxin controls bone metastasis formation in mouse through lysophosphatidic acid-dependent activation of osteoclasts. *PLoS One* **5**, e9741 (2010).
- 30 Lin, S. *et al.* Autotaxin determines colitis severity in mice and is secreted by B cells in the colon. *FASEB J* **33**, 3623-3635 (2019).
- 31 Liu, S. *et al.* Expression of autotaxin and lysophosphatidic acid receptors increases mammary tumorigenesis, invasion, and metastases. *Cancer Cell* **15**, 539-550 (2009).
- 32 Marshall, J. C. *et al.* Effect of inhibition of the lysophosphatidic acid receptor 1 on metastasis and metastatic dormancy in breast cancer. *J Natl Cancer Inst* **104**, 1306-1319 (2012).
- 33 Ledein, L. *et al.* Translational engagement of lysophosphatidic acid receptor 1 in skin fibrosis: from dermal fibroblasts of patients with scleroderma to tight skin 1 mouse. *Br J Pharmacol* **177**, 4296-4309 (2020).
- 34 Sakai, N. *et al.* The involvement of autotaxin in renal interstitial fibrosis through regulation of fibroblast functions and induction of vascular leakage. *Sci Rep* **9**, 7414 (2019).
- 35 Tager, A. M. *et al.* The lysophosphatidic acid receptor LPA1 links pulmonary fibrosis to lung injury by mediating fibroblast recruitment and vascular leak. *Nat Med* **14**, 45-54 (2008).
- 36 Kalluri, R. The biology and function of fibroblasts in cancer. *Nat Rev Cancer* **16**, 582-598 (2016).
- 37 Winkler, J., Abisoye-Ogunniyan, A., Metcalf, K. J. & Werb, Z. Concepts of extracellular matrix remodelling in tumour progression and metastasis. *Nat Commun* **11**, 5120 (2020).
- 38 Lee, Z. *et al.* Role of LPA4/p2y9/GPR23 in negative regulation of cell motility. *Mol Biol Cell* **19**, 5435-5445 (2008).
- 39 Jongsma, M., Matas-Rico, E., Rzadkowski, A., Jalink, K. & Moolenaar, W. H. LPA is a chemorepellent for B16 melanoma cells: action through the cAMP-elevating LPA5 receptor. *PLoS One* **6**, e29260 (2011).
- 40 Takahashi, K. *et al.* Lysophosphatidic acid (LPA) signaling via LPA(4) and LPA(6) negatively regulates cell motile activities of colon cancer cells. *Biochem Biophys Res Commun* **483**, 652-657 (2017).
- 41 Takeda, A. *et al.* Fibroblastic reticular cell-derived lysophosphatidic acid regulates confined intranodal T-cell motility. *Elife* **5**, e10561 (2016).
- 42 Bai, Z. *et al.* Constitutive lymphocyte transmigration across the basal lamina of high endothelial venules is regulated by the autotaxin/lysophosphatidic acid axis. *J Immunol* **190**, 2036-2048 (2013).
- 43 Knowlden, S. A. *et al.* Regulation of T cell motility in vitro and in vivo by LPA and LPA2. *PLoS One* **9**, e101655 (2014).
- 44 Ghandi, M. *et al.* Next-generation characterization of the Cancer Cell Line Encyclopedia. *Nature* **569**, 503-508 (2019).

- 45 Li, H. *et al.* Dysfunctional CD8 T Cells Form a Proliferative, Dynamically Regulated Compartment within Human Melanoma. *Cell* **176**, 775-789 e718 (2019).
- 46 Rohaan, M. W., Wilgenhof, S. & Haanen, J. Adoptive cellular therapies: the current landscape. *Virchows Arch* **474**, 449-461 (2019).
- 47 Groom, J. R. & Luster, A. D. CXCR3 ligands: redundant, collaborative and antagonistic functions. *Immunol Cell Biol* **89**, 207-215 (2011).
- 48 Shah, P. *et al.* Discovery of potent inhibitors of the lysophospholipase autotaxin. *Bioorg Med Chem Lett* **26**, 5403-5410 (2016).
- 49 Aoki, J., Inoue, A. & Okudaira, S. Two pathways for lysophosphatidic acid production. *Biochim Biophys Acta* **1781**, 513-518 (2008).
- 50 Kraemer, M. P. *et al.* Effects of diet and hyperlipidemia on levels and distribution of circulating lysophosphatidic acid. *J Lipid Res* **60**, 1818-1828 (2019).
- 51 Muinonen-Martin, A. J. *et al.* Melanoma cells break down LPA to establish local gradients that drive chemotactic dispersal. *PLoS Biol* **12**, e1001966 (2014).
- 52 Sciorra, V. A. & Morris, A. J. Roles for lipid phosphate phosphatases in regulation of cellular signaling. *Biochim Biophys Acta* **1582**, 45-51 (2002).
- 53 Keune, W. J. *et al.* Steroid binding to Autotaxin links bile salts and lysophosphatidic acid signalling. *Nat Commun* **7**, 11248 (2016).
- 54 Salgado-Polo, F. *et al.* Lysophosphatidic acid produced by autotaxin acts as an allosteric modulator of its catalytic efficiency. *J Biol Chem* **293**, 14312-14327 (2018).
- 55 Nishimasu, H. *et al.* Crystal structure of autotaxin and insight into GPCR activation by lipid mediators. *Nat Struct Mol Biol* **18**, 205-212 (2011).
- 56 Moolenaar, W. H. & Perrakis, A. Insights into autotaxin: how to produce and present a lipid mediator. *Nat Rev Mol Cell Biol* **12**, 674-679 (2011).
- 57 Gnocchi, D. *et al.* Novel lysophosphatidic acid receptor 6 antagonists inhibit hepatocellular carcinoma growth through affecting mitochondrial function. *J Mol Med (Berl)* **98**, 179-191 (2020).
- 58 Inoue, A. *et al.* Illuminating G-Protein-Coupling Selectivity of GPCRs. *Cell* **177**, 1933-1947 e1925 (2019).
- 59 Wu, V. *et al.* Illuminating the Onco-GPCRome: Novel G protein-coupled receptor-driven oncocrine networks and targets for cancer immunotherapy. *J Biol Chem* **294**, 11062-11086 (2019).
- 60 Yanagida, K. *et al.* Identification and characterization of a novel lysophosphatidic acid receptor, p2y5/LPA6. *J Biol Chem* **284**, 17731-17741 (2009).
- 61 Lin, K. Y. *et al.* Treatment of established tumors with a novel vaccine that enhances major histocompatibility class II presentation of tumor antigen. *Cancer Res* **56**, 21-26 (1996).
- 62 Ahrends, T. *et al.* CD27 Agonism Plus PD-1 Blockade Recapitulates CD4+ T-cell Help in Therapeutic Anticancer Vaccination. *Cancer Res* **76**, 2921-2931 (2016).
- 63 Ahrends, T. *et al.* CD4(+) T Cell Help Confers a Cytotoxic T Cell Effector Program Including Coinhibitory Receptor Downregulation and Increased Tissue Invasiveness. *Immunity* **47**, 848-861 e845 (2017).
- 64 Lee, S. C. *et al.* Autotaxin and LPA1 and LPA5 receptors exert disparate functions in tumor cells versus the host tissue microenvironment in melanoma invasion and metastasis. *Mol Cancer Res* **13**, 174-185 (2015).
- 65 Brindley, D. N., Tang, X., Meng, G. & Benesch, M. G. K. Role of Adipose Tissue-Derived Autotaxin, Lysophosphatidate Signaling, and Inflammation in the Progression and Treatment of Breast Cancer. *Int J Mol Sci* **21** (2020).
- 66 Jerby-Arnon, L. *et al.* A Cancer Cell Program Promotes T Cell Exclusion and Resistance to Checkpoint Blockade. *Cell* **175**, 984-997 e924 (2018).

- 67 Mariathasan, S. *et al.* TGFbeta attenuates tumour response to PD-L1 blockade by contributing to exclusion of T cells. *Nature* **554**, 544-548 (2018).
- 68 Saunders, L. P. *et al.* Kinetic analysis of autotaxin reveals substrate-specific catalytic pathways and a mechanism for lysophosphatidic acid distribution. *J Biol Chem* **286**, 30130-30141 (2011).
- 69 Baeyens, A., Fang, V., Chen, C. & Schwab, S. R. Exit Strategies: S1P Signaling and T Cell Migration. *Trends Immunol* **36**, 778-787 (2015).
- 70 Laidlaw, B. J., Gray, E. E., Zhang, Y., Ramirez-Valle, F. & Cyster, J. G. Sphingosine-1-phosphate receptor 2 restrains egress of gammadelta T cells from the skin. *J Exp Med* **216**, 1487-1496 (2019).
- 71 Kaplan, M. H., Smith, D. I. & Sundick, R. S. Identification of a G protein coupled receptor induced in activated T cells. *J Immunol* **151**, 628-636 (1993).
- 72 Webb, T. E., Kaplan, M. G. & Barnard, E. A. Identification of 6H1 as a P2Y purinoceptor: P2Y5. *Biochem Biophys Res Commun* **219**, 105-110 (1996).
- 73 Mathew, D. *et al.* LPA(5) Is an Inhibitory Receptor That Suppresses CD8 T-Cell Cytotoxic Function via Disruption of Early TCR Signaling. *Front Immunol* **10**, 1159 (2019).
- 74 Borst, J., Ahrends, T., Babala, N., Melief, C. J. M. & Kastenmuller, W. CD4(+) T cell help in cancer immunology and immunotherapy. *Nat Rev Immunol* **18**, 635-647 (2018).
- 75 De Jaeghere, E. A., Denys, H. G. & De Wever, O. Fibroblasts Fuel Immune Escape in the Tumor Microenvironment. *Trends Cancer* **5**, 704-723 (2019).
- 76 Rosato, R. R. *et al.* Evaluation of anti-PD-1-based therapy against triple-negative breast cancer patient-derived xenograft tumors engrafted in humanized mouse models. *Breast Cancer Res* **20**, 108 (2018).
- 77 Patton, E. E. *et al.* Melanoma models for the next generation of therapies. *Cancer Cell* **39**, 610-631 (2021).

Supplemental Data

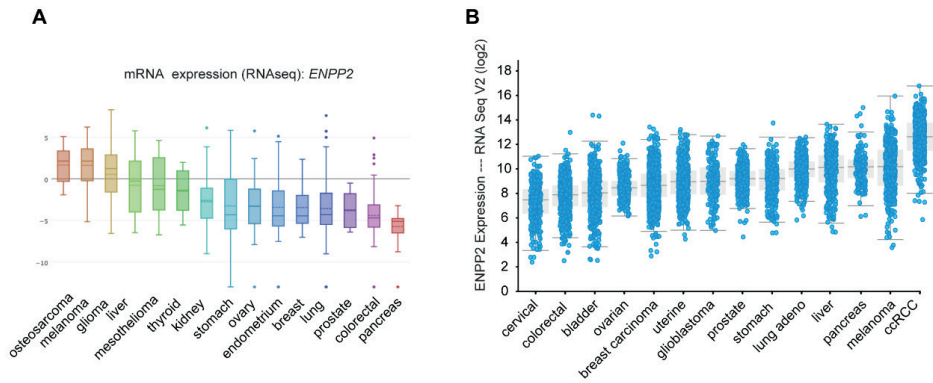


Figure S1. ATX mRNA expression in cancer cell lines and solid tumors.

(A) *ENPP2* expression in the indicated cell lines ranked according to median values. Note high *ENPP2* expression in melanoma cell lines (n=61). RNAseq expression data were retrieved from the Cancer Cell Line Encyclopedia (CCLE). (B) Pan-cancer analysis of *ENPP2* expression in the indicated solid tumors ranked according to median values (ccRCC, clear cell renal cell carcinoma). RNAseq v2 mRNA expression data were retrieved from the TCGA database (<https://www.cbioportal.org>). Note that *ENPP2* expression in cancer cell lines poorly correlates with that in the corresponding tumors, likely due to the presence of ATX-expressing stromal cells.

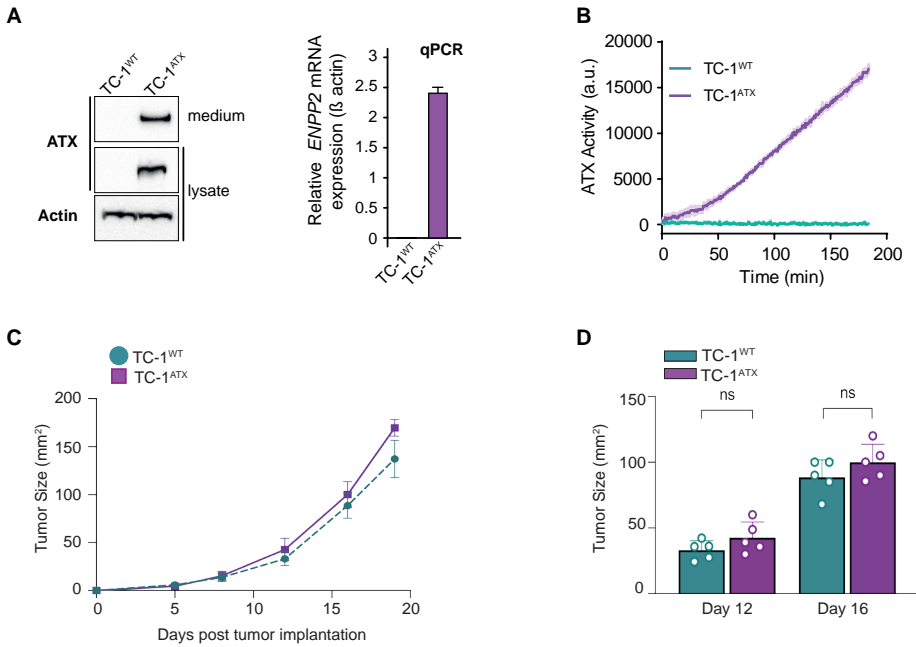


Figure S2. Characteristics of wild-type and ATX-expressing TC-1 tumors.

(A) (Left) immunoblot analysis of ATX protein expression in wild-type (TC-1^{WT}) and ATX-expressing (TC-1^{ATX}) tumor cells. Actin was used as loading control. (Right) ATX mRNA expression (relative to Cyclophilin) in TC-1^{WT} and TC-1^{ATX} cells as analyzed by qPCR. (B) Secreted ATX (lysoPLD) activity in supernatants from TC-1^{WT} and TC-1^{ATX} cells, as measured by choline release from added LPC(18:1) over time. See Methods for details. (C) TC-1^{WT} and TC-1^{ATX} tumor growth expressed as mean size in non-vaccinated mice (n=5). (D) Average tumor size in the same mice as in (C) on days 12 and 16 after s.c. tumor cell implantation. Data is depicted as mean ± SD; ns: not significant (Mann-Whitney U test).

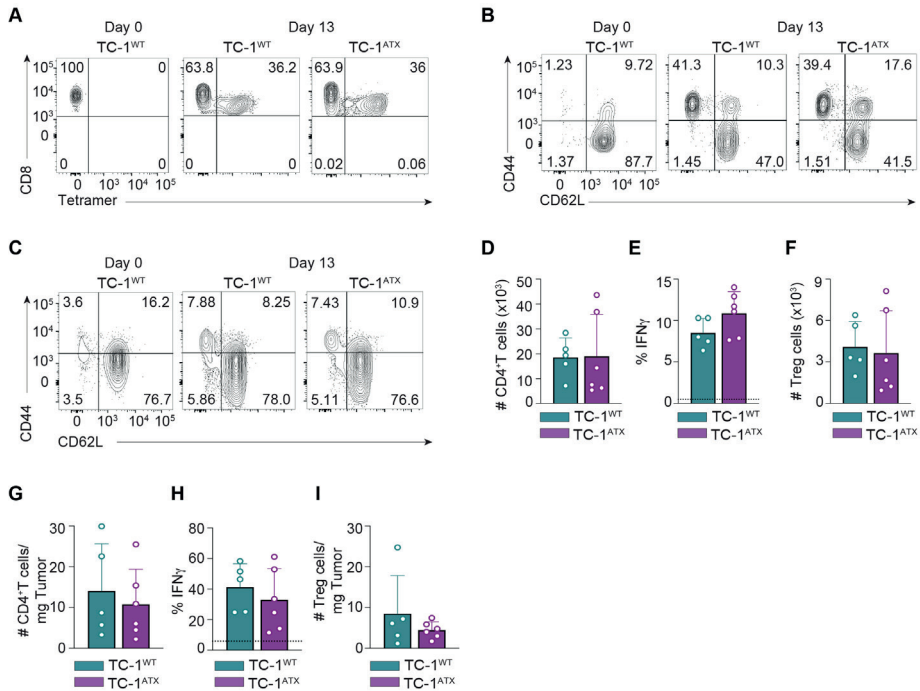


Figure S3. Enforced ATX expression in tumor cells does not affect the CD4⁺ T cell response to vaccination. (A-C) Primary data belonging to Figure 5. Representative flow cytometry plots depicting H-2D^b/E7₄₉₋₅₇ Tet⁺ cells (A) and CD44⁺CD62L⁻ effector phenotype cells among total CD8⁺ T cells (B) and total CD4⁺ T cells (C) in blood from TC-1^{WT} (n = 6) and TC-1^{ATX} (n = 5) tumor-bearing mice at day 13 post vaccination. Data at day 0 are from non-vaccinated TC-1^{WT} tumor-bearing mice. (D-I) CD4⁺ T cell populations as analyzed by flow cytometry in spleen (D-F) and tumors (G-I) of TC-1^{WT} (n = 5) and TC-1^{ATX} (n = 6) tumor-bearing mice at day 18 after tumor implantation. (D) Absolute number (#) of FOXP3⁻ CD4⁺ conventional T cells (Tconv) in spleen. (E) Frequency of IFN γ ⁺ cells among conventional CD4⁺ T cells in spleen. IFN γ was measured as outlined in Figure 5. (F) Absolute number (#) of FOXP3⁺ CD4⁺ T cells (Tregs) in spleen. (G) Absolute number (#) of CD4⁺ Tconv cells per mg tumor tissue, found in TC-1^{WT} and TC-1^{ATX} tumor-bearing mice. (H) Frequency of IFN γ ⁺ cells within CD4⁺ Tconv cells in the tumors. IFN γ was measured as outlined in Figure 5. (I) Absolute number (#) of CD4⁺ Tregs in TC-1^{WT} and TC-1^{ATX} tumors. (D-I) Data is depicted as mean \pm SD; no significance for all cell populations analyzed (Mann-Whitney U test). Data in this figure are from one experiment representative of two experiments.

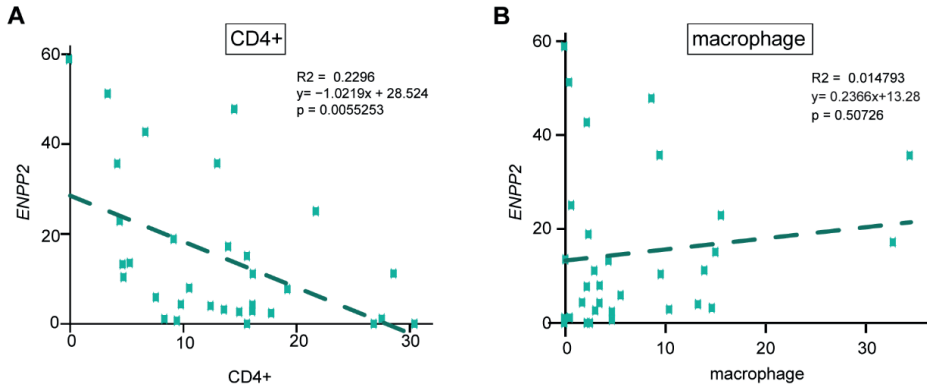


Figure S4. *ENPP2* expression and accumulation of CD4⁺ T cells (A) and macrophages (B) in melanoma tumors (n=32). Pearson's correlation between the percentage of inferred *ENPP2*-expressing cells and CD4⁺ T cells versus macrophages as indicated. For details see Figure 7.



6

General Discussion

Local radiotherapy (RT) has been used for over a century to induce DNA damage, leading to cell cycle arrest and cell death in rapidly proliferating tumor cells. To improve RT efficacy, studies have primarily focused on improving radiosensitivity by modulating DNA damage and repair. The contribution of the immune system¹, particularly CD8⁺ T cells² to RT-induced tumor regression has long been neglected. In recent years, the concept has emerged that RT is potentially immunogenic, since dying cells can release danger-associated molecular patterns (DAMPs)³ and tumor-associated antigens⁴. Such immunogenic cell death could lead to dendritic cell (DC) activation, causing tumor-specific T cell responses in the tumor-draining lymph node (TdLN)^{5,6}. This idea has greatly raised interest in using RT as an *in situ* anti-cancer vaccine. This concept was reinforced by the discovery that tumor regression outside the field of RT, known as the abscopal response⁷, is T cell mediated⁸. Consequently, numerous clinical trials were initiated to combine RT with immunotherapy (IT) strategies, in order to enhance systemic anti-tumor immune responses⁹. However, despite these efforts, clinical successes are unsatisfactory, with overall response rates generally not exceeding 18%¹⁰. In part, disappointment arises from unrealistic expectations set by mouse studies using tumor models with highly immunogenic exogenous antigens^{5,6,11,12}. Since endogenous tumor antigens are generally poorly immunogenic, these studies might overestimate the potential of RT to facilitate T cell priming to human cancer in the clinic. Additionally, while synergy between RT and IT in immune responsiveness is often claimed in mouse studies^{8,13-15}, clinical reports indicate that systemic anti-tumor immunity primarily reflects the effects induced by IT alone and do not truly represent a combined effect of RT and IT^{16,17}. For these reasons, the mechanisms that drive RT-induced T cell responses in the diversity of human cancers must be better understood. Only then can we rationally design the correct RT-IT combination strategies to synergistically increase systemic T-cell based immunity against cancer. This approach can be particularly useful for cancers that are not spontaneously immunogenic and are therefore in need of a “vaccination” approach^{18,19}.

The work described in this thesis aimed to unravel and optimize important determinants for RT-induced T cell responses in poorly immunogenic tumors. To achieve this, I addressed the following questions, which will be explored in the subsequent discussion:

1. To what extent does RT induce T cell responses against cancer?
2. Which impediments and potential IT targets can be utilized to enhanced RT-induced T cell responses in poorly immunogenic cancers?
3. Can RT be exploited to overcome local immunosuppression in the tumor microenvironment (TME)?

1) What is the potential of RT to raise systemic T-cell immunity?

RT responses are dictated by the tumor immune constellation

Traditionally, TMEs are classified as “immune-infiltrated”, “immune excluded” or “immune desert”, based on the varying levels of lymphocyte presence and localization²⁰. However, these classifications primarily rely on the density of CD3⁺ and/or CD8⁺ cells on immunohistochemistry slides²⁰ and may not accurately predict tumor responsiveness to IT. Recently, multi-omics analysis of human pan-cancer tissues revealed distinct immune constellations among tumors of the same type²¹⁻²³. These immune complexities significantly impact patient survival and response to IT^{21,22}. Tumors containing high myeloid cell content and fibroblasts, along with low presence of lymphocytes, often show negative survival outcomes and treatment responses, as opposed to tumors containing high lymphocyte abundance, combined with elevated levels of DCs and interferon type I (IFN-I) signaling²². Interestingly, FOXP3⁺ T regulatory cells (Tregs), generally considered immunosuppressive, are variably present among all immune contexts, but are typically associated with macrophage-enriched tumors²³.

Tumor responses to RT can vary, despite equal radiosensitivity *in vitro*²⁴. RT elicited systemic CD8⁺ T cell-mediated anti-tumor immunity in mouse tumor models that were spontaneously T cell-infiltrated, but not in T cell-devoid tumors^{18,24}. A recent patient study similarly identified that tumors enriched for IFN-I pathways, along with presence of CD4⁺ and CD8⁺ T cells, activated NK cells and inflammatory macrophages are associated with enhanced tumor radiosensitivity²⁵. Therefore, there appears to be a relationship between tumor immunogenicity and response to RT. In **chapter 2**, we analyzed records from The Cancer Genome Atlas (TCGA) using five pan-cancer immune phenotypes²¹. We observed reduced overall survival after RT in non-immunogenic cancers, described as “lymphocyte depleted”, in which the TME typically exhibits high myeloid-to-lymphocyte ratios²¹. We found that the transplantable TC-1 tumor model recapitulates human lymphocyte-depleted cancer and investigated the factors impeding the RT response (**chapter 2**)²¹. Despite expressing antigenic HPV16-derived E6 and E7 antigens, TC-1 tumors lack CD8⁺ T cells and have a TME enriched with myeloid cell populations, as confirmed by single-cell RNAseq analysis²⁶. This tumor model provides valuable insights into the requirements for tumor-specific T cell priming. Tumors like TC-1, which do not spontaneously provoke tumor-specific T cell responses, likely have not undergone T cell-mediated immune surveillance or pressure. As a result, they may remain susceptible to newly generated T cell responses upon RT and/or IT²⁷. In agreement, the TC-1 tumor is highly responsive to CD4⁺ and CD8⁺ T cell responses induced by vaccination (**chapter 5** and^{28,29}). Moreover, the TC-1 tumor model effectively recapitulates (dys)functional T cell priming in the TdLN³⁰. Additionally, we observed that TC-1 tumor growth triggers effector (e)Treg priming (**chapters 2, 3**) and attracts high levels of monocytes in the TdLN. These data illustrate the continuous interaction between the tumor and TdLN³¹, in this case resulting in the development of systemic immunosuppression.

In **chapter 2**, we discovered that RT of the TC-1 tumor caused priming of CD8⁺ cytotoxic T lymphocytes (CTLs) in the TdLN, necessary to mediate tumor control. However, eTreg expansion, induced by the tumor and exacerbated by RT, limited CTL priming. This mechanism may also be relevant in human cancer, as evidenced by tumor-induced Treg expansion in the TdLN in patients with challenging-to-treat cancers like breast, colorectal, and hepatocellular carcinoma³². Our finding highlights the potential of RT to stimulate tumor-specific T cell priming in lymphocyte-depleted tumors and identifies simultaneous Treg priming as a key negative regulatory mechanism. Whether prediction of anti-tumor immunity can solely rely on T cell-to-Treg ratios found in the TME remains controversial, as it appears highly influenced by the cancer molecular subtype and disease stage^{23,33}. Specifically, while the presence of Tregs is generally considered to negatively impact disease outcome, it may paradoxically be favorable for survival in head and neck, colorectal and esophageal cancer³³. This suggests that the mere presence of Tregs may not be sufficient to accurately predict disease outcomes. A patient cohort study of invasive breast cancer indicated that the ratio of effector Tregs to T cells, which contained a population with a higher suppressive phenotype, rather than the total Treg to T cell ratio, was a better predictor of treatment responses³⁴. Thus, instead of solely focusing on the entire Treg population, the functionality of the Tregs present in the TME should be considered to predict anti-tumor immune responses. Furthermore, recent RNA-seq data indicate that response to chemotherapy in Treg-enriched human cancers is associated with reduced suppressive Treg function, along with increased abundance of CD8⁺ T cells and inflammatory M1-type macrophages³⁵. Together, these findings highlight that the design of treatment strategies must encompass the broader tumor immune landscape, in addition to the Treg functional state.

The tumor-draining lymph node serves as a niche for pro- and anti-tumor immune responses

Anti-tumor immunity primarily relies on CTL responses orchestrated in the TdLN³⁶. Intravital imaging studies have revealed a two-step process for the effective priming of CTLs³⁷⁻³⁹, involving correct localization and activation of conventional (c)DCs in the TdLN. Initially, CD8⁺ and CD4⁺ T cells receive their first priming-step by encountering the cDC1 or cDC2 subset, respectively, in distinct areas of the LN. Subsequently, both T cell types interact with the same lymph-node resident or migratory cDC1s, enabling CD4⁺ T cells to provide the necessary help signals for optimizing DC activation and CTL differentiation^{37,40}. To achieve this, both cDC1s and cDC2s need appropriate activation and migration from the tumor to the TdLN^{41,42}. However, cDC paucity⁴³, inhibitory metabolic pathways^{44,45}, and negative immunoregulatory mechanisms from the tumor^{46,47} contribute to suboptimal DC activation, which extends to the TdLN and can lead to systemic immunosuppression. Additionally, tumors may enforce immunosuppression by causing

aberrant stromal remodeling and structuring in the LN, disrupting the normal dynamics required for lymphocyte interactions³² and/or by altering the cellular composition of the LN. This involves attraction of immunosuppressive myeloid cells⁴⁸ and Tregs⁴⁹ (**chapter 2** and **3**), which could limit T cell functionality^{48,50}. Notably, in the TdLN, tolerogenic cDCs may induce Treg priming and expansion⁵¹⁻⁵³, which subsequently impair CTL differentiation by inhibiting cDC1 responses⁵⁴. Aberrant immunity in the TdLN may also promote primary tumor progression and establish a microanatomic niche for metastases^{55,56}, as it is often the first tissue infiltrated³².

While the role of the LN as orchestrator for adaptive immune responses has been well-established, its function in supporting tumor immunity and response to IT has only recently been recognized^{36,57,58}. Studies in mice demonstrate that treatment efficacy of PD-1 inhibition is hindered when exit of T cells from the TdLN is blocked^{57,58}. Additionally, direct administration of anti-PD-L1 to the TdLN alone has been shown to achieve tumor control⁵⁷. Similar effects have been observed concerning CTLA-4 blockade⁵⁹. Likewise, the TdLN plays a crucial role in generating RT-induced systemic immunity¹², leading to both local (**chapter 2**) and abscopal¹¹ responses. Thus, effective anti-tumor immunity depends on the TdLN, despite potential immunosuppression. **Chapter 2** highlights the duality of this response in the context of RT, showing that RT can elicit CTL priming in the TdLN alongside Treg priming. These findings suggest that RT may support cDC1 activation by releasing DAMPs required for their migration to the TdLN. However, RT may also upregulate signals that hinder cDC1 recruitment to the TME⁶⁰, potentially limiting the number of CTLs primed in the TdLN based on the initial cDC1 population present in the tumor. Conversely, since the tumor contains high levels of cDC2s, Treg priming induced by these cDC2 cells may dominate cDC1-induced CTL priming in the TdLN after RT. IT strategies now focus on restoring cDC1 function in the tumor by alleviating cDC scarcity, supporting antigen spillage, and providing activation mimicry^{43,61,62}. However, whether these therapies are successful depends on the functional state of the TdLN^{63,64} and the ability to overcome existing immunosuppression^{57,65}.

In the clinic, the removal or irradiation of either the sentinel lymph node (the first lymph node receiving tumor drainage) or the entire LN basin is common to limit potential metastatic spread, as tumor involvement in these LNs are aberrant for survival⁶⁶. However, the therapeutic benefit of this approach is controversial⁶⁷. In view of the requirement for TdLNs to educate anti-tumor immune responses, treatment strategies should avoid removing or damaging lymph nodes when possible. In particular, in RT and RT-IT approaches, avoiding nodal irradiation is desirable, as the destruction of lymph nodes may compromise systemic anti-tumor immunity in the clinic^{63,64}. Clinical studies should determine whether tumor-infiltrated LNs can still generate effective anti-tumor immune responses⁶⁵ and whether other LNs, beyond the sentinel LN, can support anti-tumor immunity. The stage of tumor development may also impact immunity in the TdLN, with advanced tumor burden being associated with enhanced systemic immunosuppression

and reduced responses to IT⁶⁸. Therefore, preserving the TdLN may offer particular benefits for early-stage cancer, when tumor cells have not yet infiltrated in the TdLN and immunosuppression is relatively low. In **chapter 2**, we propose blockade of CD86, a costimulatory ligand expressed by cDCs and other myeloid cells, as a potential mechanism to alleviate immunosuppression in the TdLN, by disrupting Treg priming and supporting cDC1 activation (further discussed below). Particularly in advanced cancer, strategies that directly target suppressive immune responses in the TdLN may present an opportunity to salvage ineffective anti-tumor immunity.

2) Defining impediments and potential targets that prevent RT-induced systemic immune responses.

The CD28 costimulatory axis dictates RT responses in Treg-rich tumor settings

1) PD-1 and CTLA-4 blockade enable CD28 costimulation on (RT-induced) Tregs.

Clinically approved immune checkpoint blockades (ICB) of CTLA-4 and PD-(L)1 promote T cell responses by enabling cDC-mediated costimulation and aim to alleviate peripheral tolerance against the tumor. Specifically, PD-1 inhibits T cell costimulation by CD28^{69,70}. CD28 promotes antigen-specific activation and clonal expansion of CD4⁺ and CD8⁺ T-cells by various mechanisms⁷¹. Upon binding to its ligand PD-L1 or PD-L2 presented by cDCs, PD-1 recruits the SHP2 tyrosine phosphatase to its cytoplasmic tail and subsequently inhibits CD28 signaling⁷⁰. CTLA-4, constitutively expressed on Tregs and upregulated by Tconvs following antigenic activation, can downregulate the CD28 ligands CD80 and CD86 on cDCs⁷² and thereby attenuates CD28 costimulation of Tconvs⁷¹. Thus, both PD-1 and CTLA-4 prevent T cell responses by suppression of CD28 costimulation. CTLA-4 exerts its influence early during T cell priming, whereas PD-1 is upregulated following T cell activation⁷³ and each contribute to peripheral immune tolerance.

In **chapter 2**, we discovered that instead of promoting CTL responses, the blockade of CTLA-4 or PD-1 led to an increase in RT-induced eTreg expansion, which abrogated the therapeutic effects of RT. These findings highlight the limitations of current ICB approaches designed to enhance T cell responses. The majority of the costimulatory receptors are shared between both conventional T cells (Tconvs) and Tregs, which means that ICB might unintentionally activate suppressive Treg responses. Particularly, like Tconvs, Tregs require CD28 costimulation for clonal expansion⁷⁴ and may thus benefit from CTLA-4 and/or PD-1 blockade. These findings are crucial for clinical implementation of RT and ICB combinations^{9,10}. Current “one-size-fits-all” approaches may inadvertently promote adverse treatment outcomes, especially when the patient’s unique immune parameters are not considered prior to treatment. For instance, the distinction between CTL and Treg responses following PD-1 blockade appears to be influenced by the balance between these cell populations in

the TME, along with the levels of PD-1 expression⁷⁵. As a result, PD-1 blockade in cancers having high Treg-to-Tconv ratios was associated with significant tumor progression^{75,76}. Likewise, the Treg-to-Tconv ratio also seems to underlie responses to CTLA-4 blockade^{77,78}, and requires a setting in which CTLA-4 blockade favors Tconv over Treg priming. Therapeutic benefit to RT and CTLA-4 blockade has been described in mice^{13,15,79} and in patients with metastatic non-small-cell lung cancer⁸⁰ and metastatic melanoma⁸¹. Combination of RT with CTLA-4 blockade in these settings likely enhanced CTL priming, based on the observed increase in TCR diversity among tumor-infiltrating T cells^{79,80}. However, in T-cell devoid tumors, several factors may contribute to an unfavorable T cell-to-Treg ratio upon RT. This includes a higher cDC2 over cDC1 ratio in the TME (**chapter 2**), limited release of RT-induced DAMPs⁸², insufficient IFN-I responses¹⁵, and RT-induced suppressive factors hindering cDC1 maturation^{60,83}. In such cases, CTLA-4 blockade may preferentially benefit CD28 costimulation of Tregs⁸⁴, leading to their expansion and eTreg formation.

Considerable attention is directed towards improving efficacy of CTLA-4 blocking antibodies by incorporating the ability to deplete Tregs in the TME without affecting peripheral Tconvs, rather than only blocking ligand binding^{85,86}. Moreover, due to its disruption of peripheral immune tolerance against the tumor, clinical application of CTLA-4 blockade is frequently associated with grade 3-4 severe adverse immune-related events, including conditions such as diarrhea, colitis, and severe skin rashes⁸⁷. New approaches therefore aim to enhance CTL-to-Treg ratios, while limiting adverse immune-related toxicities. One strategy involves engineering antibodies that selectively bind to CTLA-4 in an acidic environment, such as the tumor site, but not in peripheral tissues, which is currently undergoing its first clinical trial⁸⁸. Furthermore, bi-specific antibodies engineered to pair PD-1 blockade with a non-Treg specific IL-2-variant are promising, as they have shown to selectively engage tumor-specific T cell responses, without targeting Tregs⁸⁹.

Collectively, our findings emphasize the importance of considering the Treg-to-Tconv ratio in the TME when contemplating RT and ICB combinations. Particularly, in tumors that provoke Treg responses, administration of PD-1 and/or CTLA-4 blockade may unintentionally enhance these responses by engaging CD28. Consequently, instead of promoting immune activation, ICBs, either alone or in combination with other treatments like RT, may inadvertently foster immune suppression. This, in part, provides insight into the lack of therapeutic responses observed in a subset of patients^{76,90,91}.

2) The differential role of the CD28 costimulatory ligands CD80 and CD86 in supporting RT-induced CTL responses.

The observed Treg response to CTLA-4 and PD-1 blockade in the TC-1 tumor model highlights that both Tconvs and Tregs benefit from CD28 costimulation mediated by its ligands CD80

and CD86, presented by cDCs. Although CD80 and CD86 diverge considerably regarding their sequence, biophysical characteristics, and cellular expression^{92,93}, they are often considered to have similar immunological functions. In **chapter 2**, we discovered that upon RT, CD80 and CD86 differentially promote Tconv and Treg responses, respectively. This discovery presents CD86 blockade as a promising therapeutic approach to boost (RT-induced) anti-tumor Tconv responses and prevent systemic immunosuppression by Tregs. In our setting, CD86 blockade countered effector Treg expansion in the TdLN. Therefore, this approach may benefit patients with advanced disease, by potentially ameliorating systemic immunosuppression. Additionally, we observed that reducing the eTreg response by CD86 blockade facilitated RT-induced cDC1 activation and CTL priming against the tumor. This result suggests that the RT-induced eTreg response directly hinders CTL priming by inhibiting cDC1 activation in the TdLN, as has recently been described in another setting⁵⁴. In the TME, Tregs rely on continuous interactions with cDCs to maintain their immunosuppressive properties, which depend on CD80 and CD86^{84,94}. Thus, next to inhibiting the eTreg response in the TdLN, CD86 blockade likely also disrupts local immunosuppressive interactions in the TME. Importantly, we found that CD86 blockade does not affect the population of central (c)Tregs in the TdLN and non-TdLN. This finding has considerable implications for translation into the clinic, as CD86 blockade may present with fewer immune-related toxicities as compared to CTLA-4 blockade⁸⁷. Specifically, because CTLA-4 is constitutively expressed on Tregs, its inhibition might inadvertently impact the entire Treg population, including those responsible for immune homeostasis. This concern could be avoided by preserving the cTreg subset.

Our discovery that CD86 is favored for CD28 costimulation of (RT-induced) Tregs can be attributed, in part, to its lower binding affinity towards CD28 and CTLA-4, unlike CD80⁹⁵. Specifically, as Tregs express both CD28 and CTLA-4, CD86 and CD80 compete for facilitating CD28 costimulation. Since CD86 has a lower affinity for CTLA-4 than CD80, CD86 may remain available for mediating CD28 costimulation, bypassing the CTLA-4 restraint. In agreement, making CD80 available by CTLA-4 blockade allowed for CD80-mediated Treg responses⁹⁶. While CD86 is constitutively expressed on cDCs, CD80 expression levels are strongly upregulated upon cDC maturation⁹⁷. Moreover, recent research has demonstrated that CD80 forms cis-heterodimers with PD-L1, providing protection from CTLA-4-mediated downregulation while retaining its CD28 costimulatory capabilities⁹⁸. These findings, together with its high affinity for CTLA-4, imply that CD80 requires tight regulation, that is apparently geared to support CD28 costimulation of Tconvs rather than Tregs, as we demonstrate. Considering the sequential expression of CD86 and CD80 on DCs⁷¹, optimal CD28 costimulation may require an initial stimulus initiated by CD86, followed by CD80. In **chapter 2**, we also observed that CTLs primed upon RT and CD86 blockade upregulated PD-1, which impaired RT-induced tumor control and survival. Thus, in presence of CD86 blockade, CD28 costimulation may still not be optimal for Tconv priming.

Recent studies indicate that the metabolic state of cDC2s dictates CD86-mediated Treg expansion^{99,100}. Since tumors generally influence the cDC maturation state^{101,102}, future treatment approaches should focus on mechanisms that alleviate these processes at a metabolic level to enhance cDC maturation and activation. For example, genetic ablation or inhibition of the prostaglandin receptors EP2 and EP4 may present an attractive strategy to promote cDC activation in the TME, warranting further investigation⁴⁴.

Collectively, our findings in **chapter 2** highlight the role of CD28 costimulation in promoting both pro- and anti-tumor T cell responses, specifically in a Treg rich tumor setting. Particularly, blockade of CD86 emerges as a promising avenue for therapeutic intervention, especially in tumor settings featuring suppressive TdLNs, as it effectively dampens Treg responses both in the TdLN and the tumor. Importantly, since this approach preserved the cTreg population, the risk of unintended adverse effects may be reduced. Furthermore, considering the effects of RT in reducing tumor burden and its immunostimulatory potential observed in **chapter 2**, its combination with CD86 blockade offers a promising strategy, as this approach holds the potential to not only mitigate prevailing systemic suppression but also to facilitate Tconv responses in Treg-enriched cancers.

Tregs as an impediment in cancer and anti-cancer therapies

As demonstrated in **chapter 2**, TC-1 tumor growth raises effector Treg responses that prevent anti-tumor immunity. In **chapter 3**, we closely examined these Tregs and found that TC-1 tumor development leads to a preferential accumulation of Helios⁺ Tregs, that are likely thymus-derived¹⁰³. These Tregs undergo initial effector differentiation before migration into the TME, where they adopt a more mature phenotype. These findings highlight the opportunity of the TC-1 tumor model to mechanistically study systemic Treg responses in an *in vivo* setting. Specifically, although the role of Tregs in driving metastatic seeding is becoming increasingly clear^{55,56}, the exact mechanisms of initial Treg responses in the TdLN remains controversial. Since Tregs accumulate in the TdLN early during tumorigenesis¹⁰⁴ (**chapter 3**), uncovering these mechanisms could reveal potential avenues to counteract early immunosuppression (e.g., CD86 inhibition - **chapter 2**). Moreover, current approaches to restrain Tregs are limited by the availability of targetable molecules exclusively expressed by Tregs, and the difficulty to distinguish tumor-specific Tregs from healthy tissue to preserve homeostatic immune tolerance. Thus, identification of *in vivo* models that may recapitulate human processes are of high importance, as they may help to elucidate the mechanisms governing Treg responses in the tumor context.

Transcriptomic analysis of human Tregs obtained from blood, adjacent healthy tissue, and tumor tissue identified many similarities in the TCR repertoire and phenotype of healthy tissue- and tumor-resident Tregs¹⁰⁵. This suggests that tumor-resident Tregs are likely specific for “self”

antigens expressed in healthy tissue rather than tumor-antigens. Similarly, in a mouse model of prostate cancer, tumor-resident Tregs were found to recognize normal prostate tissue-specific antigens, distinct from Tconv¹⁰⁶. These Tregs originated from the thymus and subsequently accumulated in the prostate-dLN in an antigen-dependent manner, irrespective of tumor presence. This aligns with our understanding of tissue-specific Treg development in a homeostatic setting, which requires priming of Treg progenitor cells in the LN or spleen before migrating to nonlymphoid tissues^{107,108}. Moreover, tumor-derived Tregs seem to follow similar adaptation trajectories as their counterparts in healthy tissue¹⁰⁹, indicating a parallel developmental pattern. This observation is supported by the identification of a preserved conservative signature encoding a tissue-repair program in tissue-resident murine and human Tregs, which may be utilized by tumor-derived Tregs to support extracellular matrix re-organization and tumor growth¹⁰⁵. Thus, given the potentially similar developmental trajectories of tumor-associated and homeostatic Tregs, the observed accumulation of Tregs in the TdLN (**chapter 2** and **3**;^{49,102}) might stem from increased exposure to self-antigens due to proliferating and dying tumor cells. However, other factors may also influence Treg expansion in the TdLN, including the DC activation state⁵³ and the LN cytokine environment^{54,110}, which requires further investigation.

In **chapter 3**, we observed that Tregs in the TME had enhanced expression of ICOS, CTLA-4, GITR, CCR8 and acquired expression of CXCR6 and CD39, compared to those found in the TdLN. These markers overlap with a mature (non-lymphoid tissue) phenotype¹⁰⁹, suggesting that Tregs undergo further maturation in the tumor tissue following their initial priming in the TdLN. In a recent study, T cell trafficking between the TdLN and tumor revealed distinct phenotypic characteristics of newly arrived Tregs in the TME compared to those already present in the tumor¹¹¹. Upon infiltration into the tumor, Tregs rapidly adopted a tumor-retained phenotype, characterized by the acquired expression of CD39 and LAG-3 and high expression of ICOS¹¹¹. Since Tregs in homeostatic settings undergo tissue adaptation in non-lymphoid tissues^{107,109}, it remains to be studied to what extent these findings truly reflect a tumor-restricted transformation. Nonetheless, studies in humans have demonstrated that tumor-resident Tregs exhibit phenotypes associated with enhanced activation and suppressor functions as compared to Tregs from healthy tissue^{112,113}. This suggests the existence of environmental factors that may sustain the intra-tumoral Treg pool and impact their molecular reprogramming, such as local interactions with DCs^{84,94} or macrophages¹¹⁴. Moreover, the presence of immunosuppressive metabolites, such as lactic acid, has also been implicated to affect intra-tumoral Tregs^{115,116}.

Importantly, recent transcriptional characterization identified the chemokine receptor CCR8 as potential marker to differentiate tumor-derived Tregs from tissue-resident Tregs^{112,113,117}. However, other studies have found that CCR8 could also be expressed on healthy tissue-resident Tregs¹⁰⁵, raising concerns regarding unwanted elimination of these Tregs in the periphery upon CCR8-

targeting. Thus, a better understanding of the factors involved to differentiate between Tregs from the tissue or tumors is necessary to identify novel therapeutic targets in a more precise manner.

The factors driving Treg expansion upon RT (**chapter 2**) are currently unclear, as most mouse studies focus on stimulating CTL responses^{14,80,118,119}. Next to pro-inflammatory responses, RT-induced tissue damage can also trigger inflammatory processes that may have counterproductive effects¹²⁰, such as releasing the active form of TGF- β , a potent suppressor of anti-tumor immune responses¹²¹. TGF- β can suppress RT-induced DC activation in the TME¹²² and may promote Treg expansion by converting CD4⁺ Tconvs to Tregs¹²³. In absence of TGF- β , RT may release activin A, a TGF- β superfamily member, which can also enhance Treg responses¹²⁴. Additionally, RT may enhance levels of IL-33, a cytokine that promotes tissue protection¹²⁵, in part by inducing Treg expansion¹²⁶. However, the roles of TGF- β and IL-33 in supporting RT-induced Tregs remain unclear, as their inhibition failed to reduce Treg expansion in irradiated tumor models¹²⁷.

While RT has been shown to promote DC activation and migration to the TdLN^{24,82,119}, the specific cues that determine Tconv versus Treg priming upon cDC encounter are not fully understood. Recent studies suggest that the metabolic rewiring of cDCs, along with the uptake of cell debris, plays a crucial role in determining their molecular differentiation state^{99,128}. RT-induced metabolic alterations¹²⁹ and upregulation of CDKN1A, a protein that protects against RT-induced DNA damage, may potentially favor enhanced Treg priming in the TdLN¹³⁰. Thus, further studies need to elucidate the metabolic and molecular pathways within cDCs that differentiate Tconv and Treg priming in the TdLN, particularly within the context of RT.

3) Overcoming local immunosuppression in the TME – The potential of RT and other strategies.

RT as a local immune modulator

Despite achieving sufficient tumor-specific CTL priming, therapeutic responses in the clinic can be impeded by local immunosuppression in the TME. In **chapter 4**, we describe a setting in which CTL priming in the TdLN was facilitated by a combined ICB approach, using a CD137 (4-1BB) agonist along with PD-1 inhibition. Addition of RT to this ICB combination enabled effective control of the primary tumor. However, it did not significantly contribute to systemic anti-tumor immune responses. This was evident by the similar outgrowth curves of a secondary non-irradiated tumor in the same mouse, treated with either ICB alone or RT combined with ICB. RNA-seq analysis indicated that RT did not induce CTL-intrinsic effects. Instead, it appeared to alleviate suppressive mechanisms imposed by the tumor, sensitizing it for CTL functionality. This effect was not observed in the non-irradiated tumor, despite high CTL infiltration, and low dose cisplatin was required to overrule immune suppression in the non-irradiated tumor. These findings emphasize

that despite raising systemic CTL responses, tumor-associated immune suppression may abrogate treatment benefit. Moreover, our results caution for the often reported “synergistic” systemic effects in clinical settings using RT in combination with ICB approaches⁸¹, since the contribution of RT to the systemic immune responses is often overestimated, especially in situations where CTL priming can be achieved with ICB treatment alone.

Specifically, CD137, a TNF receptor superfamily member, is upregulated on T cells upon antigen recognition and CD27 costimulation and plays a crucial role in mitigating cell death, promoting proliferation, facilitating memory formation, and reversing exhaustion^{131,132}. While CD137 expression is primarily confined to B-, T- and NK cells, it is also detected on several myeloid-lineage cells, including cDCs¹³². In our setting, it is likely that agonistic CD137 antibody not only directly acts on T cells, but also potentially supports cDC activation (**chapter 4**). In this context, CD137 agonism alone is probably sufficient to facilitate CTL priming, which was further assisted by PD-1 blockade. This is reinforced by the increase of CD4⁺ (FOXP3) Tconvs observed upon CD137 agonism, suggesting that anti-CD137 may contribute to enabling CD4⁺ T cell help. For instance, CTLs primed in absence of sufficient CD4⁺ T cell help lack important effector and memory functions, required to overcome negative regulation^{29,40,133} and to facilitate anti-tumor immunity³⁷. However, we found that enlargement of the tumor-specific CTL pool by therapeutic vaccination, which included an MHC-I restricted tumor-antigen alongside CD4⁺ T cell helper epitopes, did not further improve control of the non-irradiated tumor when compared to our RT and combined ICB approach (**chapter 4**). Thus, CD137 agonism together with PD-1 inhibition likely adequately supports CTL priming, either by directly facilitating CD4⁺ T cell help during priming by improving CD4⁺ T cell responses and/or by mimicking the effects of CD4⁺ T help on CTLs²⁸. Consequently, the broad range of stimuli induced by CD137 agonism, together with PD-1 inhibition, may have outweighed the potential benefits of adding RT to foster systemic anti-tumor immune responses.

Our study emphasizes the importance of engaging every step in the cancer-immunity cycle to bolster therapeutic benefits, as CTL priming alone proved insufficient to overcome local immunosuppression in the TME. Moreover, despite comparable levels of CTL infiltration, the irradiated and non-irradiated tumor significantly differed in tumor control, suggesting a local impediment in CTL functionality. This constraint was unrelated to PD-1 signaling, nor was it attributed to the presence of neutrophils or tumor-associated macrophages (TAMs) (**chapter 4**). In such cases, conventional anti-tumor approaches, like RT and chemotherapy, may sensitize tumors to CTL responses. In the clinic, effective ICB responses are most prevalent in cases of limited tumor burden⁶⁸ and when T cells are present in the TME²². In more advanced tumor settings, irradiation to all metastatic tumor sites has been suggested¹³⁴, as this may reduce tumor burden, while potentially enabling CTL priming within distinct TdLNs, situated in different anatomical locations. However, this approach is restricted to cancers presenting with identifiable

metastases on tissue sites capable of withstanding high dose RT. In settings characterized by diffuse disease spread or the presence of potential microscopic disease, other options should be considered. These encompass low-dose RT (below 2 Gy)^{135,136} or administration of minimal doses chemotherapy, like cisplatin (**chapter 4**), both proven successful in facilitating local CTL responses. Thus, especially in settings with high tumor burden, conventional anti-tumor therapies may help to alleviate local immunosuppression, provided that they are applied in a rational manner.

Autotaxin as a potential target to enable CTL-infiltration in the TME

Local CTL paucity is generally attributed to the absence of chemokine signals that guide and direct CTLs to the tumor vasculature and/or to physical obstructions, such as presence of cancer-associated fibroblasts and matrix metalloproteinases¹³⁷. In **chapter 5**, we unveil a novel function for autotaxin (ATX), a lysophospholipase D secreted by tumor cells and other cells, in repelling CTLs from the TME. Specifically, ATX generates lysophosphatidic acid (LPA), the bioactive product, from extracellularly available lysophosphatidylcholine (LPC)¹³⁸. The biological effect of ATX relies on six distinct G protein-coupled receptors (GPCRs) that LPA binds to, known as LPAR1-6. These LPARs play a significant role in various cellular responses, particularly in cell proliferation and migration¹³⁸. LPAR1-3 are part of the “endothelial differentiation gene” (EDG) subfamily of GPCRs, while LPAR4-6 are more closely associated with the purinergic receptor family of GPCRs¹³⁸. Involvement of LPAR1-3 are considered to enhance cellular responses, whereas LPAR4-6 are generally believed to counteract these responses by suppressing migration and invasion of diverse cell types^{139,140}. In **chapter 5**, we demonstrate that ATX, secreted by human melanoma cells, impedes T cell migration through chaperoning and binding of LPA to LPAR6.

Although the pleiotropic role of ATX in stimulating tumor progression and metastases formation has been widely acknowledged¹⁴¹, its function in the context of tumor immunity has only recently been appreciated¹⁴² and remains an active field of investigation. Specifically, the exact mechanisms by which LPA inhibits anti-tumor immunity remain obscure. For example, LPA may operate as a negative regulator of IFN type I production by cDCs in the TME¹⁴³, or it may act directly on T cells by disrupting early TCR signaling¹⁴⁴, preventing CTL-mediated tumor control. In the latter study, binding of LPA to LPAR5 significantly reduced the CTL functionality. In contrast, we observed that binding of LPA primarily repelled CTLs from the TME without adversely affecting their effector functions (**chapter 5**). This discrepancy could potentially be explained by the fact that T cells in the melanoma TME expressed various LPARs (**chapter 5**). Consequently, differences in LPA effects may arise from distinct molecular pathways triggered by specific activated LPA-receptors. The ultimate biological outcome is likely determined by the balance in LPA-receptors present on the T cell surface, emphasizing the need to further investigate the mechanisms underlying LPA-receptor expression. Regardless, these findings indicate that inhibition of ATX, or its mediator LPA, may act

as a potential target to enable CTL infiltration and functionality in the TME, while simultaneously mitigating its other tumor promoting effects, including the formation of tumor fibrosis¹⁴⁵. The ATX inhibitor IOA-289, currently in clinical development (clinicaltrials.gov ID NCT05586516), has shown promise by enabling CD8⁺ T cell infiltration, while simultaneously altering the chemokine milieu within the TME, improving tumor control¹⁴⁶. However, this study does not address whether ATX inhibition directly recruits CD8⁺ T cells from the periphery by alleviating its repellent effect, or if this recruitment is an indirect outcome influenced by other factors, such as reduced tumor fibrosis. Furthermore, whether the observed improved tumor control upon ATX inhibition is a direct consequence of enhanced CD8⁺ T cell infiltration has not been functionally addressed. Nevertheless, ATX inhibitors offer a promising approach to potentially benefit current treatment strategies by overcoming local immunosuppression and inviting new T cells.

Concluding remarks

The immune-modulating potential of RT to trigger systemic anti-tumor immune responses has garnered substantial interest in the past decade^{10,147}. However, its translation to the clinic has been disappointing^{10,134}, primarily due to the lack of insight into the requirements for synergy between RT and ICB approaches. The work presented in this thesis has elucidated important mechanisms that need to be considered when designing radio-immunotherapy strategies. Specifically, we provide evidence that *a priori* understanding of the effect of the tumor on the local and systemic immune response is required to rationally design treatments that benefit the vaccine potential of RT. These findings may provide a starting point for future clinical trials that aim to achieve combined responses between RT and ICB. Importantly, these trials should consider stratifying patients over immune archetype, rather than mere cancer subtype. Moreover, we propose that novel treatment strategies should extend beyond countering local suppression within the TME, as these should also focus on preserving the TdLNs and rectifying aberrant immune responses within these TdLNs. We provide evidence that combinations involving CTLA-4 and/or PD-1 blockade may inadvertently support Treg responses within Treg-enriched tumor settings, via CD28 costimulation. To address this, we suggest that CD86 blockade may alleviate CD28 costimulation to Tregs, which act both in the TdLN and tumor.

In summary, to achieve synergistic clinical responses, combined approaches involving RT requires a comprehensive understanding of how each therapeutic component contributes to optimizing anti-tumor immunity in a rational manner.

References

- 1 Stone, H. B., Peters, L. J. & Milas, L. Effect of host immune capability on radiocurability and subsequent transplantability of a murine fibrosarcoma. *J Natl Cancer Inst* **63**, 1229-1235 (1979).
- 2 North, R. J. Radiation-induced, immunologically mediated regression of an established tumor as an example of successful therapeutic immunomanipulation. Preferential elimination of suppressor T cells allows sustained production of effector T cells. *J Exp Med* **164**, 1652-1666 (1986).
- 3 Apetoh, L. *et al.* The interaction between HMGB1 and TLR4 dictates the outcome of anticancer chemotherapy and radiotherapy. *Immunol Rev* **220**, 47-59 (2007).
- 4 Chakravarty, P. K. *et al.* Flt3-ligand administration after radiation therapy prolongs survival in a murine model of metastatic lung cancer. *Cancer Res* **59**, 6028-6032 (1999).
- 5 Lugade, A. A. *et al.* Local radiation therapy of B16 melanoma tumors increases the generation of tumor antigen-specific effector cells that traffic to the tumor. *J Immunol* **174**, 7516-7523 (2005).
- 6 Lee, Y. *et al.* Therapeutic effects of ablative radiation on local tumor require CD8+ T cells: changing strategies for cancer treatment. *Blood* **114**, 589-595 (2009).
- 7 Mole, R. H. Whole body irradiation; radiobiology or medicine? *Br J Radiol* **26**, 234-241 (1953).
- 8 Demaria, S. *et al.* Ionizing radiation inhibition of distant untreated tumors (abscopal effect) is immune mediated. *Int J Radiat Oncol Biol Phys* **58**, 862-870 (2004).
- 9 Kang, J., Demaria, S. & Formenti, S. Current clinical trials testing the combination of immunotherapy with radiotherapy. *J Immunother Cancer* **4**, 51 (2016).
- 10 Pointer, K. B., Pitroda, S. P. & Weichselbaum, R. R. Radiotherapy and immunotherapy: open questions and future strategies. *Trends Cancer* **8**, 9-20 (2022).
- 11 Buchwald, Z. S. *et al.* Tumor-draining lymph node is important for a robust abscopal effect stimulated by radiotherapy. *J Immunother Cancer* **8** (2020).
- 12 Takeshima, T. *et al.* Local radiation therapy inhibits tumor growth through the generation of tumor-specific CTL: its potentiation by combination with Th1 cell therapy. *Cancer Res* **70**, 2697-2706 (2010).
- 13 Dewan, M. Z. *et al.* Fractionated but not single-dose radiotherapy induces an immune-mediated abscopal effect when combined with anti-CTLA-4 antibody. *Clin Cancer Res* **15**, 5379-5388 (2009).
- 14 Deng, L. *et al.* Irradiation and anti-PD-L1 treatment synergistically promote antitumor immunity in mice. *J Clin Invest* **124**, 687-695 (2014).
- 15 Vanpouille-Box, C. *et al.* DNA exonuclease Trex1 regulates radiotherapy-induced tumour immunogenicity. *Nat Commun* **8**, 15618 (2017).
- 16 Voorwerk, L. *et al.* Immune induction strategies in metastatic triple-negative breast cancer to enhance the sensitivity to PD-1 blockade: the TONIC trial. *Nat Med* **25**, 920-928 (2019).
- 17 McBride, S. *et al.* Randomized Phase II Trial of Nivolumab With Stereotactic Body Radiotherapy Versus Nivolumab Alone in Metastatic Head and Neck Squamous Cell Carcinoma. *J Clin Oncol* **39**, 30-37 (2021).
- 18 Lai, J. Z. *et al.* Abscopal Effects of Local Radiotherapy Are Dependent on Tumor Immunogenicity. *Front Oncol* **11**, 690188 (2021).
- 19 Arina, A. *et al.* Tumor-reprogrammed resident T cells resist radiation to control tumors. *Nat Commun* **10**, 3959 (2019).
- 20 Fridman, W. H., Zitvogel, L., Sautes-Fridman, C. & Kroemer, G. The immune contexture in cancer prognosis and treatment. *Nat Rev Clin Oncol* **14**, 717-734 (2017).
- 21 Thorsson, V. *et al.* The Immune Landscape of Cancer. *Immunity* **48**, 812-830 e814 (2018).
- 22 Luca, B. A. *et al.* Atlas of clinically distinct cell states and ecosystems across human solid tumors. *Cell* **184**, 5482-5496 e5428 (2021).

- 23 Combes, A. J. *et al.* Discovering dominant tumor immune archetypes in a pan-cancer census. *Cell* **185**, 184-203 e119 (2022).
- 24 Blair, T. C. *et al.* Dendritic Cell Maturation Defines Immunological Responsiveness of Tumors to Radiation Therapy. *J Immunol* **204**, 3416-3424 (2020).
- 25 Grass, G. D. *et al.* The Radiosensitivity Index Gene Signature Identifies Distinct Tumor Immune Microenvironment Characteristics Associated With Susceptibility to Radiation Therapy. *Int J Radiat Oncol Biol Phys* **113**, 635-647 (2022).
- 26 Ni, G. *et al.* Intratumoral injection of caerin 1.1 and 1.9 peptides increases the efficacy of vaccinated TC-1 tumor-bearing mice with PD-1 blockade by modulating macrophage heterogeneity and the activation of CD8(+) T cells in the tumor microenvironment. *Clin Transl Immunology* **10**, e1335 (2021).
- 27 Vonderheide, R. H. The Immune Revolution: A Case for Priming, Not Checkpoint. *Cancer Cell* **33**, 563-569 (2018).
- 28 Ahrends, T. *et al.* CD27 Agonism Plus PD-1 Blockade Recapitulates CD4+ T-cell Help in Therapeutic Anticancer Vaccination. *Cancer Res* **76**, 2921-2931 (2016).
- 29 Ahrends, T. *et al.* CD4(+) T Cell Help Confers a Cytotoxic T Cell Effector Program Including Coinhibitory Receptor Downregulation and Increased Tissue Invasiveness. *Immunity* **47**, 848-861 e845 (2017).
- 30 Verma, V. *et al.* PD-1 blockade in subprimed CD8 cells induces dysfunctional PD-1(+)/CD38(hi) cells and anti-PD-1 resistance. *Nat Immunol* **20**, 1231-1243 (2019).
- 31 Hiam-Galvez, K. J., Allen, B. M. & Spitzer, M. H. Systemic immunity in cancer. *Nat Rev Cancer* **21**, 345-359 (2021).
- 32 du Bois, H., Heim, T. A. & Lund, A. W. Tumor-draining lymph nodes: At the crossroads of metastasis and immunity. *Sci Immunol* **6**, eabg3551 (2021).
- 33 Shang, B., Liu, Y., Jiang, S. J. & Liu, Y. Prognostic value of tumor-infiltrating FoxP3+ regulatory T cells in cancers: a systematic review and meta-analysis. *Sci Rep* **5**, 15179 (2015).
- 34 Goda, N. *et al.* The ratio of CD8 + lymphocytes to tumor-infiltrating suppressive FOXP3 + effector regulatory T cells is associated with treatment response in invasive breast cancer. *Discov Oncol* **13**, 27 (2022).
- 35 Givechian, K. B. *et al.* Identification of an immune gene expression signature associated with favorable clinical features in Treg-enriched patient tumor samples. *NPJ Genom Med* **3**, 14 (2018).
- 36 Spitzer, M. H. *et al.* Systemic Immunity Is Required for Effective Cancer Immunotherapy. *Cell* **168**, 487-502 e415 (2017).
- 37 Ferris, S. T. *et al.* cDC1 prime and are licensed by CD4(+) T cells to induce anti-tumour immunity. *Nature* **584**, 624-629 (2020).
- 38 Eickhoff, S. *et al.* Robust Anti-viral Immunity Requires Multiple Distinct T Cell-Dendritic Cell Interactions. *Cell* **162**, 1322-1337 (2015).
- 39 Hor, J. L. *et al.* Spatiotemporally Distinct Interactions with Dendritic Cell Subsets Facilitates CD4+ and CD8+ T Cell Activation to Localized Viral Infection. *Immunity* **43**, 554-565 (2015).
- 40 Borst, J., Ahrends, T., Babala, N., Melief, C. J. M. & Kastenmuller, W. CD4(+) T cell help in cancer immunology and immunotherapy. *Nat Rev Immunol* **18**, 635-647 (2018).
- 41 Salmon, H. *et al.* Expansion and Activation of CD103(+) Dendritic Cell Progenitors at the Tumor Site Enhances Tumor Responses to Therapeutic PD-L1 and BRAF Inhibition. *Immunity* **44**, 924-938 (2016).
- 42 Binnewies, M. *et al.* Unleashing Type-2 Dendritic Cells to Drive Protective Antitumor CD4(+) T Cell Immunity. *Cell* **177**, 556-571 e516 (2019).
- 43 Hegde, S. *et al.* Dendritic Cell Paucity Leads to Dysfunctional Immune Surveillance in Pancreatic Cancer. *Cancer Cell* **37**, 289-307 e289 (2020).

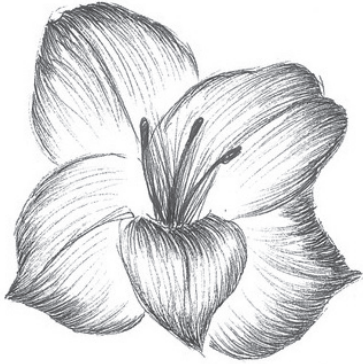
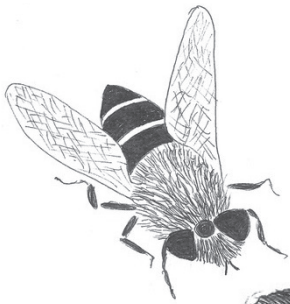
- 44 Bayerl, F. *et al.* Tumor-derived prostaglandin E2 programs cDC1 dysfunction to impair intratumoral orchestration of anti-cancer T cell responses. *Immunity* **56**, 1341-1358 e1311 (2023).
- 45 Adamik, J. *et al.* Distinct metabolic states guide maturation of inflammatory and tolerogenic dendritic cells. *Nat Commun* **13**, 5184 (2022).
- 46 Spranger, S. & Gajewski, T. F. Impact of oncogenic pathways on evasion of antitumour immune responses. *Nat Rev Cancer* **18**, 139-147 (2018).
- 47 Spranger, S. Mechanisms of tumor escape in the context of the T-cell-inflamed and the non-T-cell-inflamed tumor microenvironment. *Int Immunol* **28**, 383-391 (2016).
- 48 Lahmar, Q. *et al.* Monocytic myeloid-derived suppressor cells home to tumor-draining lymph nodes via CCR2 and locally modulate the immune response. *Cell Immunol* **362**, 104296 (2021).
- 49 Deng, L. *et al.* Accumulation of foxp3+ T regulatory cells in draining lymph nodes correlates with disease progression and immune suppression in colorectal cancer patients. *Clin Cancer Res* **16**, 4105-4112 (2010).
- 50 Matheu, M. P. *et al.* Imaging regulatory T cell dynamics and CTLA4-mediated suppression of T cell priming. *Nat Commun* **6**, 6219 (2015).
- 51 Lutz, M. B. & Schuler, G. Immature, semi-mature and fully mature dendritic cells: which signals induce tolerance or immunity? *Trends Immunol* **23**, 445-449 (2002).
- 52 Maldonado, R. A. & von Andrian, U. H. How tolerogenic dendritic cells induce regulatory T cells. *Adv Immunol* **108**, 111-165 (2010).
- 53 Ghiringhelli, F. *et al.* Tumor cells convert immature myeloid dendritic cells into TGF-beta-secreting cells inducing CD4+CD25+ regulatory T cell proliferation. *J Exp Med* **202**, 919-929 (2005).
- 54 Zagorulya, M. *et al.* Tissue-specific abundance of interferon-gamma drives regulatory T cells to restrain DC1-mediated priming of cytotoxic T cells against lung cancer. *Immunity* **56**, 386-405 e310 (2023).
- 55 Kos, K. *et al.* Tumor-educated T(regs) drive organ-specific metastasis in breast cancer by impairing NK cells in the lymph node niche. *Cell Rep* **38**, 110447 (2022).
- 56 Reticker-Flynn, N. E. *et al.* Lymph node colonization induces tumor-immune tolerance to promote distant metastasis. *Cell* **185**, 1924-1942 e1923 (2022).
- 57 Dammeijer, F. *et al.* The PD-1/PD-L1-Checkpoint Restrains T cell Immunity in Tumor-Draining Lymph Nodes. *Cancer Cell* **38**, 685-700 e688 (2020).
- 58 Fransen, M. F. *et al.* Tumor-draining lymph nodes are pivotal in PD-1/PD-L1 checkpoint therapy. *JCI Insight* **3** (2018).
- 59 van Pul, K. M. *et al.* Local delivery of low-dose anti-CTLA-4 to the melanoma lymphatic basin leads to systemic T(reg) reduction and effector T cell activation. *Sci Immunol* **7**, eabn8097 (2022).
- 60 Wennerberg, E. *et al.* CD73 Blockade Promotes Dendritic Cell Infiltration of Irradiated Tumors and Tumor Rejection. *Cancer Immunol Res* **8**, 465-478 (2020).
- 61 Oba, T. *et al.* Overcoming primary and acquired resistance to anti-PD-L1 therapy by induction and activation of tumor-residing cDC1s. *Nat Commun* **11**, 5415 (2020).
- 62 Hammerich, L. *et al.* Systemic clinical tumor regressions and potentiation of PD1 blockade with in situ vaccination. *Nat Med* **25**, 814-824 (2019).
- 63 Marciscano, A. E. *et al.* Elective Nodal Irradiation Attenuates the Combinatorial Efficacy of Stereotactic Radiation Therapy and Immunotherapy. *Clin Cancer Res* **24**, 5058-5071 (2018).
- 64 Darragh, L. B. *et al.* Elective nodal irradiation mitigates local and systemic immunity generated by combination radiation and immunotherapy in head and neck tumors. *Nat Commun* **13**, 7015 (2022).
- 65 Rahim, M. K. *et al.* Dynamic CD8(+) T cell responses to cancer immunotherapy in human regional lymph nodes are disrupted in metastatic lymph nodes. *Cell* **186**, 1127-1143 e1118 (2023).

- 66 Gershenwald, J. E. *et al.* Multi-institutional melanoma lymphatic mapping experience: the prognostic value of sentinel lymph node status in 612 stage I or II melanoma patients. *J Clin Oncol* **17**, 976-983 (1999).
- 67 Reticker-Flynn, N. E. & Engleman, E. G. Lymph nodes: at the intersection of cancer treatment and progression. *Trends Cell Biol* (2023).
- 68 Huang, A. C. *et al.* T-cell invigoration to tumour burden ratio associated with anti-PD-1 response. *Nature* **545**, 60-65 (2017).
- 69 Kamphorst, A. O. *et al.* Rescue of exhausted CD8 T cells by PD-1-targeted therapies is CD28-dependent. *Science* **355**, 1423-1427 (2017).
- 70 Hui, E. *et al.* T cell costimulatory receptor CD28 is a primary target for PD-1-mediated inhibition. *Science* **355**, 1428-1433 (2017).
- 71 Esensten, J. H., Helou, Y. A., Chopra, G., Weiss, A. & Bluestone, J. A. CD28 Costimulation: From Mechanism to Therapy. *Immunity* **44**, 973-988 (2016).
- 72 Wing, K. *et al.* CTLA-4 control over Foxp3+ regulatory T cell function. *Science* **322**, 271-275 (2008).
- 73 Willmore, Z. N. *et al.* Combined anti-PD-1 and anti-CTLA-4 checkpoint blockade: Treatment of melanoma and immune mechanisms of action. *Eur J Immunol* **51**, 544-556 (2021).
- 74 Salomon, B. *et al.* B7/CD28 costimulation is essential for the homeostasis of the CD4+CD25+ immunoregulatory T cells that control autoimmune diabetes. *Immunity* **12**, 431-440 (2000).
- 75 Kumagai, S. *et al.* The PD-1 expression balance between effector and regulatory T cells predicts the clinical efficacy of PD-1 blockade therapies. *Nat Immunol* **21**, 1346-1358 (2020).
- 76 Kamada, T. *et al.* PD-1(+) regulatory T cells amplified by PD-1 blockade promote hyperprogression of cancer. *Proc Natl Acad Sci U S A* **116**, 9999-10008 (2019).
- 77 Quezada, S. A., Peggs, K. S., Curran, M. A. & Allison, J. P. CTLA4 blockade and GM-CSF combination immunotherapy alters the intratumor balance of effector and regulatory T cells. *J Clin Invest* **116**, 1935-1945 (2006).
- 78 Kavanagh, B. *et al.* CTLA4 blockade expands FoxP3+ regulatory and activated effector CD4+ T cells in a dose-dependent fashion. *Blood* **112**, 1175-1183 (2008).
- 79 Rudqvist, N. P. *et al.* Radiotherapy and CTLA-4 Blockade Shape the TCR Repertoire of Tumor-Infiltrating T Cells. *Cancer Immunol Res* **6**, 139-150 (2018).
- 80 Formenti, S. C. *et al.* Radiotherapy induces responses of lung cancer to CTLA-4 blockade. *Nat Med* **24**, 1845-1851 (2018).
- 81 Twyman-Saint Victor, C. *et al.* Radiation and dual checkpoint blockade activate non-redundant immune mechanisms in cancer. *Nature* **520**, 373-377 (2015).
- 82 Blair, T. C. *et al.* Fluorescent tracking identifies key migratory dendritic cells in the lymph node after radiotherapy. *Life Sci Alliance* **5** (2022).
- 83 Hsieh, R. C. *et al.* ATR-mediated CD47 and PD-L1 up-regulation restricts radiotherapy-induced immune priming and abscopal responses in colorectal cancer. *Sci Immunol* **7**, eabl9330 (2022).
- 84 Marangoni, F. *et al.* Expansion of tumor-associated Treg cells upon disruption of a CTLA-4-dependent feedback loop. *Cell* **184**, 3998-4015 e3919 (2021).
- 85 Simpson, T. R. *et al.* Fc-dependent depletion of tumor-infiltrating regulatory T cells co-defines the efficacy of anti-CTLA-4 therapy against melanoma. *J Exp Med* **210**, 1695-1710 (2013).
- 86 Ha, D. *et al.* Differential control of human Treg and effector T cells in tumor immunity by Fc-engineered anti-CTLA-4 antibody. *Proc Natl Acad Sci U S A* **116**, 609-618 (2019).
- 87 Martins, F. *et al.* Adverse effects of immune-checkpoint inhibitors: epidemiology, management and surveillance. *Nat Rev Clin Oncol* **16**, 563-580 (2019).

- 88 Humphries, P. A. & Lo, W. L. Two CTLA-4 ligands, separate pHates. *Nat Immunol* **23**, 1297-1299 (2022).
- 89 Ren, Z. *et al.* Selective delivery of low-affinity IL-2 to PD-1+ T cells rejuvenates antitumor immunity with reduced toxicity. *J Clin Invest* **132** (2022).
- 90 Robert, C. *et al.* Pembrolizumab versus ipilimumab in advanced melanoma (KEYNOTE-006): post-hoc 5-year results from an open-label, multicentre, randomised, controlled, phase 3 study. *Lancet Oncol* **20**, 1239-1251 (2019).
- 91 Schadendorf, D. *et al.* Pooled Analysis of Long-Term Survival Data From Phase II and Phase III Trials of Ipilimumab in Unresectable or Metastatic Melanoma. *J Clin Oncol* **33**, 1889-1894 (2015).
- 92 Collins, M., Ling, V. & Carreno, B. M. The B7 family of immune-regulatory ligands. *Genome Biol* **6**, 223 (2005).
- 93 Bhatia, S., Edidin, M., Almo, S. C. & Nathenson, S. G. B7-1 and B7-2: similar costimulatory ligands with different biochemical, oligomeric and signaling properties. *Immunol Lett* **104**, 70-75 (2006).
- 94 Bauer, C. A. *et al.* Dynamic Treg interactions with intratumoral APCs promote local CTL dysfunction. *J Clin Invest* **124**, 2425-2440 (2014).
- 95 Collins, A. V. *et al.* The interaction properties of costimulatory molecules revisited. *Immunity* **17**, 201-210 (2002).
- 96 Halliday, N. *et al.* CD86 Is a Selective CD28 Ligand Supporting FoxP3+ Regulatory T Cell Homeostasis in the Presence of High Levels of CTLA-4. *Front Immunol* **11**, 600000 (2020).
- 97 Sharpe, A. H. & Freeman, G. J. The B7-CD28 superfamily. *Nat Rev Immunol* **2**, 116-126 (2002).
- 98 Zhao, Y. *et al.* PD-L1:CD80 Cis-Heterodimer Triggers the Co-stimulatory Receptor CD28 While Repressing the Inhibitory PD-1 and CTLA-4 Pathways. *Immunity* **51**, 1059-1073 e1059 (2019).
- 99 Pelgrom, L. R. *et al.* LKB1 expressed in dendritic cells governs the development and expansion of thymus-derived regulatory T cells. *Cell Res* **29**, 406-419 (2019).
- 100 Wang, Y. *et al.* LKB1 orchestrates dendritic cell metabolic quiescence and anti-tumor immunity. *Cell Res* **29**, 391-405 (2019).
- 101 Scarlett, U. K. *et al.* Ovarian cancer progression is controlled by phenotypic changes in dendritic cells. *J Exp Med* **209**, 495-506 (2012).
- 102 van Pul, K. M. *et al.* Selectively hampered activation of lymph node-resident dendritic cells precedes profound T cell suppression and metastatic spread in the breast cancer sentinel lymph node. *J Immunother Cancer* **7**, 133 (2019).
- 103 Thornton, A. M. *et al.* Expression of Helios, an Ikaros transcription factor family member, differentiates thymic-derived from peripherally induced Foxp3+ T regulatory cells. *J Immunol* **184**, 3433-3441 (2010).
- 104 Darrasse-Jeze, G. *et al.* Tumor emergence is sensed by self-specific CD44hi memory Tregs that create a dominant tolerogenic environment for tumors in mice. *J Clin Invest* **119**, 2648-2662 (2009).
- 105 Delacher, M. *et al.* Single-cell chromatin accessibility landscape identifies tissue repair program in human regulatory T cells. *Immunity* **54**, 702-720 e717 (2021).
- 106 Malchow, S. *et al.* Aire-dependent thymic development of tumor-associated regulatory T cells. *Science* **339**, 1219-1224 (2013).
- 107 Delacher, M. *et al.* Precursors for Nonlymphoid-Tissue Treg Cells Reside in Secondary Lymphoid Organs and Are Programmed by the Transcription Factor BATF. *Immunity* **52**, 295-312 e211 (2020).
- 108 Li, C. *et al.* TCR Transgenic Mice Reveal Stepwise, Multi-site Acquisition of the Distinctive Fat-Treg Phenotype. *Cell* **174**, 285-299 e212 (2018).
- 109 Miragaia, R. J. *et al.* Single-Cell Transcriptomics of Regulatory T Cells Reveals Trajectories of Tissue Adaptation. *Immunity* **50**, 493-504 e497 (2019).

- 110 Fujita, T. *et al.* Inhibition of transforming growth factor-beta-mediated immunosuppression in tumor-draining lymph nodes augments antitumor responses by various immunologic cell types. *Cancer Res* **69**, 5142-5150 (2009).
- 111 Li, Z. *et al.* In vivo labeling reveals continuous trafficking of TCF-1+ T cells between tumor and lymphoid tissue. *J Exp Med* **219** (2022).
- 112 De Simone, M. *et al.* Transcriptional Landscape of Human Tissue Lymphocytes Unveils Uniqueness of Tumor-Infiltrating T Regulatory Cells. *Immunity* **45**, 1135-1147 (2016).
- 113 Plitas, G. *et al.* Regulatory T Cells Exhibit Distinct Features in Human Breast Cancer. *Immunity* **45**, 1122-1134 (2016).
- 114 Casanova-Acebes, M. *et al.* Tissue-resident macrophages provide a pro-tumorigenic niche to early NSCLC cells. *Nature* **595**, 578-584 (2021).
- 115 Kumagai, S. *et al.* Lactic acid promotes PD-1 expression in regulatory T cells in highly glycolytic tumor microenvironments. *Cancer Cell* **40**, 201-218 e209 (2022).
- 116 Watson, M. J. *et al.* Metabolic support of tumour-infiltrating regulatory T cells by lactic acid. *Nature* **591**, 645-651 (2021).
- 117 Kidani, Y. *et al.* CCR8-targeted specific depletion of clonally expanded Treg cells in tumor tissues evokes potent tumor immunity with long-lasting memory. *Proc Natl Acad Sci U S A* **119** (2022).
- 118 Deng, L. *et al.* STING-Dependent Cytosolic DNA Sensing Promotes Radiation-Induced Type I Interferon-Dependent Antitumor Immunity in Immunogenic Tumors. *Immunity* **41**, 843-852 (2014).
- 119 Gupta, A. *et al.* Radiotherapy promotes tumor-specific effector CD8+ T cells via dendritic cell activation. *J Immunol* **189**, 558-566 (2012).
- 120 Cytlak, U. M. *et al.* Immunomodulation by radiotherapy in tumour control and normal tissue toxicity. *Nat Rev Immunol* **22**, 124-138 (2022).
- 121 Pickup, M., Novitskiy, S. & Moses, H. L. The roles of TGFbeta in the tumour microenvironment. *Nat Rev Cancer* **13**, 788-799 (2013).
- 122 Vanpouille-Box, C. *et al.* TGFbeta Is a Master Regulator of Radiation Therapy-Induced Antitumor Immunity. *Cancer Res* **75**, 2232-2242 (2015).
- 123 Chen, W. *et al.* Conversion of peripheral CD4+CD25- naive T cells to CD4+CD25+ regulatory T cells by TGF-beta induction of transcription factor Foxp3. *J Exp Med* **198**, 1875-1886 (2003).
- 124 De Martino, M. *et al.* Activin A Promotes Regulatory T-cell-Mediated Immunosuppression in Irradiated Breast Cancer. *Cancer Immunol Res* **9**, 89-102 (2021).
- 125 Liew, F. Y., Girard, J. P. & Turnquist, H. R. Interleukin-33 in health and disease. *Nat Rev Immunol* **16**, 676-689 (2016).
- 126 Faustino, L. D. *et al.* Interleukin-33 activates regulatory T cells to suppress innate gammadelta T cell responses in the lung. *Nat Immunol* **21**, 1371-1383 (2020).
- 127 Muroyama, Y. *et al.* Stereotactic Radiotherapy Increases Functionally Suppressive Regulatory T Cells in the Tumor Microenvironment. *Cancer Immunol Res* **5**, 992-1004 (2017).
- 128 Maier, B. *et al.* A conserved dendritic-cell regulatory program limits antitumour immunity. *Nature* **580**, 257-262 (2020).
- 129 van Gisbergen, M. W., Zwilling, E. & Dubois, L. J. Metabolic Rewiring in Radiation Oncology Toward Improving the Therapeutic Ratio. *Front Oncol* **11**, 653621 (2021).
- 130 Price, J. G. *et al.* CDKN1A regulates Langerhans cell survival and promotes Treg cell generation upon exposure to ionizing irradiation. *Nat Immunol* **16**, 1060-1068 (2015).
- 131 Peperzak, V., Xiao, Y., Veraar, E. A. & Borst, J. CD27 sustains survival of CTLs in virus-infected nonlymphoid tissue in mice by inducing autocrine IL-2 production. *J Clin Invest* **120**, 168-178 (2010).

- 132 Melero, I. *et al.* CD137 (4-1BB)-Based Cancer Immunotherapy on Its 25th Anniversary. *Cancer Discov* **13**, 552-569 (2023).
- 133 Ahrends, T. *et al.* CD4(+) T cell help creates memory CD8(+) T cells with innate and help-independent recall capacities. *Nat Commun* **10**, 5531 (2019).
- 134 Arina, A., Gutiontov, S. I. & Weichselbaum, R. R. Radiotherapy and Immunotherapy for Cancer: From “Systemic” to “Multisite”. *Clin Cancer Res* **26**, 2777-2782 (2020).
- 135 Herrera, F. G. *et al.* Low-Dose Radiotherapy Reverses Tumor Immune Desertification and Resistance to Immunotherapy. *Cancer Discov* **12**, 108-133 (2022).
- 136 Barsoumian, H. B. *et al.* Low-dose radiation treatment enhances systemic antitumor immune responses by overcoming the inhibitory stroma. *J Immunother Cancer* **8** (2020).
- 137 Melssen, M. M., Sheybani, N. D., Leick, K. M. & Slingluff, C. L., Jr. Barriers to immune cell infiltration in tumors. *J Immunother Cancer* **11** (2023).
- 138 Perrakis, A. & Moolenaar, W. H. Autotaxin: structure-function and signaling. *J Lipid Res* **55**, 1010-1018 (2014).
- 139 Jongsma, M., Matas-Rico, E., Rzadkowski, A., Jalink, K. & Moolenaar, W. H. LPA is a chemorepellent for B16 melanoma cells: action through the cAMP-elevating LPA5 receptor. *PLoS One* **6**, e29260 (2011).
- 140 Takahashi, K. *et al.* Lysophosphatidic acid (LPA) signaling via LPA(4) and LPA(6) negatively regulates cell motile activities of colon cancer cells. *Biochem Biophys Res Commun* **483**, 652-657 (2017).
- 141 Benesch, M. G. K., MacIntyre, I. T. K., McMullen, T. P. W. & Brindley, D. N. Coming of Age for Autotaxin and Lysophosphatidate Signaling: Clinical Applications for Preventing, Detecting and Targeting Tumor-Promoting Inflammation. *Cancers (Basel)* **10** (2018).
- 142 Lee, S. C. *et al.* Regulation of Tumor Immunity by Lysophosphatidic Acid. *Cancers (Basel)* **12** (2020).
- 143 Chae, C. S. *et al.* Tumor-Derived Lysophosphatidic Acid Blunts Protective Type I Interferon Responses in Ovarian Cancer. *Cancer Discov* **12**, 1904-1921 (2022).
- 144 Mathew, D. *et al.* LPA(5) Is an Inhibitory Receptor That Suppresses CD8 T-Cell Cytotoxic Function via Disruption of Early TCR Signaling. *Front Immunol* **10**, 1159 (2019).
- 145 Benesch, M. G. K., Tang, X. & Brindley, D. N. Autotaxin and Breast Cancer: Towards Overcoming Treatment Barriers and Sequelae. *Cancers (Basel)* **12** (2020).
- 146 Deken, M. A. *et al.* Characterization and translational development of IOA-289, a novel autotaxin inhibitor for the treatment of solid tumors. *Immunooncol Technol* **18**, 100384 (2023).
- 147 Ngwa, W. *et al.* Using immunotherapy to boost the abscopal effect. *Nat Rev Cancer* **18**, 313-322 (2018).



A

Addenda

English summary

Nederlandse samenvatting

Publications

PhD portfolio

Curriculum Vitae

Acknowledgements

English Summary

In this thesis, I describe the role of T cells in eliminating cancer cells, alone or in combination with radiotherapy (RT), immunotherapy (IT) or conventional chemotherapy. Since therapeutic interventions have advanced to combat infectious diseases, cancer, along with cardiovascular diseases, has emerged as a prominent global health challenge in the 20th century. Although cancer is typically considered a single disease, it is now clear that it encompasses a multitude of diseases determined by the tissue of origin, the underlying genetic alterations, and the presence of non-tumorous cells, including immune cells. During tumor development and treatment, these cells are in continuous crosstalk with each other, giving rise to evolving cellular ecosystems.

Cancers are generally treated with conventional therapies designed to kill rapidly dividing tumor cells, like RT and chemotherapy. RT is a local treatment that aims to reduce tumor masses, without harming the surrounding healthy tissue. Therefore, RT generally has less severe side effects than chemotherapy, which is administered throughout the body to combat systemic cancer spread. However, RT efficacy is limited by intrinsic and acquired resistance of cancer cells.

While it was originally thought that RT primarily acts by causing tumor cell cycle arrest and death, it is now evident that it also has the capacity to activate immune cells, including T cells. The evolutionary role of CD8⁺ and CD4⁺ T cells is to protect us against infection by viruses and other micro-organisms. Particularly, CD8⁺ T cells can mature into cytotoxic T lymphocytes (CTLs), which are highly effective in directly killing infected cells by recognizing pathogen-derived, foreign (“non-self”) molecules, called antigens. CD8⁺ T cells are activated (primed) to expand and differentiate into CTLs in tissue draining lymph nodes (TdLN) in response to antigen recognition and specific costimulatory signals and cytokines delivered by conventional dendritic cells (cDCs). After priming, these CTLs exit the lymph node and migrate through the blood to the infected tissue. CD4⁺ T cells are crucial to provide help for effective CTL and antibody responses. Besides combating infections, T cells can also employ the same mechanisms to target cancer cells.

Since tumors originate from the body’s own cells, they are not easily recognized as “foreign” and therefore do not typically raise a T cell response. RT can help to overcome this problem, since RT-induced tumor cell damage and death can cause the release of inflammatory molecules and antigens that can activate cDCs and tumor-specific T cell responses. However, tumors also develop immunoregulatory mechanisms that prevent or inhibit T cell responses. These inhibitory processes can act locally in the tumor microenvironment (TME) but can also involve the TdLN and may therefore become systemic. Not only can these processes interfere with the generation of new T cell responses, but they can also facilitate the spread of cancer beyond the primary tumor. One such mechanism used by the tumor is the recruitment and expansion of FOXP3⁺ CD4⁺

T regulatory (Tregs) cells. Tregs employ multiple mechanisms that suppress T cell activity, either directly or indirectly (i.e., via cDCs). Therefore, they play an essential role in preventing excessive and self-reactive immunity.

To enhance efficacy by overcoming immune suppression, clinical trials often combine RT with IT, particularly utilizing antibody-mediated immune checkpoint blockade (ICB) targeting inhibitory receptors such as PD-1 or CTLA-4. ICB aims to enhance anti-tumor T cell responses by either blocking of immune inhibitory receptors or engaging immune stimulatory molecules. The combined approach of RT and IT holds the potential to enhance the effectiveness of local RT and generate systemic anti-tumor T cell responses, which are crucial for preventing metastatic progression. However, achieving improved combined responses in the clinical setting remains challenging, primarily due to a lack in understanding of the mechanisms that drive RT-induced T cell responses across the diversity of human cancers. By improving our understanding of the factors required to initiate and support RT-induced T cell responses, we can enhance the clinical efficacy of RT. This may lead to a rational use of treatment strategies that can effectively overcome local or systemic immune suppression. This thesis contributes to a deeper understanding of how RT affects T cell responsiveness and provides guidelines for optimizing the combination of RT with IT.

In **chapter 2**, we analyzed publicly available records from The Cancer Genome Atlas (TCGA) and observed that RT was negatively associated with survival of patients with cancer types that have low lymphocyte- and high myeloid cell content. The transplantable TC-1 tumor model in mice replicated these immune characteristics and was therefore used to study the spontaneous and RT-induced T cell response. We found that TC-1 tumor development was associated with systemic immunosuppression, indicated by increased monocyte and Treg cell levels in the TdLN and tumor. RT to TC-1 tumors induced CTL priming in the TdLN. However, concurrent Treg priming, initiated by the tumor and further exacerbated by RT, inhibited overt CTL responses and CTL-based tumor rejection. We found, contrary to our expectations, that blockade with CTLA-4- or PD-1, further increased RT-induced Treg responses and did not promote tumor rejection. This is an important observation since similar effects could potentially occur in human tumors of this type. We elucidated that Treg expansion was caused by engagement of the costimulatory receptor CD28 on Treg cells. Therefore, this type of ICB may unintentionally support immunosuppressive Treg responses in tumor settings that favor Tregs over T cells. Our research further revealed that the CD28 ligands CD80 and CD86, expressed by cDCs, differentially promote T cell and Treg responses, respectively. Blocking CD86, but not CD80, attenuated RT-induced Treg responses and supported RT-induced CTL priming. Additional PD-1 blockade to this combination treatment improved RT-induced tumor control and overall survival. This study reveals the potential of RT to induce CTL responses even in the presence of Treg-mediated immunosuppression and highlights CD86 blockade as a promising therapeutic approach to increase CTL-based immunity in such tumors.

The influence of Tregs on preventing anti-tumor immunity has garnered significant attention in recent years. However, the exact mechanisms responsible for tumor-induced Treg priming in the TdLN remain unclear. Tregs can develop in the thymus (tTregs) in response to self-antigens, after which they migrate to the lymph nodes in an immature state to undergo initial Treg differentiation. Subsequently, these Tregs migrate to the tissue where they further adapt a tissue-resident phenotype. Alternatively, Tregs can emerge from the conversion of mature CD4⁺ T cells in the periphery (pTregs) that are specific against non-self antigens.

In **chapter 3**, we characterize the Treg response initiated upon TC-1 tumor development in the TdLN and tumor. We reveal that TC-1 tumor growth preferentially drives expansion and effector differentiation of tTregs in the TdLN and their increased presence in the tumor, where they adapt a more mature phenotype. We propose future experiments that can elucidate the mechanisms governing tumor-induced Treg responses in the TdLN and the developmental trajectories of Tregs in healthy tissues and tumors. This information is essential for identifying novel therapeutic targets to prevent tumor-associated Treg responses without eliciting immune-related adverse effects.

Chapter 4 details the contribution of RT to systemic anti-tumor CTL responses within the context of combined ICB treatment, involving blockade of the inhibitory receptor PD-1 and stimulation of the costimulatory receptor CD137, in a transplantable breast carcinoma model. In this setting, the combined anti-PD-1 and anti-CD137 treatment promoted CTL priming. Contrarily, RT did not directly contribute to a systemic T cell response, but enabled CTL activity in the TME. Accordingly, rejection of a non-irradiated tumor implanted on the contralateral flank in the same mouse was not improved upon combined treatment with RT and ICB compared to ICB alone. This study highlights that RT can enable tumor rejection by overcoming local immunosuppression within the TME. Furthermore, we show that low-dose chemotherapy infusion, in the form of cisplatin, enabled CTL activity in the non-irradiated tumor, leading to improved overall survival. This chapter emphasizes that in settings where CTL priming can be achieved by ICB treatment alone, conventional treatments like RT and low dose chemotherapy, can help override local immunosuppression when applied in a rational manner, based on mechanistic insights.

In **chapter 5**, we uncover a novel role of autotaxin (ATX), a lysophospholipase D secreted by tumor cells and other cells, in repelling CTLs from the TME. Mechanistically, we reveal that lysophosphatidic acid (LPA), the bioactive product of ATX, hinders T cell migration primarily by binding to the G protein-coupled receptor 6 (LPAR6). We experimentally enforced ATX overexpression in TC-1 tumor cells and implanted these cells in mice. ATX production by the tumor cells did not disrupt the induction of a systemic CTL response by vaccination but impeded the infiltration of these CTLs into the TME, resulting in significantly reduced mouse survival. Given that ATX inhibitors are currently in development for clinical use, these findings reveal a promising

therapeutic opportunity for enhancing anti-tumor immunity. Together with our findings in **chapter 4**, this study emphasizes that treatments designed to facilitate CTL activity, such as conventional ICB approaches, may not succeed unless we have a comprehensive understanding of the specific CTL inhibitory mechanisms at play and address them carefully.

Finally, in **chapter 6**, I discuss the findings described in this thesis and provide context within the current literature. Additionally, I explore future perspectives regarding the valuable role of RT in enhancing the anti-tumor immunity, particularly within the diverse human tumor landscapes. Together, these findings contribute to a rational application of RT to establish durable anti-tumor immune responses against a range of cancer types.

Nederlandse Samenvatting

In dit proefschrift beschrijf ik hoe T-cellen kunnen bijdragen aan het opruimen van kankercellen, vooral na radiotherapie (RT), en hoe immunotherapie (IT) hierbij kan helpen. Tegenwoordig zijn infectieziekten veelal effectief te voorkomen of bestrijden en daarom zijn kanker en hart- en vaatziekten, nu de belangrijkste gezondheidsproblemen. Kanker wordt vaak beschouwd als een enkele ziekte, maar eigenlijk is het een begrip dat verschillende ziekten omvat die worden bepaald door het weefsel van oorsprong, de onderliggende genetische veranderingen en de aanwezigheid van niet-tumorcellen, waaronder immuuncellen. Tijdens de ontwikkeling en behandeling van tumoren zijn deze cellen voortdurend in gesprek met elkaar, wat leidt tot evoluerende cellulaire ecosystemen.

Kankers worden in de eerste plaats behandeld door chirurgie, maar als de kanker (mogelijk) is uitgezaaid, of moeilijk te verwijderen door een operatie worden RT en chemotherapie toegepast. Deze conventionele therapieën zijn geselecteerd en ontworpen om snel delende tumorcellen te doden. RT is een lokale behandeling die tot doel heeft tumormassa's te verminderen zonder het omliggende gezonde weefsel te schaden. Daarom heeft RT over het algemeen minder ernstige bijwerkingen dan chemotherapie, die door het hele lichaam wordt toegediend om systemische kankerverspreiding te bestrijden. Kankercellen kunnen echter van origine resistent zijn tegen RT, of dit worden in de loop van de behandeling.

Oorspronkelijk werd gedacht dat RT alleen werkt door de celdeling van tumorcellen te stoppen en celdood teweeg te brengen door DNA-schade. Recent is duidelijk geworden dat RT ook T-cellen activeert die bijdragen aan het therapeutisch effect. Ook andere immuuncellen in de tumor reageren op RT. CD8⁺ en CD4⁺ T-cellen zijn ontstaan in de evolutie om ons te beschermen tegen infectie door virussen en andere micro-organismen. Ziekteverwekkers die ons lichaam binnendringen, kunnen worden herkend door T cellen. CD8⁺ T-cellen vermeerderen zich na deze herkenning en veranderen in celdodende T-lymfocyten (CTLs), die heel effectief geïnfecteerde cellen kunnen doden. CD8⁺ T-cellen kunnen ook reageren op tumorcellen als daar lichaamsvreemde moleculen in zitten. In alle gevallen worden T cellen geactiveerd om te delen en CTLs te worden in lymfeklieren die nabij het geïnfecteerde weefsel of de tumor liggen. Dendritische cellen (cDCs) die in de weefsels zitten, nemen resten van dode cellen in zich op en brengen deze naar de lymfeklieren. Ze verteren de celresten en presenteren de vreemde moleculen in kleine stukjes (peptiden) aan T cellen. Die peptiden heten antigenen. Nadat CTLs op deze manier zijn geactiveerd, verlaten ze de lymfeklier en gaan ze via het bloed naar het geïnfecteerde (of tumor) weefsel waar ze hun doelwitcellen doodmaken. CD4⁺ T-cellen zijn cruciaal om hulp te bieden voor effectieve CTL- en antilichaamreacties.

Aangezien tumoren afkomstig zijn van lichaamseigen cellen, worden ze niet gemakkelijk herkend als "vreemd" en roepen ze meestal geen T-celreactie op. RT-geïnduceerde schade en dood

van tumorcellen kunnen helpen om een T-celreactie op te wekken. Er komen na RT namelijk ontstekingsmoleculen en vreemde moleculen vrij die cDCs activeren en tumor-specifieke T-celreacties teweeg kunnen brengen. Tumoren stellen zich teweeg tegen aanvallen van T cellen door deze op diverse manieren te onderdrukken via andere immuuncellen, zowel lokaal in de tumor, alsook in de lymfeklieren en zelfs door het hele lichaam heen. Deze processen kunnen T-celreacties remmen, maar ook de uitzaaiing van kanker vergemakkelijken. Een belangrijk celtype dat de CTL-reactie onderdrukt is de regulatoire T cel (Treg). Deze Tregs gebruiken meerdere mechanismen om T-celactiviteit te onderdrukken, direct of indirect (bijvoorbeeld via cDCs). Daarom spelen ze een essentiële rol bij het voorkomen van overmatige en zelf-reactieve immuniteit.

Om het therapeutisch effect van RT te verbeteren, worden klinische studies vaak gecombineerd met IT. Hierbij wordt vooral gebruik gemaakt van zogenoemde antilichaam-gebaseerde immuuncheckpointblokkade (ICB) tegen receptoren die zich op T cellen bevinden en hun functie belemmeren, zoals PD-1 of CTLA-4. ICB heeft tot doel T-celreacties tegen tumoren te versterken door ofwel immuunremmende receptoren te blokkeren of immuunstimulerende moleculen te activeren. De gecombineerde benadering van RT en IT heeft het potentieel om de effectiviteit van lokale RT te verbeteren en tegelijkertijd systemische T-celreacties tegen tumoren op te wekken, wat cruciaal is om uitzaaiing van tumorcellen te remmen. Het is moeilijk om succesvolle combinaties van RT en ICB in de klinische praktijk toe te passen, vooral omdat we nog niet goed begrijpen hoe de T cel respons op RT wordt opgewekt en hoe dit verloopt in de verschillende kankertypen. We willen daarom beter begrijpen welke factoren nodig zijn om RT-geïnduceerde T-celreacties te initiëren en te ondersteunen. Zo kunnen we op basis van het verkregen inzicht meer rationeel behandelingsstrategieën ontwerpen, die dan effectief lokale of systemische immuunonderdrukking kunnen overwinnen. Dit proefschrift draagt bij aan een dieper begrip van hoe RT de T-cel respons beïnvloedt en biedt richtlijnen voor het rationaliseren van RT/IT combinaties.

In **hoofdstuk 2** hebben we openbaar beschikbare gegevens van The Cancer Genome Atlas (TCGA) gebruikt om de invloed van RT op de overleving kankerpatiënten te onderzoeken. We ontdekten dat RT minder effectief is bij patiënten met kankers die gekenmerkt worden door weinig T cellen en veel myeloïde cellen. Om dit fenomeen beter te begrijpen, maakten we gebruik van tumorcellen die we in muizen implanteren. Voor een bepaald tumormodel (TC-1) stelden we vast dat het lijkt op de tumoren in de mens, waar veel Tregs en myeloïde cellen inzitten en die slecht op RT reageren. Dit model zijn we daarom gaan bestuderen. We ontdekten dat TC-1-tumoren tijdens hun ontwikkeling een Treg respons opwekken door het hele lichaam heen en dat die Treg cellen dus ook verhoogd aanwezig zijn in de tumor en de drainerende lymfeklier. In die lymfeklier moet de CTL-respons worden opgewekt. Het bleek dat RT van de TC-1 tumor wel een CTL-respons in de lymfeklier opwekt, maar tegelijkertijd ook een Treg respons, die de tumorafstoting door CTLs verhindert. We hadden verwacht dat blokkade van CTLA-4 of PD-1 de CTL-respons zou

verbeteren, maar het verbeterde juist de Treg-respons. Dit is een belangrijke observatie, omdat vergelijkbare effecten zich mogelijk ook voordoen bij menselijke tumoren van dit type. Tijdens de ontwikkeling van TC-1-tumoren ontstaat een Treg-respons in het hele lichaam, wat leidt tot verhoogde aanwezigheid van Treg-cellen in de tumor en de drainerende lymfeklier. We ontdekten dat deze Treg respons wordt gedreven door de costimulerende receptor CD28 op de Treg-cellen. CD28 is ook essentieel voor het op gang brengen van CTL-responsen. We vroegen ons daarom af hoe bepaald wordt of de CTL of de Treg profiteren van CD28 costimulatie, vooral wanneer er veel Treg-cellen aanwezig zijn in de lymfeklier. Dit hebben wij opgelost door de bijdrage van CD80 en CD86 te onderzoeken. Deze moleculen zijn de bindingspartners van CD28 en bepalen of CD28 wordt geactiveerd. Deze zogenaamde liganden zitten op cDC. We vonden door selectief CD86 or CD80 te blokkeren in combinatie met RT, dat de Treg-respons specifiek werd gedreven door CD86. Door CD86 te blokkeren konden we de CTL-respons verbeteren, dankzij onderdrukking van de Treg respons. Onder deze omstandigheden verbeterde PD-1 blokkade tumorbestrijding en overleving. We laten met deze studie zien dat ook in tumortypen die een sterke Treg respons opwekken, RT een CTL-respons kan opwekken, die effectief de tumor kan bestrijden als je de Treg respons remt. Dit lukt dan niet met de standaard ICB benaderingen, zoals PD-1 of CTLA-4 blokkade, die het tegengestelde resultaat hebben, maar wel met CD86 blokkade. We denken dat onze ontdekking dat CD86 specifiek Treg responsen drijft tot nieuwe strategieën kan leiden.

De rol van Tregs in het onderdrukken van de immuunrespons tegen tumoren heeft de laatste jaren veel aandacht gekregen. Toch begrijpen we nog niet volledig hoe tumoren zorgen voor de activatie van Tregs in de lymfeklieren. Er zijn twee manieren waarop Tregs kunnen ontstaan: in de thymus (tTregs), waar ze uitrijpen in respons op lichaamseigen antigenen en dan naar de lymfeklieren migreren om hun functies uit te oefenen en zich verder te ontwikkelen. Of ze kunnen ontstaan doordat volwassen CD4⁺ T-cellen veranderen in Tregs die reageren op niet-lichaamseigen antigenen.

In **hoofdstuk 3** karakteriseren we de respons van Tregs in de lymfeklieren en de tumor tijdens de ontwikkeling van TC-1 tumoren. Het blijkt dat dit type tumor de groei en differentiatie van tTregs in de lymfeklieren bevordert, wat resulteert in een grotere aanwezigheid van deze cellen in de tumor, waar ze een meer volwassen fenotype aannemen. We stellen experimenten voor om beter te begrijpen hoe tumoren deze Tregs activeren in de lymfeklieren en hoe Treg ontwikkeling in de tumoren zich onderscheidt van gezonde weefsels. We leggen in dit hoofdstuk uit dat we Treg responsen opgewekt door tumoren willen remmen, maar niet alle Tregs willen verwijderen tijdens de kankerbestrijding, want dan krijgt de patient ongewenste immuunbijwerkingen.

Hoofdstuk 4 beschrijft hoe RT gecombineerd kan worden met immunotherapie (ICB) om CTL-responsen tegen kanker op te wekken, die in het hele lichaam effect kunnen hebben, dus ook kunnen werken in geval van uitgezaaide kanker. In dit geval hebben we voor ICB zowel de

remmende receptor PD-1 geblokkeerd en de costimulerende receptor CD137 geactiveerd met behulp van antistoffen. In een muismodel van lokale borstkanker bevorderde deze combinatie behandeling CTL-responsen tegen de tumor. Toen we een tweede tumor in dezelfde muis lieten groeien, zagen we dat RT in combinatie met deze ICB de afstoting van de bestraalde tumor verbeterde, maar niet de afstoting van deze tweede, niet-bestraalde tumor. We vonden dat CTLs die door de gecombineerd behandeling werden opgewekt, beter tumorcellen konden doodmaken in de bestraalde dan in de onbestraalde tumor. Om een vergelijkbaar effect te bereiken in de niet-bestraalde tumor hebben we lage dosis chemotherapie, in de vorm van cisplatine, toegepast. Dit stimuleerde de activiteit van CTLs in de niet-bestraalde tumor en resulteerde in een verbeterde algehele overleving. Dit hoofdstuk benadrukt dat in situaties waarin CTL-activering kan worden bereikt door ICB-behandeling alleen, conventionele behandelingen zoals RT en lage dosis chemotherapie nuttig kunnen zijn om lokale immuun onderdrukking in de tumor te overwinnen, mits ze strategisch worden ingezet op basis van begrip van de werkingsmechanismen.

In **hoofdstuk 5** ontdekken we een nieuwe rol van een molecuul genaamd autotaxine (ATX) bij het afweren van CTLs uit tumoren. We hebben vastgesteld dat ATX, dat wordt uitgescheiden door zowel tumorcellen als andere cellen, T-cel migratie naar de tumor voornamelijk belemmert door te binden aan een receptor, genaamd LPAR6. Om dit te onderzoeken, hebben we tumorcellen gemanipuleerd zodat ze extra ATX produceerden en deze cellen bij muizen geïmplantteerd. Zo konden we vaststellen dat ATX geproduceerd door de tumor geen invloed had op het opwekken van een CTL-respons door middel van vaccinatie, maar wel verhinderde dat deze CTLs de tumor binnendrongen, wat resulteerde in een aanzienlijk lagere overlevingskans voor de muizen. Er zijn al chemische remmers van ATX in ontwikkeling voor klinisch gebruik, met het idee dat deze uitzaaiing van tumorcellen kunnen remmen. Onze bevindingen voegen nu toe dat het mes aan twee kanten snijdt, want de remmers kunnen er ook voor zorgen dat de CTL-respons tegen de kanker wordt versterkt. Samen met onze bevindingen in **hoofdstuk 4**, benadrukt deze studie dat behandelingen die gericht zijn op het stimuleren van CTL-activiteit, zoals conventionele ICB, mogelijk niet succesvol zullen zijn, tenzij we een diepgaand begrip hebben van de specifieke CTL-remmende mechanismen, en deze op een gerichte manier tegengaan.

Tenslotte bespreek ik in **hoofdstuk 6** de bevindingen die in dit proefschrift beschreven zijn en bied ik context binnen de huidige wetenschappelijke literatuur. Bovendien verken ik hoe in de toekomst RT waardevol kan zijn bij het verbeteren van de immuunrespons tegen tumoren, met name binnen de diverse landschappen van menselijke tumoren. Samen dragen deze bevindingen bij aan een rationele toepassing van RT om effectieve immuunreacties tegen verschillende soorten kanker mogelijk te maken.

Publications

1. **Autotaxin impedes anti-tumor immunity by suppressing chemotaxis and tumor infiltration of CD8⁺ T cells.**

Matas-Rico E*, **Frijlink E***, van der Haar Àvila I, Menegakis A, van Zon M, Morris AJ, Koster J, Salgado-Polo F, de Kivit S, Lança T, Mazzocca A, Johnson Z, Haanen J, Schumacher TN, Perrakis A, Verbrugge I, van den Berg JH, Borst J#, Moolenaar WH#.

Cell Rep. 2021 Nov 16;37(7):110013. doi: 10.1016/j.celrep.2021.110013. PMID: 34788605

2. **Radiotherapy and Cisplatin Increase Immunotherapy Efficacy by Enabling Local and Systemic Intratumoral T-cell Activity.**

Kroon P*, **Frijlink E***, Iglesias-Guimaraes V, Volkov A, van Buuren MM, Schumacher TN, Verheij M, Borst J#, Verbrugge I#.

Cancer Immunol Res. 2019 Apr;7(4):670-682. doi: 10.1158/2326-6066.CIR-18-0654. Epub 2019 Feb 19 PMID: 30782666.

3. **Effects of valproic acid on histone deacetylase inhibition in vitro and in glioblastoma patient samples.**

Berendsen S, **Frijlink E**, Kroonen J, Spliet WGM, van Hecke W, Seute T, Snijders TJ, Robe PA.

Neurooncol Adv. 2019 Nov 12;1(1):vdz025. doi: 10.1093/noonl/vdz025. eCollection 2019 May-Dec .PMID: 32642660 .

4. **Characterization and modulation of anti- $\alpha\beta$ TCR antibodies and their respective binding sites at the β TCR chain to enrich engineered T cells.**

Kierkels GJJ*, van Diest E*, Hernández-López P*, Scheper W*, de Bruin ACM, **Frijlink E**, Aarts-Riemens T, van Dooremalen SFJ, Beringer DX, Oostvogels R, Kramer L, Straetmans T, Uckert W, Sebestyén Z, Kuball J.

Mol Ther Methods Clin Dev. 2021 Jun 24;22:388-400. doi: 10.1016/j.omtm.2021.06.011. eCollection 2021 Sep 10. PMID: 34514030

Manuscript accepted for publication:

1. **PD-1 and CTLA-4 blockade promote CD86-driven Treg responses upon radiotherapy of lymphocyte-depleted cancer in mice.**

Frijlink E, Bosma DMT, Busselaar J, Battaglia TW, Staal MD, Verbrugge I, Borst J.

J Clin Invest. 2024

*Shared first author

#Shared senior author

PhD portfolio

Courses and Workshops

2016	Qlucore hands on training, NKI & VUmc (Amsterdam)
2016	Biostatistics workshop prof. Bing Zhang, OOA/VUmc (Amsterdam)
2017	Advanced Immunology Course, OOA & VUmc (Amsterdam)
2019	Poster: Cell Death in Immunity and Inflammation, EMBO (Crete, Greece)
2021	Basic methods & reasoning in Statistics, LUMC (Leiden)
2021	OMIQ hands on training, LUMC (Leiden)
2023	Ethics and Integrity in Science, OOA & NKI (Amsterdam)

Conferences, retreats, and meetings

2017	Poster: Annual OOA retreat, OOA (Renesse)
2017	Poster: ImmunoRad conference on Immunotherapy and Radiotherapy combinations (New York City, USA)
2017 – 22	Poster: Annual NVVI (Dutch Society for Immunology), (Noordwijk)
2017 – 22	EOS consortium (Belgium)
2019	Jon van Rood symposium, (Noordwijk)
2019/21	NKI-LUMC Immunology symposium, NKI & LUMC (Leiden)
2020 – 22	Speaker: Annual department of Immunology retreat, LUMC (Leiden)
2021	Guest speaker: f-TALES Tumor Immunology and Immunotherapy Conference (Leuven, Belgium)
2021	Bridging Radiotherapy & Immunotherapy Conference, UMC Radboud (Nijmegen)
2022	Poster: Annual conference British Society of Immunology (Liverpool, UK)

Curriculum Vitae

Elselien Stephanie Frijlink was born on March 15, 1989 in Naarden, the Netherlands. In 2008, she completed her high school education at the Baudartius College in Zutphen, majoring in Economics and Culture. Since her interest was directed towards life sciences, she enrolled in the Bètbrug traject in 2009, offered by the University of Amsterdam, to obtain the required life science certifications. The following year, she started the bachelors program in Biomedical Sciences at the Vrije Universiteit in Amsterdam, during which she completed a minor in Genetics and Bioengineering at Yeditepe University in Istanbul, Turkey. Following her graduation in 2012, she continued with the Master of Science program in Infection and Immunity at Utrecht University, which she completed *cum laude* in 2015. During her masters, she investigated different GMP-compatible methods to improve the safety and efficacy of T cell receptor (TCR)-engineered T cells for the treatment of hematological malignancies in the laboratory of Prof. dr. Jürgen Kuball at the University Medical Center Utrecht. Subsequently, she studied the interactions between perturbed microbial communities in the colon and systemic estrogen levels in the lab of Prof. dr. Martin Blaser at the New York University Langone Medical Center in New York City, USA. After obtaining her masters degree, she continued as a junior researcher in the T&P Bohnenn laboratory for neuro-oncology at the University Medical Center Utrecht under the supervision of Prof. dr. Pierre Robe, where she focused on enhancing the CD4⁺ T cell response in glioma cells by inducing CIITA-mediated MHC Class II expression. Having developed a strong interest in the field of cancer immunology, she joined the group of Prof. dr. Jannie Borst at the Netherlands Cancer Institute in Amsterdam as a PhD student in 2016, under the joint supervision of dr. Inge Verbrugge. The results of this work are presented in this thesis.

Acknowledgements

The final and most-read part of the thesis, condensed into 800 words. This achievement would not have been possible without the invaluable support of the people listed below:

My promotor and copromotor: Jannie Borst and Inge Verbrugge.

My paranymphs: Douwe Bosma and Shanna Handgraaf.

Netherlands Cancer Institute:

Marcel Verheij, Heinz Jacobs, Hein te Riele, Karin de Visser, Leila Akkari, Marleen Kok, Ton Schumacher, Karin van der Heijden, Evert de Vries, Yanling Xiao, Paula Kroon, Irene van der Haar Àvila, Andriy Volkov, Victoria Iglesias, Nika Babala, Astrid Bovens, Mark Mensink, Sander de Kivit, Xin Lei, Tom de Wit, Xiaohang Qiao, Mercedes Machuca Ostos, Joleen Traets, Hatice Karabulut, Tisee Hau, Kim Vrijland, Hannah Garner, Noor Bakker, Max Wellenstein, Danique Duits, Olga Blomberg, Lorenzo Spagnuolo, Kevin Kos, Wietske Pieters, Serena Vegna, Luuk van Hooren, Awa Gassama, Daan Kloosterman, Efi Tsouri, Christel Ramirez, Marnix de Groot, Camiel Göbel, Ronak Shah, Aldo Spanjaard, Daniel de Groot, Rachele Niccolai, Frank van Gemert, Iris Glykofridis, Chiara Cattaneo, Vivien Veninga, Iris Mimpfen, Rhianne Voogd, Wouter Scheper, Felipe Rojas Rodriguez, Michael Schubert all the other members at the B3 and B6 department.

Martijn van Baalen, Frank van Diepen, Guido de Roo, Monique van Vlastuin, Jeroen van Os, Marissa Kollee, Brechtje Theijn-Rijnbout, Tania Maidment, Natalie Proost, Ben van de Graaff, Marieke van de Ven, Maaïke van der Meulen, Sin-Ming Sit, Mijke de Vreij-Kruidenier, Doreen Ram, Mahdi Hamidi Shishavan and all the other members of the T building.

Leiden University Medical Center:

Jetty Hagen, Julia Busselaar, Lotte Verleng, Mo Staal, Ellen Schrama, Fiamma Salerno, Annemarthé van der Veen, Timo Oosenbrug, Jorn Stok, Eloisa Vega Quiroz, Dennis Gravekamp, Laurens ter Haar, Ben Thompson, Ferry Ossendorp, Ramon Arens, Frank Staal, Tetje van der Sluis, Floor van Haften.

Ghent University:

Sofie Rennen and Sophie Janssens.

Outside of my academic life:

My ultimate cheerleaders: Loes Aaldering, Gilat Ben Yehuda, Abi Herschberg, Channah Herschberg, Janneke Rinzema, Caroline Rotenberg, Lotte Stiekema, Marlies Thomassen, Stephanie Wentink, Lexane van der Zee.

My VU-buddies and beyond: Amber Hol Horeman and Stacey Joosten.

Dames 7: Cecilia Sellmeijer, Anna de Wilde and Lotte Zonneberg.

My favorite Zwollenaar: Brett Hahn.

My book club friend: Johanna Erhani.

The couple that appreciates my dinner-hosting skills: Soufiane Mourragui and Lisa Koob.

My amazing – above and beyond – family: Papa, Mama, Margriet, Elmar, Sverre, Kalle, Irene, Carlien, Boaz, Ilya, Hein-Carl, Mitzi, Miny, Evert and Sjaantje.

And last, but definitely not least, My Love: Thomas Battaglia.

My sincere thanks to all of you for:

- Providing intelligent input.
- Letting me vent when necessary.
- Cheering me on.
- Believing in me.
- And for your continuous (mental) support.

